

UCSF

UC San Francisco Electronic Theses and Dissertations

Title

Pharmacokinetics and delivery of proteins modified with FcRn binding ligands

Permalink

<https://escholarship.org/uc/item/0m17q8hv>

Author

Sockolosky, Jonathan

Publication Date

2013

Peer reviewed|Thesis/dissertation

**Pharmacokinetics and Delivery of Proteins Modified with FcRn Binding
Ligands**

by

Jonathan T. Sockolosky

DISSERTATION

Submitted in partial satisfaction of the requirements for the degree of

DOCTOR OF PHILOSOPHY

in

Pharmaceutical Science and Pharmacogenomics

in the

GRADUATE DIVISION

of the

UNIVERSITY OF CALIFORNIA, SAN FRANCISCO

Copyright 2013

By

Jonathan T. Sockolosky

Dedication

This thesis is dedicated to my Mother, Shelley Sockolosky. You are the beating of my heart. Without you I would not be. I love you today, tomorrow, and always.

Acknowledgments

I would first and foremost like to thank my mentor, Dr. Frank Szoka, who has provided me with the foundation, ethics, intuition, creativity, and determination to become an independent researcher. I am forever in debt to Frank for enabling my development as a young scientist by trusting my decisions and allowing me to pursue personal research interests without restriction. I have never doubted Frank's passion for his students and science and I can only hope that one day I will be a loved and respected mentor like Frank. I would not be where I am today without his guidance and support over the last 4 years. Frank has given me a realistic perspective on research and life as an academic and has taught me that above all passion is the driving force for doing good science. I feel so fortunate to have trained with Frank.

I would like to thank all the other mentors who have been instrumental in my graduate career. Especially Dr. Dean Sheppard and Dr. Walt Finkbeiner for serving on my dissertation committee and providing me with valuable feedback and mentorship. I would also like to thank Dr. Leslie Benet, Dr. Max Krummel, and Dr. Kathy Giacomini for serving on my qualifying exam committee. And of course Dr. Deanna Kroetz who has been a wonderful mentor over the years and a fearless director of the PSPG graduate program. Deanna works tirelessly to preserve the integrity of the PSPG program and graciously donates her time to support not only her own students, but also all students in the PSPG program. Deanna has had a profound impact on my graduate career at UCSF and I am so thankful for all the wonderful opportunities she has

provided me. I would also like to thank Debbie Acoba-Idlebi for making life as a student in the PSPG program simple.

Words cannot even begin to describe how thankful I am for my family, especially my Mom and Dad, Shelley and Gary Sockolosky, for always encouraging me to follow my own path, their unconditional love, and their endless support not only during my graduate studies but throughout my entire life. I am so lucky and fortunate to have a family that makes me laugh, that I look forward to being around, and that I wish I could spend every day of my life with. Who I am today is because of my family and of course my sisters, Nicole and Danielle Sockolosky, who I love more than words on paper can describe. I am also in debt to my Grandma, Jean Sockolosky, who helped raise me as a child and gave me strong morals and ethics. Although we are now spread around the country, I have never felt as close with my family as I do today. As the years pass and our lives change, the one thing that remains is our family bond. My Mom is my inspiration for doing science and I can only hope that one day I can contribute to the discovery and development of medicines that directly impact human health and perhaps save a life. I feel strongly that my duty as an academic is to push myself and others to do science for the good of humanity. I love you Mom, Dad, Danielle, Nicole, and Grandma.

Of course where would I be without my partner and better half, Le Truong. I am so fortunate to have someone in my life that brings me back to earth when I am up in space and that has supported me, without question, in all my endeavors over the years. Thank you for continuing to believe in me all these years. The home and relationship we have built together is the most important aspect of my life. You are the peanut butter to my bread. I just couldn't imagine living without you.

I am also so very thankful for my dear friend and my old manager Dr. Matthew Hutchinson. Matt always pushed for my personal and professional development when I was just starting my scientific career and was never afraid to provide me with candid feedback. I am so thankful that I had the opportunity to work with Matt and even more thankful that our relationship has continued to grow and develop. And to the rest of the Hutchison family, especially Boone, who is like a sister to me. And to Olivia and Ashton who I wish I could take home with me every day but am so fortunate to be in their lives and to watch them grow over the years to come. Thank you Hutchinson's for being my family away from family. It brings me to tears of joy thinking about how influential you have been in my life. No matter where life takes us from here I hope that there will always be a place in it for each other.

Thank you to my San Francisco family, especially Marc Lopez, Kevin Morley, Rich Fidler, Jen Naidu, Srinivas Naidu, Jenifer Lundberg, Maddie Thies, and Aparna Chhibber. Thank you for all the lifelong memories we have created together and being there for me all these years. I would not be complete without such fantastic friends.

I would like to thank all Szoka lab members that I have had the pleasure to work with over the years. I especially would like to thank Dr. Matt Tiffany who took me in under his wings as a rotation student and transferred to me a solid foundation in molecular biology. I cannot imagine what my graduate career would have been like without Matt. I will miss working together in lab but will continue to look forward to our bike rides. I would also like to thank Dr. Saul Kivimae, Aditya Kohli, Dr. Vince Venditto, and Dr. Juliane Nguyen who have all been integral in shaping the way I do science.

Finally, I would like to thank my funding sources that have made both my research and professional development possible: NIH 1 R21 EB015520-01 and NIH TG T32 GM007175 and past and current fellowship support from the American Foundation for Pharmaceutical Education (AFPE), UCSF Graduate Dean's Chancellor's Fellowship, UCSF Graduate Student Research Award, and the Pharmaceutical Research and Manufacturers of America (PhRMA) foundation. I am so fortunate to be able to come to work every single day and do what truly makes me happy.

Pharmacokinetics and Delivery of Proteins Modified with FcRn Binding Ligands

Jonathan T. Sockolosky

Abstract

The importance of therapeutic recombinant proteins in medicine has led to a variety of tactics to increase their circulation time or to enable routes of administration other than injection. One clinically successful tactic to improve protein circulation and delivery is to fuse the Fc-domain of immunoglobulin G (IgG) to therapeutic proteins so that the resulting fusion proteins interact with the neonatal Fc receptor (FcRn). Although successful, Fc-fusion proteins significantly increase molecular weight thereby restricting tissue penetration, decrease protein function, and are limited to mammalian expression systems. As an alternative to grafting the high molecular weight Fc-domain to therapeutic proteins, we have modified their N- and/or C-terminus with a short peptide sequence that interacts with FcRn. Our strategy was motivated by results from Mezo and coworkers [Mezo et al. (2008) PNAS 105:2337-42] who identified peptides that compete with human IgG for FcRn. The small size and simple structure of the FcRn binding peptide (FcBP) allows for expression of FcBP fusion proteins in *E. coli* and results in their pH-dependent binding to FcRn with an affinity comparable to that of hIgG1. The FcBP fusion proteins are internalized, recycled and transcytosed across cell monolayers that express FcRn. Although FcBP fusion proteins mimic the human IgG1 interaction with human FcRn *in vitro*, the half-life of FcBP fusion proteins in wild type C57BL/6J and human FcRn transgenic mice is independent of FcRn binding, whereas the half-life of human and mouse IgG1 correlate with their species matched FcRn-binding affinity. These results promoted a detailed investigation into potential factors that may contribute to the lack of correlation between the *in vitro* and *in vivo* results including: serum stability, serum competition, renal clearance, and the function of the hybrid

human-mouse FcRn/ β 2m receptor; however, no single variable explains the FcRn-independent half-life of FcBP fusion proteins. We speculate that an additional component(s), in collaboration with FcRn, regulates IgG homeostasis *in vivo* and is not replicated by FcBP fusion. If such a novel FcRn regulatory component exists, it would have a significant impact on FcRn biology and provide new opportunities to engineer IgG or alternative FcRn-targeted molecules for enhanced serum persistence.

Table of Contents

Dedication	iii
Acknowledgments	iii
Table of Contents	ix
List of Figures	xv
List of Tables	xviii
Abbreviations	xix
Chapter 1: The neonatal Fc receptor, FcRn, as a molecular target to improve the drug-like properties of proteins and macromolecules.....	1
1.1 FcRn discovery, structure, biology, and function	1
1.1.1 The Brambell hypothesis	1
1.1.2 The discovery of FcRn.....	2
1.1.3 FcRn structure and mechanism of IgG and albumin binding	4
1.1.4 The site of FcRn protection of IgG <i>in vivo</i>	8
1.1.5 The mechanism of FcRn-mediated recycling and transcytosis of IgG	9
1.2 Modulating the IgG-FcRn interaction.....	11
1.2.1 Fc-engineering to increase the half-life of therapeutic antibodies.....	11
1.2.2 Inhibitors of the IgG-FcRn interaction	17
1.3 Fc-fusion for half-life extension, non-invasive protein delivery, and as vaccines	19
1.3.1 Fc-fusion as a versatile half-life extension platform.....	20
1.3.2 Oral and pulmonary protein delivery via FcRn transcytosis	21
1.3.3 Fc-fusion proteins for vaccination	24
1.4 Alternative strategies that target FcRn.....	27
1.4.1 Albumin fusion	27
1.4.2 Low molecular weight FcRn binding ligands	30
1.4 Conclusion	32
1.5 References.....	33

Chapter 2: Engineering FcRn-mediated recycling and transcytosis in recombinant proteins by short N- and C-terminal peptide extensions..... 43

2.1 Introduction.....	43
2.2 Methods.....	45
2.2.1 Materials	45
2.2.2 Cell Culture	45
2.2.3 Mammalian expression vectors.....	46
2.2.4 MDCK h β 2M and MDCK hFcRn-EYFP/h β 2M cell line generation.....	47
2.2.5 <i>E. coli</i> expression vectors	47
2.2.6 Protein expression and purification	50
2.2.7 Mass spectrometry	50
2.2.8 Fluorescent spectra measurements.....	51
2.2.9 Affinity measurements by surface plasmon resonance.....	51
2.2.10 FACS cellular accumulation assay	52
2.2.11 mKate fluorescence in MDCK hFcRn-EYFP/h β 2M cells after intracellular pH clamping.....	52
2.2.12 Fluorescence microscopy.....	53
2.2.13 FcRn mediated recycling and transcytosis assay	54
2.2.14 FcRn-mediated recycling versus transcytosis in MDCK hFcRn-EYFP/h β 2M cells.	55
2.2.15 Statistical analysis	56
2.3 Results.....	57
2.3.1 Protein expression and characterization.....	57
2.3.2 Binding kinetics between FcRn and FcBP modified mKates	58
2.3.3 Cellular accumulation of FcBP modified mKates by FACS	61
2.3.4 Fluorescence imaging of FcBP modified mKates	64
2.3.5 Recycling from FcRn expressing MDCK cells	68
2.3.6 Transcytosis across FcRn expressing MDCK cell monolayers	69

2.3.7 FcRn-mediated Recycling versus Transcytosis in MDCK hFcRn-EYFP/h β ₂ m cell monolayers	70
2.3.8 Tyr12 to His FcBP mutant with altered affinity for FcRn	72
2.4 Conclusions	73
2.5 References	76
Chapter 3: Correlations between cross-species IgG and albumin binding to FcRn <i>in vitro</i> and plasma clearance <i>in vivo</i> validate the human FcRn transgenic mouse model	80
3.1 Introduction	80
3.2 Methods	83
3.2.1 Materials	83
3.2.2 Cell Culture	83
3.2.3 Mice	83
3.2.4 mKate-cFcBP protein expression and purification	84
3.2.5 Size exclusion chromatography	84
3.2.6 Affinity measurements by surface plasmon resonance	85
3.2.7 Cellular accumulation of IgG, albumin, and mKate-cFcBP in MDCK hFcRn-EYFP/h β ₂ M by FACS	86
3.2.8 Plasma clearance in mice	86
3.3 Results	88
3.3.1 Protein expression, purification, and characterization	88
3.3.2 Binding kinetics between FcRn and mouse, rabbit, and human IgG	90
3.3.3 Binding kinetics between FcRn and mouse and human serum albumin	93
3.3.4 Accumulation of FcRn ligands in MDCK hFcRn-EYFP/h β ₂ M cells by FACS	95
3.3.5 Plasma clearance of mouse and human IgG1 in mice	96
3.3.7 Plasma clearance of mouse and human serum albumin in mice	99
3.4 Conclusion	101
3.5 References	105
Chapter 4: The <i>in vivo</i> fate of FcBP fusion proteins and liposomes in wild type and human FcRn transgenic mice	109

4.1 Introduction.....	109
4.2 Methods.....	112
4.2.1 Materials	112
4.2.2 Cell Culture.....	113
4.2.3 Mice	113
4.2.4 Mammalian expression vectors.....	115
4.2.5 <i>E. coli</i> expression vectors	116
4.2.6 Synthetic FcRn binding peptides	117
4.2.7 FcBP modified mKate protein expression and purification.....	117
4.2.8 Affinity measurements by surface plasmon resonance.....	118
4.2.9 Size exclusion chromatography	118
4.2.10 FACS cellular accumulation, serum competition, ligand competition, and serum stability assays	118
4.2.11 Analysis of ligand binding to hybrid FcRn/ β 2m receptors in MDCK cells	119
4.2.12 Western blot analysis of FcRn, β 2m, and β -actin.....	120
4.2.13 PEGylation of N-&-C-Term Linear FcBP mKate (mKate-IFcBP).....	121
4.2.14 Preparation of synthetic FcBP modified liposomes.....	121
4.2.15 Preparation of mIgG1-SMCC-FcBP	122
4.2.16 Plasma clearance in mice.....	123
4.3 Results.....	124
4.3.1 Binding kinetics between N-&-C-Term Cyclic FcBP mKate (mKate-cFcBP) and mouse and human FcRn.....	124
4.3.2 Plasma clearance of mKate and FcBP modified mKate	125
4.3.3 Ligand binding to hybrid FcRn/ β 2m receptor <i>in vitro</i>	128
4.3.4 mKate-cFcBP plasma clearance in FcRn knockout and Tg35/Tg55 heterozygous mice	131
4.3.5 PEGylation of mKate-IFcBP to reduce renal clearance.....	133
4.3.6 Whole blood stability of FcBP modified mKates and hIgG1	136

4.3.7 Serum competition for FcBP modified mKate and hIgG1 accumulation in MDCK hFcRn-EYFP/h β 2M cells.....	137
4.3.8 FcBP modified liposomes to probe the role of molecular weight and valency	141
4.3.9 mIgG1-SMCC-FcBP to probe alternative IgG regulatory mechanism.....	145
4.4 Conclusion	148
4.5 References.....	155
Chapter 5: Conclusions	159
5.1 Overview.....	159
5.2 Summary of findings.....	160
5.3 Historical and future perspectives: the not so well characterized neonatal Fc receptor? .	162
5.4 References.....	166
Appendix A: Periplasmic production via the pET expression system of soluble, bioactive human growth hormone	169
A.1 Introduction.....	169
A.2 Methods.....	171
A.2.1 Materials.....	171
A.2.2 <i>E. coli</i> expression vectors.....	171
A.2.3 Protein expression and purification.....	172
A.2.4 Matrix-assisted laser desorption and ionization (MALDI)-time of flight (TOF) mass spectrometry.....	173
A.2.5 Size exclusion chromatography.....	174
A.2.6 In vitro receptor binding assay.....	174
A.2.7 Nb2 cell proliferation assay.....	175
A.2.8 Affinity measurements by surface plasmon resonance.....	175
A.3 Results.....	177
A.3.1 Construction of pET22b hGH expression vectors.....	177
A.3.2 Protein expression, purification, and characterization.....	179
A.3.3 Affinity measurement by surface plasmon resonance and ELISA.....	183

A.3.4 Nb2 cell bioassay for growth hormone activity.....	186
A.4 Conclusion	187
A.5 References.....	188
Appendix B	191
B.1 Amino acid sequences of proteins studied in this dissertation.....	191

List of Figures

Figure 1.1 The γ-globulin concentration versus catabolism effect in mice.	2
Figure 1.2 Structure of human FcRn in contact with hIgG1 and human serum albumin.	4
Figure 1.3 Amino acid residues on the human IgG1 Fc-domain involved in binding to human FcRn and that have been mutated to alter human IgG half-life.	6
Figure 1.4 The FcRn-mediated recycling and transcytosis model.	10
Figure 1.5 Schematic of various fusion protein domains that can hijack FcRn.	29
Figure 2.1 Construction and characterization of FcBP modified mKate's.	58
Figure 2.2 FcBP modified mKates exhibit pH dependent binding to hFcRn by SPR.	60
Figure 2.3 <i>In vitro</i> characterization of FcBP modified mKates in MDCK cells expressing hFcRn-EYFP by FACS.	62
Figure 2.4 Cellular accumulation of FcBP modified mKates in various cell lines.	63
Figure 2.5 Influence of pH clamping of MDCK hFcRn-EYFP/hB2M cells at pH 4, 5, or 7.4 on cell associated mKate fluorescence.	63
Figure 2.6 Fluorescence Imaging of FcBP modified mKates in MDCK cells expressing hFcRn-EYFP.	65
Figure 2.7 Cyclic FcBP modified mKate's colocalize with hFcRn-EYFP in MDCK cells.	66
Figure 2.8 N-&-C-Term Cyclic FcBP mKate is trafficked by hFcRn-EYFP in MDCK cells.	67
Figure 2.9 FcBP fusion enables FcRn-mediated recycling and transcytosis.	68
Figure 2.10 Dose-dependent transcytosis of N-&-C-Term Cyclic FcBP mKate and transport of FITC-inulin across MDCK hFcRn/hB2M cell monolayers.	70
Figure 2.11 Recycling versus transcytosis of FcBP modified mKates, hIgG1, and transferrin in MDCK MDCK hFcRn/hB2M cell monolayers.	71
Figure 2.12 Tyr-12 to His mutation of the Cyclic FcBP improved pH dependent binding to hFcRn.	73
Figure 3.1. Size exclusion chromatograms of IgGs, albumins, and mKate-cFcBP pre (a) and post (b) size exclusion chromatography purification.	89
Figure 3.2. Reducing and non-reducing SDS-PAGE analysis of IgGs, albumins, and mKate-cFcBP.	90
Figure 3.3 Surface plasmon resonance sensograms of IgG binding to mouse and human FcRn at pH 6.	92

<u>Figure 3.4 Surface plasmon resonance sensograms of mouse, rabbit, and human IgG binding to mouse and human FcRn at pH 7.4</u>	92
<u>Figure 3.5 Surface plasmon resonance sensograms of mouse and human serum albumin binding to mouse and human FcRn at pH 6</u>	94
<u>Figure 3.6 Surface plasmon resonance sensograms of mouse and human serum albumin binding to mouse and human FcRn at pH 7.4</u>	94
<u>Figure 3.7 <i>In vitro</i> characterization of FcRn ligand accumulation in MDCK cells expressing hFcRn-EYFP/hβ2M by FACS</u>	96
<u>Figure 3.8 Plasma clearance of mouse and human IgG1 in wild type and human FcRn transgenic mice</u>	98
<u>Figure 3.9 Plasma clearance of rabbit serum IgG and human IgG1 in Tg32 mice</u>	99
<u>Figure 3.10 Plasma clearance of mouse and human serum albumin in wild type and human FcRn transgenic mice</u>	100
<u>Figure 4.1. Surface plasmon resonance sensograms of mKate-cFcBP binding to mouse and human FcRn at pH 6 and pH 7.4</u>	124
<u>Figure 4.2. Plasma clearance of mKate and FcBP modified mKates in wild type and human FcRn transgenic mice</u>	127
<u>Figure 4.3. Ligand accumulation in MDCK cells expressing hybrid human FcRn / β2m receptors</u>	130
<u>Figure 4.4. Ligand accumulation in MDCK cells expressing hybrid mouse or rabbit FcRn / β2m receptors</u>	131
<u>Figure 4.5. Plasma clearance of N-&-C-Term Cyclic FcBP mKate in FcRn knockout and Tg32/Tg55 transgenic mice</u>	133
<u>Figure 4.6. PEGylation does not impact FcRn-binding or result in human FcRn specific half-life extension in mice</u>	135
<u>Figure 4.7. Whole blood stability of hIgG1, mKate-cFcBP, and mKate-IFcBP</u>	137
<u>Figure 4.8. Serum competition of hIgG1, mKate-cFcBP, and mKate-IFcBP accumulation in MDCK hFcRn-EYFP/hβ2M cells by FACS</u>	139
<u>Figure 4.9. Purified hIgG1 and human serum albumin competition of mKate-cFcBP accumulation in MDCK hFcRn-EYFP/hβ2M cells by FACS</u>	140
<u>Figure 4.10. FcBP modified liposomes exhibit dose, pH, and FcRn dependent accumulation in MDCK hFcRn-EYFP/hβ2M cells</u>	143
<u>Figure 4.11. Plasma clearance of FcBP modified liposomes in wild type and human FcRn transgenic mice</u>	144

Figure 4.12. mIgG1-SMCC-FcBP fusion binds human FcRn but does not have an extended half-life in human FcRn transgenic mice	147
Figure 4.13. Alternative IgG salvage theories that act in combination with FcRn	154
Figure A.1 Schematic depicting the construction of pET22b-pelB hGH (left) and pET22b-ompA hGH (right) expression vectors	178
Figure A.2 Reducing and non-reducing SDS-PAGE analysis of recombinant hGH	181
Figure A.3 Size exclusion chromatography (a-c) and MALF-TOF (d-f) analysis of TEV-TROPIN (a,d), pelB-hGH (b,e), and ompA-hGH (c,f)	182
Figure A.4 <i>In vitro</i> hGH receptor binding ELISA (a) and Nb2 cell potency bioassay (b)	184
Figure A.5 Surface plasmon resonance sensograms of hGH binding to immobilized hGH-R .	185

List of Tables

<u>Table 1.1. Summary of Fc mutations that validate the IgG-FcRn affinity at pH 6 to serum half-life relationship.</u>	15
<u>Table 1.2. Summary of Fc mutations that refute the IgG-FcRn affinity at pH 6 to serum half-life relationship.</u>	16
<u>Table 2.1 Primer sequences used in this study.</u>	49
<u>Table 2.2 Binding kinetics to human FcRn and <i>in vitro</i> uptake of FcBP modified mKates and hIgG1 in FcRn expressing MDCK cells.</u>	60
<u>Table 3.1 Binding kinetics and affinity of IgG to human and mouse FcRn at pH 6 and pH 7.4.</u>	91
<u>Table 3.2 Binding kinetics and affinity of mouse and human serum albumin to human and mouse FcRn at pH 6 and pH 7.4</u>	93
<u>Table 3.3. Plasma half-life of hIgG1, mIgG1, HSA, and MSA in wild type and human FcRn transgenic mice.</u>	98
<u>Table 4.1 Primers used in this study</u>	117
<u>Table 4.2. Plasma half-life of mKate, FcBP modified mKates, ABP modified mKate in wild type, human FcRn transgenic, and human FcRn α-chain null (FcRn KO) mice.</u>	128
<u>Table 4.3. Summary of IC₅₀ values derived from serum and plasma competition of IgG, albumin, and FcBP modified mKate accumulation in MDCK hFcRn-EYFP/hβ2M cells at pH 6 shown in Fig. 4.8.</u>	140
<u>Table A.1 Primers used in this study</u>	177
<u>Table A.2 Binding affinity to hGH receptor measured by SPR and ELISA and <i>in vitro</i> hGH potency in Nb2 cell growth bioassay.</u>	183

Abbreviations

Nucleic acids:

mRNA - messenger ribonucleic acid
DNA - deoxyribonucleic acid
cDNA - complementary deoxyribonucleic acid
MCS - multiple cloning site

Proteins/Protein complexes:

EGF - epidermal growth factor
FcRn – neonatal Fc receptor
Fc γ R – Fc γ receptor
FcBP – FcRn binding peptide
ABP – albumin binding peptide
FSH – follicle stimulating hormone
EPO - erythropoietin
TfR – transferrin receptor
Tf – transferrin
 β 2M - β 2-microglobulin
IC – immune complex
GLP-1 – glucagon-like peptide-1
hGH – human growth hormone
hGHR – human growth hormone receptor
MHC - major histocompatibility complex
IVIg – intravenous immunoglobulin G
OVA - ovalbumin
His6 - hexahistidine
mKate - monomeric Katushka
GFP - green fluorescent protein
YFP - yellow fluorescent protein
CFP - cyan fluorescent protein
LAMP-1 - lysosome associated membrane protein 1
VEGF – vascular endothelial growth factor
EGFR – epidermal growth factor receptor
BSR – B-cell receptor
HepBV – Hepatitis B virus
HEL – hen egg lysozyme
TNF α – tumor necrosis factor alpha
INF α 2 – interferon alpha-2
INF γ - interferon gamma
TSG-6 – tumor necrosis factor alpha-induced protein 6
GCSF-3 – granulocyte colony-stimulating factor 3
RSV – respiratory syncytial virus
HIV – human immunodeficiency virus
HER2 – human epidermal growth factor receptor 2
CD80 – cluster of differentiation 80

CLTA4 – cytotoxic T-Lymphocyte Antigen 4
TRIM21 – tripartite motif-containing protein 21
spA – staphylococcus aureus protein A
spG – streptococcal protein G
Fc – fragment crystalizable
Fab – fragment antigen binding
C_H2 – immunoglobulin constant heavy chain domain 2
C_H3 – immunoglobulin constant heavy chain domain 3
CDR – complementarity determining region
IL6 – interleukin 6
HRP – horseradish peroxidase
mAb – monoclonal antibody
hIgG1 – human immunoglobulin G1
mIgG1 – mouse immunoglobulin G1
rabIgG – rabbit immunoglobulin G
HSA – human serum albumin
MSA – mouse serum albumin
RSA – rabbit serum albumin

Lipids/Polymers:

HSPC – L- α -phosphatidylcholine, hydrogenated (Soy)
Chol – cholesterol
DPPE-Rho - 1,2-dipalmitoyl-*sn*-glycero-3-phosphoethanolamine-N-(lissamine rhodamine B sulfonyl)
PEG-DSPE - 1,2-distearoyl-*sn*-glycero-3-phosphoethanolamine-N-[amino(polyethylene glycol)-2000]
MAL-PEG-DSPE - 1,2-distearoyl-*sn*-glycero-3-phosphoethanolamine-N-[maleimide(polyethylene glycol)-2000]
PEG – polyethyleneglycol
mPEG-MAL-20 - α -[3-(3-Maleimido-1-oxopropyl)amino]propyl- ω -methoxy, polyoxyethylene, 20 kDa
mPEG-MAL-40 - α -[3-(3-Maleimido-1-oxopropyl)amino]propyl- ω -methoxy, polyoxyethylene, 40 kDa

Units:

nts - nucleotides
bp - base pair
 $\times g$ - times (\times) gravity
g - gram
pmoles - picomoles
mg - miligram
 μg - microgram
M - molar
mM - milimolar
 μM - micromolar
nM - nanomolar

mm - milimeter
μm - micrometer
nm - nanometer
L - liter
mL - mililiter
μL - microliter
ms - milisecond
kDa - kiloDalton
rpm - revolutions per minute
s.d. - standard deviation
K_D – equilibrium dissociation constant
k_a – association rate constant
k_d – dissociation rate constant
IC₅₀ - inhibitory concentration for 50% inhibition
ED₅₀ - effective dose for 50% effect
U_{1/2,max} - concentration for 50% uptake
MWCO - molecular weight cutoff
MFI – mean fluorescent intensity

Chemicals:

EDTA - Ethylenediaminetetraacetic acid
HEPES - 4-(2-hydroxyethyl)-1-piperazineethanesulfonic acid
NAC - N-acetyl-L-cysteine
IAM – iodoacetimide
DTT – dithiothreitol
TCEP - Tris(2-carboxyethyl)phosphine hydrochloride
G418 - Geneticin
Tris - tris(hydroxymethyl)aminomethane
MES - 2-(N-morpholino)ethanesulfonic acid
NaCl – sodium chloride
IPTG - isopropylthio-β-galactoside
PES - polyethylene sulfate
PVDF – polyvinylidene difluoride
FITC - fluorescein isothiocyanate
DAPI - 4',6-diamidino-2-phenylindole
HBFA – heptafluorobutyric acid
5-TAMRA - 5-Carboxytetramethylrhodamine
SMCC - Succinimidyl-4-(N-maleimidomethyl)cyclohexane-1-carboxylate

Cells:

MDCK – madin-darby canine kidney
APC – antigen presenting cells
DC – dendritic cell

Media:

D-PBS - phosphate buffered saline without calcium and magnesium

PBS - phosphate buffered saline

HBSS – hanks balanced salt solution

FBS - fetal bovine serum

TB - terrific broth

NEAA – non-essential amino acids

MEM – minimal essential medium

RPMI – roswell park memorial institute

Techniques:

FACS - Fluorescence-activated cell sorting

ELISA – enzyme-linked immunosorbent assay

SPR – surface plasmon resonance

SEC – size exclusion chromatography

DLS – dynamic light scattering

SDS-PAGE - sodium dodecyl sulfate polyacrylamide gel electrophoresis

PCR - polymerase chain reaction

RT-PCR – reverse transcription polymerase chain reaction

LC-MS/MS – liquid chromatography tandem mass spectrometry mass spectrometry

MALDI – matrix assisted laser desorption/ionization

Other:

Abdeg – antibodies that enhance IgG degradation

GI – gastrointestinal

FDA – food and drug administration

Chapter 1: The neonatal Fc receptor, FcRn, as a molecular target to improve the drug-like properties of proteins and macromolecules

1.1 FcRn discovery, structure, biology, and function

1.1.1 The Brambell hypothesis

Immunoglobulin G (IgG) and albumin, although widely disparate in biological function, share an exceptionally long plasma half-life of ~ 20 days in humans as a result of salvage from intracellular catabolism by the neonatal Fc receptor (FcRn). The discovery of the FcRn is a fascinating story that was enabled through a number of elegant studies and remarkable foresight by Francis William Rogers Brambell in the 1940s-1960s who focused much of his career studying IgG transmission and passive immunity. Brambell proposed a number of hypotheses regarding a receptor-mediated and intimately related process of IgG transmission from mother to fetus and IgG catabolism based on the observations that IgG but not other serum proteins or immunoglobulins were selectively transported across the yolk sac of fetal rabbits and the intestine of neonatal rats, transport was mediated entirely by the Fc but not Fab domain of IgG, and that the half-life of IgG decreased as the serum concentration of IgG increased in mice¹ (Fig. 1.1). Thus, Brambell put forth the following paraphrased hypothesis in 1964²:

“...of the γ -globulin so isolated in a special [cellular] compartment, only those molecules which attached to receptors are saved and returned to the circulation. It is suggested that the isolation is effected by pinocytosis and that the receptors are intracellular in the walls of the vesicles. Similar cellular mechanisms may underlie the catabolism of circulating γ -globulin and the transmission of passive immunity.”

Brambell retired in 1968 and passed away in 1970 leaving a gap in expertise pertaining to the study of IgG transport and catabolism; however, his hypotheses were eventually confirmed.

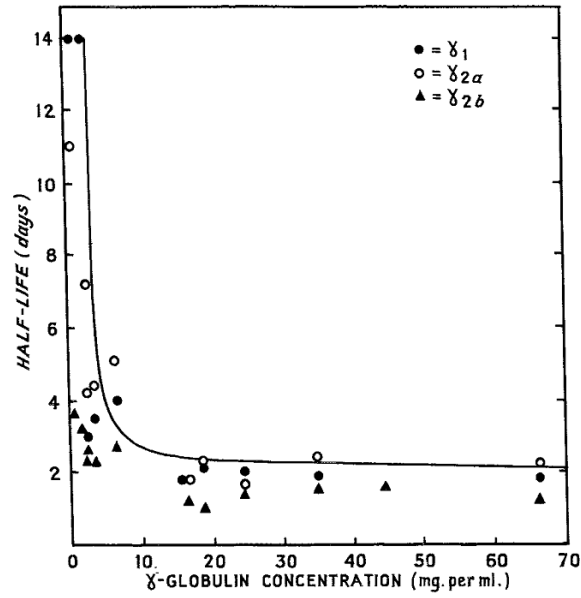


Figure 1.1 The γ -globulin concentration versus catabolism effect in mice. The data shown were obtained by Fahey and Sell³ and reproduced by Brambell¹.

1.1.2 The discovery of FcRn

The first major discovery after Brambell's contribution to the field was the pH-dependent nature of IgG binding to the neonatal rat intestinal brush border suggesting the existence of an IgG specific receptor on the surface of intestinal cells responsible for the acquisition of IgG from maternal milk^{4,5}. The binding at acidic (pH < 6.5) but not neutral pH was exploited by Rodewald and co-workers to affinity purify FcRn from rat enterocytes, which was then described as a heterodimer of ~ 51 kDa and ~ 14 kDa subunits⁶. FcRn was subsequently cloned from the neonatal rat intestine, hence the neonatal Fc receptor, in 1989 by Simster and Mostov⁷ who identified the p51 subunit of FcRn (α -chain) as a homolog of MHC Class I molecules and the p14 subunit as β 2-microglobulin (β 2m). Studies in β 2m-null mice, which we now know lack functional FcRn, provided evidence regarding the requirement of FcRn for the acquisition of maternal IgG by neonatal mice⁸. β 2m null mice also had low serum IgG levels⁸ suggesting that the receptor involved in the transport and catabolism of IgG were in fact the same, as originally hypothesized by Brambell 30 years prior.

Ward and colleagues connected the link between the dual functions of FcRn in controlling the maternofetal transfer and catabolism of IgG by identifying the Fc-domain amino acid residues responsible for mIgG1 binding to FcRn and that influence IgG half-life in mice⁹. Soon after, three independent groups including Ward and colleagues demonstrated that IgG half-life in β 2m null mice is abnormally short and that FcRn α -chain mRNA is present in numerous adult animal tissues indicating that FcRn is responsible for IgG catabolism and transmission¹⁰⁻¹². Eventually, the observations in β 2m null mice were recapitulated in FcRn α -chain null mice¹³ providing definitive evidence that a single receptor, FcRn, controls maternal to fetal IgG transfer and IgG serum persistence. Brambell's prescient hypothesis was spot on!

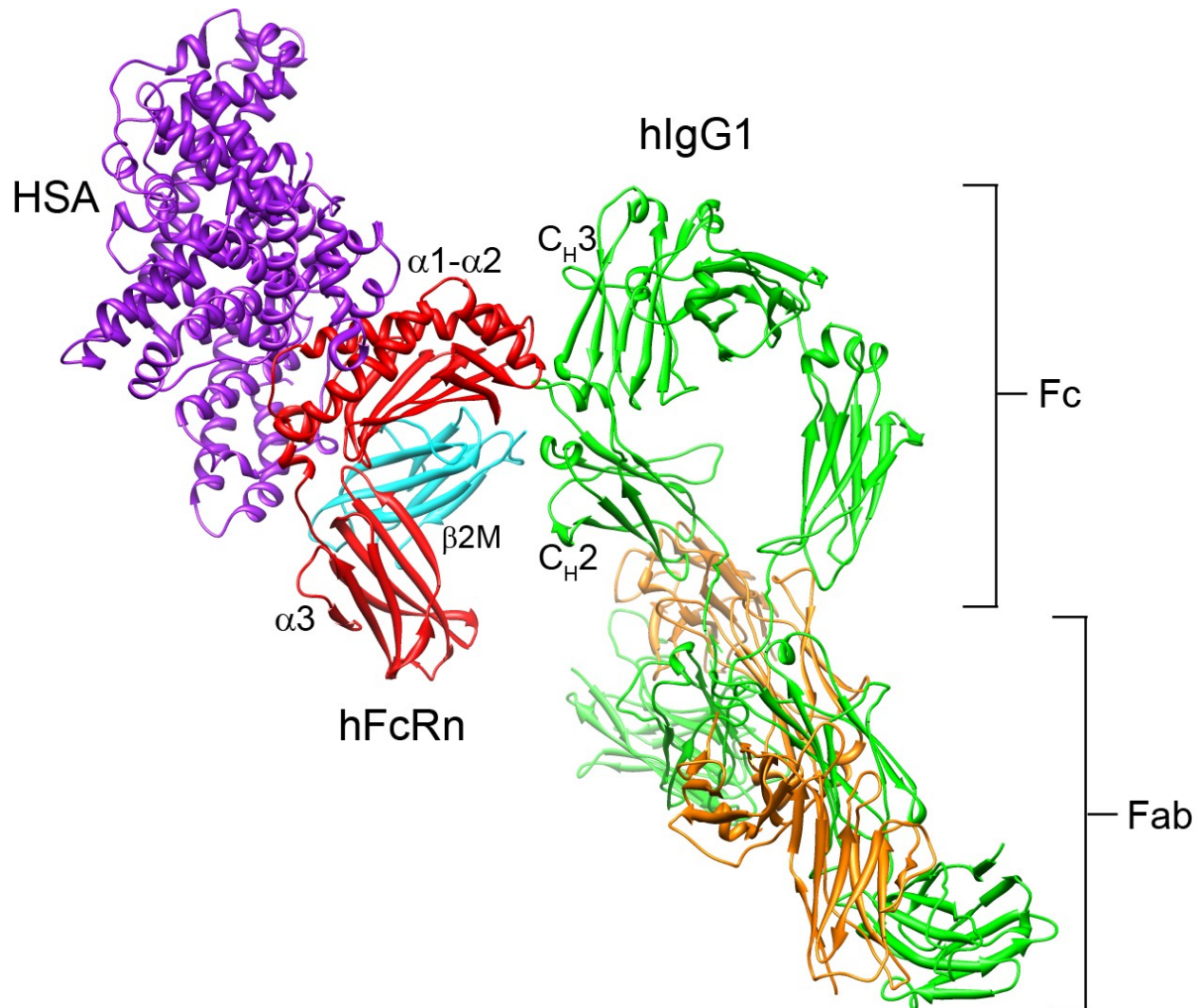


Figure 1.2 Structure of human FcRn in contact with hIgG1 and human serum albumin.

Human IgG1 (green) contacts the $\alpha 2$ domain of human FcRn (red) and N-terminus of $\beta 2M$ (cyan) at the intersection of the C_{H2} - C_{H3} domains within the Fc portion of IgG. Human serum albumin (purple) contacts a distinctly different binding site that spans the $\alpha 1$ - $\alpha 2$ domains of FcRn and $\beta 2M$. The HSA/hFcRn/hIgG1 model in this figure is based upon the HSA/hFcRn structure (PDB code 4K71) and the full length human IgG1 structure (PDB code 1HZH). As there is no crystal structure of the hIgG1/FcRn complex, full length hIgG1 was aligned to human FcRn based upon the rat Fc/FcRn structure (PDB code 1FRT) using Chimera v1.6.1 (UCSF, San Francisco, CA).

1.1.3 FcRn structure and mechanism of IgG and albumin binding

FcRn is structurally homologous to the MHC Class I heterodimeric receptor family¹⁴ consisting of a type I transmembrane heavy chain that non-covalently associates with the soluble light chain, $\beta 2$ -microglobulin ($\beta 2m$). $\beta 2m$ is absolutely necessary for the proper folding,

transport, and function of FcRn, as well as other MHC Class I homologs, both *in vitro* and *in vivo*. The FcRn heavy chain contains three soluble domains ($\alpha 1$, $\alpha 2$, and $\alpha 3$), a single transmembrane helix, and a cytoplasmic tail (Fig. 1.2). Unlike MHC Class I molecules, FcRn does not directly present antigen to T-cells due to point mutations on the top face of FcRn that disrupt peptide binding. The human and mouse FcRn α -chain and $\beta 2m$ light chain share $\sim 65\%$ and $\sim 70\%$ amino acid sequence identity, respectively, although the residues important in IgG and albumin binding are generally conserved across species.

The ability of FcRn to protect IgG from otherwise certain catabolism is the result of a specific, pH-dependent interaction with the Fc portion of IgG. IgG binds FcRn in a strictly pH-dependent manner at acidic (< 6.5) but not neutral pH (> 7) mediated by electrostatics between titratable histidine residues in the Fc C_{H2} - C_{H3} domains of IgG and acidic residues on the $\alpha 2$ -domain of FcRn¹⁵⁻¹⁸ (Fig. 1.2 and Fig. 1.3). Binding is further stabilized by a series of hydrophobic interactions and hydrogen bonds between Fc and residues within the FcRn $\alpha 2$ -domain and the $\beta 2m$ light chain N-terminus¹⁹. One IgG molecule can simultaneously bind two FcRn molecules due to the homodimeric nature of IgG^{20,21} resulting in a high affinity interaction between FcRn and IgG at pH 6 due to avidity. The 2:1 interaction between FcRn and IgG is critical for efficient binding, recycling, and transcytosis *in vitro*²² and to preserve the long serum persistence of IgG *in vivo*¹⁶.

The FcRn binding site on IgG overlaps with the staphylococcal protein A (spA), streptococcal protein G (spG), and rheumatoid factor binding site²³ but is distinct from the classical Fc γ receptors¹⁸ and the C1q component of complement^{24,25} that bind near the upper C_{H2} domain and hinge region. IgG binding to FcRn is independent of glycosylation²⁶ in contrast to glycan dependent IgG binding to classical Fc γ receptors.

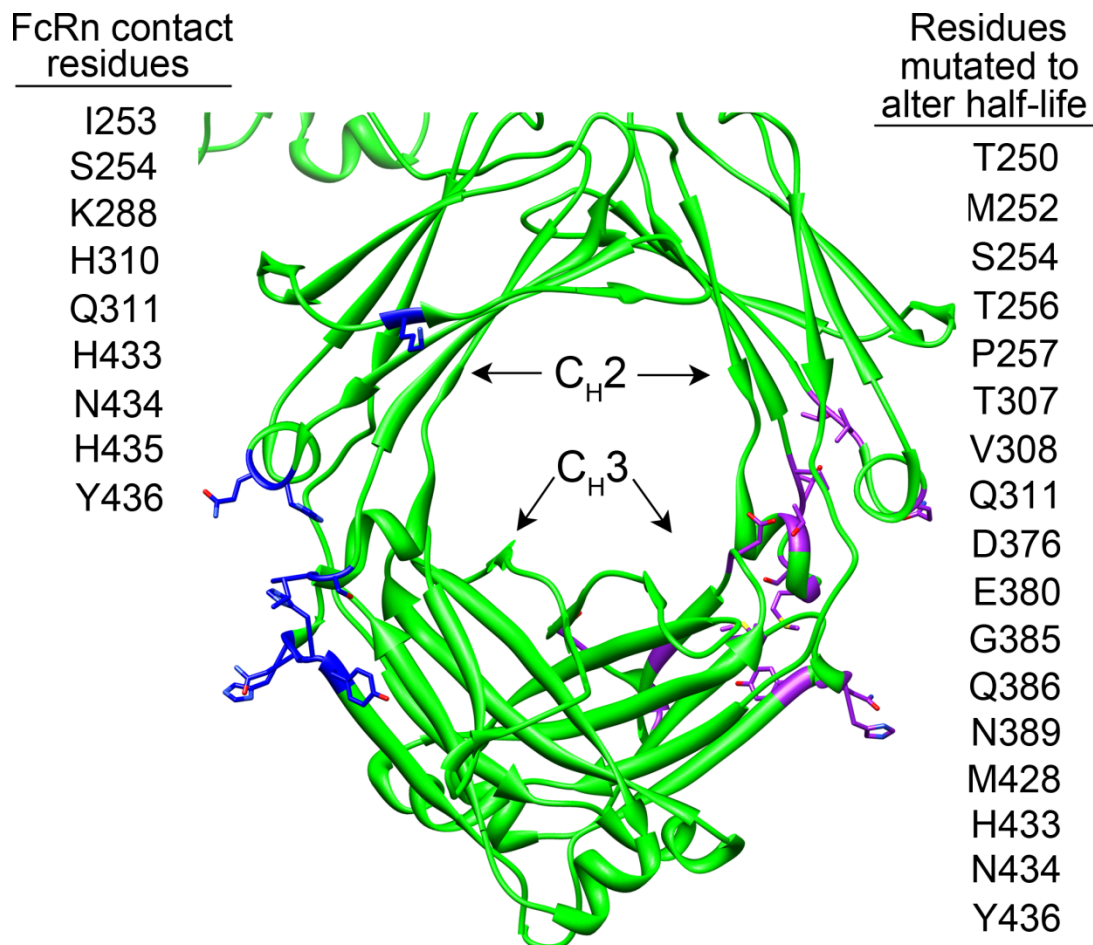


Figure 1.3 Amino acid residues on the human IgG1 Fc-domain involved in binding to human FcRn and that have been mutated to alter human IgG half-life.

Human IgG1 Fc-domain residues involved in pH-dependent binding to human FcRn are shown as blue side chains on the left. The residues predominately cluster at the C_{H2} - C_{H3} domain interface and include the three key protonatable histidine residues H310, H433, H435. The residues in the Fc-domain of hIgG1 that have been mutated to alter the binding affinity to human FcRn are shown as purple side chains on the right. Again the residues cluster at the C_{H2} - C_{H3} domain interface and most are distinct from the FcRn contact residues shown on the left. The human IgG1 Fc-domain model in this figure is based upon the full length human IgG1 structure (PDB code 1HZH).

The amino acid residues involved in the IgG-FcRn interaction have been determined by mutagenesis¹⁸, molecular modeling¹⁹, and crystallography^{15,17,27} (Fig. 1.3). The IgG-FcRn interface is composed of three subsites: a hydrophobic core and two electrostatic sites. Ile253 on IgG is conserved across species and is critical for interaction with FcRn making numerous hydrophobic contacts with $\alpha 2$ domain amino acids Leu112, Phe117, and Trp131 on FcRn¹⁹. The

hallmark pH-dependent binding is driven by two key histidine residues, His310 and His435, and to a lesser extent His433 on IgG that become positively charged as the pH approaches 6.0-6.5 resulting in the formation of salt bridges with Glu115, Glu116, Asp130, and Glu133 residues on FcRn. Ile1 on β 2m also contributes to IgG binding as mutation to Ala abrogates rat IgG binding to rat FcRn²⁸.

In addition to IgG, albumin binds FcRn through a series of pH-dependent ionic interactions between conserved histidine and glutamic acid residues located within the α 1 and α 2-domains of FcRn²⁹ (Fig. 1.2), characteristic of the IgG-FcRn interaction. As a result, albumin is recycled by FcRn and also has a long half-life in humans of \sim 19 days. Molecular modeling, structure guided mutagenesis, and the recent crystal structure of an engineered albumin-FcRn complex indicates that albumin binds to a distinct site on FcRn opposite that of IgG^{29,30}. IgG and albumin can simultaneously and non-cooperatively bind FcRn *in vitro*^{31,32} in agreement with their distinctly different binding sites; however, whether a single FcRn molecule can transport both IgG and albumin concurrently has not been determined.

Although the pH-dependent FcRn binding mechanism is similar between IgG and albumin, the 1:1 stoichiometry of the FcRn-albumin interaction³¹ results in a significantly lower equilibrium binding affinity of albumin-FcRn compared to the 2:1 stoichiometry of the FcRn-IgG interaction, which has a significantly higher affinity due to avidity^{21,27}. In addition, the IgG-FcRn interaction is predominately driven by electrostatics whereas the albumin-FcRn interaction is predominantly hydrophobic³⁰. Both IgG and albumin exhibit significant cross-species differences in their interaction with mouse and human FcRn³². Human FcRn is selective for evolutionarily related IgG species but ignores rodent IgGs while mouse FcRn is promiscuous in its interaction with IgG from various species³³. FcRn is less restrictive towards albumin across

species as both mouse and human albumin bind mouse and human FcRn albeit with species-specific kinetics and affinity³². The cross-species binding specificities of IgG and albumin are important considerations when choosing appropriate pre-clinical animal models to study the *in vivo* properties of FcRn ligands.

1.1.4 The site of FcRn protection of IgG *in vivo*

The major cells types involved in the FcRn-mediated protection of IgG from degradation have been deduced in the mouse. IgG clearance is accelerated in irradiated wild-type mice reconstituted with bone marrow from FcRn α -chain null mice³⁴ indicating the hematopoietic compartment is a major contributor to IgG homeostasis. FcRn is expressed in human intestinal macrophages, peripheral blood monocytes, and dendritic cells as well as in mouse splenic macrophages, B cells, dendritic cells, and monocytes^{35,36}; however, it is unknown if a particular hematopoietic cell type or many are important in maintaining serum IgG levels.

Conditional deletion of FcRn in mouse vascular endothelial cells, and to some extent in hematopoietic cells, results in rapid clearance of IgG and reduced steady state levels of IgG and albumin, indicating that the vascular endothelium is also a major contributor to IgG homeostasis³⁶ in the mouse, as was expected given the close contact between the vascular endothelium and IgG in blood. Thus, endothelial cells and hematopoietic cells including monocytes, macrophages, dendritic cells, and possibly B cells are important regulators of IgG clearance in the mouse.

FcRn expression at the mRNA level in mice is highest in the liver followed by kidneys, skin, lungs, spleen, and muscle³⁷. The relative IgG tissues-to-plasma area under the curve ratios in wild type and FcRn α -chain null mice indicate that FcRn contributes significantly to IgG exposure in the skin and muscle³⁸, which are presumed to be the major sites of IgG catabolism in

humans. FcRn is also expressed in a wide variety of human tissues; however, the contribution of human endothelial cells to the FcRn-mediated protection of IgG is a point of debate as there are conflicting reports on the extent of FcRn expression in human endothelial cell lines³⁹ versus human tissues⁴⁰. Regardless, expression of FcRn in human tissue resident dendritic cells, macrophages, and neutrophils, muscle endothelial cells, and a range of epithelial cells^{40,41} is consistent with data in the mouse^{36,42}. Therefore, the sites of FcRn function in humans is likely tissue specific endothelial cells, such as in the muscle and/or skin, hematopoietic cells, and potentially tissue specific epithelial cells although this warrants further investigation.

1.1.5 The mechanism of FcRn-mediated recycling and transcytosis of IgG

The ability of FcRn to protect IgG from intracellular catabolism has been deduced through a series of *in vitro* cellular trafficking studies⁴³⁻⁴⁵. The albumin-FcRn salvage pathway has not been studied *in vitro* but it is widely believed to follow a fate similar to IgG. In almost all cell types FcRn is localized predominantly to intracellular vesicles such as early and recycling endosomes and sorting tubules. FcRn expression on the cell surface is limited and the pH of the extracellular environment is not favorable for an IgG-FcRn interaction; therefore, IgG is believed to enter cells through non-specific, fluid-phase pinocytosis (Fig. 1.4a). Endocytosed IgG is trafficked along the endosomal pathway and encounters FcRn in the early endosome where the acidic microenvironment ($\text{pH} \cong 6$) favors a productive IgG-FcRn interaction. The FcRn-IgG complex is trafficked away from the lysosomal pathway and back to the plasma membrane, where upon membrane fusion the FcRn-IgG complex disassociates due to the elevated extracellular pH, returning IgG to the extracellular space, such as the blood, thus extending the serum half-life of IgG. Serum proteins that are not associated with a recycling receptor or IgGs that do not dissociate from FcRn⁴⁵ are destined for lysosomal degradation. In addition to

recycling, FcRn can transcytosis IgG across polarized cell monolayers via a similar cellular pathway delivering IgG from the blood into tissue interstitial space and vice versa (Fig. 1.4b).

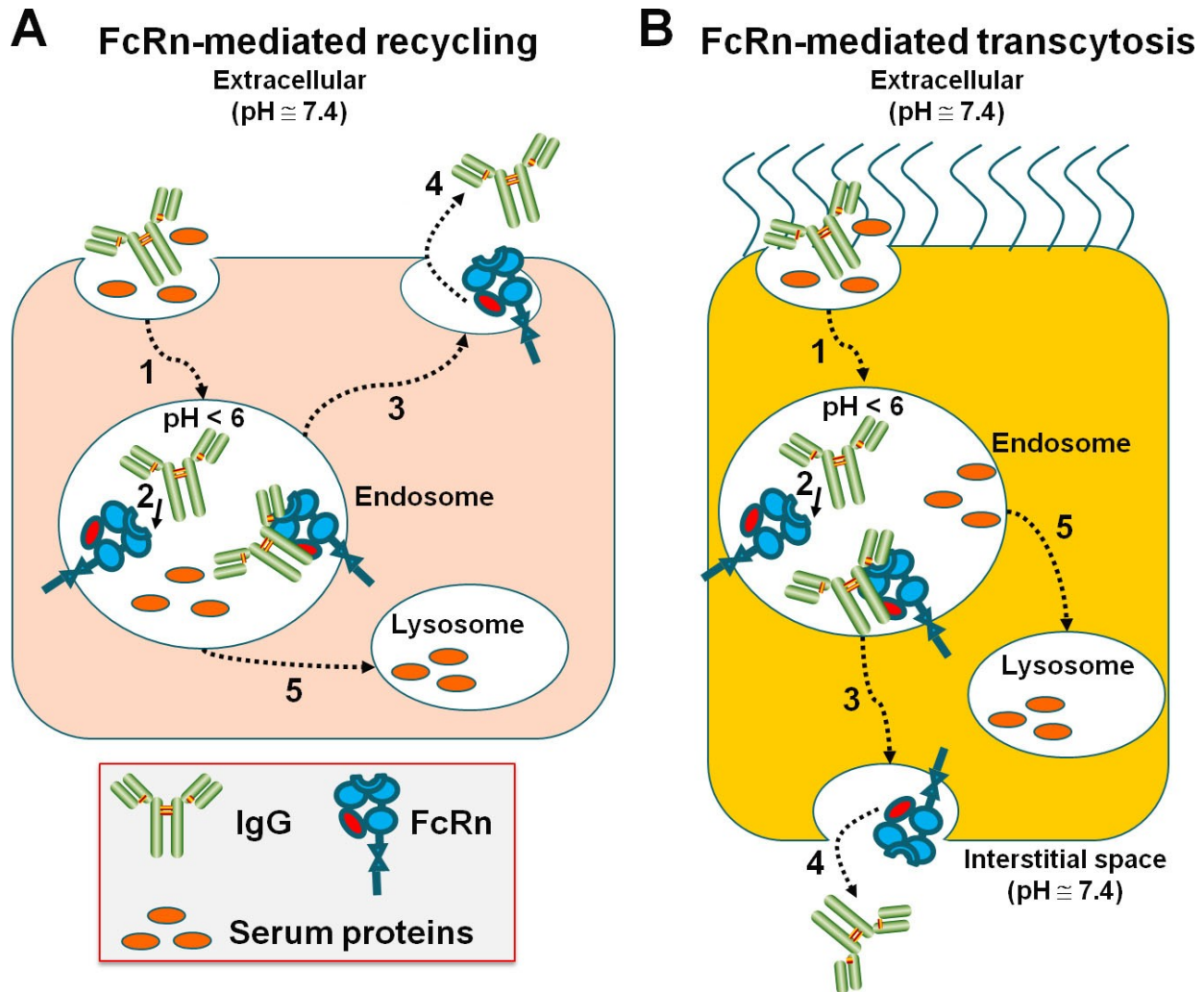


Figure 1.4 The FcRn-mediated recycling and transcytosis model.

(a) FcRn-mediated recycling initiates upon non-specific fluid-phase pinocytosis of serum IgG into FcRn expressing endothelial or hematopoietic cells. As IgG is trafficked along the endosomal pathway (1) the pH decreases to 6 resulting in association with endosomal FcRn (2). The IgG-FcRn complex is sorted and trafficked back to the plasma membrane (3) where IgG is released into blood due to its weak affinity for FcRn at blood pH (4). Serum proteins that do not bind a recycling receptor are trafficked to the lysosome and catabolized (5). (b) FcRn-mediated transcytosis of IgG across polarized epithelial cells, such as in the gut or lung, follows a similar cellular trafficking mechanism as in (a). IgG enters FcRn-expressing epithelial cells by fluid-phase pinocytosis (1), is captured by FcRn in the endosome (2), and is subsequently trafficked to the opposing cell membrane (3) where upon endosomal fusion IgG is released into the tissue interstitial space due to the elevated pH (4).

1.2 Modulating the IgG-FcRn interaction

Because FcRn contributes significantly to the half-life of IgG and its transport across cellular barriers, a number of engineering approaches have been devised to modulate the IgG-FcRn interaction. These approaches have focused around mutation of Fc-domain amino acid residues in proximity to the FcRn binding site. Modulating the IgG-FcRn interaction to increase antibody half-life could enable in less frequent dosing while still maintaining efficacy. Conversely, reducing the half-life of antibodies used for tumor imaging may improve signal-to-noise by enabling antibody accumulation in the tumor but rapid clearance from the blood⁴⁶. Finally, inhibiting the endogenous IgG-FcRn interaction has therapeutic potential for the treatment of IgG-mediated autoimmune disease.

1.2.1 Fc-engineering to increase the half-life of therapeutic antibodies

The identification of the amino acid residues involved in the regulating the catabolism and transcytosis of IgG indicated a strong correlation between serum half-life and affinity for FcRn at pH 6^{9,16,47}. This suggested that increasing the affinity of the IgG-FcRn interaction at pH 6 would result in an engineered IgG with increased serum persistence. Ghetie, Ward and colleagues randomly mutated three residues in close proximity to the IgG-FcRn binding interface and selected Fc variants that bound FcRn with increasing stringency by phage display⁴⁸. One mouse Fc mutant (T252L/T254S/T256F) with an ~ 3.5-fold increase in affinity for mouse FcRn at pH 6 while still maintaining pH-dependent binding had a modest but significantly increased half-life in mice⁴⁸. This seminal study was the first to demonstrate that it is possible to increase the serum persistence of Fc, and likely IgG, by increasing affinity toward FcRn at pH 6.

Mutation of the same amino acid residues in human IgG (M252Y/S254T/T256E) results in an ~ 10-fold increase in affinity for human FcRn at pH 6 without increasing affinity at pH 7.4

and an ~ 4-fold increase in half-life in monkeys⁴⁹. Importantly, the M252Y/S254T/T256E human IgG1 mutant was recently shown to also have an increased half-life in healthy adult humans⁵⁰. This is a major validation of engineering efforts to increase IgG affinity for FcRn at pH 6 as a means to increase serum persistence in humans. Unfortunately, the IgG-FcRn affinity to half-life relationship is not straightforward as an alternative IgG mutant (N434H) with an ~ 3-fold increase in affinity for human FcRn at pH 6 and an ~ 2-fold increase in half-life in baboons did not translate to an increased half-life in diseased humans⁵¹. Thus, disease state and antibody target resulting in FcRn-independent IgG clearance mechanisms are potential confounding factors when translating engineered IgGs from pre-clinical models into the clinic.

A number of additional mutations to the Fc-domain of IgG that alter pH-dependent binding to FcRn (Fig. 1.3, Table 1.1, and Table 1.2) have now been described and are reviewed extensively in references^{37,52,53}. Increasing IgG affinity toward FcRn at pH 6 while maintaining little to no binding at pH 7.4 is a validated mechanism to increase antibody half-life and in general a ~ 5-10 fold increase in affinity at pH 6 translates to an ~ 2-4-fold increase in half-life. However, the FcRn affinity to half-life correlation is not always clear in pre-clinical animal models as was also observed in humans.

In one example, the pharmacokinetics of anti-tumor necrosis factor α (TNF α) IgG1 variants with increased affinity to human, monkey, and mouse FcRn at pH 6 were evaluated in CD-1 mice and cynomolgus monkeys⁵⁴. In mice, the anti-TNF α IgG1 variants were rapidly eliminated compared to wild-type IgG1 despite the ~ 17 – 200-fold increase in affinity for mouse FcRn at pH 6. The equilibrium binding affinity at pH 7.4 was not reported; however, the percentage of variant IgG1s that remained bound to mouse FcRn at pH 7.4 by ELISA was in some cases up to 80%, suggesting that each variant has substantial affinity for mouse FcRn at pH

7.4. Thus, the accelerated clearance of the anti-TNF α IgG1 variants in mice is likely due to the failure to dissociate from FcRn at physiological pH resulting in catabolism of bound IgG1 during FcRn turnover.

The same IgG1 variants have an \sim 50 - 80-fold increase in affinity for monkey FcRn at pH 6 but retained pH-dependent binding. However, despite the substantial increase in affinity at pH 6 the IgG1 variants (P257I/N434H or D376V/N434H) had a similar half-life in monkeys compared to wild-type IgG1⁵⁴.

Conversely, a separate set of IgG1 mutations (M428L/N434S) that resulted in an \sim 11-fold improvement in affinity for human FcRn at pH 6 also resulted in an \sim 4-fold and \sim 3-fold increase in half-life in human FcRn transgenic mice (Tg276) and monkeys, respectively⁵⁵. In this case the IgG1 mutations were introduced into the anti-vascular endothelial growth factor (VEGF) antibody bevacizumab and the anti-epidermal growth factor receptor (EGFR) antibody cetuximab. Both antibodies cross-react with their respective monkey antigen but only cetuximab exhibited significant target mediated, non-linear clearance; however, increased FcRn affinity in both cases resulted in half-life extension. Affinity at pH 7.4 was not quantified although dissociation at pH 7.4 was monitored by SPR and the variant appears to behave like WT hIgG1 suggesting that the M428L/N434S mutation does not substantially alter affinity at pH 7.4. This was the first study to demonstrate that an FcRn-dependent increase in half-life in mice translates to an improvement in anti-tumor activity *in vivo*, indicating that at least in these particular mouse cancer models increased drug exposure through half-life extension preserves efficacy and enables less frequent dosing.

A number of additional reports that either support^{49,55-65} or a few that refute^{54,64,66} the IgG-FcRn affinity to half-life relationship are in the literature. In all cases, the extent of IgG

characterization with FcRn varies making it difficult to draw useful comparisons between studies. Analysis of the IgG-FcRn affinity to half-life relationship is listed in Table 1.1. To address these issues, future studies evaluating the impact of FcRn affinity on IgG pharmacokinetics should consider numerous factors in addition to simply measuring affinity at pH 6 such as: 1) binding kinetics including on and off-rates 2) binding affinity and kinetics at pH 7.4, 3) species matched FcRn binding affinities, and 4) alternative FcRn-independent clearance mechanisms. Despite the conflicting reports, it is clear that modulating the IgG-FcRn interaction via Fc mutation results in the generation of antibodies with altered *in vivo* properties and that maintaining pH-dependent binding to FcRn is critical for half-life extension.

Table 1.1. Summary of Fc mutations that validate the IgG-FcRn affinity at pH 6 to serum half-life relationship.

IgG Isotype	Antigen	Mutation	K _D , pH 6 (nM)*	Fold increase in K _D , pH 6	Binding at pH 7.4 ^v	PK Species	Half-life (days)	Fold increase in half-life	Ref.
hlgG1	anti-BSR	WT	1700	---	n.b.	Cynomolgus monkey	6.2	---	59
		N434A	570	3	negligible		14.5	2.3	
		N434W	44	39	10-100 nM		9.7	1.6 (n.s.)	
hlgG1	anti-RSV	WT	1196	---	n.b.	Cynomolgus monkey	6.1	---	49
		M252Y/S254T/T256E	134	9	n.b.		21.2	3.5	
hlgG1	anti-RSV	WT	269	---	n.b.	BALB/C mice	3.2	---	56
		M252Y/S254T/T256E	27	10	~ 42%		3.0	0.9	
		G385D/Q386P/N389S	187	1	weak		2.8	0.9	
		H433K/N434F/Y436H	14	19	~ 51%		n.r.	---	
hlgG2	anti-HepBV	WT	n.d.	---	n.r.	Rhesus monkey	14.6	---	60
		M428L	n.d.	7	n.r.		26.8	1.8	
		T250Q/M428L	n.d.	28	n.r.		27.2	1.9	
hlgG1	anti-HepBV	WT	10	---	n.b.	Rhesus monkey	14.0	---	57
		T250Q/M428L	0.4	28	slight ↑ vs WT		34.9	2.5	
hlgG1	anti-HEL	WT	32	---	n.b.	Swiss-webster	10.4	---	61
		H433K/N434F	2	21	82		2.6	0.3	
hlgG1	anti-VEGF	WT	2460	---	n.r.	Tg276 hFcRn mice	2.8	---	55
		M428L/N434S	218	11	n.r.		12.0	4.3	
hlgG1	anti-VEGF	WT	2460	---	n.r.	Cynomolgus monkey	9.7	---	55
		M428L/N434S	218	11	n.r.		31.1	3.2	
hlgG1	anti-EGFR	WT	n.r.	---	n.r.	Tg276 hFcRn mice	2.9	---	55
		M428L/N434S	n.r.	---	n.r.		13.9	4.8	
hlgG1	anti-EGFR	WT	n.r.	---	n.r.	Cynomolgus monkey	1.5	---	55
		M428L/N434S	n.r.	---	n.r.		4.7	3.1	
hlgG1	anti-VEGF	WT	2400	---	> 10 μM	Cynomolgus monkey	11.4	---	65
		N434H	450	5	~ 12 μM		18.6	1.6	
		T307Q/N434A	240	10	~ 10 μM		24.9	2.2	
		T307Q/N434S	195	12	~ 10 μM		22.4	2.0	
		T307Q/E380A/N434A	153	16	~ 9 μM		21.7	1.9	
		V308P/N434A	67	36	~ 5 μM		20.5	1.8	
hlgG1	anti-HER2	WT	n.r.	---	n.r.	Tg32 hFcRn mice	6.5	---	58
		I253A	n.r.	< 0.1	n.r.		1.1	0.2	
		N434A	n.r.	3	n.r.		10.6	1.6	
		T307A/E380A/N434A	n.r.	12	n.r.		9.7	1.5	
hlgG1	anti-HER2	WT	n.r.	---	n.r.	Tg276 hFcRn mice	1.7	---	58
		I253A	n.r.	< 0.1	n.r.		1.0	0.6	
		N434A	n.r.	3	n.r.		3.9	2.2	
		T307A/E380A/N434A	n.r.	12	n.r.		4.4	2.5	
hlgG4 (A1)	n.r.	WT	65	---	6.4	Cynomolgus monkey	13.7	---	64
		V308P	2	43	6.9		26.5	1.9	
hlgG4 (E1)	n.r.	WT	160	---	6.4	Cynomolgus monkey	3.9	---	64
		V308P	1	114	6.7		12.9	3.3	
		T250Q/M428L	13	12	6.7		10.3	2.6	
Fc-CTLA4 fusion (hlgG1 Fc)	anti-CD80	WT	2460	---	n.r.	Cynomolgus monkey	5.4	---	63
		M428L/N434S	218	11	n.r.		7.5	1.4	
hlgG1	anti-IL6	WT	1160	---	n.r.	Cynomolgus monkey	8.5	---	62
		M252Y/S254T/T256E	365	3	n.r.		28.4	3.4	

Table 1.2. Summary of Fc mutations that refute the IgG-FcRn affinity at pH 6 to serum half-life relationship.

IgG Isotype	Antigen	Mutation	K _D , pH 6 (nM) [*]	Fold increase in K _D , pH 6	Binding at pH 7.4 [‡]	PK Species	Half-life (days)	Fold increase in half-life	Ref.
hlgG1	anti-TNF α	WT	209	---	6.3	Cynomolgus monkey	6.0	---	54
		P257I/N434H	4	52	6.5		4.3	0.7	
		D376V/N434H	4	52	6.3		4.8	0.8	
		P257I/Q311I	3	80	6.5		n.r.	---	
hlgG1	anti-TNF α	WT	118	---	6.6	CD-1 mice	11.6	---	54
		P257I/N434H	1	197	7.6		0.4	0.0	
		D376V/N434H	7	17	7.2		1.1	0.1	
		P257I/Q311I	5	25	7.3		1.2	0.1	
hlgG1	anti-TNF α	WT	209	---	6.3	Cynomolgus monkey	5.0	---	61
		P257I/Q311I	3	80	6.5		4.8	0.9	
		T250Q/M428L	5	40	6.3		4.7	0.9	
hlgG1	anti-TNF α	WT	118	---	6.6	CD-1 mice	15.3	---	61
		P257I/Q311I	5	25	7.3		n.r.	---	
		T250Q/M428L	0.2	513	7.0		16.7	1.1	
hlgG4 (A1)	n.r.	WT	65	---	6.4	Cynomolgus monkey	13.7	---	63
		T250Q/M428L	3	24	6.6		11.9	0.9	
Chimeric IgG1	anti-dansyl	WT	71	---	3.7	BALB/C mice	6.0	---	66
		T307A/E380A/N434A	10	7	17.8		5.7	1.0	
Chimeric IgG1	anti-dansyl	WT	71	---	3.7	BALB/C mice	6.0	---	66
Chimeric IgG2		WT	40	2	25		10.5	1.8	
Chimeric IgG3		WT	27	3	34		3.0	0.5	
Chimeric IgG4		WT	91	1	21		2.6	0.4	

*Affinity reported at pH 6 is toward the same species of FcRn as the animals used for PK studies except for ref. 55 and 58 which are both affinity for human FcRn. Affinity at pH 6 in ref. 49, 55, 56, 59, 63, 64, and 65 are monovalent (e.g. IgG captured on chip) as determined by SPR. Affinity at pH 6 in ref. 54, 61, 62, 66 are bivalent (e.g. FcRn captured on chip) as determined by SPR and the high affinity binding site value is reported in the table. Affinity at pH 6 in ref. 57 and 60 are based on a cell-based binding assay with human FcRn displayed on the cell surface. Fold increase in affinity to FcRn reported in ref. 58 is based on a human FcRn ELISA.

[‡]Binding data at pH 7.4 is reported as measured in the respective reference. In most cases affinity at pH 7.4 was not reported. The “binding at pH 7.4” value reported in ref. 56 is the percentage of IgG that remained bound to FcRn at pH 7.4 compared to pH 6. The “binding at pH 7.4” reported in ref. 54, 62, and 64 is the pH at which 50% of IgG dissociates from FcRn as determined by SPR. The “binding at pH 7.4” reported in ref. 66 is the dissociation rate constant at pH 7.4 ($10^{-2}/s$) by SPR derived from a dual bivalent analyte model. The K_D at pH 7.4 reported in ref. 65 was estimated based on binding curves provided in the supplemental information.

Chimeric IgG: mouse variable heavy and light chain, human constant chains.

Abbreviation: n.r., not reported; n.b., no binding; n.s., not statistical.

1.2.2 Inhibitors of the IgG-FcRn interaction

Pathogenic IgGs that are reactive toward a self antigen is a hallmark of numerous autoimmune disorders resulting in tissue and organ damage⁶⁷. Because FcRn contributes to the serum persistence of IgG, therapeutics that block the IgG-FcRn interaction represent a potential treatment modality for IgG-mediated autoimmunity. Mice deficient in FcRn are protected against IgG-mediated disease^{68,69} indicating that FcRn contributes, at least in part, to autoimmunity by maintaining pathogenic IgGs in circulation. High dose intravenous immunoglobulin (IVIg) therapy is FDA-approved for the treatment of numerous immune diseases and provides a therapeutic benefit in IgG-mediated autoimmunity in part by saturation of FcRn thereby increasing the catabolism of pathogenic IgG⁷⁰. However, IVIg therapy is expensive requiring IgG extraction from the plasma of many blood donors, thus recombinant approaches may provide alternative cost-effective treatment options.

IgG based antagonists have been developed to inhibit the endogenous IgG-FcRn interaction. One approach to interfere with the IgG-FcRn interaction is the use of monoclonal antibodies directed against FcRn or $\beta 2m$ via the classical antibody:antigen binding mechanism between the IgG fragment antigen binding (Fab) domain and antigen. One such antibody, 1G3⁷¹, binds the rat FcRn heavy chain with an affinity of 1.9 nM and 5.8 nM at pH 6 and pH 7.4, respectively, inhibits IgG binding to FcRn *in vitro*, accelerates the clearance of endogenous serum IgG in rats, and reduces disease severity in rat models of myasthenia gravis⁷². In a similar approach, the anti-rat $\beta 2m$ antibody, 4C9⁷¹, also inhibits IgG binding to FcRn and accelerates the clearance of a model IgG autoantibody in rats with ~ 50-fold increased potency compared to IVIg⁷³. However, as $\beta 2m$ is the common light chain of numerous MHC Class I like molecules¹⁴ the off targets effect of 4C9 should be carefully monitored.

An alternative antibody engineering approach to reduce IgG levels in serum is to engineer the Fc-domain of IgG to have high affinity for FcRn at both pH 6 and pH 7.4, termed antibodies that enhance IgG degradation (Abdegs). A series of five Fc mutations located at the IgG-FcRn binding interface resulted in an engineered IgG with a 1.2 nM and 7.4 nM affinity for mouse FcRn at pH 6 and pH 7.4, respectively, similar to 1G3. Abdegs, inhibit FcRn-mediated recycling of wild-type IgG *in vitro*, accelerate the clearance of exogenous IgG, and reduce endogenous IgG concentrations in mice⁷⁴. The high affinity at pH 7.4 presumably enables Abdegs to bind FcRn transiently present on the surface of cells during exocytosis⁴³ preventing any subsequent interaction with endogenous IgG. Abdegs, are effective in treating a murine model of arthritis at 25- to 50-fold lower doses than IVIg therapy⁷⁵ indicating that potent antagonists of the IgG-FcRn interaction represent an alternative therapeutic intervention in autoimmunity. The Abdeg technology is currently in clinical development by the Netherlands based biotech company, arGEN-X.

More recently, synthetic peptides that compete with IgG for binding to FcRn were identified from a phage library⁷⁶. The phage identified FcRn binding peptides (FcBP) interacts with FcRn at the same position as the Fc-domain of IgG, despite the complete lack of sequence homology between the two FcRn binding molecules⁷⁷ and is highly specific for human and monkey FcRn, with an approximate 1000-fold weaker binding to mouse and rat FcRn⁷⁶. The phage identified FcBP monomer binds FcRn with micromolar affinity at pH 6 and pH 7.4 and inhibits IgG binding to FcRn *in vitro* but is not effective at accelerating the clearance of IgG in mice presumably due to its weak affinity and rapid clearance. A chemically optimized peptide dimer (SYN1436) that bound FcRn with subnanomolar affinity at pH 6 and pH 7.4 was effective at increasing the clearance of exogenous IgG in mice as well as endogenous IgG in monkeys⁷⁶

but has not been evaluated in a therapeutic model of IgG-mediated autoimmunity. Small molecule inhibitors of the IgG-FcRn interaction have also been reported⁷⁸. Although less potent than IgG- and peptide-based inhibitors, these compounds represent a significant step toward the development of orally available IgG-FcRn inhibitors.

Additional molecules that bind Fc at the C_H2-C_H3 domain interface and may block the IgG-FcRn interaction have been described in the literature including 1) a 13-amino acid cyclic peptide selected by phage display²³ and 2) an endogenous Fc receptor, TRIM21. Both bind Fc with nanomolar affinity at pH 6 and pH 7.4 predominantly driven by interaction with the Fc residues Met-252, Ile-253, Ser-254, Asn-434, and His-435. The same set of Fc amino acid residues is critical for pH-dependent binding to FcRn and spA and spG binding; therefore, it is likely that both peptide and TRIM21 would inhibit IgG binding to FcRn, although this has not been determined experimentally. The multitude of human and non-human ligands that bind at the C_H2-C_H3 domain interface on Fc indicates this region is naturally poised for interaction with distinct molecules with remarkable plasticity in binding mechanism and likely biological function. Thus, it would not be surprising to discover additional endogenous human proteins that bind Fc at the C_H2-C_H3 domain interface.

The major limitation of the current IgG-FcRn antagonists as drugs is their short half-life which necessitates frequent dosing to maintain therapeutic concentrations in blood. In addition, because IgG-based inhibitors can exert additional immunomodulatory functions through the engagement of Fcγ receptors and complement, it remains to be seen whether inhibition of the IgG-FcRn interaction alone, as is the case for SYN1436, is sufficient to produce a therapeutic benefit in IgG-mediated autoimmune disease.

1.3 Fc-fusion for half-life extension, non-invasive protein delivery, and as vaccines

The first Fc-fusion protein described in 1989 by Genentech⁷⁹ came well before detailed knowledge of the Fc-FcRn interaction. The promising outcomes in this pioneering study demonstrated that Fc-fusion can endow a protein with unique effector functions mediated by Fc receptor binding and complement fixation. Additional molecular knowledge of the Fc domain and its biological functions has accelerated the use of Fc-fusion proteins in the clinic and as research reagents. Dissection of the Fc-FcRn structure in combination with a more detailed understanding of FcRn biology has resulted in numerous protein drug delivery strategies that take advantage of the unique biological properties of both the Fc domain and FcRn.

1.3.1 Fc-fusion as a versatile half-life extension platform

The Fc-domain of IgG alone is sufficient for a direct interaction with FcRn. Genetic fusion of a protein to the Fc-domain of IgG, or Fc-fusion, results in half-life extension by hijacking the FcRn recycling and salvage pathway and reducing renal clearance through the increase in molecular weight due to the size of the Fc-domain (~ 50 kDa). Typical Fc-fusions are constructed by fusing the C-terminus of an effector molecule to the N-terminus of the IgG hinge region followed by the Fc-domain of IgG (Fig. 1.5c). A number of Fc-fusion proteins are approved for clinical use resulting, in some cases, a half-life of up to 13 days in humans⁸⁰. The success of Fc-fusion proteins as a strategy to improve protein circulation is illustrated by Enbrel, a Fc-fusion protein containing the human soluble p75 TNF receptor and marketed for the treatment of psoriasis and rheumatoid arthritis (RA). The half-life of Enbrel is 5 times that of the monomeric-soluble TNF receptor⁸¹ due to its interaction with FcRn. However, there are drawbacks to this approach including: production, which is preferred in eukaryotic expression systems due to the disulfide bond pattern and glycosylation of Fc, reduced stability of Fc-fusion proteins⁸², lower activity of the fusion partner⁸³, and the large size of the Fc domain that may

adversely affect tissue penetration of the fusion protein. Interestingly, Fc-fusion proteins in clinical use cannot achieve the same ~ 21-day half-life as intact IgG. This may be due to a multitude of factors including steric hindrance between the Fc-domain and fusion partner that reduce protein stability or binding to FcRn, alternative clearance pathways dependent on the protein fused to Fc, contribution of the Fab domain to antibody half-life, or molecular architecture. A number of alternative Fc-fusion formats have been devised to address these issues⁸⁴ but await clinical validation. Regardless, Fc-fusion represents one of the most clinically successful protein half-life extension strategies to date and has been extensively reviewed recently^{53,84}.

1.3.2 Oral and pulmonary protein delivery via FcRn transcytosis

In addition to recycling, FcRn transports its ligands across cellular monolayers providing a feasible route for the transport of protein cargo across epithelial barriers and into the blood stream. There are currently no commercially available protein therapeutics administered by non-parenteral routes. Administration of protein therapeutics by the oral route remains the ‘holy grail’ of protein drug delivery; however, the low pH, harsh proteolytic environment of the GI tract, and low protein permeability of the intestinal epithelium are major hurdles. FcRn is expressed in the neonatal mouse¹⁰ and adult human intestine^{85,86} and can transport IgG across polarized intestinal epithelial cell monolayers *in vitro*⁸⁷ and in mice⁸⁸. Fc-fusion in addition to prolonging circulation can hijack FcRn transport for delivery of protein cargos across epithelial barriers, which has been evaluated by Syntonix Pharmaceuticals (now Biogen Idec) as a potential non-invasive protein delivery strategy. Oral delivery of a follicle stimulating hormone-Fc fusion (FSH-Fc) protein in a neonatal rat model resulted in systemic exposure of FSH-Fc that translated to an increase in testicular weight when compared to FSH or vehicle⁸⁹. Although a valuable

proof-of-concept study, the FSH-Fc bioavailability was not reported and the barrier properties of the neonatal rat intestine are a potential confounding factor as they do not mimic an adult rat or human⁹⁰. Unfortunately, rodent FcRn expression in the intestine declines rapidly after weaning^{91,92}; therefore, adult rodents are not useful models to study FcRn-mediated intestinal IgG transport.

The lung represents an additional organ for the non-invasive delivery of proteins by inhalation. Compared to the intestine, the lung pH is neutral, the proteolytic activity is reduced, and the epithelium is naturally permeable to small peptide and proteins⁹³. In fact, inhaled insulin was a clinical success resulting in FDA-approval but was subsequently withdrawn from the market due to poor sales contributed mostly to the bulky and inconvenient inhalation device. FcRn is also expressed in bronchial epithelial cells of the adult human, non-human primate, and mouse lung⁹⁴ and studies with Fc-fusion proteins confirmed that FcRn is a viable target for transporting protein cargos across the lung^{83,94}. Pulmonary delivery of an erythropoietin Fc (EPO-Fc) fusion protein enables FcRn-specific transport from the lung air space and into systemic circulation with a bioavailability similar to subcutaneous administration (~ 35%) and an ~ 2-fold increase over EPO. An EPO-Fc monomer that contains a single EPO molecule fused to a Fc dimer exhibited higher pulmonary uptake and efficacy compared to the EPO-Fc dimer, suggesting that in addition to FcRn binding, alternative factors such as molecular weight or steric hindrance may also impact pulmonary absorption of Fc-fusion proteins. Absorption of EPO-Fc was higher in monkeys when deposited in the central airways compared to the deep lung, in agreement with the FcRn expression pattern in primates⁸³. Studies with Fc-fusion proteins validate FcRn as a target to enable non-invasive protein delivery and the pulmonary route

appears more promising than the oral route to achieve non-invasive protein delivery. Indeed, delivery of EPO-Fc fusion proteins by inhalation has been translated to humans⁹⁵.

Although hijacking FcRn to enable non-invasive protein delivery appears promising, the transport capacity of FcRn in the lung or intestine is unknown. The maximum serum concentration of EPO-Fc in humans increased from 0.2 ng/mL to 7.1 ng/mL as the dose increased from 3 $\mu\text{g}/\text{kg}$ to 30 $\mu\text{g}/\text{kg}$ ⁹⁵. Although sufficient to produce a biological response, EPO is an extremely potent drug. Typical intravenous or subcutaneous doses of EPO range from 1 $\mu\text{g}/\text{kg}$ to 3 $\mu\text{g}/\text{kg}$ resulting in plasma concentrations at steady state between 1 and 10 ng/mL⁹⁶. Villasaliu and colleagues estimated the IgG-FcRn transport capacity in the lung to be $\sim 6.5 \mu\text{g}/\text{hr}$ based upon transcytosis rates of monomeric IgG across a model Calu-3 cell monolayer and the assumed surface area of the human bronchi⁹⁷. Extending this analysis and assuming that IgG has a maximum lifespan in the lung of about 24 hours⁹³ and that distribution is limited to plasma (~ 3 L), approximately 150 μg of protein could be absorbed into systemic circulation resulting in maximum serum concentrations not exceeding 50 ng/mL. Monoclonal antibody doses are typically between $\sim 2 - 10 \text{ mg}/\text{kg}$ and require significantly higher serum concentrations in the $\mu\text{g}/\text{mL}$ range to elicit a biological effect^{98,99}; therefore, pulmonary/oral delivery of antibodies, and other low potency proteins, is likely constrained by the FcRn transport capacity. Nonetheless, FcRn transport may be a viable strategy for non-parenteral administration of potent proteins including EPO, human growth hormone, glucagon like peptide-1, and other potent cytokines and growth factors.

Packaging protein molecules into a carrier, such as a liposome or polymer, decorated with an FcRn binding ligand on the surface, such as Fc, has been proposed to increase the total amount of protein that can be delivered across an epithelial barrier by FcRn⁹⁷. In fact, oral

delivery of a hybrid polymeric nanoparticle encapsulating insulin was recently shown to reduce blood glucose in fasting mice only when the Fc domain of IgG was present on the nanoparticle surface and mice expressed FcRn¹⁰⁰.

However, care must be taken when designing multivalent FcRn-targeted nanoparticle systems. FcRn present at mucosal barriers serves a dual role in transporting IgG-immune complexes across epithelial barriers for subsequent phagocytosis by antigen presenting cells (APCs)¹⁰¹ and once internalized FcRn regulates immune complex sorting to the appropriate intracellular major histocompatibility complex (MHC) loading compartment^{102,103}. Multivalent immune complexes that cross-link FcRn are typically sorted away from the recycling pathway and diverted to lysosomes¹⁰⁴. Thus, Fc-decorated protein nanocontainers delivered to the lung or intestine may be phagocytosed by tissues resident APCs, degraded in the lysosome, and peptide antigens loaded onto MHC molecules for subsequent presentation to T-cells resulting in immune induction. Nonetheless, this recent report is an important proof-of-concept study that may also have utility in the development of oral or intranasal vaccines or to improve the efficacy of locally administered drugs for treatment of intestinal or pulmonary disease. Moving forward it will be important to understand the cellular fate of Fc-modified nanoparticles delivered to the lung or intestine and their potential for immune induction *in vivo*.

1.3.3 Fc-fusion proteins for vaccination

FcRn participates in immune surveillance at mucosal barriers, such as in the intestine and lung, through bidirectional transport of IgG from the tissue interstitial space to the lumen, and vice versa¹⁰¹. Monomeric IgG delivered to the lung airspace or intestinal lumen can neutralize antigen through the formation of IgG immune complexes (ICs), be transported back across the epithelial barrier by FcRn, and be delivered to tissues resident APCs¹⁰¹. FcRn is also expressed

in professional APCs, such as macrophages and dendritic cells, and participates in MHC Class I and Class II antigen presentation to T-cells^{35,102,103} as well as in polymorphonuclear neutrophils and facilitates the phagocytosis of IgG opsonized bacteria¹⁰⁵. The immunologic functions of FcRn in phagocytes, epithelial cells, and antigen presenting cells at mucosal surfaces make it an ideal target for protein subunit vaccination, mucosal vaccination, and pathogen neutralization strategies.

Ward and colleagues demonstrated that *in vitro* and *in vivo* there is a fine balance between the role of FcRn and Fc γ receptor engagement to induce antigen specific T-cell expansion¹⁰⁶. Although *in vitro* Fc-antigen fusions that engage Fc γ receptors and have a high, pH-independent affinity to FcRn (Fc-mut) induce the most potent antigen specific T-cell response, Fc-mut has poor stimulatory capacity *in vivo*. In contrast, Fc-antigen fusions that retain pH-dependent binding to FcRn and engage Fc γ receptors (Fc-wt) induce weak T-cell responses *in vitro* but are the most potent *in vivo*. The shorter *in vivo* half-life of Fc-mut compared to Fc-wt indicates that length of antigen exposure *in vivo* is more important than FcRn targeting, at least for antigen administered systemically. In all cases, Fc γ receptor binding is crucial to induce antigen specific T-cell responses against Fc-antigen fusions *in vivo*. The studies suggest that fine tuning the Fc-FcRn interaction (or Fc-Fc γ R interactions) to increase antigen processing by APCs without significantly altering serum persistence may be a viable strategy to improve antigen specific immune responses to Fc-fusions *in vivo*.

Typical vaccination strategies rely on intramuscular or subcutaneous injection yet most viral and bacterial infections occur at mucosal barriers. Thus, the ideal vaccination strategy would induce both systemic and mucosal immunity. Towards this goal Zhu and colleagues developed a mucosal vaccination strategy mediated by FcRn by fusing the herpes simplex virus

type-2 glycoprotein gD to the Fc-domain of IgG (Fc-gD)¹⁰⁷. Intranasal administration of Fc-gD to mice induced gD-specific local and peripheral T-cell responses resulting in the induction of gD-specific memory B-cells in the spleen and most importantly protection against a subsequent intravaginal HSV-2 challenge that persisted for 6 months post immunization. Protection was both dependent on FcRn expression in mice and also Fc binding to FcRn. The role of Fcγ receptor engagement was not evaluated but the mouse IgG isotype used (IgG2a) binds the high affinity Fcγ receptor I (FcγRI) expressed on the surface of dendritic cells¹⁰⁸. Thus, a common theme of FcRn targeted vaccination strategies is the necessity for FcγR engagement on antigen presenting cells to facilitate antigen endocytosis and intracellular processing. Zhu and colleagues have also extended their Fc-fusion based mucosal vaccination strategy to induce protection against HIV infection with similar successes indicating this strategy may be general and not be restricted to a particular viral antigen¹⁰⁹.

Pathogen neutralization by IgG is a primary line of defense against invading viruses, such as influenza, and FcRn dependent deposition of neutralizing IgG in the mucosa is an important pathway in IgG-mediated host defense^{91,110}. Recently, Zhu and colleagues also described an intracellular FcRn-mediated neutralization mechanism. An influenza hemagglutinin-specific monoclonal antibody, Y8-10C2, that neutralizes a particular influenza strain (PR8) only at acidic pH (e.g. only in acidic intracellular compartment) was used to demonstrate that FcRn expression in MDCK cells delivers Y8-10C2 to the early endosome where it can bind PR8 and divert the neutralized virus to the lysosome *in vitro*¹¹¹. Importantly this was dependent on FcRn expression in MDCK cells and Y8-10C2 binding to PR8; however, a Y8-10C2 that lacks FcRn binding was not evaluated. Mice pre-dosed with Y8-10C2 results in protection from a subsequent lethal, intranasal PR8 challenge for up to 9 days. Mice pre-dosed with an irrelevant IgG control or

vehicle died of infection within 6 days of viral challenge. FcRn knockout mice that received Y8-10C2 were partially protected indicating alternative FcRn-independent pathways of presumably intracellular viral neutralization. Although this study sheds new light on the role of FcRn in IgG-mediated viral inhibition, prophylactic administration of neutralizing antibody in the clinic is unlikely; therefore, the utility of this approach as a therapeutic intervention to attenuate disease progression after onset should be determined.

1.4 Alternative strategies that target FcRn

Aside from Fc-fusion a number of additional engineering approaches have been devised to target proteins to FcRn. These strategies include fusion to albumin, engineered Fc domains, or synthetic peptides. To date, these strategies are not clinically validated although albumin based drugs are FDA-approved and albumin fusions are likely to follow. Regardless, alternative strategies that target proteins to FcRn to enable half-life extension, non-invasive delivery, or immune modulation are likely to become important new reagents that expand our understanding of FcRn biology.

1.4.1 Albumin fusion

Albumin is the most abundant protein in human serum and has an extraordinarily long half-life as a result of its size and direct interaction with the FcRn. The interaction between albumin and FcRn has been exploited as a mechanism to increase the circulation time of proteins that are covalently or non-covalently bound to albumin¹¹². Direct interaction with FcRn is achieved by genetic fusion or covalent attachment of a protein cargo to the terminus or single free cysteine, respectively, of recombinant serum albumin (Fig. 1.5b) that in some cases results in half-lives ranging from 9-15 days in humans¹¹³. There are currently no albumin fusion proteins approved for clinical use; however, a GLP-1 albumin fusion (albiglutide) developed by

Human Genome Sciences (acquired by GSK) extends the half-life of GLP-1 by ~ 3600-fold¹¹⁴ (~ 2 min to ~ 5 days) and awaits a decision from the FDA expected in early 2014.

Non-covalent binding of therapeutic proteins and peptides to albumin enables an indirect interaction with FcRn. Albumin binds a number of endogenous compounds including fatty acids. Conjugation of a C16 fatty acid to GLP-1 results in non-covalent attachment to albumin and half-life extension and is FDA-approved for the treatment of type 2 diabetes¹¹⁵. Fatty acids inhibit albumin binding to FcRn³⁰ therefore fatty acid conjugated drugs bound to albumin may not be productively salvaged by FcRn *in vivo*. Alternative albumin binding molecules have been engineered such as peptides¹¹⁶, albumin binding domains from streptococcal protein G¹¹⁷, and antibody based scaffolds¹¹⁸. In general, non-covalent albumin binding fusion proteins have only a modest increase in circulation time likely due to dissociation of the protein cargo before or during FcRn interaction resulting in excretion or catabolism of the protein cargo. The immunogenicity of non-human albumin binding proteins is still a concern, especially for therapeutics intended for long term use. Nonetheless, the use of albumin as a drug carrier is a clinically successful platform for half-life extension and more details are presented in two recent reviews^{112,113}.

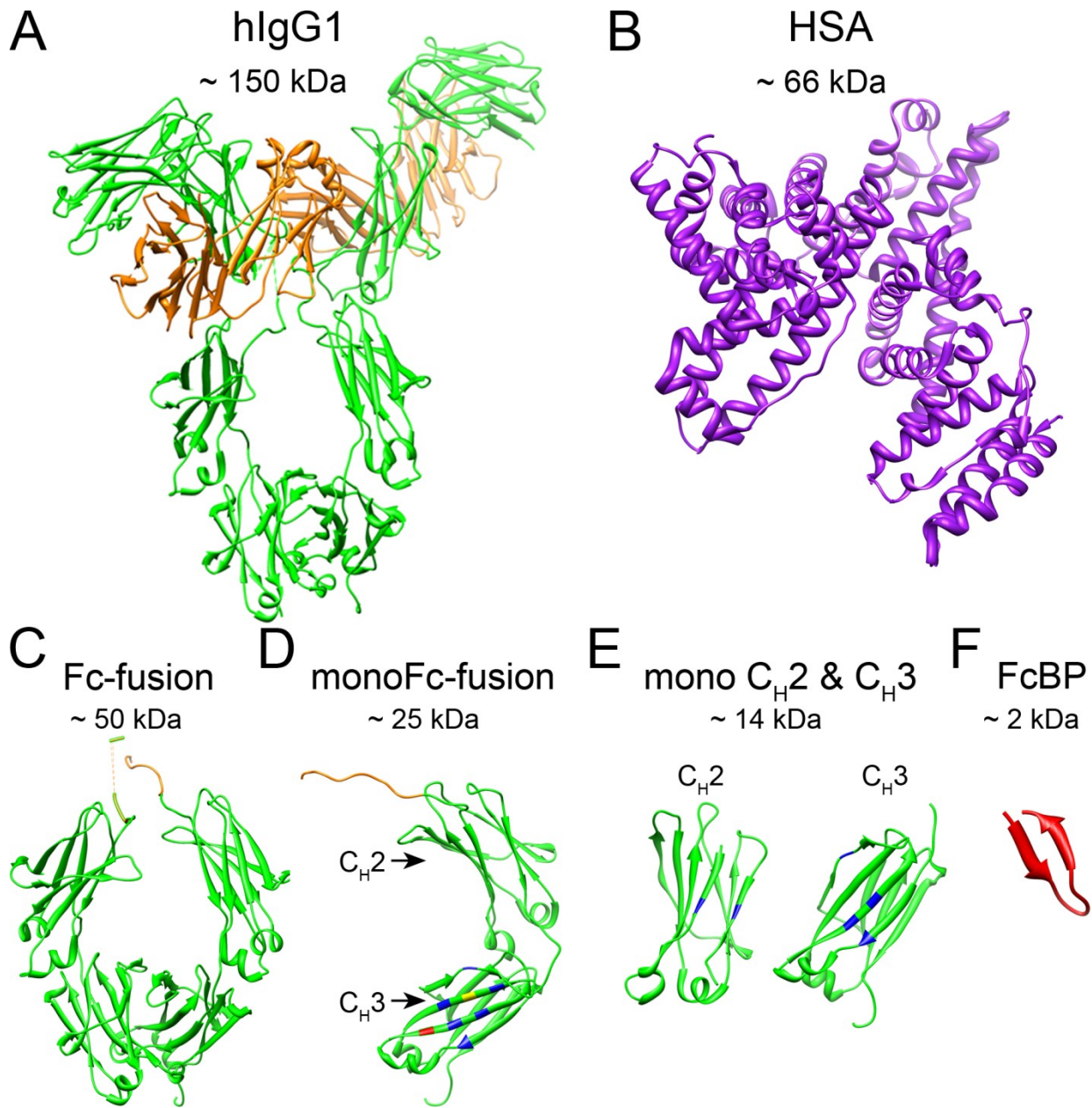


Figure 1.5 Schematic of various fusion protein domains that can hijack FcRn.

(a) The crystal structure of full length human IgG1 (PDB code 1HZH) and (b) HSA (PDB code 4K71) are shown on the top. (c) The Fc-domain of hIgG1 used to construct Fc-fusion proteins. The C_{H2} and C_{H3} domains are shown in green and the hinge region in orange. Typical Fc-fusions are constructed by fusing the C-terminus of a protein of interest to the N-terminus of the Fc hinge. (d) Monomeric Fc-domain. Fc-domain residues mutated to generate monoFc-fusions are shown in blue, red, and yellow. The yellow and red residues were mutated to incorporate N-linked glycans resulting in a monomeric Fc. The blue and red residues indicate mutants that were selected from phage panning resulting in an alternative monomeric Fc-domain. (e) Monomeric C_{H2} and C_{H3} . The amino acid residues mutated to generate monomeric C_{H2} and C_{H3} domains are shown in blue. (f) FcBP fusion (PDB code 3M17).

1.4.2 Low molecular weight FcRn binding ligands

The molecular weight of protein therapeutics, or hydrodynamic radius, is inversely proportional to diffusivity and capillary permeability¹¹⁹. Monoclonal antibodies are proven anti-cancer agents but heterogeneous distribution in tumor tissues can result in restricted tumor cell exposure and poor efficacy. Antibody distribution through a tumor is the result of numerous factors including length of systemic exposure, extent of tumor vasculature, convection, diffusion, and antigen binding¹²⁰. However, it is recognized that the concentration gradient between blood and tumor is a major driving force in protein accumulation within a tumor that can be controlled by modulating circulation time¹²¹. Low molecular weight proteins have excellent tumor penetration properties but rapid clearance limits their use as therapeutics¹²⁰. Strategies that increase serum persistence without substantially increasing molecular weight may improve the distribution of drugs in tumors (and other tissues) without compromising dosing frequency.

Towards this goal Dimitrov and colleagues generated a variety of engineered monomeric C_{H2}, C_{H3}, and Fc domains¹²²⁻¹²⁴ (Fig. 1.5d,e). Although substantially smaller than dimeric Fc (~ 15 kDa vs 50 kDa), monomeric C_{H2} and C_{H3} bind weakly to FcRn as expected given the contribution of amino acid residues that span both the C_{H2} and C_{H3} domains to FcRn binding¹⁶. The terminal half-life of monomeric C_{H2} is ~ 17 hrs and ~ 9 hrs in wild type and human FcRn transgenic mice, respectively¹²⁵, whereas mutation of residues involved in binding to FcRn reduced the half-life to ~ 8 hrs and ~ 3 hrs. Monomeric C_{H3} has not been evaluated *in vivo*. Monomeric C_{H2} and C_{H3} fusion proteins are unlikely to achieve circulation times comparable to Fc-fusion as they cannot make a bivalent, high-affinity interaction with FcRn. Additional mutations to increase affinity toward FcRn may improve the *in vivo* properties of monomeric C_{H2} and C_{H3} domains.

Fc is a dimer composed of two C_{H2}-C_{H3} chains (Fig. 1.5c). Fc dimerization is mainly mediated by hydrophobic interactions between two C_{H3} domains and stabilized by disulfide bonds in the hinge region preceding the C_{H2} domain. Fc dimerization empowers IgG with bivalent antigen binding as well as bivalent Fc receptor binding. Monomeric Fc domains have recently been described by either mutation of hydrophobic residues at the C_{H3}-C_{H3} dimer interface¹²⁶ or introduction of N-linked glycosylation sites on the C_{H3} domain¹²⁷ (Fig. 1.5d). Both formats retain pH-dependent binding to FcRn and a Fc monomer Fab fusion protein (Fab-monoFc) has a FcRn dependent half-life in mice; however, the half-life of Fab-monoFc compared to Fab alone was not determined. Nonetheless, monomeric Fc domains represent the smallest reported IgG domain (~ 25 kDa) that exhibit pH-dependent binding to FcRn. A more thorough investigation into the FcRn binding, circulating, and tumor penetrating properties of monomeric Fc compared to alternative formats (e.g. dimeric Fc fusion) is warranted to realize fully the potential of this novel half-life extension platform.

In this dissertation we describe an alternative strategy to engineer FcRn-mediated recycling and transcytosis in recombinant proteins by genetic fusion of short FcRn binding peptides⁷⁶ (FcBP) to the termini of a model fluorescent protein¹²⁸ (Fig. 1.5e). Our approach was motivated by results of Mezo and colleagues who identified peptides that compete with IgG for binding to FcRn⁷⁶. Proteins modified with FcBPs exhibit pH-dependent binding to FcRn with an affinity comparable to human IgG1 and are recycled and transcytosed across cell monolayers that express human FcRn. *In vitro*, FcBP fusion proteins are highly mimetic of the hIgG1-FcRn interaction. To date, FcBP fusion represents the smallest protein modification (~ 2 – 4 kDa) approach to target FcRn without compromising affinity or pH-dependent binding. However, we found that the plasma clearance of FcBP fusion proteins *in vivo* is independent of human FcRn

binding, whereas the clearance of IgG and albumin is FcRn dependent. We speculate that alternative unknown factors are important regulators of IgG homeostasis *in vivo* that is not replicated by FcBP fusion.

1.4 Conclusion

In recent years a number of advancements in our understanding of FcRn biology have translated to the development of novel FcRn based drug delivery strategies. Most notably, the recently elucidated immunological functions of FcRn have been exploited to improve delivery and efficacy of protein subunit vaccines¹⁰⁷ and neutralizing antibodies¹¹¹ for treatment of infection diseases. The continual exploitation of the classical roles of FcRn in regulating IgG homeostasis and transport across cellular barriers have also resulted in a number of novel engineering approaches that hijack FcRn-mediated recycling and transcytosis to improve protein half-life and delivery. Most approaches focus on engineering higher affinity IgG Fc-domains or albumins for use as therapeutics or fusion partners; however, a number of novel FcRn targeting strategies are in their infancy. Engineered IgGs with higher affinity toward FcRn to improve half-life, a concept that originated almost 20 years ago⁴⁸, have finally been evaluated in humans^{50,51}. The recent crystal structure of an albumin variant in complex with FcRn³⁰ should accelerate the development of albumin based therapeutics and underlying FcRn-albumin biology, which has lagged IgG. The future is bright for FcRn as a molecular target to improve the drug-like properties of proteins and macromolecule drug carriers. The plethora of known and almost certain discovery of new biological functions of FcRn provide vast opportunities to develop therapeutics that treat human disease.

1.5 References

1. Brambell, F. W. The transmission of immunity from mother to young and the catabolism of immunoglobulins. *Lancet* **2**, 1087–93 (1966).
2. Brambell, F. W., Hemmings, W. A. & Morris, I. G. A theoretical model of gamma-globulin catabolism. *Nature* **203**, 1352–4 (1964).
3. Fahey, J. L. & Sell, S. The immunoglobulins of mice: V. The metabolic (catabolic) properties of the five immunoglobulin classes. *J. Exp. Med.* **122**, 41–58 (1965).
4. Rodewald, R. pH-dependent binding of immunoglobulins to intestinal cells of the neonatal rat. *J. Cell Biol.* **71**, 666–9 (1976).
5. Jones, E. A. & Waldmann, T. A. The mechanism of intestinal uptake and transcellular transport of IgG in the neonatal rat. *J. Clin. Invest.* **51**, 2916–27 (1972).
6. Rodewald, R. & Kraehenbuhl, J. P. Receptor-mediated transport of IgG. *J. Cell Biol.* **99**, 159s–164s (1984).
7. Simister, N. E. & Mostov, K. E. An Fc receptor structurally related to MHC class I antigens. *Nature* **337**, 184–7 (1989).
8. Israel, E. J., Patel, V. K., Taylor, S. F., Marshak-Rothstein, A. & Simister, N. E. Requirement for a beta 2-microglobulin-associated Fc receptor for acquisition of maternal IgG by fetal and neonatal mice. *J. Immunol.* **154**, 6246–51 (1995).
9. Kim, J. K., Tsen, M. F., Ghetie, V. & Ward, E. S. Identifying amino acid residues that influence plasma clearance of murine IgG1 fragments by site-directed mutagenesis. *Eur. J. Immunol.* **24**, 542–8 (1994).
10. Ghetie, V. *et al.* Abnormally short serum half-lives of IgG in beta 2-microglobulin-deficient mice. *Eur. J. Immunol.* **26**, 690–6 (1996).
11. Israel, E. J., Wilsker, D. F., Hayes, K. C., Schoenfeld, D. & Simister, N. E. Increased clearance of IgG in mice that lack beta 2-microglobulin: possible protective role of FcRn. *Immunology* **89**, 573–8 (1996).
12. Junghans, R. P. & Anderson, C. L. The protection receptor for IgG catabolism is the beta2-microglobulin-containing neonatal intestinal transport receptor. *Proc. Natl. Acad. Sci. U. S. A.* **93**, 5512–6 (1996).
13. Roopenian, D. C. *et al.* The MHC class I-like IgG receptor controls perinatal IgG transport, IgG homeostasis, and fate of IgG-Fc-coupled drugs. *J. Immunol.* **170**, 3528–33 (2003).

14. Wilson, I. A. & Bjorkman, P. J. Unusual MHC-like molecules: CD1, Fc receptor, the hemochromatosis gene product, and viral homologs. *Curr. Opin. Immunol.* **10**, 67–73 (1998).
15. Martin, W. L., West Jr., A. P., Gan, L. & Bjorkman, P. J. Crystal structure at 2.8 Å of an FcRn/heterodimeric Fc complex: mechanism of pH-dependent binding. *Mol Cell* **7**, 867–877 (2001).
16. Kim, J. K., Tsen, M. F., Ghetie, V. & Ward, E. S. Catabolism of the murine IgG1 molecule: evidence that both CH2-CH3 domain interfaces are required for persistence of IgG1 in the circulation of mice. *Scand. J. Immunol.* **40**, 457–65 (1994).
17. Burmeister, W. P., Gastinel, L. N., Simister, N. E., Blum, M. L. & Bjorkman, P. J. Crystal structure at 2.2 Å resolution of the MHC-related neonatal Fc receptor. *Nature* **372**, 336–43 (1994).
18. Shields, R. L. *et al.* High resolution mapping of the binding site on human IgG1 for Fc gamma RI, Fc gamma RII, Fc gamma RIII, and FcRn and design of IgG1 variants with improved binding to the Fc gamma R. *J Biol Chem* **276**, 6591–6604 (2001).
19. Huang, X., Zheng, F. & Zhan, C.-G. Binding structures and energies of the human neonatal Fc receptor with human Fc and its mutants by molecular modeling and dynamics simulations. *Mol. Biosyst.* **9**, 3047–58 (2013).
20. West, A. P. & Bjorkman, P. J. Crystal Structure and Immunoglobulin G Binding Properties of the Human Major Histocompatibility Complex-Related Fc Receptor †, ‡. *Biochemistry* **39**, 9698–9708 (2000).
21. Martin, W. L. & Bjorkman, P. J. Characterization of the 2:1 complex between the class I MHC-related Fc receptor and its Fc ligand in solution. *Biochemistry* **38**, 12639–47 (1999).
22. Tesar, D. B., Tiangco, N. E. & Bjorkman, P. J. Ligand Valency Affects Transcytosis, Recycling and Intracellular Trafficking Mediated by the Neonatal Fc Receptor. *Traffic* **7**, 1127–1142 (2006).
23. DeLano, W. L. Convergent Solutions to Binding at a Protein-Protein Interface. *Science* **287**, 1279–1283 (2000).
24. Idusogie, E. E. *et al.* Mapping of the C1q binding site on rituxan, a chimeric antibody with a human IgG1 Fc. *J. Immunol.* **164**, 4178–84 (2000).
25. Duncan, A. R. & Winter, G. The binding site for C1q on IgG. *Nature* **332**, 738–40 (1988).
26. Simmons, L. C. *et al.* Expression of full-length immunoglobulins in *Escherichia coli*: rapid and efficient production of aglycosylated antibodies. *J. Immunol. Methods* **263**, 133–47 (2002).

27. West, A. P. & Bjorkman, P. J. Crystal structure and immunoglobulin G binding properties of the human major histocompatibility complex-related Fc receptor. *Biochemistry* **39**, 9698–708 (2000).
28. Vaughn, D. E. *et al.* Identification of critical IgG binding epitopes on the neonatal Fc receptor. *J. Mol. Biol.* **274**, 597–607 (1997).
29. Andersen, J. T. *et al.* Structure-based mutagenesis reveals the albumin-binding site of the neonatal Fc receptor. *Nat. Commun.* **3**, 610 (2012).
30. Schmidt, M. M. *et al.* Crystal Structure of an HSA/FcRn Complex Reveals Recycling by Competitive Mimicry of HSA Ligands at a pH-Dependent Hydrophobic Interface. *Structure* **21**, 1966–78 (2013).
31. Chaudhury, C., Brooks, C. L., Carter, D. C., Robinson, J. M. & Anderson, C. L. Albumin binding to FcRn: distinct from the FcRn-IgG interaction. *Biochemistry* **45**, 4983–90 (2006).
32. Andersen, J. T., Daba, M. B., Berntzen, G., Michaelsen, T. E. & Sandlie, I. Cross-species binding analyses of mouse and human neonatal Fc receptor show dramatic differences in immunoglobulin G and albumin binding. *J. Biol. Chem.* **285**, 4826–36 (2010).
33. Ober, R. J., Radu, C. G., Ghetie, V. & Ward, E. S. Differences in promiscuity for antibody-FcRn interactions across species: implications for therapeutic antibodies. *Int Immunol* **13**, 1551–1559 (2001).
34. Akilesh, S., Christianson, G. J., Roopenian, D. C. & Shaw, A. S. Neonatal FcR Expression in Bone Marrow-Derived Cells Functions to Protect Serum IgG from Catabolism. *J. Immunol.* **179**, 4580–4588 (2007).
35. Zhu, X. *et al.* MHC class I-related neonatal Fc receptor for IgG is functionally expressed in monocytes, intestinal macrophages, and dendritic cells. *J Immunol* **166**, 3266–3276 (2001).
36. Montoyo, H. P. *et al.* Conditional deletion of the MHC class I-related receptor FcRn reveals the sites of IgG homeostasis in mice. *Proc. Natl. Acad. Sci.* **106**, 2788–2793 (2009).
37. Chen, Y. & Balthasar, J. P. Evaluation of a catenary PBPK model for predicting the in vivo disposition of mAbs engineered for high-affinity binding to FcRn. *AAPS J.* **14**, 850–9 (2012).
38. Garg, A. & Balthasar, J. P. Physiologically-based pharmacokinetic (PBPK) model to predict IgG tissue kinetics in wild-type and FcRn-knockout mice. *J. Pharmacokinet. Pharmacodyn.* **34**, 687–709 (2007).

39. Ward, E. S. Evidence to support the cellular mechanism involved in serum IgG homeostasis in humans. *Int. Immunol.* **15**, 187–195 (2003).
40. Cianga, C., Cianga, P., Plamadeala, P. & Amalinei, C. Nonclassical major histocompatibility complex I-like Fc neonatal receptor (FcRn) expression in neonatal human tissues. *Hum. Immunol.* **72**, 1176–87 (2011).
41. Roopenian, D. C. & Akilesh, S. FcRn: the neonatal Fc receptor comes of age. *Nat. Rev. Immunol.* **7**, 715–725 (2007).
42. Borvak, J. *et al.* Functional expression of the MHC class I-related receptor, FcRn, in endothelial cells of mice. *Int. Immunol.* **10**, 1289–98 (1998).
43. Ober, R. J. Exocytosis of IgG as mediated by the receptor, FcRn: An analysis at the single-molecule level. *Proc. Natl. Acad. Sci.* **101**, 11076–11081 (2004).
44. Ward, E. S. *et al.* From Sorting Endosomes to Exocytosis: Association of Rab4 and Rab11 GTPases with the Fc Receptor, FcRn, during Recycling. *Mol. Biol. Cell* **16**, 2028–2038 (2005).
45. Gan, Z., Ram, S., Vaccaro, C., Ober, R. J. & Ward, E. S. Analyses of the Recycling Receptor, FcRn, in Live Cells Reveal Novel Pathways for Lysosomal Delivery. *Traffic* **10**, 600–614 (2009).
46. Wu, A. M. Engineered antibodies for molecular imaging of cancer. *Methods* (2013). doi:10.1016/j.ymeth.2013.09.015
47. Medesan, C., Matesoi, D., Radu, C., Ghetie, V. & Ward, E. S. Delineation of the amino acid residues involved in transcytosis and catabolism of mouse IgG1. *J. Immunol.* **158**, 2211–7 (1997).
48. Ghetie, V. *et al.* Increasing the serum persistence of an IgG fragment by random mutagenesis. *Nat. Biotechnol.* **15**, 637–40 (1997).
49. Dall’Acqua, W. F., Kiener, P. A. & Wu, H. Properties of human IgG1s engineered for enhanced binding to the neonatal Fc receptor (FcRn). *J Biol Chem* **281**, 23514–23524 (2006).
50. Robbie, G. J. *et al.* A Novel Investigational Fc-Modified Humanized Monoclonal Antibody, Motavizumab-YTE, Has an Extended Half-Life in Healthy Adults. *Antimicrob. Agents Chemother.* **57**, 6147–53 (2013).
51. Zheng, Y. *et al.* Translational pharmacokinetics and pharmacodynamics of an FcRn-variant anti-CD4 monoclonal antibody from preclinical model to phase I study. *Clin. Pharmacol. Ther.* **89**, 283–90 (2011).

52. Kuo, T. T. & Aveson, V. G. Neonatal Fc receptor and IgG-based therapeutics. *MAbs* **3**, 422–30 (2011).
53. Rath, T. *et al.* Fc-fusion proteins and FcRn: structural insights for longer-lasting and more effective therapeutics. *Crit. Rev. Biotechnol.* (2013). doi:10.3109/07388551.2013.834293
54. Datta-Mannan, A. *et al.* Humanized IgG1 variants with differential binding properties to the neonatal Fc receptor: relationship to pharmacokinetics in mice and primates. *Drug Metab. Dispos.* **35**, 86–94 (2007).
55. Zalevsky, J. *et al.* Enhanced antibody half-life improves in vivo activity. *Nat. Biotechnol.* **28**, 157–159 (2010).
56. Dall'Acqua, W. F. *et al.* Increasing the affinity of a human IgG1 for the neonatal Fc receptor: biological consequences. *J. Immunol.* **169**, 5171–80 (2002).
57. Hinton, P. R. *et al.* An engineered human IgG1 antibody with longer serum half-life. *J. Immunol.* **176**, 346–56 (2006).
58. Petkova, S. B. *et al.* Enhanced half-life of genetically engineered human IgG1 antibodies in a humanized FcRn mouse model: potential application in humorally mediated autoimmune disease. *Int Immunol* **18**, 1759–1769 (2006).
59. Yeung, Y. A. *et al.* Engineering human IgG1 affinity to human neonatal Fc receptor: impact of affinity improvement on pharmacokinetics in primates. *J Immunol* **182**, 7663–7671 (2009).
60. Hinton, P. R. *et al.* Engineered human IgG antibodies with longer serum half-lives in primates. *J. Biol. Chem.* **279**, 6213–6 (2004).
61. Vaccaro, C., Bawdon, R., Wanjie, S., Ober, R. J. & Ward, E. S. Divergent activities of an engineered antibody in murine and human systems have implications for therapeutic antibodies. *Proc. Natl. Acad. Sci.* **103**, 18709–18714 (2006).
62. Finch, D. K. *et al.* Whole-Molecule Antibody Engineering: Generation of a High-Affinity Anti-IL-6 Antibody with Extended Pharmacokinetics. *J. Mol. Biol.* **411**, 791–807 (2011).
63. Bernett, M. J. *et al.* Immune suppression in cynomolgus monkeys by XPro9523: An improved CTLA4-Ig fusion with enhanced binding to CD80, CD86 and neonatal Fc receptor FcRn. *MAbs* **5**, 384–96 (2013).
64. Datta-Mannan, A. *et al.* FcRn affinity-pharmacokinetic relationship of five human IgG4 antibodies engineered for improved in vitro FcRn binding properties in cynomolgus monkeys. *Drug Metab. Dispos.* **40**, 1545–55 (2012).

65. Yeung, Y. A. *et al.* A therapeutic anti-VEGF antibody with increased potency independent of pharmacokinetic half-life. *Cancer Res.* **70**, 3269–77 (2010).
66. Gurbaxani, B., Dela Cruz, L. L., Chintalacharuvu, K. & Morrison, S. L. Analysis of a family of antibodies with different half-lives in mice fails to find a correlation between affinity for FcRn and serum half-life. *Mol Immunol* **43**, 1462–1473 (2006).
67. Elkon, K. & Casali, P. Nature and functions of autoantibodies. *Nat. Clin. Pract. Rheumatol.* **4**, 491–8 (2008).
68. Li, N. *et al.* Complete FcRn dependence for intravenous Ig therapy in autoimmune skin blistering diseases. *J. Clin. Invest.* **115**, 3440–50 (2005).
69. Akilesh, S. *et al.* The MHC class I-like Fc receptor promotes humorally mediated autoimmune disease. *J. Clin. Invest.* **113**, 1328–33 (2004).
70. Yu, Z. & Lennon, V. A. Mechanism of intravenous immune globulin therapy in antibody-mediated autoimmune diseases. *N. Engl. J. Med.* **340**, 227–8 (1999).
71. Raghavan, M., Chen, M. Y., Gastinel, L. N. & Bjorkman, P. J. Investigation of the interaction between the class I MHC-related Fc receptor and its immunoglobulin G ligand. *Immunity* **1**, 303–315 (1994).
72. Liu, L. *et al.* Amelioration of experimental autoimmune myasthenia gravis in rats by neonatal FcR blockade. *J. Immunol.* **178**, 5390–8 (2007).
73. Getman, K. E. & Balthasar, J. P. Pharmacokinetic effects of 4C9, an anti-FcRn antibody, in rats: implications for the use of FcRn inhibitors for the treatment of humoral autoimmune and alloimmune conditions. *J. Pharm. Sci.* **94**, 718–29 (2005).
74. Vaccaro, C., Zhou, J., Ober, R. J. & Ward, E. S. Engineering the Fc region of immunoglobulin G to modulate in vivo antibody levels. *Nat. Biotechnol.* **23**, 1283–1288 (2005).
75. Patel, D. a *et al.* Neonatal Fc receptor blockade by Fc engineering ameliorates arthritis in a murine model. *J. Immunol.* **187**, 1015–22 (2011).
76. Mezo, A. R. *et al.* Reduction of IgG in nonhuman primates by a peptide antagonist of the neonatal Fc receptor FcRn. *Proc. Natl. Acad. Sci. U. S. A.* **105**, 2337–42 (2008).
77. Mezo, A. R., Sridhar, V., Badger, J., Sakorafas, P. & Nienaber, V. X-ray Crystal Structures of Monomeric and Dimeric Peptide Inhibitors in Complex with the Human Neonatal Fc Receptor, FcRn. *J. Biol. Chem.* **285**, 27694–27701 (2010).

78. Wang, Z., Fraley, C. & Mezo, A. R. Discovery and structure-activity relationships of small molecules that block the human immunoglobulin G-human neonatal Fc receptor (hIgG-hFcRn) protein-protein interaction. *Bioorg. Med. Chem. Lett.* **23**, 1253–6 (2013).
79. Capon, D. J. *et al.* Designing CD4 immunoadhesins for AIDS therapy. *Nature* **337**, 525–31 (1989).
80. Suzuki, T. *et al.* Importance of neonatal FcR in regulating the serum half-life of therapeutic proteins containing the Fc domain of human IgG1: a comparative study of the affinity of monoclonal antibodies and Fc-fusion proteins to human neonatal FcR. *J Immunol* **184**, 1968–1976 (2010).
81. Madhusudan, S. *et al.* A phase II study of etanercept (Enbrel), a tumor necrosis factor alpha inhibitor in patients with metastatic breast cancer. *Clin Cancer Res* **10**, 6528–6534 (2004).
82. Fast, J. L., Cordes, A. A., Carpenter, J. F. & Randolph, T. W. Physical Instability of a Therapeutic Fc Fusion Protein: Domain Contributions to Conformational and Colloidal Stability. *Biochemistry* **48**, 11724–11736 (2009).
83. Bitonti, A. J. *et al.* Pulmonary delivery of an erythropoietin Fc fusion protein in non-human primates through an immunoglobulin transport pathway. *Proc. Natl. Acad. Sci.* **101**, 9763–9768 (2004).
84. Czajkowsky, D. M., Hu, J., Shao, Z. & Pleass, R. J. Fc-fusion proteins: new developments and future perspectives. *EMBO Mol. Med.* **4**, 1015–28 (2012).
85. Israel, E. J. *et al.* Expression of the neonatal Fc receptor, FcRn, on human intestinal epithelial cells. *Immunology* **92**, 69–74 (1997).
86. Kliwinski, C. *et al.* Contribution of FcRn binding to intestinal uptake of IgG in suckling rat pups and human FcRn-transgenic mice. *Am. J. Physiol. Gastrointest. Liver Physiol.* **304**, G262–70 (2013).
87. Dickinson, B. L. *et al.* Bidirectional FcRn-dependent IgG transport in a polarized human intestinal epithelial cell line. *J Clin Invest* **104**, 903–911 (1999).
88. Yoshida, M. *et al.* Human neonatal Fc receptor mediates transport of IgG into luminal secretions for delivery of antigens to mucosal dendritic cells. *Immunity* **20**, 769–783 (2004).
89. Low, S. C., Nunes, S. L., Bitonti, A. J. & Dumont, J. A. Oral and pulmonary delivery of FSH-Fc fusion proteins via neonatal Fc receptor-mediated transcytosis. *Hum Reprod* **20**, 1805–1813 (2005).

90. Israel, E. Neonatal necrotizing enterocolitis, a disease of the immature intestinal mucosal barrier. *Acta Paediatr.* **83**, 27–32 (1994).
91. Yoshida, M. *et al.* Neonatal Fc receptor for IgG regulates mucosal immune responses to luminal bacteria. *J. Clin. Invest.* **116**, 2142–2151 (2006).
92. Hornby, P. J. *et al.* Human and Non-Human Primate Intestinal FcRn Expression and Immunoglobulin G Transcytosis. *Pharm. Res.* (2013). doi:10.1007/s11095-013-1212-3
93. Patton, J. S. & Byron, P. R. Inhaling medicines: delivering drugs to the body through the lungs. *Nat Rev Drug Discov* **6**, 67–74 (2007).
94. Spiekermann, G. M. *et al.* Receptor-mediated Immunoglobulin G Transport Across Mucosal Barriers in Adult Life: Functional Expression of FcRn in the Mammalian Lung. *J. Exp. Med.* **196**, 303–310 (2002).
95. Dumont, J. A. *et al.* Delivery of an erythropoietin-Fc fusion protein by inhalation in humans through an immunoglobulin transport pathway. *J Aerosol Med* **18**, 294–303 (2005).
96. Krzyzanski, W., Jusko, W. J., Wacholtz, M. C., Minton, N. & Cheung, W. K. Pharmacokinetic and pharmacodynamic modeling of recombinant human erythropoietin after multiple subcutaneous doses in healthy subjects. *Eur. J. Pharm. Sci.* **26**, 295–306 (2005).
97. Vllasaliu, D., Alexander, C., Garnett, M., Eaton, M. & Stolnik, S. Fc-mediated transport of nanoparticles across airway epithelial cell layers. *J. Control. Release* **158**, 479–86 (2012).
98. Wang, W., Wang, E. Q. & Balthasar, J. P. Monoclonal antibody pharmacokinetics and pharmacodynamics. *Clin. Pharmacol. Ther.* **84**, 548–58 (2008).
99. Leyland-Jones, B. *et al.* Pharmacokinetics, safety, and efficacy of trastuzumab administered every three weeks in combination with paclitaxel. *J. Clin. Oncol.* **21**, 3965–71 (2003).
100. Pridgen, E. M. *et al.* Transepithelial Transport of Fc-Targeted Nanoparticles by the Neonatal Fc Receptor for Oral Delivery. *Sci. Transl. Med.* **5**, 213ra167–213ra167 (2013).
101. Yoshida, M. *et al.* Human neonatal Fc receptor mediates transport of IgG into luminal secretions for delivery of antigens to mucosal dendritic cells. *Immunity* **20**, 769–783 (2004).
102. Liu, X. *et al.* The neonatal FcR-mediated presentation of immune-complexed antigen is associated with endosomal and phagosomal pH and antigen stability in macrophages and dendritic cells. *J. Immunol.* **186**, 4674–86 (2011).

103. Baker, K. *et al.* Neonatal Fc receptor for IgG (FcRn) regulates cross-presentation of IgG immune complexes by CD8-CD11b⁺ dendritic cells. *Proc. Natl. Acad. Sci. U. S. A.* **108**, 9927–32 (2011).
104. Weflen, A. W. *et al.* Multivalent immune complexes divert FcRn to lysosomes by exclusion from recycling sorting tubules. *Mol. Biol. Cell* **24**, 2398–405 (2013).
105. Vidarsson, G. *et al.* FcRn: an IgG receptor on phagocytes with a novel role in phagocytosis. *Blood* **108**, 3573–9 (2006).
106. Mi, W. *et al.* Targeting the neonatal fc receptor for antigen delivery using engineered fc fragments. *J. Immunol.* **181**, 7550–61 (2008).
107. Ye, L., Zeng, R., Bai, Y., Roopenian, D. C. & Zhu, X. Efficient mucosal vaccination mediated by the neonatal Fc receptor. *Nat. Biotechnol.* **29**, 158–63 (2011).
108. Bruhns, P. Properties of mouse and human IgG receptors and their contribution to disease models. *Blood* **119**, 5640–9 (2012).
109. Lu, L. *et al.* A neonatal Fc receptor-targeted mucosal vaccine strategy effectively induces HIV-1 antigen-specific immunity to genital infection. *J. Virol.* **85**, 10542–53 (2011).
110. Li, Z. *et al.* Transfer of IgG in the female genital tract by MHC class I-related neonatal Fc receptor (FcRn) confers protective immunity to vaginal infection. *Proc. Natl. Acad. Sci. U. S. A.* **108**, 4388–93 (2011).
111. Bai, Y. *et al.* Intracellular neutralization of viral infection in polarized epithelial cells by neonatal Fc receptor (FcRn)-mediated IgG transport. *Proc. Natl. Acad. Sci. U. S. A.* **108**, 18406–11 (2011).
112. Sleep, D., Cameron, J. & Evans, L. R. Albumin as a versatile platform for drug half-life extension. *Biochim. Biophys. Acta* **1830**, 5526–34 (2013).
113. Elsadek, B. & Kratz, F. Impact of albumin on drug delivery--new applications on the horizon. *J. Control. Release* **157**, 4–28 (2012).
114. Rosenstock, J., Reusch, J., Bush, M., Yang, F. & Stewart, M. Potential of albiglutide, a long-acting GLP-1 receptor agonist, in type 2 diabetes: a randomized controlled trial exploring weekly, biweekly, and monthly dosing. *Diabetes Care* **32**, 1880–6 (2009).
115. Garber, A. J. Long-acting glucagon-like peptide 1 receptor agonists: a review of their efficacy and tolerability. *Diabetes Care* **34 Suppl 2**, S279–84 (2011).
116. Dennis, M. S. *et al.* Albumin binding as a general strategy for improving the pharmacokinetics of proteins. *J Biol Chem* **277**, 35035–35043 (2002).

117. Andersen, J. T. *et al.* Extending half-life by indirect targeting of the neonatal Fc receptor (FcRn) using a minimal albumin binding domain (ABD). *J Biol Chem* **286**, 5234–41 (2010).
118. Tijink, B. M. *et al.* Improved tumor targeting of anti-epidermal growth factor receptor Nanobodies through albumin binding: taking advantage of modular Nanobody technology. *Mol. Cancer Ther.* **7**, 2288–97 (2008).
119. Pluen, A. *et al.* Role of tumor-host interactions in interstitial diffusion of macromolecules: cranial vs. subcutaneous tumors. *Proc. Natl. Acad. Sci. U. S. A.* **98**, 4628–33 (2001).
120. Sofou, S., Yu, Y. B., Thurber, G. M., Schmidt, M. M. & Wittrup, K. D. Antibody tumor penetration: Transport opposed by systemic and antigen-mediated clearance. *Adv. Drug Deliv. Rev.* **60**, 1421–1434 (2008).
121. Kenanova, V. *et al.* Radioiodinated versus radiometal-labeled anti-carcinoembryonic antigen single-chain Fv-Fc antibody fragments: optimal pharmacokinetics for therapy. *Cancer Res.* **67**, 718–26 (2007).
122. Ying, T., Chen, W., Gong, R., Feng, Y. & Dimitrov, D. S. Soluble Monomeric IgG1 Fc. *J. Biol. Chem.* **287**, 19399–408 (2012).
123. Gong, R., Wang, Y., Feng, Y., Zhao, Q. & Dimitrov, D. S. Shortened engineered human antibody CH2 domains: increased stability and binding to the human neonatal receptor. *J. Biol. Chem.* **286**, 27288–93 (2011).
124. Ying, T. *et al.* Engineered soluble monomeric IgG1 CH3 domain: generation, mechanisms of function, and implications for design of biological therapeutics. *J. Biol. Chem.* **288**, 25154–64 (2013).
125. Gehlsen, K. *et al.* Pharmacokinetics of engineered human monomeric and dimeric CH2 domains. *MAbs* **4**, 466–74 (2012).
126. Ying, T., Chen, W., Gong, R., Feng, Y. & Dimitrov, D. S. Soluble monomeric IgG1 Fc. *J. Biol. Chem.* **287**, 19399–408 (2012).
127. Ishino, T. *et al.* Engineering a monomeric Fc domain modality by N-glycosylation for the half-life extension of biotherapeutics. *J. Biol. Chem.* **288**, 16529–37 (2013).
128. Sockolosky, J. T., Tiffany, M. R. & Szoka, F. C. Engineering neonatal Fc receptor-mediated recycling and transcytosis in recombinant proteins by short terminal peptide extensions. *Proc. Natl. Acad. Sci. U. S. A.* **109**, 16095–16100 (2012).

Chapter 2: Engineering FcRn-mediated recycling and transcytosis in recombinant proteins by short N- and C-terminal peptide extensions

2.1 Introduction

It is remarkable that IgG and albumin have exceptionally long plasma half-lives whereas most other human proteins exhibit rapid blood clearance¹. The extended circulation of IgG contributes to the success of antibody therapeutics² whereas the rapid clearance of non-IgG proteins limits their therapeutic potential due to the need for frequent injection or continuous infusion. This long half-life of IgG and albumin is a result of interaction with FcRn which creates an intracellular protein reservoir that is protected from lysosomal degradation and subsequently recycled to the extracellular space³. A number of chemical and recombinant methods have been devised to improve protein half-life. The most common chemical approach pioneered by Abuchowski and coworkers in 1977⁴ depends upon the attachment of polyethylene glycol (PEG) chains. Although there are numerous FDA approved PEGylated proteins⁵, the approach decreases their potency and contributes to their heterogeneity and immunoreactivity. The use of alternative polymers or polymerization strategies address these issues⁶ but require additional processing steps to prepare the polymer-protein conjugate. Genetic fusion between a therapeutic protein and either the Fc-domain of IgG, albumin, or long, flexible polypeptide extensions⁷ have been introduced to extend protein circulation. Fusion to the Fc-domain or albumin is a widely adapted strategy to improve protein circulation via a combination of interaction with FcRn and the substantial increase in molecular weight, which reduces renal clearance. Although a number of such fusion proteins are used clinically, the large size of the Fc-domain and albumin adversely affects tissue penetration and reduces the specific activity of the fusion partner⁸. There have been extensive protein engineering efforts to overcome these limitations by reducing the size of

the Fc-domain^{9,10} or albumin¹¹; however, alternative ligands that target proteins to FcRn have not been explored.

In addition to enabling long circulation, recycling receptors such as FcRn or transferrin expressed in the lung and intestinal epithelia provide a route for transport of protein cargos across the epithelium and into the blood stream^{12,13}. A Fc-Erythropoietin (Fc-EPO) fusion protein when administered into the lung was transported via the FcRn across the lung epithelium in humans¹⁴; however, the Fc-EPO bioavailability is low perhaps due to the large size of the Fc-fusion. Thus, non-invasive protein delivery remains a major challenge¹⁵.

We have devised a strategy for engineering proteins to interact with FcRn through the genetic fusion of a short FcBP sequence to the N- and/or C-terminus of a model fluorescent protein, monomeric Katushka (mKate)¹⁶. We chose FcRn as the molecular target of our engineered proteins due to its ability to both prolong protein circulation and enable epithelial transcytosis. This approach may overcome limitations associated with chemical modifications, be easy to manufacture, and provide a solution to the rapid elimination and limited protein delivery routes. As an initial step on the path to more convenient protein delivery, we demonstrate that FcBP fusion proteins can be readily expressed in *E. coli*, exhibit pH dependent binding to FcRn, and undergo FcRn-mediated recycling and transcytosis.

2.2 Methods

2.2.1 Materials

All cell culture reagents were purchased from the UCSF Cell Culture Facility. Ovalbumin, ampicillin, Inulin-FITC, DAPI, Terrific Broth (TB), and all buffer salts were purchased from Sigma-Aldrich (St. Louis, MO). The humanized anti-VEGF IgG1 antibody (Bevacizumab) was obtained from the UCSF medical center. Nickel Sepharose high performance resin prepacked in 5 mL HiTrap columns (HisTrap FF), PD-10 desalting columns, and HiPrep 16/60 Sephacryl S-100 HR size exclusion chromatography (SEC) column were purchased from GE Healthcare (Piscataway, NJ). Complete EDTA-free protease inhibitor cocktail tablets, isopropyl β -D-1-thiogalactopyranoside (IPTG), and G418 were purchased from Roche Diagnostics (Indianapolis, IN). Dextran Cascade Blue (10kDa) and Hygromycin B were from Invitrogen, Life Technologies (Grand Island, NY). All primers were purchased from IDT (San Diego, CA) and all restriction enzymes were purchased from New England BioLabs (Ipswich, MA).

2.2.2 Cell Culture

MDCK wild type cells (purchased from the UCSF cell culture facility) were maintained in MEM supplemented with 10% FBS, 1% non-essential amino acids (NEAA), 1% L-glutamine, 1% sodium pyruvate, and 1% penicillin and streptomycin. MDCK human β_2 -microglobulin (h β_2 M) cells were maintained in MDCK wild type cell media but under constant drug selection by addition of 0.3 mg/mL hygromycin B. MDCK hFcRn-YFP/h β_2 M cells were maintained in MDCK wild type cell media but under constant drug selection by addition of 0.4 mg/mL G418 and 0.3 mg/mL hygromycin B. B16F10 cells were maintained in MEM supplemented with 10% FBS, 1% NEAA, and 1% sodium pyruvate. All cells were maintained in a humidified environment at 37 °C and 5% CO₂.

2.2.3 Mammalian expression vectors

The mammalian expression plasmid encoding human FcRn linked to N-terminus of enhanced YFP was generated by polymerase chain reaction (PCR) amplification of human FcRn (hFcRn) cDNA with primers to incorporate 5' EcoRI and 3' AgeI restriction sites along with DNA encoding a [Gly₄Ser]₂ linker separating the C-terminus of hFcRn from the N-terminus of EYFP. The resulting PCR product was restriction cloned into the 5' EcoRI and 3' AgeI sites of the mammalian expression vector pEYFP-N1 (kindly provided by Dr. Alan Verkman, UCSF). Human FcRn cDNA was obtained from OpenBiosystems (Huntsville, AL) and maintained in the vector pINCY.

The mammalian expression plasmid encoding human β 2M was generated by PCR amplification of h β _{2m} cDNA from the vector pCMV-SPORT6 (OpenBiosystems) followed by restriction cloning into the 5' BamHI and 3' XhoI sites of the mammalian expression vector pcDNATM3.1/Hygro (+) (kindly provided by Dr. Kathy Giacomini, UCSF).

The mammalian expression plasmid encoding LAMP1 linked to the C-terminus of mTurquoise was generated by Matthew R. Tiffany, Ph.D. in the Szoka lab by PCR amplification of LAMP1 from a cDNA library prepared from M28 human mesothelioma cells with primers designed to incorporate 5' XhoI and 3' BamHI restriction sites. The resulting PCR product was restriction cloned into the 5' XhoI and 3' BamHI sites of the mammalian expression vector pmTurquoise-C1 (kindly provided by Kurt Thorn, UCSF). All plasmids were confirmed by DNA sequencing (McLab; South San Francisco, CA).

2.2.4 MDCK h β 2M and MDCK hFcRn-EYFP/h β 2M cell line generation

To generate MDCK cells stably expressing h β 2M, MDCK wild type cells were transfected with the h β 2m expression vector described in section 2.2.3 using Lipofectamine 2000 (Invitrogen; Carlsbad, CA) and selected with 0.3 mg/mL hygromycin B (Invitrogen). Resistant clonal colonies were selected and expanded for further analysis. A cDNA library was generated from the propagated clones by isolation of mRNA using TRIzol® and conversion to cDNA using the Superscript® III first-strand synthesis kit and oligo(dT) primers following the manufacturers recommend protocol (Invitrogen). The cDNA prepared from the isolated clones was evaluated by RT-PCR to confirm the presence of h β 2m mRNA.

To generate MDCK cells stably expressing both hFcRn-EYFP and h β 2M MDCK, wild type cells were co-transfected with expression vectors encoding full-length hFcRn-EYFP and h β 2M using Lipofectamine 2000 (Invitrogen) and first selected with 0.3 mg/mL hygromycin B (Invitrogen) followed by selection with 1.0 mg/mL G418 (Roche). Resistant colonies were evaluated by fluorescence microscopy to confirm expression of hFcRn-EYFP, selected, and expanded for further analysis. Propagated clones were further evaluated for binding of fluorescently labeled hIgG1 at pH 6 and co-localization with hFcRn-EYFP by fluorescence microscopy. Furthermore, the presence of hFcRn and h β 2m mRNA were confirmed by RT-PCR. All stably transfected cells were maintained in MDCK wild type media under constant drug selection (0.4 mg/mL G418 and/or 0.3 mg/mL hygromycin B).

2.2.5 *E. coli* expression vectors

The bacterial expression vector for mKate was generated as previously described¹⁷. The genes encoding mKate modified at its C-terminus with FcRn binding polypeptide (FcBP) sequences were constructed by PCR amplification of mKate with primers designed to insert

DNA encoding a cyclic or linear FcBP sequence (Cyclic: QRFCTGHFGGLYPCNG; Linear: QRFVTGHFGGLYPANG) separated from the C-terminus of mKate by a flexible linker (GGGGS). The resulting PCR products were purified and restriction cloned into the NdeI and BamHI restriction sites of the bacterial expression vector pET15b (Novagen; San Diego, CA). The solvent exposed cysteine residues of mKate (Cys134 and Cys242) were mutated to serine with mutagenic oligonucleotides using the QuikChange Lightning mutagenesis kit (Agilent Technologies; Santa Clara, CA) to yield the final expression vectors pETmKcC and pETmKcI, corresponding to mKate modified at its C-terminus with a cyclic or linear FcBP, respectively. The same method was used to create the expression vector for mKate modified at its N-terminus with the cyclic FcBP sequence (pETmKnc).

The gene encoding mKate modified at its N-&-C-terminus with the cyclic FcBP sequence was generated by PCR amplification of C-terminal modified mKate from pETmKc with primers designed to add an N-terminal cyclic FcBP sequence. The resulting PCR product was restriction cloned into the NdeI and BamHI restriction sites of the bacterial expression vector pET15b and the three amino acids between the thrombin cleavage site and start of the N-terminal cyclic FcBP sequence (Ser, His, Met) were deleted with a mutagenic oligonucleotide using the QuikChange Lightning mutagenesis kit to yield the vector pETmKnc. The pET15b vectors for expression of the Tyr-12 to His mutant of N-&-C-Term Cyclic FcBP mKate (pETmKncCcY286H), N-Linear/C-Cyclic FcBP mKate (pETmKnicC), and N-&-C-Term Linear FcBP mKate (pETmKnicI) were created by mutagenesis of pETmKncCc. All plasmids were confirmed by DNA sequencing. A complete list of primers used in this study is provided in the Table 2.1. Amino acid sequences of proteins used in this study are also provided in the Appendix A.

Table 2.1 Primer sequences used in this study.

Protein	Primer Pair	Restriction Site
Human FcRn-YFP	F= 5'-AAG CTT CGA ATT CCT CAG CAT GGG GTC-3'	EcoRI
	R= 5'-GCG ACC GGT CCG GAC CCC CCC CCC CCG GAC CCC CCC CCC CCG GCG GTG GCT GGA ATC ACA-3'	AgeI
Human β 2M	F= 5'-CGA GCT CGG ATC CGC CGA GAT GTC TCG CTC CGT GG-3'	BamHI
	R= 5'-CTC TAG ACT CGA GTT ACA TGT CTC GAT CCC ACT TAA C-3'	XhoI
hLAMP1-mTurquoise	F= 5'-GATCTCGAGCGCCACCATGGCGGCCCGCCGAGC-3'	XhoI
	R= 5'-GGTGGATCCGGGATAGTCTGGTAGCCTGC-3'	BamHI
C-Term Cyclic FcBP mKate	F= 5'-CGGCAGCCATATGTCTGAACTGATCA-3'	NdeI
	R= 5'-GCA GCC GGA TCC TTA GCC GTT GCA CGG ATA CAG GCC GCC AAA ATG GCC GGT GCA AAA GCG CTG CGA GCC GCC GCC TTT ATG GCC CAG TTT AGA-3'	BamHI
C-Term Linear FcBP mKate	F= 5'-CGGCAGCCATATGTCTGAACTGATCA-3'	NdeI
	R= 5'-GCA GCC GGA TCC TTA GCC GTT CGC CGG ATA CAG GCC GCC AAA ATG GCC GGT CAC AAA GCG CTG CGA GCC GCC GCC TTT ATG GCC CAG TTT AGA-3'	BamHI
N-Term Cyclic FcBP mKate	F= 5'-CAG CCA TAT GCA ACG TTT CTG TAC CGG TCA CTT CGG TGG TCT GTA CCC GTG TAA TGG TGG TGG TGG TGG TTC GTC TGA ACT GAT CAA AGA-3'	NdeI
	R= 5'-GCCGGATCCTTATTTATGGCCAGTT-3'	BamHI
N-&-C-Term Cyclic FcBP mKate	F= 5'-CAG CCA TAT GCA ACG TTT CTG TAC CGG TCA CTT CGG TGG TCT GTA CCC GTG TAA TGG TGG TGG TGG TGG TTC GTC TGA ACT GAT CAA AGA-3'	NdeI
	R= 5'-GCA GCC GGA TCC TAG CCG TTG-3'	BamHI
N-&-C-Term Cyclic FcBP mKate Y286H Mutagenesis	5'-ATT TTG GCG GCC TGC ATC CGT GCA ACG GC-3'	---
N-Linear & C-Cyclic FcBP mKate C22V Mutagenesis	5'-CGC GGC CAA CGT TTC GTT ACC GGT CAC TTC GG-3'	---
N-Linear & C-Cyclic FcBP mKate C32A Mutagenesis	5'-GGT GGT CTG TAC CCG GCT AAT GGT GGT GGT GG-3'	---
N-&-C-Term Linear FcBP mKate C278V Mutagenesis	5'-GGCGGCTCGCAGCGCTTTGTACCG-3'	---
N-&-C-Term Linear FcBP mKate C288V Mutagenesis	5'-GCGGCCTGTATCCGGCCAACGGCTA-3'	---
N-Terminal SHM Deletion Mutagenesis	5'-TGG TGC CGC GCG GCC AAC GTT TCT GTA C-3'	---
qPCR hFcRn Forward	5'-CCT GGC TTT TCC GTG CTT AC-3'	---
qPCR hFcRn Reverse	5'-TTT GAC TGT TAG TGA CGA CGA G-3'	---
qPCR h β 2M Forward	5'-GAG GCT ATC CAG CGT ACT CCA-3'	---
qPCR h β 2M Reverse	5'-CGG CAG GCA TAC TCA TCT TTT-3'	---

2.2.6 Protein expression and purification

Expression of mKate and FcBP modified mKates was carried out in BL21-Codon Plus (DE3)-RIPL *E. coli* cells (Stratagene; La Jolla, CA) harboring expression vectors described in section 2.2.5. A 100 mL overnight *E. coli* culture was used to inoculate a 1 L culture of Terrific Broth containing 100 µg/mL ampicillin and 0.1 mM IPTG. Cells were cultured at 37 °C for 8 hrs and harvested by centrifugation. Cells were lysed by free-thaw and lysozyme treatment (1 mg/mL, 2 hr, 4 °C) followed by sonication and centrifugation. The supernatant containing soluble proteins were purified by Ni²⁺ affinity chromatography followed by size exclusion chromatography on a HiPrep 16/60 Sephacryl S-100. The N-terminal poly-histidine tag was cleaved with thrombin (Amersham Biosciences; Piscataway, NJ) and removed by Ni²⁺ affinity chromatography. Purity was confirmed by SDS-PAGE.

2.2.7 Mass spectrometry

Mass spectrometry was performed by the Proteomics/Mass Spectrometry Laboratory at UC Berkeley. For LC-MS/MS analysis, proteins were digested in solution with LysC (Promega). The protein solution was adjusted to 8M urea, subjected to carboxyamidomethylation of cysteines, and digested with LysC. The sample was then desalted using a C18 spec tip (Varian). A nano LC column was packed in a 100 µm inner diameter glass capillary with an emitter tip. The column consisted of 10 cm of Polaris C18 5 µm packing material (Varian). The column was loaded by use of a pressure bomb and washed extensively with buffer A (see below). The column was then directly coupled to an electrospray ionization source mounted on a Thermo-Fisher LTQ XL linear ion trap mass spectrometer. An Agilent 1200 HPLC equipped with a split line so as to deliver a flow rate of 30 nL/min was used for chromatography. Peptides were eluted using a linear gradient from 100% buffer A to 60% buffer B. Buffer A was 5% acetonitrile,

0.02% heptafluorobutyric acid (HBFA); buffer B was 80% acetonitrile, 0.02% HBFA. The programs SEQUEST and DTASELECT^{18,19} were used to identify peptides from a database consisting of the protein sequence plus a database of common contaminants using a partial tryptic search.

2.2.8 Fluorescent spectra measurements

All fluorescent spectra were measured on a Spex Fluorolog fluorometer (Horiba Jobin Yvon; Edison, NJ) with 5 nm band width excitation and emission slits. To compare fluorescent emission spectra between unmodified mKate or FcBP-modified mKates, proteins were diluted to 500 nM in D-PBS, excited at 588 nm, and the emission spectra was recorded. Quantification of protein samples by fluorometry was done by comparing unknown samples to a standard curve specific for each protein.

2.2.9 Affinity measurements by surface plasmon resonance

SPR measurements were obtained using a BIAcore T100 instrument (BIAcore Inc.; Piscataway, NJ). The extracellular region of human FcRn (a kind gift of Dr. E. Sally Ward, UT Southwestern) was captured on a CM5 sensor chip at pH 5 by amine coupling to a final immobilization density of ~550 or ~100 resonance units. Un-reacted sites were blocked with 1M ethanolamine. A control flow cell without immobilized hFcRn was prepared for reference subtraction. All binding experiments were performed as previously described for the synthetic FcBP²⁰ with the following modifications. The flow rate used for all methods was 30 μ L/min and injection times were 60 sec. Proteins were dissociated from the chip for 45 sec in running buffer followed by regeneration with 45 sec injections of HBS-P (10mM Hepes, 150 mM NaCl, 0.005% Tween 20, pH 7.4) and/or Tris, pH 9 buffer (50 mM Tris, 100 mM NaCl, 0.01% Tween 20, pH 9). Binding kinetics were derived by analysis of the generated sensograms using the

Biacore T100 evaluation software. Sensograms were fit to either a steady-state affinity model, a one-site kinetic binding model, or a bivalent analyte kinetic model included in the evaluation software.

2.2.10 FACS cellular accumulation assay

Due to the far red fluorescent properties of mKate (Ex/Em: 588/620), cell associated FcBP modified mKate can be quantified via fluorescence-activated cell sorting (FACS). MDCK hFcRn-EYFP/h β_2 m cells were washed twice in binding buffer [Hank's Balanced Salt Solution (HBSS), 1% ovalbumin, 50 mM MES, pH 6] and incubated with serial dilutions of proteins for 1 hr at 37 °C to permit cellular uptake. Cells were washed twice with cold binding buffer to remove unbound protein, trypsinized, and analyzed on a FACS Array cell sorter (BD Biosciences; San Jose, CA). Mean fluorescent intensities (MFI) for each test population were derived after gating for live and EYFP positive cells. Binding at pH 7.4 was as described above except all incubations and washes were done in HBSS(+), pH 7.4 [HBSS, 1% ovalbumin, 50 mM HEPES, pH 7.4]. Protein accumulation in MDCK h β_2 m, wild type MDCK, and B16F10 cells at pH 6 was as described above. All FACS data were analyzed using FlowJo (Tree Star Inc.; Ashland, OR). All incubations were done in triplicate and data is represented as mean \pm SD.

2.2.11 mKate fluorescence in MDCK hFcRn-EYFP/hB2M cells after intracellular pH clamping

MDCK hFcRn-EYFP/h β_2 m cells seeded in a 12-well plate (250,000 c/well) were washed twice in binding buffer [HBSS(+), pH 6] and incubated with either 25 μ M mKate or 2.5 μ M N-&-C-Term Cyclic FcBP for 1 hr at pH 6, 37 °C to permit cellular uptake. Cells were washed three times with cold binding buffer to remove unbound protein, trypsinized, and collected by centrifugation. The pH in all cellular compartments was clamped by re-suspending cells in high

K⁺ solutions containing inhibitors and ionophores (50 mM Hepes, pH 7.4 or 50 mM acetic acid, pH 5 or pH 4, containing 140 mM KCl, 2 mM CaCl₂, 1 mM MgCl₂, 5 mM glucose, 100 nM bafilomycin A1, 10 μM nigericin, 10 μM valinomycin, and 10 μM CCCP) as described ²¹. After pH clamp cells were analyzed by FACS to determine differences in mKate MFI as a function of pH.

2.2.12 Fluorescence microscopy

Widefield epifluorescence images of protein co-localization with FcRn-EYFP in MDCK cells were obtained on a Nikon Eclipse Ti-E inverted microscope equipped with an In Vivo Scientific temperature controlled chamber with humidification and CO₂ control, infrared autofocus, 60x 1.4 numerical aperture Plan Apo objective, Photometrics Coolsnap HQ2 CCD camera, and Sutter Lambda XL lamp.

MDCK cells were transiently transfected with 1 μg hFcRn-EYFP expression plasmid in combination with 4 μg hβ₂M expression plasmid using Lipofectamine 2000 (Invitrogen) following the manufacturers recommended 6-well plate protocol. Cells were incubated with Lipofectamine / DNA complexes in OptiMEM reduced serum media for 6 – 8 hrs, the media was exchanged with MDCK cell culture media described in section 2.2.2, and cells were cultured overnight to allow for gene/protein expression. Transfected MDCK cells were washed twice with 1 mL HBSS(+), pH 6 binding buffer, pulsed with 1 mL of protein solution in binding buffer at varying concentrations as indicated in the figure legends for 1 hr at 37 °C, washed three times with binding buffer, and imaged live on a temperature controlled stage.

The distribution of hFcRn-EYFP, N-&-C-Term Cyclic FcBP mKate, and LAMP1-mTourquoise in MDCK hFcRn-EYFP/hβ₂m cells was determined by transient transfection with the mammalian expression vector encoding LAMP1-mTourquoise. Cells were pulsed as

described above, washed, and chased in HBSS, pH 7.4 at 37 °C for 1 hr or 4 hrs before imaging.

Confocal images were obtained on a Zeiss Axiovert 200M inverted microscope equipped with a Yokogawa CSU10 spinning disc unit. Dextran pulse chase studies were as follows. MDCK hFcRn-EYFP/h β_2 m cells were pulsed with 1 mg/mL of 10 kDa Dextran-Blue for 2 hrs at 37 °C, washed, and chased for 1 hr at 37 °C in HBSS, pH 7.4. Cells were then pulsed with 1 μ M of N-&-C-Term Cyclic FcBP mKate for 1 hr at 37 °C, pH 6, washed, and chased for 1 hr at 37 °C in HBSS, pH 7.4 prior to imaging.

All image analysis was performed using ImageJ (NIH; Bethesda, MD). Widefield epifluorescent images were deconvoluted to remove out of focus light using the 2D parallel spectral deconvolution plugin.

2.2.13 FcRn mediated recycling and transcytosis assay

FcRn-mediated recycling and transcytosis were assessed as previously described for Fc domains²² with minor modifications. Recycling was assessed on non-polarized MDCK hFcRn-EYFP/h β_2 m or MDCK h β_2 m cells pulsed with 2.5 μ M of mKate, 2.5 μ M mKates modified with a single FcBP, 1 μ M mKate modified at both termini, or 1 μ M labeled hIgG1 for 1 hr at 37 °C in binding buffer to permit uptake. Cells were washed 4 times with cold HBSS(+), pH 8.5 [HBSS, 1% ovalbumin, 50 mM Tris, pH 8.5] to remove surface bound protein and chased with pre-warmed HBSS(+), pH 7.4 for 2 hrs at 37 °C. The media containing recycled proteins was collected, centrifuged to remove dead or detached cells, and the amount of protein in the supernatant was quantified by fluorometry. Controls including recycling at 4 °C, pH 7.4, and in hFcRn negative MDCK cells were conducted as described above with the appropriate modification.

FcRn-mediated transcytosis was assessed across polarized wild type MDCK or MDCK hFcRn-EYFP/h β ₂m cell monolayers cultured on Transwell® filters (12 mm diameter, 0.4 μ m pore size; Corning Life Sciences; Lowell, MA). Cell confluence was confirmed by a transepithelial electrical resistance (TEER) greater than 250 Ω /cm² prior to experiments typically conducted 4 days after initial cell seeding of 250,000 cells/well. Cells were washed three times with 1 mL of HBSS(+), pH 6 in the apical compartment and 1 mL of HBSS(+), pH 7.4 in the basolateral compartment. Apical-to-basolateral transcytosis was measured by incubating the apical chamber with 0.5 mL of 2.5 μ M of mKate, 2.5 μ M N-&-C-Term Cyclic FcBP mKate, or 0.5 μ M labeled hIgG1 in HBSS(+), pH 6 or pH 7.4 and the basolateral chamber with 1 mL of HBSS(+), pH 7.4. FITC-inulin (4 μ g/mL) was co-incubated with protein in the apical compartment as a marker for paracellular transport and monolayer consistency across transwells. The amount of protein and FITC-inulin transported to the basolateral chamber after a 2 hr continuous incubation at 37 °C or 4 °C was quantified by fluorometry.

2.2.14 FcRn-mediated recycling versus transcytosis in MDCK hFcRn-EYFP/h β 2M cells

The fractional recycling versus transcytosis of hIgG1, FcBP modified mKates, and transferrin was evaluated in polarized MDCK hFcRn-EYFP/h β ₂m cell monolayers cultured on Transwell® filters cultured as described in section 2.2.13. Cells were pulsed with 2.5 μ M mKate, N-&-C-Term Cyclic FcBP mKate, N-&-C Term Linear FcBP mKate, hIgG1-TAMRA, or Transferrin-Alexa568 (Invitrogen, Molecular Probes; Cat. T23365) for 1 hr at 37 °C in HBSS(+), pH 6 to facilitate cellular accumulation. Cells were washed three times with 1 mL of ice cold HBSS, 50 mM Tris, pH 8.5 to remove surface bound protein in both the apical and basolateral compartments. Cells were then chased with 0.5 mL of HBSS, pH 7.4 in both the apical and basolateral compartments for 4 hr at 37 °C. The apical and basolateral medium was

collected and assayed via fluorometry. The cells were then washed three times with 1 mL of HBSS, pH 7.4 to removed residual protein and lysed with 0.5 mL of luciferase cell culture lysis reagent (Promega; Madison, WI). All samples were centrifuged at 14,000 rpm in a tabletop centrifuge to remove cell debris prior to analysis via fluorometry. The amount of protein recycled, transcytosed, or that remained intracellular was determined based on standard curves and the fraction recycled, transcytosed, or intracellular for each protein was calculated by normalizing the amount of protein in each fraction to the total amount of protein in the three fractions.

2.2.15 Statistical analysis

Comparison between two groups was analyzed for statistical significance using an unpaired, Student's *t*-test (two-sided). Comparison between multiple groups was analyzed for statistical significance using a one-way ANOVA and Bonferroni post-test. All statistical analysis was performed in Prism 5 (GraphPad Software; La Jolla, CA) on un-transformed data.

2.3 Results

2.3.1 Protein expression and characterization

To test whether proteins genetically modified with a FcBP sequence enables interaction with FcRn, we created *Escherichia coli* expression vectors encoding mKate modified at its N- and/or C-terminus with FcBP sequences (Fig. 2.1a). We chose mKate as a model protein for proof-of-concept studies due to its far-red fluorescent properties, which allows for multi-fluorophore microscopy studies and simple quantification techniques. The 16 amino acid FcBP gene sequence was fused to the 5' and/or 3' end of the gene encoding mKate separated by a flexible Gly₄Ser linker and subsequently restriction cloned downstream of a 5' poly-histidine tag and thrombin cleavage site in the pET15b vector. The thrombin site was modified such that cleavage removes the poly-histidine tag, leaving a single glycine residue as the first amino acid followed by the FcBP sequence.

All proteins were adequately expressed in the soluble *E. coli* fraction and following purification, no significant differences in fluorescence emission between unmodified and modified mKates were observed (Fig. 2.1b), suggesting that FcBP fusion does not result in major structural changes that disrupt chromophore assembly during protein folding. FcBP fusion results in a subtle change in migration by SDS-PAGE (Fig. 2.1c) from ~27 kDa to ~30 kDa for mKate and N-&-C terminal modified mKates, respectively, in stark contrast to Fc or albumin fusions which increase molecular weight by ~50 – 70 kDa. Tandem mass spectrometry analysis (LC MS/MS) confirmed expression of mKate modified at its C-terminus with a Gly₄Ser linker followed by the cyclic FcBP sequence (Fig. 2.1d).

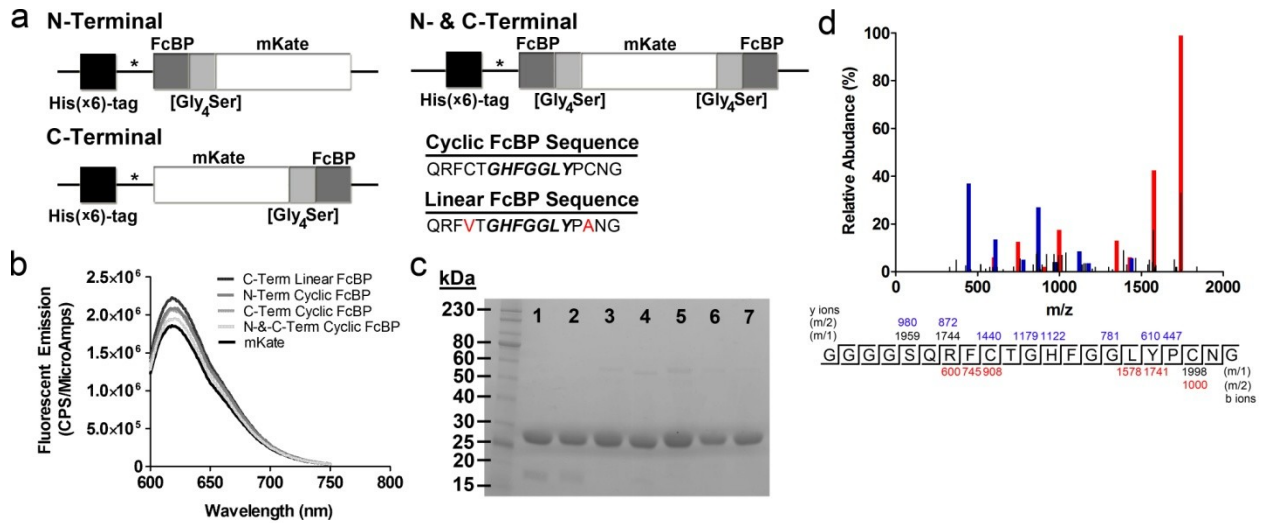


Figure 2.1 Construction and characterization of FcBP modified mKate's.

(a) Diagram of the gene sequences encoding mKate modified at its N- and/or C-terminus with a cyclic or linear FcBP sequence. (b) Fluorescence emission spectra comparing equal molar concentrations (500 nM) of mKate (black line) and FcBP modified mKates (grey lines). (c) SDS-PAGE analysis of purified mKate (lane 1), C-Term Linear FcBP mKate (lane 2), C-Term Cyclic FcBP mKate (lane 3), N-Term Cyclic FcBP mKate (lane 4), N-&-C-Term Cyclic FcBP mKate (lane 5), N-&-C-Term Cyclic FcBP mKate Y286H (lane 6), and N-Linear & C-Cyclic FcBP mKate (lane 7). 7.5 ug of protein was loaded in each lane. (d) LC MS/MS identification of the peptide containing the Gly₄Ser linker and cyclic FcBP sequence from a LysC digest of C-Term Cyclic FcBP mKate. The blue and red peaks correspond to the identified y and b ions, respectively, within the peptide sequence.

2.3.2 Binding kinetics between FcRn and FcBP modified mKates

We characterized the binding kinetics between FcBP modified mKate and human FcRn by surface plasmon resonance (SPR). The ability of FcRn to protect IgG from intracellular catabolism is based on two critical properties: pH-dependent binding and bivalency. The interaction between IgG and FcRn occurs at slightly acidic pH (< 6.5) with little to no binding at physiological pH. In addition, one IgG molecule contains two FcRn-binding sites allowing the formation of a 2:1 complex between FcRn and IgG²³. Both properties translate to more efficient binding, recycling, and transcytosis²² as well as a longer *in vivo* half-life of IgG²⁴ and are important considerations when engineering protein mimetics of the IgG:FcRn interaction. mKate modified with a cyclic FcBP at either its N- or C-terminus binds FcRn independent of FcBP orientation (N-to-C or C-to-N) with an affinity similar to that reported for the synthetic

FcBP²⁰, indicating that genetic fusion and recombinant expression does not alter its FcRn binding properties (Table 2.2). Modification of both the N- and C-termini of mKate (N-&-C-Term Cyclic FcBP mKate) results in an apparent affinity of 1023 nM, an ~11-fold increase over the single modified mKates, consistent with the role of avidity due to a bivalent interaction with FcRn. This affinity is comparable to that of hIgG1 at pH 6 ($K_D = 986$ nM by SPR). Unmodified mKate does not bind FcRn which confirms that binding to FcRn is mediated solely through the FcBP sequence.

We also engineered mKate modified at its C-terminus with a linearized FcBP to eliminate potential disulfide heterogeneity within the FcBP sequence. The C-Term Linear FcBP mKate bound FcRn similar to the C-Term Cyclic FcBP mKate indicating the disulfide is not a requirement for binding to FcRn (Table 2.2). In addition, a fusion bearing a N-terminal linear and C-terminal cyclic FcBP or N-&-C-terminal linear FcBP bound FcRn with an affinity close to that of N-&-C-Term Cyclic FcBP mKate at both pH 6 and pH 7.4 (Table 2.2).

At pH 7.4, binding of all FcBP modified mKates to FcRn is dramatically reduced compared to pH 6 demonstrating that FcBP fusion confers pH-dependent binding to FcRn (Table 2.2). However, unlike hIgG1 which has no detectable binding to FcRn at pH 7.4 under the conditions tested, binding of FcBP modified mKates is detectable by SPR at pH 7.4 (Fig. 2.2). Because of the low levels of binding, the K_D at pH 7.4 measured by SPR should be viewed as relative and used as a comparator, not as a true affinity.

Table 2.2 Binding kinetics to human FcRn and *in vitro* uptake of FcBP modified mKates and hIgG1 in FcRn expressing MDCK cells.

(*) Data were fit to a steady state affinity model for derivation of apparent K_D . SPR data are the mean of two independent experiments.

Molecule	FcBP Sequence	K_D (SPR)* pH 6, (nM)	K_D (SPR)* pH 7.4, (μ M)	$U_{1/2max}$ (FACS) pH 6, (nM)	$U_{1/2max}$ (FACS) pH 7.4, (μ M)
mKate	None	No binding	No binding	No binding	No binding
C-Term Linear FcBP	QRFVTGHHFGGLYPANG	9253	154	9230	> 200
C-Term Cyclic FcBP	QRFCTGHHFGGLYPCNG	14625	207	14417	> 200
N-Term Cyclic FcBP	QRFCTGHHFGGLYPCNG	11290	252	7077	> 200
N-&-C-Term Cyclic FcBP	QRFCTGHHFGGLYPCNG	1023	78	814	2.6
N-&-C-Term Cyclic FcBP (Y286H)	QRFCTGHHFGGLHPCNG	1480	> 1000	1529	21.2
N-Term Linear & C-Term Cyclic FcBP	N: QRFVTGHHFGGLYPANG C: QRFCTGHHFGGLYPCNG	1159	148	1440	2.1
N-&-C-Term Linear FcBP	QRFVTGHHFGGLYPANG	1210	99	1002	20.6
hIgG1	None	986	No binding	1267	No binding

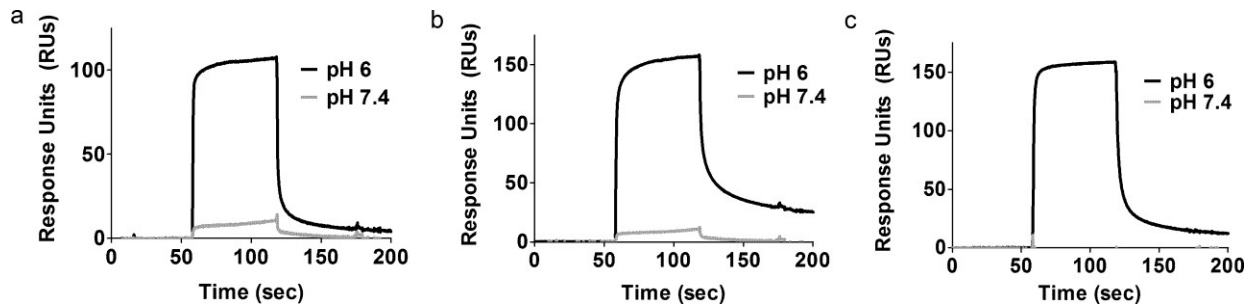


Figure 2.2 FcBP modified mKates exhibit pH dependent binding to hFcRn by SPR.

SPR sensograms of 12.5 μ M N-Term Cyclic FcBP mKate (a), 5 μ M N-&-C-Term Cyclic FcBP mKate (b), and 5 μ M hIgG1 (c) binding to hFcRn at pH 6 (black line) and pH 7.4 (grey line). FcBP modified mKates or hIgG1 was injected over immobilized hFcRn as described in Materials and Methods. FcRn immobilization density for the data shown is \sim 550 RU. All data were baseline adjusted and reference-cell subtracted.

2.3.3 Cellular accumulation of FcBP modified mKates by FACS

We quantitatively measured cellular accumulation of FcBP modified mKates in MDCK cells stably expressing hFcRn-EYFP/h β_2 m by FACS. Transfected MDCK cells have been widely used as an *in vitro* model for studying FcRn-mediated endocytosis, recycling, and transcytosis²⁵. The concentration at which half-maximal uptake ($U_{1/2max}$) occurs for each protein was determined by pulsing MDCK hFcRn-EYFP/h β_2 m cells with increasing concentrations of protein at either pH 6 or pH 7.4 and fitting the resulting data to a one-site total binding model in Prism (Fig. 2.3). The $U_{1/2max}$ values at pH 6 and pH 7.4 correlate with affinity measurements by SPR (Table 2.2). N-&-C-Term Cyclic FcBP mKate and hIgG1 have a similar $U_{1/2max}$ of 814 nM and 1267 nM, respectively, at pH 6. Taken together with binding affinities measured by SPR, this data demonstrate that mKate modified at both its N- and C-terminus with the cyclic FcBP sequence mimics the IgG:FcRn interaction at pH 6. Cellular accumulation of FcBP modified mKates and labeled hIgG1 is significantly reduced ($P < 0.001$) when co-incubated with excess unlabeled hIgG1 or when incubated at pH 7.4 (Fig. 2.3b), and accumulation in MDCK h β_2 m, wild type MDCK, and the murine melanoma cell line B16F10 was negligible due to the absence of human FcRn in these cells (Fig. 2.4).

Since the fluorescent intensity of mKate is pH dependent¹⁶ we also determine the mean fluorescent intensity (MFI) of mKate in cells in which we clamped the pH at 4.0, 5.0, and 7.4. There is no difference in MFI between mKate pulsed cells clamped at pH 7.4 compared to cells without ionophore treatment indicating that the small amount of internalized mKate is not underestimated due to accumulation in low pH compartments and subsequent loss of fluorescence (Fig. 2.5). An increase in MFI was observed in N-&-C-Term Cyclic FcBP mKate pulsed cells clamped at pH 7.4 compared to cells without ionophore treatment (Fig. 2.5). N-&-

C-Term Cyclic FcBP mKate is predominantly localized to FcRn-containing endosomes with an expected pH of ~ 6 ; therefore, the increase in MFI is consistent with the pH-dependent increase in mKate fluorescence as the pH of the cellular compartments is adjusted to 7.4. Collectively, these FACS data indicate that FcBP modified mKates interact specifically with FcRn which facilitates uptake through a FcRn-mediated endocytosis process and is not distorted by non-specific uptake of the mKate portion of the fusion protein in MDCK hFcRn-EYFP/h β_2 m cells.

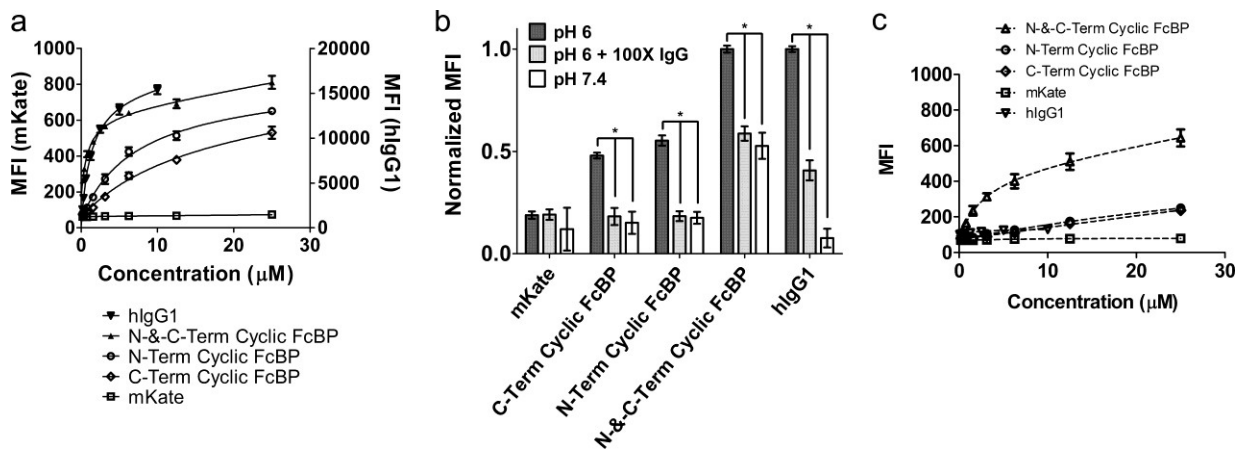


Figure 2.3 *In vitro* characterization of FcBP modified mKates in MDCK cells expressing hFcRn-EYFP by FACS.

(a) Cellular accumulation of FcBP modified mKates and labeled hlgG1 at pH 6 in MDCK hFcRn-EYFP/h β_2 m cells. Solid lines represent data fit to a one-site total binding model in Prism. MFI, mean fluorescent intensity, for mKates and hlgG1 is shown on left and right axes, respectively. (b) Cellular accumulation of FcBP modified mKates and labeled hlgG1 at pH 6 in the presence of 100 mol excess unlabeled hlgG or at pH 7.4. Cells were incubated with 2.5 μ M mKate, 2.5 μ M mKates modified with a single FcBP, 1 μ M N-&-C-Term Cyclic FcBP mKate, or 1 μ M labeled hlgG1 with or without 100 mol excess unlabeled hlgG1 as a competitor. The MFI for modified and unmodified mKates was normalized to the maximum MFI for N-&-C-Term Cyclic FcBP mKate. hlgG1 was normalized to itself given that the fluorescent intensity between the two fluorophores (mKate and TAMRA) are different. * indicates significance with $P < 0.001$. (c) Cellular accumulation of FcBP modified mKates and labeled hlgG1 at pH 7.4 in MDCK hFcRn-EYFP/h β_2 m cells. Dashed lines represent data fit to a one-site total binding model in Prism. The data shown in each panel are the mean ($n=3$) and error bars indicate s.d.

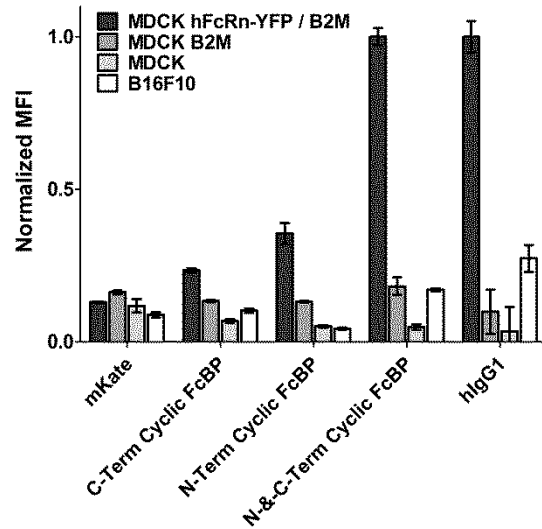


Figure 2.4 Cellular accumulation of FcBP modified mKates in various cell lines.

Cells were pulsed with 1.5 μ M of the specified protein for 1 hr at pH 6 and 37 $^{\circ}$ C, washed, trypsinized, and analyzed for cellular accumulation by FACS. The MFI, mean fluorescent intensity, for modified and unmodified mKates was normalized to the maximum MFI for N-&-C-Term Cyclic FcBP mKate. hIgG1 was normalized to itself given that the fluorescent intensity between the two fluorophores (mKate and TAMRA) are different.

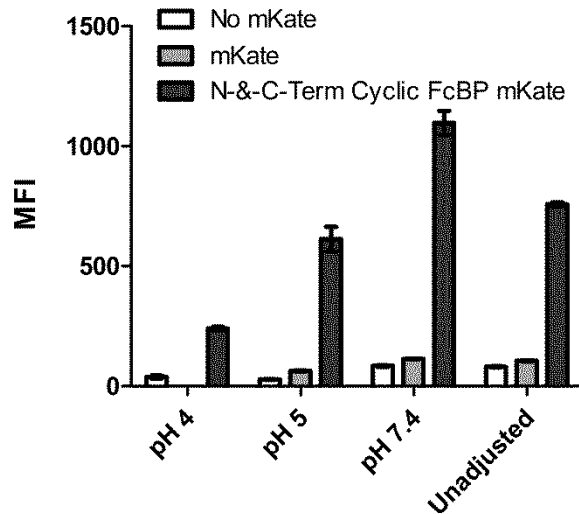


Figure 2.5 Influence of pH clamping of MDCK hFcRn-EYFP/hB2M cells at pH 4, 5, or 7.4 on cell associated mKate fluorescence.

Cells were pulsed with 25 μ M mKate or 2.5 μ M N-&-C-Term Cyclic FcBP mKate for 1 hr at pH 6 and 37 $^{\circ}$ C, washed, trypsinized, and the intracellular pH was clamped to either pH 4, 5, or 7.4 as described in section 2.2.11. The data shown are the mean (n=3) and error bars indicate s.d. MFI, mean fluorescent intensity.

2.3.4 Fluorescence imaging of FcBP modified mKates

To further understand the fate of FcBP fusion proteins after internalization we used fluorescence imaging as well as *in vitro* assays to evaluate FcRn-mediated transport and recycling. The ability of FcRn to salvage protein cargo, particularly IgG, from catabolism initiates in the early endosome²⁶, where the acidic environment promotes binding to FcRn. FcRn-bound proteins are subsequently trafficked away from the lysosomal pathway²⁶ and back to the plasma membrane²⁷ where the elevated extracellular pH results in dissociation from FcRn. Similar to hIgG1, FcBP modified mKates reside primarily in punctate, endosomal compartments and extensively co-localize with FcRn-EYFP in MDCK cells (Fig. 2.6a and Fig. 2.7). N-&-C-Term Cyclic FcBP mKate is predominately excluded from lysosomal compartments labeled with either the lysosomal associated membrane protein 1 (LAMP1) or the lysosomal pathway marker dextran (Fig. 2.6b); however, due to the pH dependent fluorescence of mKate¹⁶ we cannot exclude the possibility that some lysosomal accumulation occurs but is undetectable due to lysosomal degradation or the reduction of mKate fluorescence in low pH environments (pH <5). N-&-C-Term Cyclic FcBP mKate not only co-localizes with FcRn-EYFP compartments, but is also trafficked by FcRn-EYFP in a dynamic fashion. A number of well characterized FcRn-IgG intracellular sorting events²⁸ are observed between N-&-C-Term Cyclic FcBP mKate and FcRn-EYFP including: full endosomal fusion, vesicle budding, and tubule-mediated transfers (Fig. 2.8), suggesting that the cellular processing of FcBP modified cargo has a fate similar to IgG.

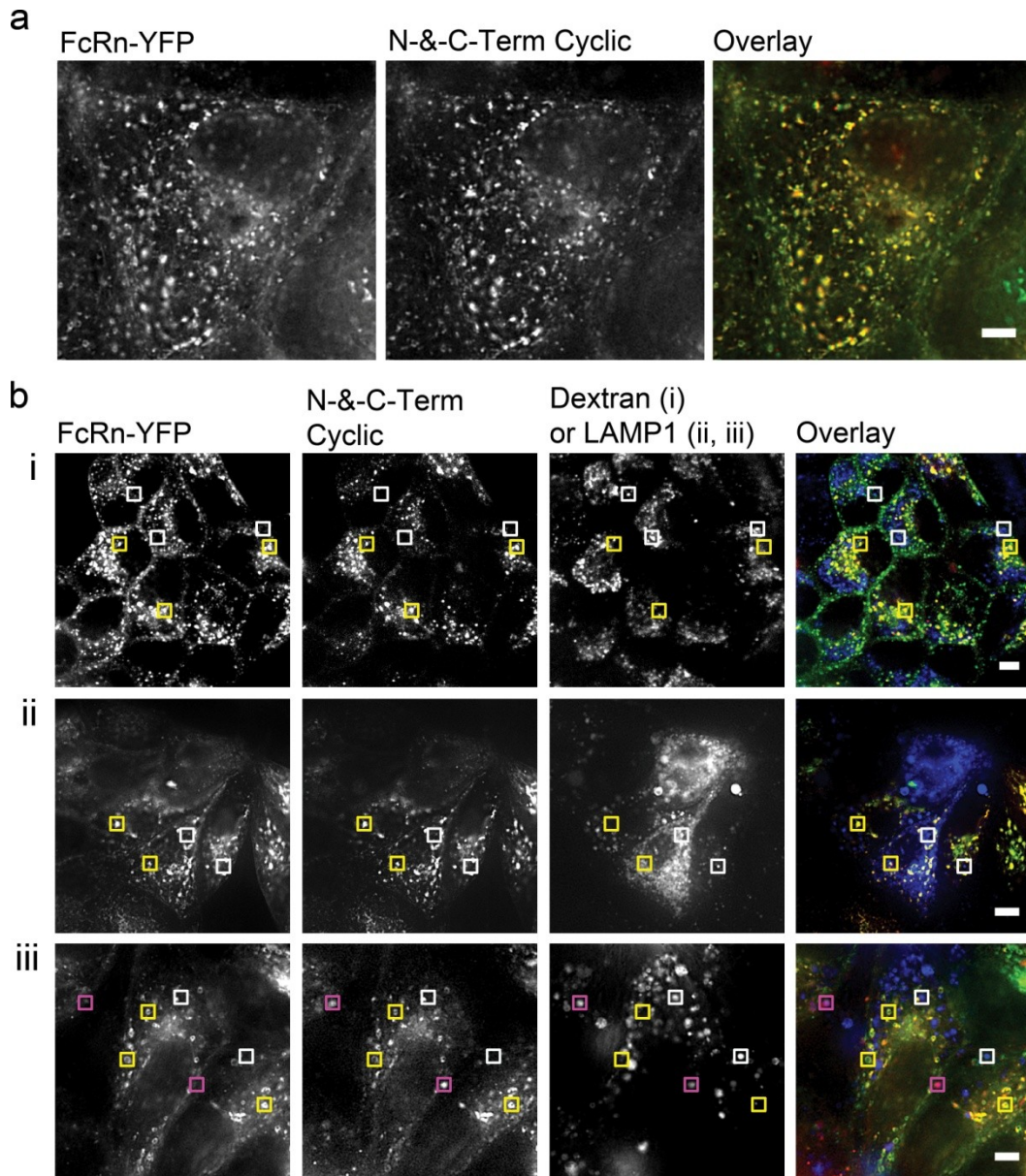


Figure 2.6 Fluorescence Imaging of FcBP modified mKates in MDCK cells expressing hFcRn-EYFP.

(a) Widefield epifluorescence image of N-&-C-Term Cyclic FcBP mKate co-localization with hFcRn-EYFP in MDCK cells. Scale bar, 5 μm . (b) (i) Confocal images of MDCK hFcRn-EYFP/h $\beta_2\text{m}$ cells showing the distribution of hFcRn-EYFP, N-&-C-Term Cyclic FcBP mKate, and 10 kDa Dextran. (ii,iii) Widefield epifluorescence images of MDCK hFcRn-EYFP/h $\beta_2\text{m}$ cells showing the distribution of hFcRn-EYFP, N-&-C-Term Cyclic FcBP mKate, and LAMP1-mTourquoise after a 1 hr (ii) or 4 hr (iii) chase at 37 $^{\circ}\text{C}$ in HBSS, pH 7.4 prior to imaging. Yellow boxes indicate areas of co-localization between N-&-C-Term Cyclic FcBP mKate and FcRn-EYFP, white boxes indicate LAMP1-mTourquoise compartments that do not contain N-&-C-Term Cyclic FcBP mKate or FcRn-EYFP, and pink boxes indicate areas of co-localization between N-&-C-Term Cyclic FcBP mKate and LAMP1-mTourquoise. Scale bar, (i) 10 μm ; (ii,iii) 5 μm . The overlays are pseudocolored as follows: Green = hFcRn-EYFP, Red = N-&-C-Term Cyclic FcBP mKate, Blue = Dextran or LAMP1-mTourquoise, Yellow indicates co-localization between FcRn and N-&-C-Term Cyclic FcBP mKate, Pink indicates co-localization between N-&-C-Term Cyclic FcBP mKate and LAMP1.

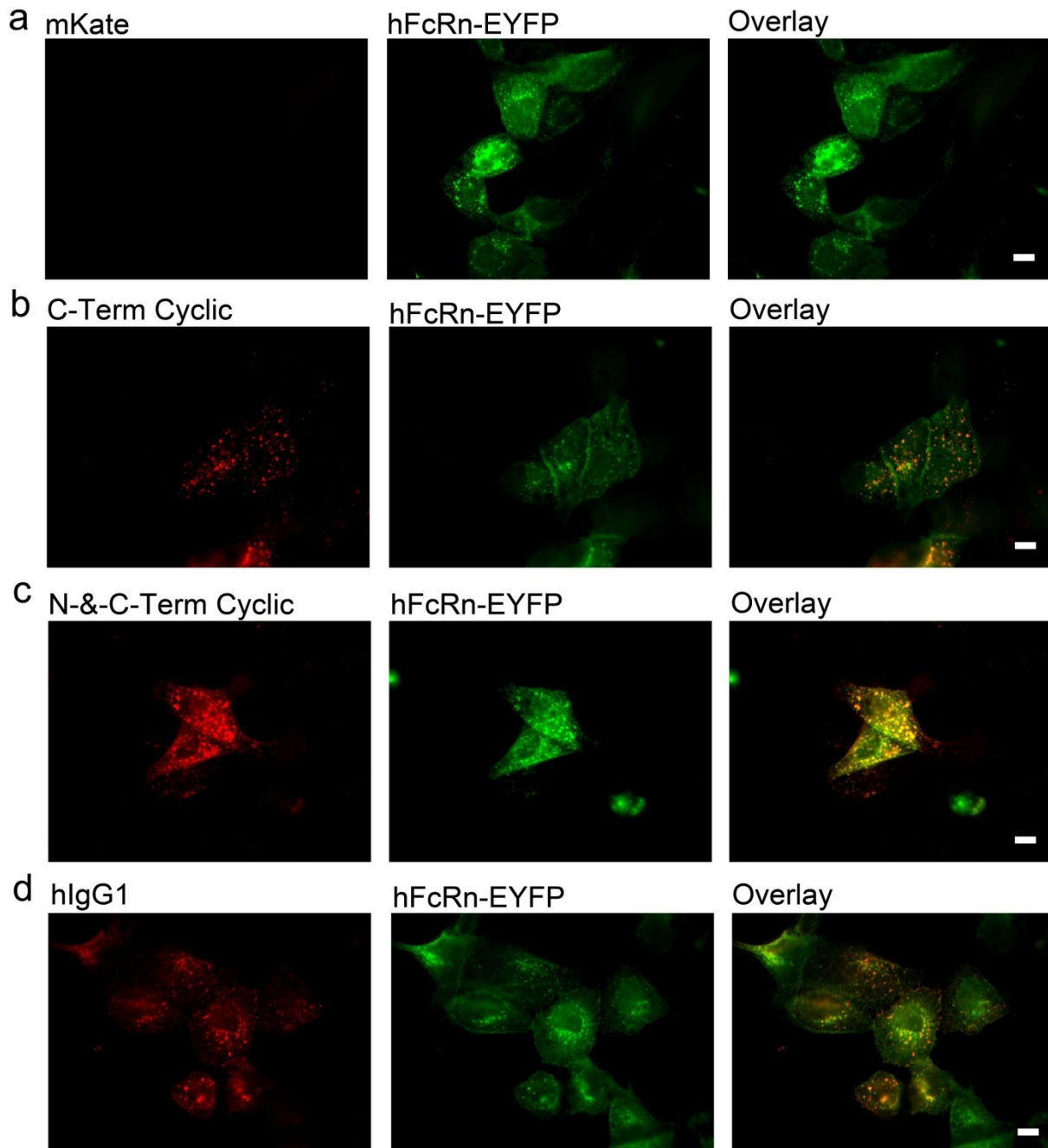


Figure 2.7 Cyclic FcBP modified mKate's colocalize with hFcRn-EYFP in MDCK cells.

Uptake of 5 μM mKate (a), 5 μM C-Term Cyclic FcBP mKate (b), 1 μM N-&-C-Term Cyclic FcBP mKate (c), or 1 μM Alexa-labeled hIgG1 (d) by MDCK cells transfected with hFcRn-EYFP and $\beta 2\text{m}$ at 37 $^{\circ}\text{C}$. Cells were pulsed for 1 hr with protein at pH 6, washed, fixed and imaged. The same imaging and processing conditions were used for all images. mKates and Alexa-labeled hIgG1 are pseudocolored in red and hFcRn-EYFP in green. Yellow indicates co-localization between mKates (red) and hFcRn (green). Scale bars, 10 μm .

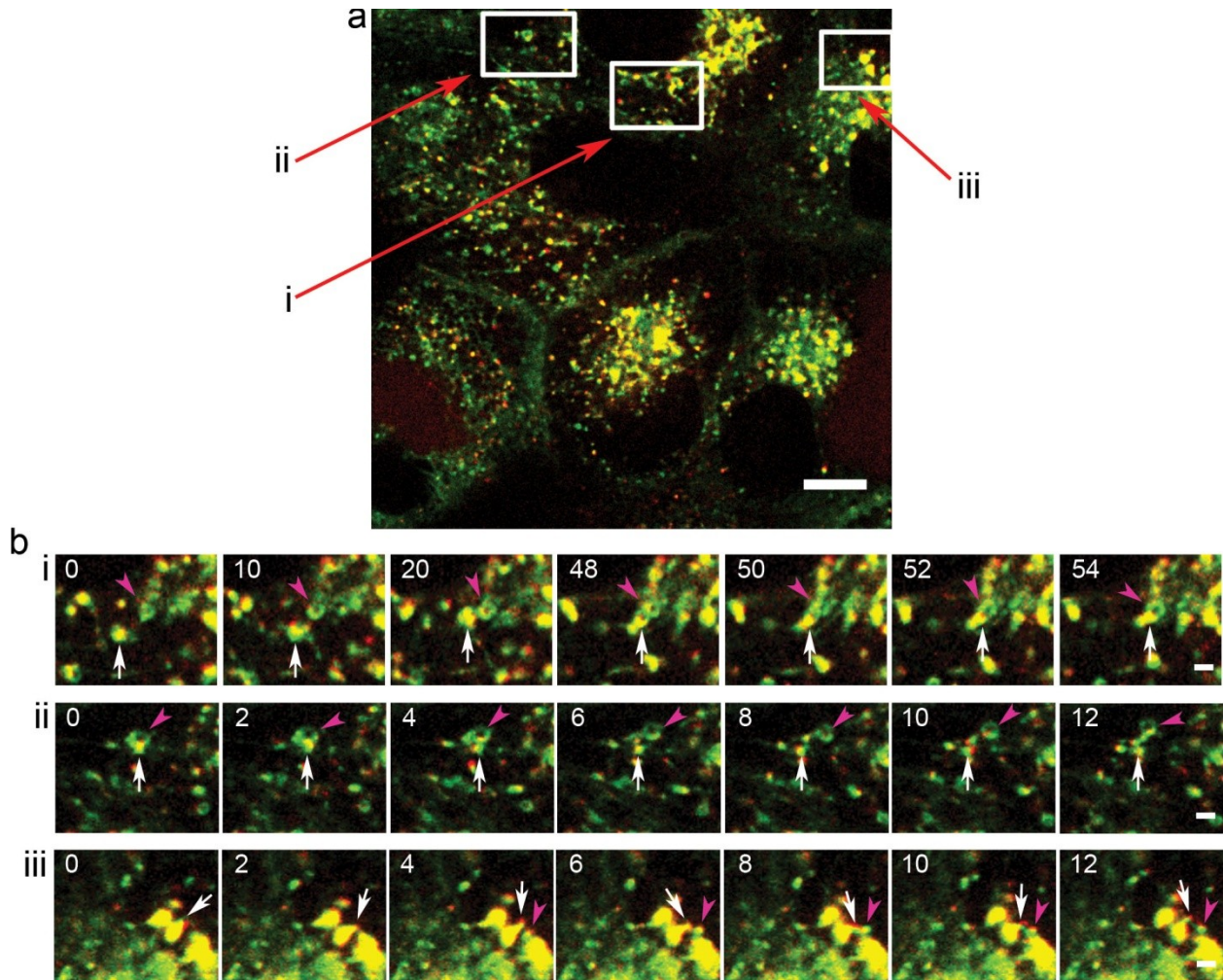


Figure 2.8 N-&-C-Term Cyclic FcBP mKate is trafficked by hFcRn-EYFP in MDCK cells. MDCK hFcRn-EYFP/h β_2 m cells were pulsed with 1 μ M of N-&-C-Term cyclic FcBP mKate for 1 hr at 37 $^{\circ}$ C and pH 6, washed, and imaged immediately on a stage preheated to 37 $^{\circ}$ C. (a) Full size confocal image depicting areas presented as cropped images in (b, i-iii). (b) Confocal images depicting (i) endosomal fusion, (ii) vesicle budding, and (iii) tubule-mediated transfer events. The arrow in (i) marks a FcRn-YFP and N-&-C-Term Cyclic FcBP mKate positive compartment that eventually fuses with the FcRn-YFP positive vesicle marked by the pink arrowhead. The arrow in (ii) marks a subset of an endosomal vesicle (pink arrowhead) that eventually buds and trafficks away from the parent FcRn-YFP positive vesicle (pink arrowhead). The arrow in (iii) marks a FcRn-YFP and N-&-C-Term Cyclic FcBP mKate positive compartment in which a tubule rapidly extends, makes contact with another FcRn-YFP compartment (pink arrowhead), and retracts. Time, in seconds, of each frame relative to the first frame is shown in the top left corner of each image. Images were pseudocolored such that FcRn-YFP is depicted in green, N-&-C-Term Cyclic FcBP mKate in red, and yellow indicates co-localization of FcRn-YFP and N-&-C-Term Cyclic FcBP mKate. Scale bars, 10 μ m.

2.3.5 Recycling from FcRn expressing MDCK cells

To assess recycling, MDCK hFcRn-EYFP/h β_2 m cells were pulsed with proteins at pH 6 to promote FcRn-dependent internalization of the protein cargo. After removal of non-internalized protein, recycling was determined by measuring the amount of protein returned to the culture medium after a 2 hr chase at 37 °C. FcBP modified mKates are recycled by FcRn in MDCK hFcRn-EYFP/h β_2 m cells and the amount of recycled protein increases with increasing affinity to FcRn (Fig. 2.9a). Recycling is significantly reduced when incubated at 4 °C ($P < 0.001$) confirming the role of an energy dependent recycling process. Similarly, recycling is significantly reduced ($P < 0.001$) when pulsed with protein at pH 7.4, a pH that does not favor FcRn-mediated internalization. We also evaluated recycling in MDCK h β_2 m cells, which lack FcRn, and found that in all cases the amount of protein recycled is significantly reduced ($P < 0.001$) when compared to recycling from MDCK hFcRn-EYFP/h β_2 m cells.

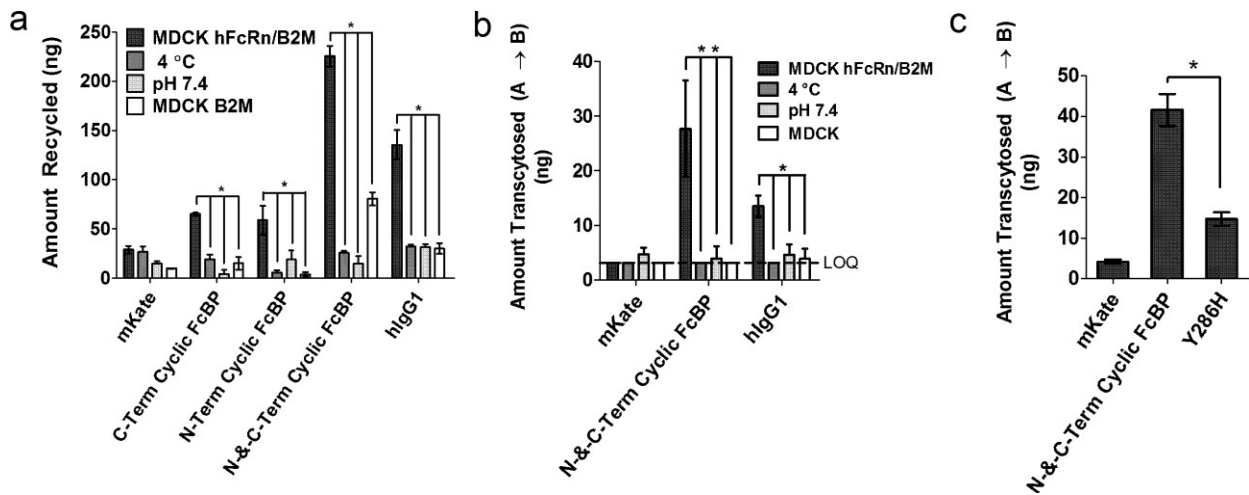


Figure 2.9 FcBP fusion enables FcRn-mediated recycling and transcytosis.

(a) *In vitro* FcRn-mediated recycling from MDCK hFcRn-EYFP/h β_2 m cells. * indicates significance with $P < 0.001$. (b) *In vitro* FcRn-mediated transcytosis across MDCK hFcRn-EYFP/h β_2 m or wild type MDCK cell monolayers grown on Transwell inserts. The data shown are the amount of protein transported to the basolateral compartment after a 2 hr continuous incubation with 2.5 μ M mKate or FcBP modified mKates, and 1 μ M labeled-hlgG1 in the apical compartment. The apical chamber was equilibrated to pH 6, unless noted, and the basolateral to pH 7.4 in all cases. ** indicates that transcytosis is statistically significant between the specified groups, with $P < 0.001$. * indicates significance with $P <$

0.01. Transport below the limit of quantification (LOQ) is indicated by the dashed line at 3.1 ng. (c) Transcytosis of 5 μ M mKate or FcBP modified mKates in the apical to basolateral direction after a 5 hr continuous incubation at 37 °C with both compartments equilibrated to pH 7.4. * indicates significance with $P < 0.001$. The data shown for each panel are the mean (n=3) and error bars indicate s.d.

2.3.6 Transcytosis across FcRn expressing MDCK cell monolayers

Unlike small molecule drugs, proteins and other large macromolecules are unable to passively cross epithelial barriers due to their large size and hydrophilicity. Therefore, for proteins to penetrate epithelial barriers, without disrupting tight junctions, they must be actively transported. FcRn actively transports endogenous IgG across epithelial barriers in the gut and lung. We predicted that FcRn can be hijacked by alternative FcRn-binding cargo, such as FcBP fusion proteins, to enable epithelial transcytosis. N-&-C-Term Cyclic FcBP mKate and hIgG1 are transported from the apical-to-basolateral compartment by FcRn expressed in MDCK hFcRn-EYFP/h β_2 m cells, whereas unmodified mKate is unable to cross the MDCK cell barrier (Fig. 2.9b). Transcytosis of N-&-C-Term Cyclic FcBP mKate across MDCK hFcRn-EYFP/h β_2 m cells is dose-dependent, indicating a FcRn-dependent transcytosis process (Fig. 2.10a). Transcytosis of all proteins across MDCK cells lacking FcRn is undetectable indicating that FcRn is necessary to deliver proteins across the MDCK epithelial cell barrier. Transport of the paracellular probe FITC-inulin was similar across transwells (Fig. 2.10b), indicating the formation of a tight, uniform barrier between the apical and basolateral chambers and that differences in transport between proteins were mediated by FcRn.

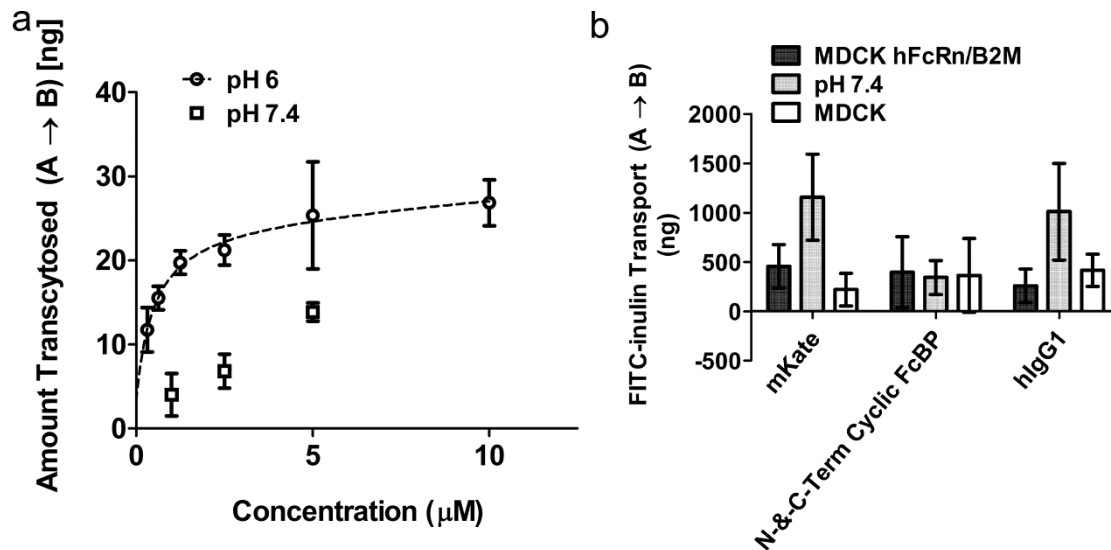


Figure 2.10 Dose-dependent transcytosis of N-&C-Term Cyclic FcBP mKate and transport of FITC-inulin across MDCK hFcRn/hB2M cell monolayers.

(a) Transcytosis of N-&C-Term Cyclic FcBP mKate in the apical to basolateral direction after a 2 hr continuous incubation with increasing concentrations of protein in the apical chamber equilibrated to either pH 6 or pH 7.4. The basolateral chamber was equilibrated to pH 7.4 in both cases. The data shown for each panel are the mean (n=3) and error bars indicate s.d. The dashed line represents a curve fit to a one-site total binding model in Prism. (b) The paracellular transport probe FITC-inulin (4 μg/mL) was co-incubated with each protein during transcytosis experiments in figure 2.9 to ensure the integrity of cell monolayers across transwells. The amount of FITC-inulin transported is similar across transwells indicating that differences in protein transport is not due to defects in the cell monolayer. The data shown are mean (n=3) and error bars indicate s.d.

2.3.7 FcRn-mediated Recycling versus Transcytosis in MDCK hFcRn-EYFP/hβ₂m cell monolayers

FcRn-mediated transport of IgG across polarized cell monolayers is bidirectional both *in vitro*^{29,30} and *in vivo*^{14,31,32}; however, the fraction of FcBP modified proteins recycled or transcytosed by FcRn is unknown. Therefore, we determined the fractional recycling and transcytosis of IgG, FcBP modified mKates, and transferrin in MDCK FcRn-EYFP/hβ₂m cells. FcBP modified mKates and hIgG1 are recycled and transcytosed by FcRn to a similar degree whereas unmodified mKate is not detected in any fraction (Fig. 2.11a), indicating that recycling and transcytosis is dependent on a productive interaction with FcRn. Transferrin on the other hand is predominately recycled from MDCK hFcRn-EYFP/hβ₂m cells in agreement with the

function of the transferrin receptor as a classical recycling receptor³³. A small fraction of transferrin is transcytosed; however, with a dramatically reduced efficiency compared to recycled transferrin. All ligands are predominantly intracellular after a 37 °C pulse and 4 °C chase confirming the role of an energy dependent recycling and transcytosis process (Fig. 2.11b). Collectively, the data indicate that FcRn acts as a bidirectional transporter in MDCK hFcRn-EYFP/h β 2m cells and the relative fraction of recycling versus transcytosis is similar between hIgG1 and FcBP modified mKates.

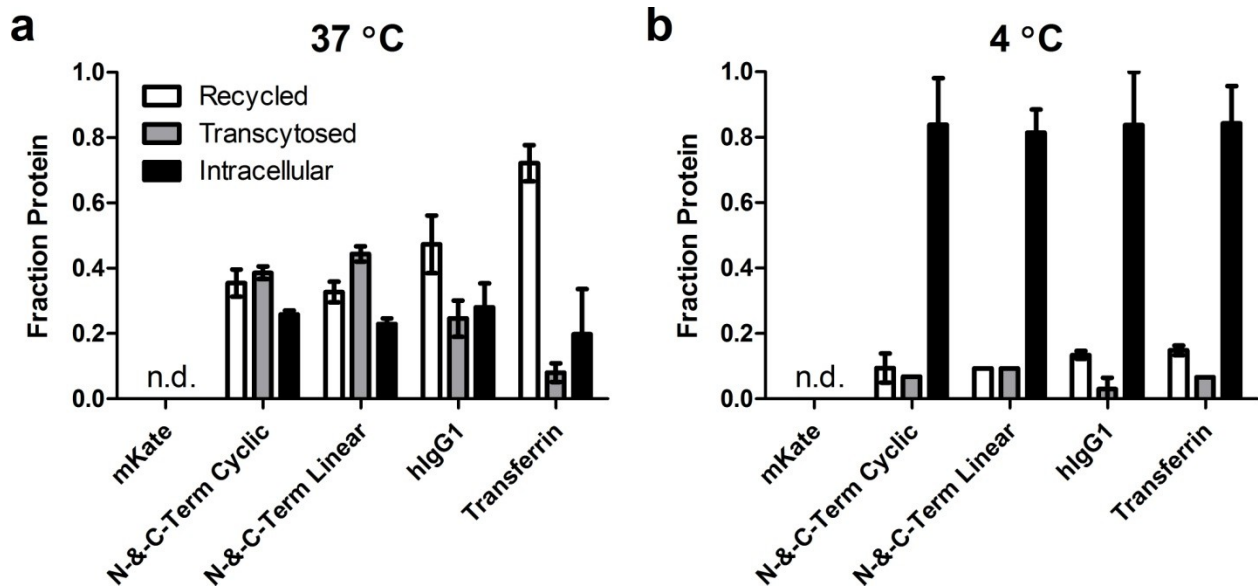


Figure 2.11 Recycling versus transcytosis of FcBP modified mKates, hIgG1, and transferrin in MDCK MDCK hFcRn/h β 2M cell monolayers.

Recycling versus transcytosis of mKate, FcBP modified mKates, hIgG1, and transferrin in MDCK hFcRn-EYFP/h β 2M cells after a 1 hr apical pulse at 37 °C, pH 6 followed by a 4 hr apical and basolateral chase at pH 7.4 and either 37 °C (a) or 4 °C (b). The amount of protein returned to the apical compartment (recycled), delivered to the basolateral compartment (transcytosed) or that remained intracellular was determined as described in section 2.2.14. The data shown are mean (n=3) and error bars indicate s.d.

2.3.8 Tyr12 to His FcBP mutant with altered affinity for FcRn

Using a rational design approach we identified a simple point mutation (Tyr-12 to His) in the FcBP sequence that improves pH-dependent binding to human FcRn (Table 2.2 and Fig. 2.12). Based on the crystal structure³⁴, the phenolic hydroxyl of Tyr-12 in the FcBP sequence makes an end-on-end hydrogen bond with Tyr-88 of FcRn, an interaction that likely contributes to binding at pH 7.4. We tested if mutation of Tyr-12 to His eliminates this hydrogen bond and creates a pH-dependent salt bridge between His and the nearby Glu-133 of FcRn (Fig. 2.12b). Indeed, mutation of the C-terminal FcBP Tyr to His of N-&-C-Term Cyclic FcBP mKate (Y286H variant) retains affinity and half-maximal uptake at pH 6 with little to no binding or cellular accumulation at pH 7.4 (Table 2.2 and Fig. 2.12c). We also evaluated the transport of the Y286H variant across MDCK hFcRn-EYFP/h β_2 m cell monolayers with both the apical and basolateral chambers equilibrated to pH 7.4, conditions that are more representative of the lung air and interstitial space. Significantly more ($P < 0.001$) N-&-C-Term Cyclic FcBP mKate was transported across the MDCK hFcRn-EYFP/h β_2 m cell monolayer compared to the Y286H variant (Fig. 2.9c). These findings support the hypothesis that low to moderate affinity at pH 7.4 for FcRn promotes transport across epithelial cell monolayers and may enhance systemic accumulation of pulmonary administered FcBP fusion proteins.

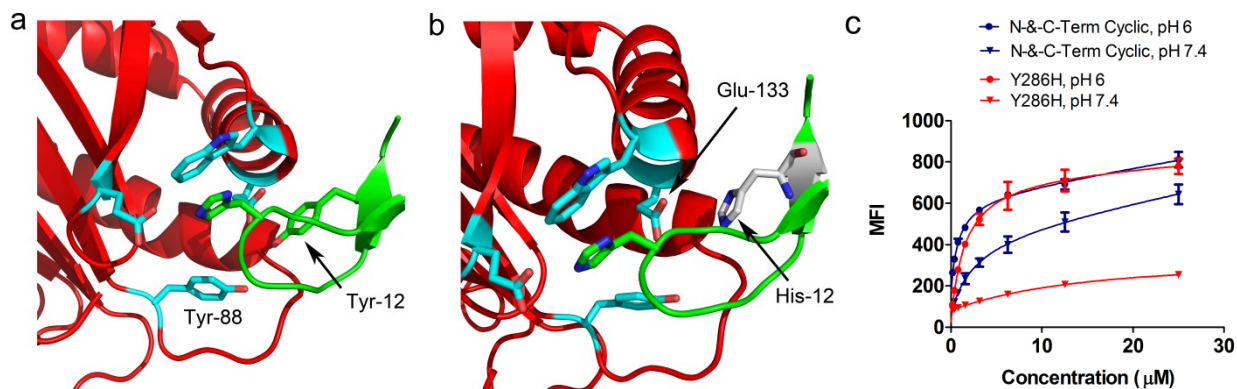


Figure 2.12 Tyr-12 to His mutation of the Cyclic FcBP improved pH dependent binding to hFcRn.

(a) Crystal structure of the cyclic FcBP (green) in complex with hFcRn (red backbone and blue side chains). (b) Crystal structure of the cyclic FcBP in complex with hFcRn showing the Tyr-12 to His mutation and its proximity to Glu-133 of hFcRn. The images in a,b were generated from the published crystal structure³⁴ using PyMOL (PDB # 3M17). (c) Cellular accumulation of N-&-C-Term Cyclic FcBP mKate (blue) and N-&-C-Term Cyclic FcBP mKate Y286H mutant (red) showing reduced accumulation in MDCK hFcRn-EYFP/h β_2 m cells at pH 7.4 with no effect on accumulation at pH 6. Cells were pulsed with increasing concentrations of protein for 1 hr at 37 °C, washed, trypsinized, and analyzed by FACS. The data shown are the mean (n=3) and error bars indicate s.d. Solid lines represent curve fit to a one-site total binding model in Prism. MFI, mean fluorescent intensity.

2.4 Conclusions

In this chapter, we demonstrate that proteins can be engineered to interact with FcRn by recombinant fusion of a short FcBP sequence at a proteins N- and/or C-terminus. This strategy is to our knowledge the only report of proteins engineered to interact with FcRn from non-Fc or albumin domains. Our strategy was motivated by results of Mezo and colleagues²⁰ who identified and engineered peptides that compete with IgG for binding to FcRn as potential therapeutics for the treatment of IgG-mediated autoimmune disease. We built upon the Mezo approach and hypothesized that the phage identified peptide sequence would be an ideal ligand for genetically engineering proteins to interact with FcRn for a number of reasons. First, the identified FcBPs exhibited binding to FcRn at pH 6 with a significant reduction in binding at pH 7.4, a critical property for FcRn-mediated protection from lysosomal degradation. Second, peptide dimerization resulted in a dramatic increase in affinity, which based on the crystal

structure was due to avidity from a 2:1 interaction with FcRn³⁴. Third, the small size and simple structure of the FcBP would enable expression of FcBP fusions in *E. coli*. Finally, a recombinant peptide tag that improves protein pharmacokinetics and delivery may overcome limitations associated with protein-polymer conjugates and Fc- or albumin fusion, which significantly increases molecular weight and decreases biological activity and tissue penetration.

A family of FcBP fusion proteins were engineered and characterized using molecular and cell-based assays. FcBP fusion at the N- and/or C-terminus of mKate results in a pH dependent interaction with FcRn that is modulated by altering the FcBP sequence or number of FcBPs fused to the protein. A majority of FcRn binding and trafficking properties are similar between IgG and FcBP fusions; however, a difference occurs at pH 7.4. IgG has no appreciable FcRn-mediated cellular accumulation in FcRn expressing MDCK cells at pH 7.4 or detectable binding by SPR, whereas significant accumulation and binding of N-&-C-Term Cyclic FcBP mKate occurs. Therefore, we rationally designed a Y286H variant of N-&-C-Term Cyclic FcBP mKate with negligible binding to FcRn at pH 7.4 to probe the role of affinity at pH 7.4 on FcRn transport.

There have been a number of reports on the relationship between affinity for FcRn at physiological pH and *in vivo* circulation time³⁵⁻³⁷. In general, variant IgGs with appreciable affinity for FcRn at physiological pH have reduced circulation time and increased clearance compared to wild type IgG, likely due to catabolism of variant IgGs that do not dissociate from FcRn during receptor turnover. However, moderate affinity for FcRn at pH 7.4 may be advantageous for low molecular weight proteins that exhibit rapid renal clearance. This affinity may promote salvage of FcBP fusion proteins by FcRn expressed in renal proximal tubule cells³⁸ resulting in re-absorption of intact protein filtered through the glomerulus. Similarly, moderate

affinity at physiological pH may improve absorption of FcBP fusion proteins from the lung airway by FcRn expressed on the apical surface of bronchial epithelial cells¹². Indeed, we found that N-&-C-Term Cyclic FcBP mKate was transported to a greater extent than the Y286H variant across FcRn expressing MDCK cell monolayers. Additional modifications that generate FcBP fusion proteins with differential FcRn binding properties will provide interesting tools to further probe the biology of FcRn related to protein drug delivery.

In summary, our results demonstrate proteins can be engineered to interact with FcRn from non-IgG domains based on a simple recombinant fusion to a small polypeptide resulting in protein mimetics of the IgG:FcRn interaction. These findings suggest that FcBP fusion may be an effective strategy to improve protein pharmacokinetics and/or delivery that is applicable to a wide-range of rapidly eliminated protein therapeutics, such as a number of clinically relevant cytokines (IFN α 2, IFN γ , TSG-6), hormones (hGH), and growth factors (EPO, GCSF-3) whose termini are not involved in receptor binding³⁹, or next generation protein therapeutics including small antibody fragment and engineered protein scaffolds, although additional *in vivo* studies are necessary to fully realize the potential of the FcBP fusion platform. In addition, this strategy may be applicable to alternative systems including liposomes, polymers, dendrimers, nucleic acids, or small molecules as a means to improve drug delivery by targeting FcRn.

2.5 References

1. Kontermann, R. E. Strategies for extended serum half-life of protein therapeutics. *Curr. Opin. Biotechnol.* **22**, 868–76 (2011).
2. Wang, W., Wang, E. Q. & Balthasar, J. P. Monoclonal antibody pharmacokinetics and pharmacodynamics. *Clin. Pharmacol. Ther.* **84**, 548–58 (2008).
3. Roopenian, D. C. & Akilesh, S. FcRn: the neonatal Fc receptor comes of age. *Nat. Rev. Immunol.* **7**, 715–725 (2007).
4. Abuchowski, A., McCoy, J. R., Palczuk, N. C., van Es, T. & Davis, F. F. Effect of covalent attachment of polyethylene glycol on immunogenicity and circulating life of bovine liver catalase. *J. Biol. Chem.* **252**, 3582–3586 (1977).
5. Alconcel, S. N. S., Baas, A. S. & Maynard, H. D. FDA-approved poly(ethylene glycol)–protein conjugate drugs. *Polym. Chem.* **2**, 1442 (2011).
6. Gao, W., Liu, W., Christensen, T., Zalutsky, M. R. & Chilkoti, A. In situ growth of a PEG-like polymer from the C terminus of an intein fusion protein improves pharmacokinetics and tumor accumulation. *Proc. Natl. Acad. Sci. U. S. A.* **107**, 16432–7 (2010).
7. Schellenberger, V. *et al.* A recombinant polypeptide extends the in vivo half-life of peptides and proteins in a tunable manner. *Nat. Biotechnol.* **27**, 1186–90 (2009).
8. Vallee, S. *et al.* Pulmonary Administration of Interferon Beta-1a-Fc Fusion Protein in Non-Human Primates Using an Immunoglobulin Transport Pathway. *J. Interferon Cytokine Res.* **32**, 178–84 (2011).
9. Gong, R., Wang, Y., Feng, Y., Zhao, Q. & Dimitrov, D. S. Shortened engineered human antibody CH2 domains: increased stability and binding to the human neonatal Fc receptor. *J. Biol. Chem.* **286**, 27288–93 (2011).
10. Ying, T., Chen, W., Gong, R., Feng, Y. & Dimitrov, D. S. Soluble Monomeric IgG1 Fc. *J. Biol. Chem.* **287**, 19399–408 (2012).
11. Andersen, J. T. *et al.* Extending half-life by indirect targeting of the neonatal Fc receptor (FcRn) using a minimal albumin binding domain. *J. Biol. Chem.* **286**, 5234–41 (2011).
12. Spiekermann, G. M. *et al.* Receptor-mediated Immunoglobulin G Transport Across Mucosal Barriers in Adult Life: Functional Expression of FcRn in the Mammalian Lung. *J. Exp. Med.* **196**, 303–310 (2002).
13. Amet, N., Wang, W. & Shen, W.-C. Human growth hormone-transferrin fusion protein for oral delivery in hypophysectomized rats. *J. Control. Release* **141**, 177–82 (2010).

14. Dumont, J. A. *et al.* Delivery of an erythropoietin-Fc fusion protein by inhalation in humans through an immunoglobulin transport pathway. *J Aerosol Med* **18**, 294–303 (2005).
15. Patton, J. S. & Byron, P. R. Inhaling medicines: delivering drugs to the body through the lungs. *Nat Rev Drug Discov* **6**, 67–74 (2007).
16. Shcherbo, D. *et al.* Bright far-red fluorescent protein for whole-body imaging. *Nat Methods* **4**, 741–746 (2007).
17. Platt, V. *et al.* Influence of multivalent nitrilotriacetic acid lipid-ligand affinity on the circulation half-life in mice of a liposome-attached His6-protein. *Bioconjug. Chem.* **21**, 892–902 (2010).
18. Eng, J. K., McCormack, A. L. & Yates, J. R. An approach to correlate tandem mass spectral data of peptides with amino acid sequences in a protein database. *J. Am. Soc. Mass Spectrom.* **5**, 976–989 (1994).
19. Tabb, D. L., McDonald, W. H. & Yates, J. R. DTASelect and Contrast: Tools for Assembling and Comparing Protein Identifications from Shotgun Proteomics. *J. Proteome Res.* **1**, 21–26 (2002).
20. Mezo, A. R. *et al.* Reduction of IgG in nonhuman primates by a peptide antagonist of the neonatal Fc receptor FcRn. *Proc. Natl. Acad. Sci. U. S. A.* **105**, 2337–42 (2008).
21. Sonawane, N. D., Szoka, F. C. & Verkman, A. S. Chloride accumulation and swelling in endosomes enhances DNA transfer by polyamine-DNA polyplexes. *J. Biol. Chem.* **278**, 44826–31 (2003).
22. Tesar, D. B., Tiangco, N. E. & Bjorkman, P. J. Ligand Valency Affects Transcytosis, Recycling and Intracellular Trafficking Mediated by the Neonatal Fc Receptor. *Traffic* **7**, 1127–1142 (2006).
23. West, A. P. & Bjorkman, P. J. Crystal Structure and Immunoglobulin G Binding Properties of the Human Major Histocompatibility Complex-Related Fc Receptor † , ‡. *Biochemistry* **39**, 9698–9708 (2000).
24. Kim, J. K., Tsen, M. F., Ghetie, V. & Ward, E. S. Catabolism of the murine IgG1 molecule: evidence that both CH2-CH3 domain interfaces are required for persistence of IgG1 in the circulation of mice. *Scand. J. Immunol.* **40**, 457–65 (1994).
25. Tesar, D. B. & Björkman, P. J. An intracellular traffic jam: Fc receptor-mediated transport of immunoglobulin G. *Curr. Opin. Struct. Biol.* **20**, 226–233 (2010).

26. Ober, R. J., Martinez, C., Vaccaro, C., Zhou, J. & Ward, E. S. Visualizing the Site and Dynamics of IgG Salvage by the MHC Class I-Related Receptor, FcRn. *J. Immunol.* **172**, 2021–2029 (2004).
27. Prabhat, P. *et al.* Elucidation of intracellular recycling pathways leading to exocytosis of the Fc receptor, FcRn, by using multifocal plane microscopy. *Proc. Natl. Acad. Sci.* **104**, 5889–5894 (2007).
28. Gan, Z., Ram, S., Vaccaro, C., Ober, R. J. & Ward, E. S. Analyses of the Recycling Receptor, FcRn, in Live Cells Reveal Novel Pathways for Lysosomal Delivery. *Traffic* **10**, 600–614 (2009).
29. Dickinson, B. L. *et al.* Bidirectional FcRn-dependent IgG transport in a polarized human intestinal epithelial cell line. *J Clin Invest* **104**, 903–911 (1999).
30. Claypool, S. M. *et al.* Bidirectional transepithelial IgG transport by a strongly polarized basolateral membrane Fcγ-receptor. *Mol Biol Cell* **15**, 1746–1759 (2004).
31. Bitonti, A. J. *et al.* Pulmonary delivery of an erythropoietin Fc fusion protein in non-human primates through an immunoglobulin transport pathway. *Proc. Natl. Acad. Sci.* **101**, 9763–9768 (2004).
32. Yoshida, M. *et al.* Human neonatal Fc receptor mediates transport of IgG into luminal secretions for delivery of antigens to mucosal dendritic cells. *Immunity* **20**, 769–83 (2004).
33. Cardone, M. H. Phorbol myristate acetate-mediated stimulation of transcytosis and apical recycling in MDCK cells. *J. Cell Biol.* **124**, 717–727 (1994).
34. Mezo, A. R., Sridhar, V., Badger, J., Sakorafas, P. & Nienaber, V. X-ray Crystal Structures of Monomeric and Dimeric Peptide Inhibitors in Complex with the Human Neonatal Fc Receptor, FcRn. *J. Biol. Chem.* **285**, 27694–27701 (2010).
35. Yeung, Y. A. *et al.* Engineering human IgG1 affinity to human neonatal Fc receptor: impact of affinity improvement on pharmacokinetics in primates. *J Immunol* **182**, 7663–7671 (2009).
36. Yeung, Y. A. *et al.* A therapeutic anti-VEGF antibody with increased potency independent of pharmacokinetic half-life. *Cancer Res.* **70**, 3269–77 (2010).
37. Acqua, W. F. D. *et al.* Increasing the Affinity of a Human IgG1 for the Neonatal Fc Receptor: Biological Consequences. *J. Immunol.* **169**, 5171–5180 (2002).
38. Kobayashi, N. *et al.* FcRn-mediated transcytosis of immunoglobulin G in human renal proximal tubular epithelial cells. *Am J Physiol Ren. Physiol* **282**, F358–65 (2002).

39. Wang, X., Lupardus, P., Laporte, S. L. & Garcia, K. C. Structural biology of shared cytokine receptors. *Annu. Rev. Immunol.* **27**, 29–60 (2009).

Chapter 3: Correlations between cross-species IgG and albumin binding to FcRn *in vitro* and plasma clearance *in vivo* validate the human FcRn transgenic mouse model

3.1 Introduction

The neonatal Fc receptor (FcRn) has the exceptional capacity to divert intracellular immunoglobulin G (IgG) and albumin from the lysosome, transport to the plasma membrane, and release IgG and albumin into the extracellular space. As a result, FcRn regulates the homeostasis of the two most abundant serum proteins and participates in a plethora of biological processes including pre- and postnatal immunity, immune surveillance at mucosal barriers, antigen presentation, and its most well known function in regulating the serum persistence of IgG and albumin^{1,2}. The mechanism by which FcRn carries out these diverse functions is based upon a pH-dependent interaction with the Fc-domain of IgG or albumin. Binding occurs at acidic pH (pH < 6), such as in the endosome, with rapid dissociation upon exposure to increased pH (pH > 7), such as in the blood or interstitial tissue space.

FcRn is structurally homologous to the MHC Class I heterodimeric receptor family³ consisting of a type I transmembrane heavy chain that non-covalently associates with the soluble light chain, β 2-microglobulin (β 2m). β 2m is absolutely necessary for the proper folding, transport, and function of FcRn, as well as other MHC Class I homologs, both *in vitro*⁴ and *in vivo*⁵⁻⁷. The pH dependence of the FcRn-IgG interaction is mediated by electrostatics between titratable histidine residues in the Fc C_H2-C_H3 domains and acidic residues on the α 2-domain of FcRn^{8,9} and is responsible for the extraordinarily long half-life of IgG in humans (~ 21 days) and mice^{6,10}.

In addition to IgG, albumin binds FcRn through a series of pH-dependent ionic interactions

between conserved histidine and glutamic acid residues located within the $\alpha 1$ and $\alpha 2$ -domains of FcRn¹¹, characteristic of the IgG-FcRn interaction. As a result, albumin also has a long half-life in humans (~ 19 days) and an FcRn-dependent half-life in mice¹². Molecular modeling, structure guided mutagenesis, and the recent crystal structure of an engineered albumin-FcRn complex indicates that albumin binds to a distinct site on FcRn opposite that of IgG^{11,13}. IgG and albumin can simultaneously and non-cooperatively bind FcRn *in vitro*^{14,15} in agreement with their distinctly different binding sites. Both IgG and albumin exhibit significant cross-species differences in their interaction with mouse and human FcRn^{15,16}. Human FcRn is selective for evolutionarily related IgG species but ignores rodent IgGs while mouse FcRn is promiscuous in its interaction with IgG from various species¹⁶. FcRn is less restrictive towards albumin across species as both mouse and human albumin bind mouse and human FcRn albeit with species-specific kinetics and affinity¹⁵.

Because FcRn contributes significantly to the half-life of IgG and albumin, a number of engineering strategies that hijack the FcRn-mediated recycling process have been devised to extend protein circulation, including Fc-¹⁷ and albumin-fusion¹⁸ or modified formats of these endogenous ligands¹⁹. However, there are surprisingly few reports of FcRn ligands derived from non-IgG or albumin domains²⁰⁻²². In chapter 2 we described a strategy to engineer proteins to interact with FcRn through genetic fusion of a short FcRn binding peptide (FcBP) sequence to the termini of a model protein, termed FcBP fusion, with the goal of enabling long circulation and/or non-invasive protein administration without altering molecular weight²³. FcBP fusion proteins mimic the hIgG1-hFcRn interaction *in vitro*, are selective for hFcRn with little to no binding to mFcRn, and are recycled and transcytosed across cell monolayers that express human FcRn^{20,23}. The lack of FcBP binding to mouse FcRn necessitates alternative animal models to

evaluate the *in vivo* properties of FcBP fusion proteins.

Species differences in IgG and albumin binding to mouse FcRn also impose limitations on the use of wild type mice to accurately determine FcRn-dependent pharmacokinetics *in vivo*¹⁶. To address these issues, human FcRn transgenic mice that express a hybrid human-mouse FcRn/ β 2m receptor on a murine FcRn-null background were developed by the Jackson Laboratory^{10,24}. The human FcRn transgenic mice are useful for the evaluation of human IgG and Fc-based therapeutics engineered to enhance binding to human FcRn¹⁰, therapeutics that disrupt the IgG-FcRn interaction^{20,25,26}, and prediction of IgG pharmacokinetics in non-human primates and humans^{27,28}. In contrast, very little is known about the behavior of albumin or FcBP fusion proteins in these mice.

In this chapter we built upon previous knowledge of the IgG and albumin interaction with FcRn across species^{15,16} to validate the human FcRn transgenic mouse models. We characterized the cross-species IgG and albumin interaction with both mouse and human FcRn *in vitro* and determined the impact on their plasma clearance *in vivo* in both wild-type and human FcRn transgenic mice. The results described in this chapter confirm the importance of the FcRn in regulating IgG and albumin clearance *in vivo*, suggest a relationship between IgG and albumin affinity to FcRn and half-life in mice, and validate the use of human FcRn transgenic mice for the pharmacokinetic evaluation of human IgG and albumin-based therapeutics. Thus, the human FcRn transgenic mice should also be useful to evaluate the *in vivo* fate of an exogenous class of human FcRn specific ligands, FcBP fusion proteins.

3.2 Methods

3.2.1 Materials

Human IgG1 (Avastin®, bevacizumab) was obtained from the UCSF Medical Center and Mouse IgG1 (MOPC-21 isotype control) was obtained from the UCSF Monoclonal Antibody Core facility. Human and mouse serum albumin (A8763 and A3559, respectively), rabbit serum IgG (I5006), ovalbumin, ampicillin, Terrific Broth (TB), heparin, and all buffer salts were purchased from Sigma-Aldrich (St. Louis, MO). AnaTag™ 5 – TAMRA protein labeling kit was purchased from AnaSpec (Fremont, CA). Nickel Sepharose high performance resin prepacked in 5 mL HiTrap columns (HisTrap FF), PD-10 desalting columns, and Superdex 75 size exclusion chromatography (SEC) column were purchased from GE Healthcare (Piscataway, NJ). Complete EDTA-free protease inhibitor cocktail tablets and isopropyl β -D-1-thiogalactopyranoside (IPTG) were purchased from Roche Diagnostics (Indianapolis, IN). Stericup 0.45 μ m vacuum filters and Amicon 10 kDa MWCO spin filters were from Millipore (Billerica, MA).

3.2.2 Cell Culture

MDCK hFcRn-EYFP/h β 2M cells were generated as previously described in reference 23²³ and in Chapter 2, Section 2.2.4 and maintained in MDCK wild type media supplemented with 0.3 mg/mL Hygromycin B and 0.4 mg/mL G418. All cells were maintained in a humidified environment at 37 °C and 5% CO₂.

3.2.3 Mice

All mice used in this study were purchased from The Jackson Laboratory (Bar Harbor, ME), bred, and maintained under pathogen-free conditions at the University of California, San Francisco (UCSF). All breeding schemes and mouse procedures were approved by the UCSF

Institutional Animal Care and Use Committee (IACUC). Three mouse strains were used in this study: control C57BL/6J (wild type; stock number 000664), B6.Cg-*Fcgrt*^{tm1Dcr} Tg(CAG-FCGRT)276Dcr/DcrJ (Tg276 homoz.; stock number 004919), and B6.Cg-*Fcgrt*^{tm1Dcr} Tg(FCGRT)32Dcr/DcrJ (Tg32 homoz.; stock number 014565). C57BL/6J mice are wild type at both the mouse *Fcgrt* and beta-2 microglobulin ($m\beta 2m$) locus resulting in a fully murine FcRn / $\beta 2m$ receptor. Tg276 homoz. mice are knock out for mouse *Fcgrt* and express a human *FCGRT* cDNA under the control the human cytomegalovirus immediate early promoter/enhancer with chicken beta-actin/rabbit beta-globin hybrid promoter (CAG). Tg32 homoz. mice are knock out for mouse *Fcgrt* and express a human *FCGRT* gene under control of the human *FCGRT* promoter by insertion of a 33-Kb cosmid clone including the complete *FCGRT* gene (approximately 11 kb as well as 10 kb of 5' and 3' flanking sequences). Both the Tg276 and Tg32 mice are wild type at the murine $\beta 2m$ locus and therefore express a hybrid hFcRn / $m\beta 2m$ heterodimeric receptor at the protein level.

3.2.4 mKate-cFcBP protein expression and purification

Expression of N-&-C Term Cyclic FcBP mKate, named mKate-cFcBP for the rest of this dissertation, was carried out in BL21-Codon Plus (DE3)-RIPL *E. coli* cells (Stratagene; La Jolla, CA) harboring expression vectors described in reference 23²³ and Chapter 2, Section 2.2.5. Protein expression and purification was as described in Chapter 2, Section 2.2.6.

3.2.5 Size exclusion chromatography

All proteins used in this chapter were purified by size exclusion chromatography on a Dionex FPLC equipped with a Superdex 75 column (GE Healthcare) as previously described²⁹. The column was operated at a flow rate of 0.5 mL/min in D-PBS and the eluate was monitored at 280 nm. Fractions containing monomeric protein were pooled, concentrated using Amicon 10

kDa MWCO spin filters, and exchanged into the appropriate running buffer for *in vitro* and *in vivo* studies.

3.2.6 Affinity measurements by surface plasmon resonance

SPR measurements for human IgG1, rabbit serum IgG, and mouse IgG1 binding to human and mouse FcRn were obtained using a BIAcore T100 instrument (BIAcore Inc.; Piscataway, NJ) as previously described²³ with minor modifications. The extracellular region of human FcRn and mouse FcRn (a kind gift of Dr. E. Sally Ward, UT Southwestern) were captured on a CM5 sensor chip at pH 5 by amine coupling to a final immobilization density of ~ 415 and ~ 225 resonance units (RUs), respectively. Un-reacted sites were blocked with 1M ethanolamine. Two control flow cell lanes without immobilized FcRn were blocked with 1M ethanolamine for reference subtraction. The flow rate used for all methods was 30 μ L/min and injection times were 120 sec in either PBS-T, pH 6 (PBS, 50 mM MES, 0.01% Tween 20, pH 6) or PBS-T, pH 7.4 (PBS, 50 mM Hepes, 0.01% Tween 20, pH 7.4) running buffer. Proteins were dissociated from the chip for 120 sec in running buffer followed by regeneration with one 60 sec injection of PBS-T, pH 7.4 and two 45 sec injections of Tris, pH 9 buffer (50 mM Tris, 100 mM NaCl, 0.01% Tween 20, pH 9). Binding kinetics were derived by analysis of the generated sensograms using the BIAcore T100 evaluation software. All sensograms were baseline adjusted and reference subtracted. Sensograms were fit to a bivalent analyte model for derivation of binding kinetics and to a steady-state affinity model for derivation of the apparent binding affinity.

We were unable to accurately quantify human or mouse albumin binding to immobilized FcRn using the method described above or previously described methods^{15,30,31} due to a high degree of non-specific binding to the reference flow cells. To circumvent this issue we made the

following modifications to the above method: 1) hFcRn and mFcRn were coupled to a CM5 chip to a final density of ~ 1400 RUs and ~ 1200 RUs, respectively, 2) ovalbumin was coupled to the reference flow cells to a final density of ~ 1800 RUs prior to the 1M ethanolamine quench, and 3) 2% (w/v) ovalbumin was added to the PBS-T, pH 6 and pH 7.4 running/sample buffers. All other parameters were as described above for IgG. The modifications significantly reduced non-specific binding and enabled quantification of the albumin:FcRn binding kinetics.

3.2.7 Cellular accumulation of IgG, albumin, and mKate-cFcBP in MDCK hFcRn-EYFP/h β 2M by FACS

IgGs and albumins were labeled with 5-carboxytetramethylrhodamine (5-TAMRA; Ex/Em: 547/574) using the AnaTagTM 5-TAMRA protein labeling kit at a ratio ~ 2 – 3 mol 5-TAMRA per mol protein to enable detection by FACS. All proteins were labeled for 2 hr at room temperature, desalted over a PD-10 column equilibrated in D-PBS, and further purified by size exclusion chromatography as described in Section 3.2.5. Labeled protein accumulation in MDCK hFcRn-EYFP/h β 2m cells was quantified as previously described in reference 23²³ and in Chapter 2, Section 2.2.10.

3.2.8 Plasma clearance in mice

The plasma clearance of IgGs and albumins were evaluated in wild type C57BL/6J, Tg276 homoz., and Tg32 homoz. mice. IgGs and albumins were labeled with 5-carboxytetramethylrhodamine (5-TAMRA; Ex/Em: 547/574) using the AnaTagTM 5-TAMRA protein labeling kit at a ratio ~ 2 – 3 mol 5-TAMRA per mol protein to enable detection in mouse plasma via fluorescence. Mice (n = 9 per group) received a 10 mg/kg intravenous (IV) tail vein injection of IgGs or albumins in 200 μ L D-PBS and blood samples were collected into heparinized tubes through submandibular cheek pouch bleeds. Blood was centrifuged at 6,000 rpm for 6 min and the plasma was diluted 1:10 into D-PBS and assayed by fluorometry on a

Spex Fluorolog fluorometer (Horiba Jobin Yvon; Edison, NJ) with 5 nm excitation and emission slits. All plasma samples were normalized to the maximum fluorescence observed in the first bleed 5 min after injection and plotted as % injected dose (%ID) versus time. The α - and β -phase half-life of the IgGs were calculated by fitting the plasma clearance curves (%ID vs. time) to a 2-compartment PK model, $Y = C_0e^{k_1*x} + C_1e^{k_2*x}$, using Prism 5 (GraphPad Software; La Jolla, CA). The α - and β - phase half-lives of albumin were calculated by separately fitting the α -phase and β - phase to a semilog line model, $Y = 10^{(k*x+Y_0)}$, in Prism 5 due to an insufficient number of data points to accurately fit a 2-compartment PK model.

3.3 Results

3.3.1 Protein expression, purification, and characterization.

The binding affinity between FcRn and its ligands is dependent on valency. The homodimeric nature of the IgG Fc-domain allows one IgG to simultaneously bind 2 FcRn molecules³² whereas albumin can only bind 1 FcRn molecule¹⁴. The bivalent interaction between IgG and FcRn results in a higher apparent affinity compared to the monovalent interaction between albumin and FcRn. Therefore, it is important to evaluate binding using monomeric protein preparations. HSA, MSA, and rabIgG purchased from Sigma, and mKate-cFcBP isolated from *E. coli* contain a significant fraction of high molecular weight impurities (Fig. 3.1a) that were removed by size exclusion chromatography (Fig. 3.1b). All proteins migrate at their expected molecular weight by SDS-PAGE under non-reducing conditions with decent purity, albeit all contain low levels of product related impurities (Fig. 3.2a). Rabbit serum IgG migrates as a smear (Fig. 3.2a,b; lane 3) likely due to the heterogeneous nature of the serum IgG repertoire. All IgGs migrate as two separate bands at ~ 50 kDa and ~ 25 kDa under reducing conditions corresponding to the heavy and light chains, respectively (Fig. 3.2; lanes 1,2,3). The observed shift in electrophoretic mobility of albumin under reducing versus non-reducing conditions indicates the presence of native disulfide bonds resulting in a more compact tertiary structure and faster migration under non-reducing conditions (Fig. 3.2; lanes 4,5).

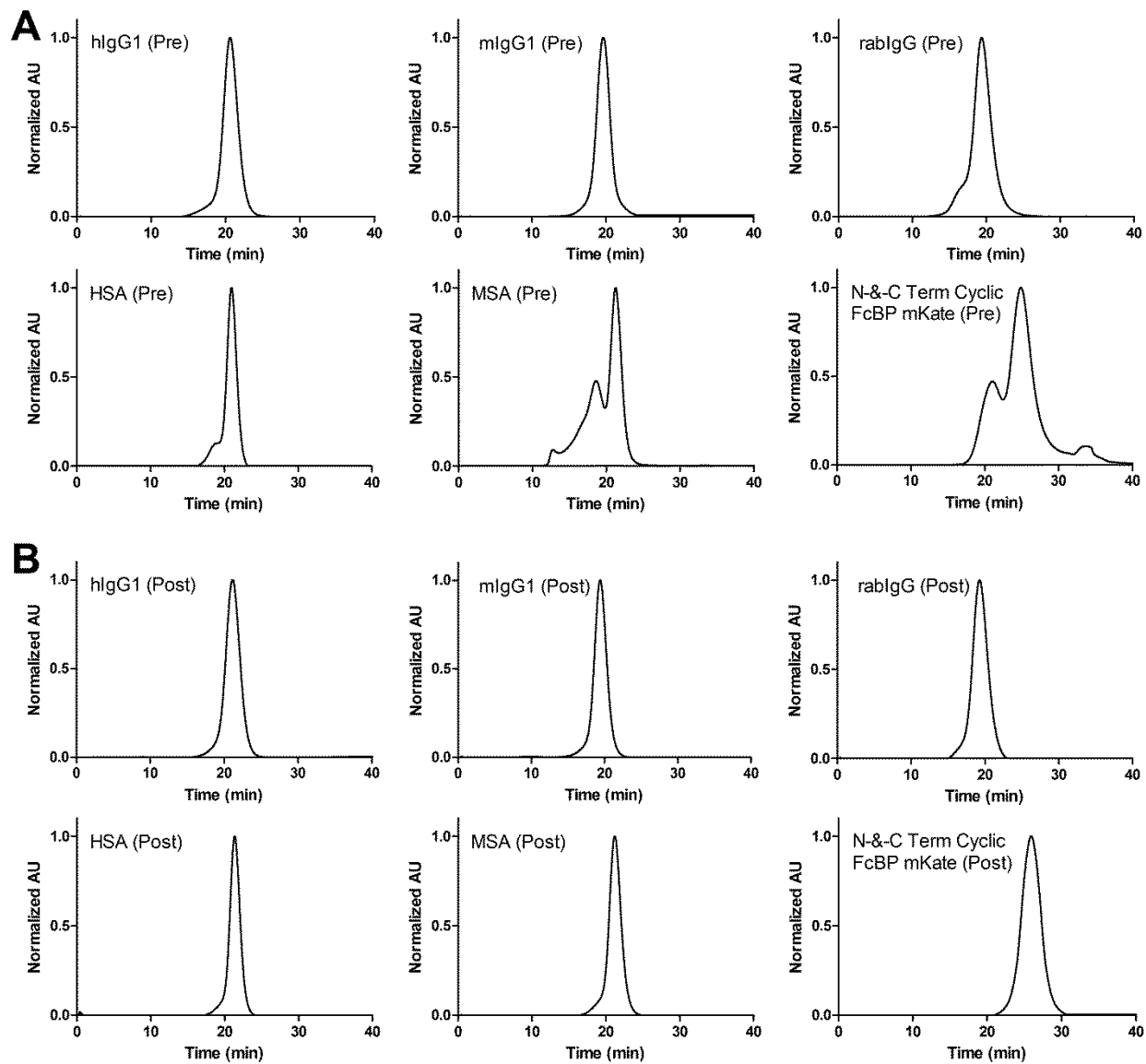


Figure 3.1. Size exclusion chromatograms of IgGs, albumins, and mKate-cFcBP pre (a) and post (b) size exclusion chromatography purification.

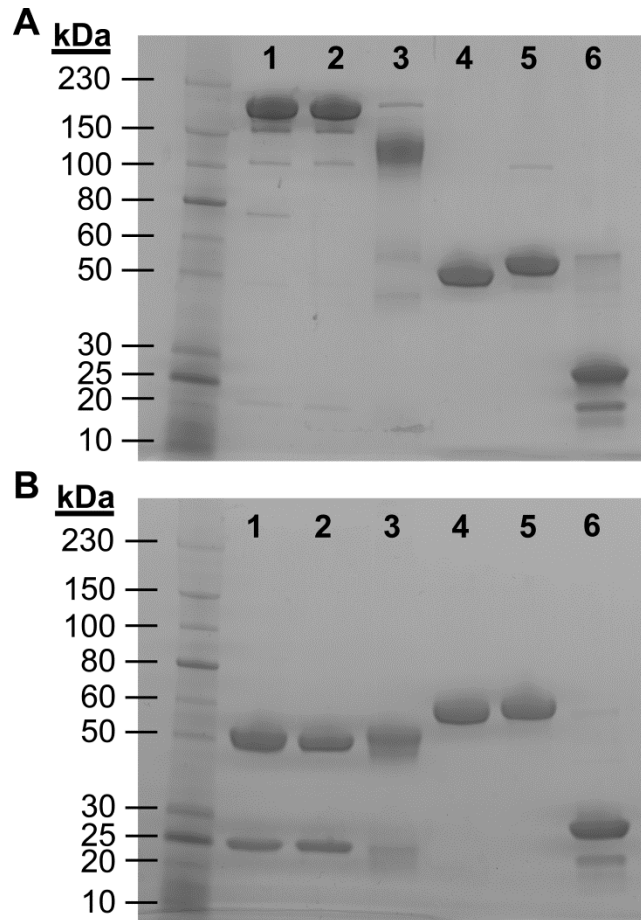


Figure 3.2. Reducing and non-reducing SDS-PAGE analysis of IgGs, albumins, and mKate-cFcBP.

Non-reduced (a) and reduced (b) 4-15% SDS-PAGE gel of size exclusion chromatography purified hIgG1 (lane 1), mIgG1 (lane 2), rabbit serum IgG (lane 3), human serum albumin (lane 4), mouse serum albumin (lane 5), FcBP-mKate (lane 6). 7.5 μ g of protein were loaded in each lane.

3.3.2 Binding kinetics between FcRn and mouse, rabbit, and human IgG

We determined the binding kinetics of hIgG1, rabIgG, and mIgG1 to both human and mouse FcRn by surface plasmon resonance (SPR). Dilutions of ligand were injected over immobilized mouse or human FcRn as this assay format allows ligand-induced receptor cross linking, mimicking the presumed intracellular IgG-FcRn binding mechanism. Human IgG1 and rabIgG bind human FcRn at pH 6 with similar kinetics and affinity whereas mIgG1 lacks binding to human FcRn under these conditions (Table 3.1 and Fig. 3.3a-c). All IgGs evaluated bind

mouse FcRn at pH 6 (Fig. 3.3d-f), consistent with the known promiscuity of the mouse FcRn-IgG interaction across species¹⁶, but with significant differences in affinity, kinetics and pH-dependency compared to human FcRn (Table 3.1). In general, IgG affinity for mouse FcRn is significantly higher than for human FcRn due to a substantial decrease in the rate of IgG dissociation from mouse compared to human FcRn. At pH 7.4, binding of all ligands to mouse and human FcRn is dramatically reduced or not detectable compared to pH 6 (Fig. 3.4). However, unlike species matched IgG-FcRn interactions that have no detectable binding at pH 7.4, cross-species binding of hIgG1 and rabIgG to mouse FcRn occurs at pH 7.4 albeit with significantly lower affinity than at pH 6 (Table 3.1 and Fig. 3.4d,f). The rank order affinities at pH 6 from highest to lowest are as follows: rabIgG:mFcRn \cong hIgG1:mFcRn > mIgG1:mFcRn > hIgG1:hFcRn \cong rabIgG:hFcRn >>> mIgG1:hFcRn.

Table 3.1 Binding kinetics and affinity of IgG to human and mouse FcRn at pH 6 and pH 7.4.

Molecule	FcRn Species	k_{a1} pH 6 (10^4 /Ms)	k_{d1} pH 6 (1/s)	K_{D1}^* pH 6 (nM)	K_D pH 6, SSA (nM)	$U_{1/2, \max}$ pH 6, (nM)	K_D pH 7.4, SSA (μ M)
hIgG1	Human	9.0	0.24	2617	2323	2943	NQ
hIgG1	Mouse	18.4	0.03	153	215	nd	15.6
mIgG1	Human	---	---	NQ	NQ	NQ	NQ
mIgG1	Mouse	4.8	0.07	1415	812	nd	NQ
rabIgG	Human	5.2	0.29	5586	2508	1488	NQ
rabIgG	Mouse	16.0	0.02	97	187	nd	6.3

(*) Data were fit to a bivalent analyte kinetic model for derivation of K_{D1} . nd, not determined. NQ, not quantifiable due to no or weak binding. SSA, steady state affinity model

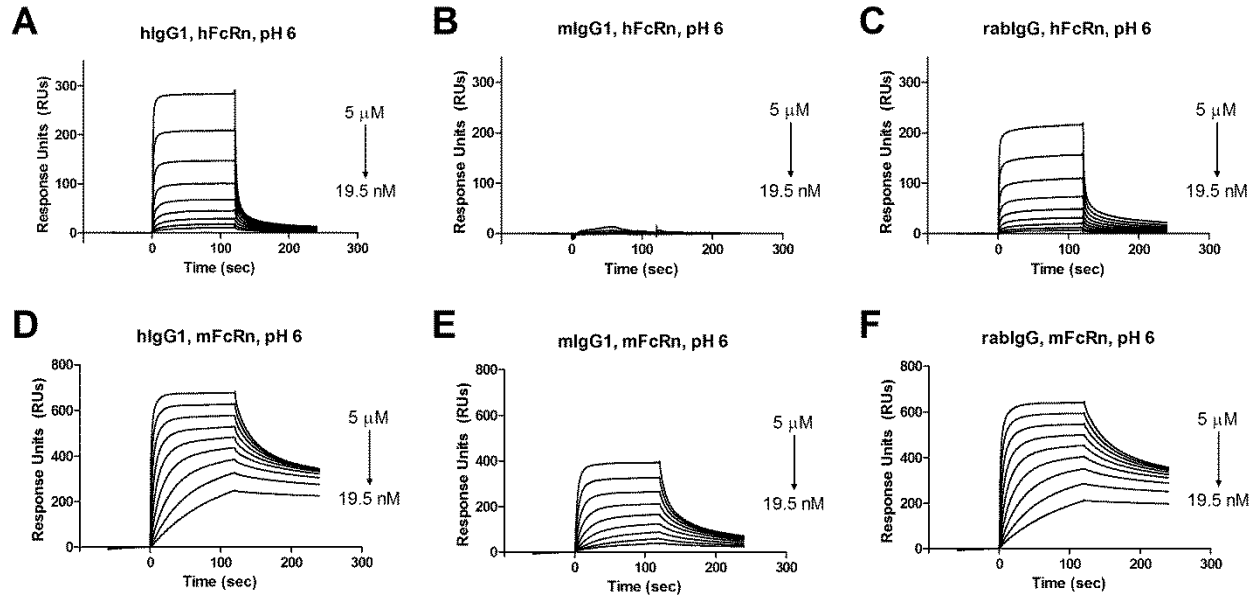


Figure 3.3 Surface plasmon resonance sensograms of IgG binding to mouse and human FcRn at pH 6.

Serial dilutions of hIgG1 (a,e), mIgG1 (b,f), rabIgG (c,g) and mKate-cFcBP (d,h) were injected over immobilized human (a-d) and mouse FcRn (e-f) at pH 6. The resulting sensograms were fit to the bivalent analyte model for derivation of binding kinetics and affinity summarized in Table 3.1.

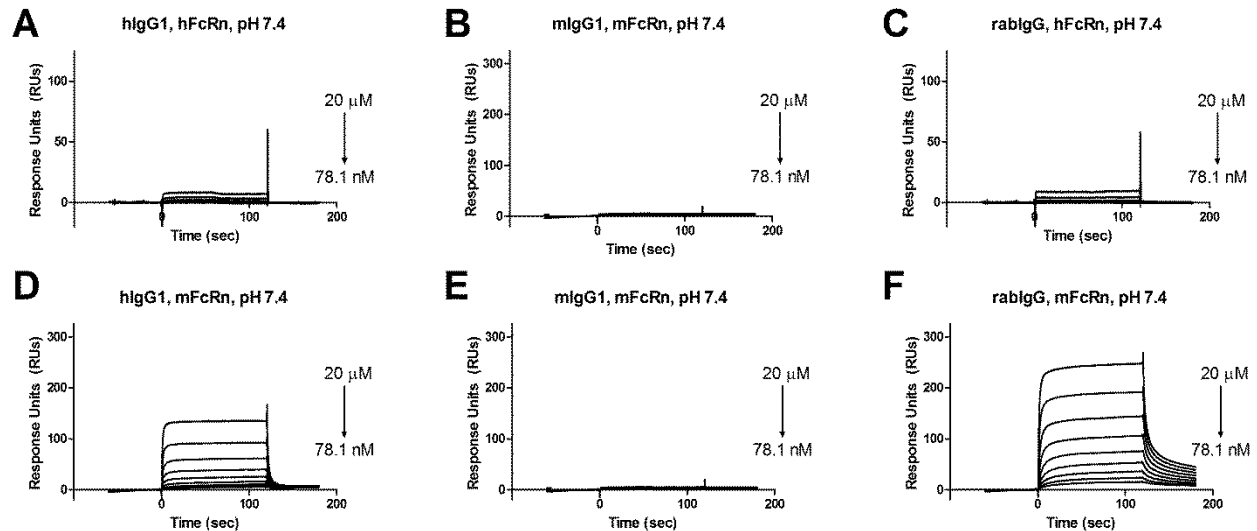


Figure 3.4 Surface plasmon resonance sensograms of mouse, rabbit, and human IgG binding to mouse and human FcRn at pH 7.4

Serial dilutions of hIgG1 (a,e), mIgG1 (b,f), rabIgG (c,g) and mKate-cFcBP (d,h) were injected over immobilized human (a-d) and mouse FcRn (e-f) at pH 7.4. The resulting sensograms were fit to the bivalent analyte model for derivation of binding kinetics and affinity summarized in Table 3.1.

3.3.3 Binding kinetics between FcRn and mouse and human serum albumin

We also evaluated the cross-species binding of albumin to FcRn by SPR. We had difficulties reproducing previous albumin-FcRn SPR methods^{14,15} and even with major modifications to block non-specific binding our albumin-FcRn kinetic data and calculated affinities are much lower than previous reports. Therefore, the data should be viewed as relative. Human FcRn is less selective in its interaction with albumins compared to IgGs as both MSA and HSA bind human FcRn with micromolar affinity at pH 6 (Table 3.2 and Fig. 3.5a,b). Cross-species binding of HSA to mouse FcRn is notably weaker than to human FcRn with rapid rates of association and dissociation (Fig. 3.5a,c). MSA and HSA also bind mouse FcRn at pH 6 and in general MSA binds both FcRn species with higher affinity than HSA (Fig. 3.5b,d). Only weak non-specific binding to FcRn at high albumin concentrations (> 50 μM) was observed at pH 7.4 across all species (Fig. 3.6) confirming the pH dependence of the albumin-FcRn interaction. The rank order affinities at pH 6 from highest to lowest are as follows: MSA:mFcRn > MSA:hFcRn > HSA:hFcRn >> HSA:mFcRn.

Table 3.2 Binding kinetics and affinity of mouse and human serum albumin to human and mouse FcRn at pH 6 and pH 7.4

Molecule	FcRn Species	k_a pH 6 (1/Ms)	k_d pH 6 (1/s)	K_D^* pH 6 (μM)	K_D pH 6, SSA (μM)	$U_{1/2, \max}$ pH 6, (μM)	K_D pH 7.4, SSA (μM)
HSA	Human	257.8	0.15	586	121	17.9	NQ
HSA	Mouse	3341	2.53	758	215	nd	NQ
MSA	Human	246.6	0.02	93	84	4.2	NQ
MSA	Mouse	1302	0.03	21	19	nd	NQ

(*) Data were fit to a 1:1 binding kinetic model for derivation of K_D . nd, not determined. NQ, not quantifiable due to weak or non-specific binding. SSA, steady state affinity model.

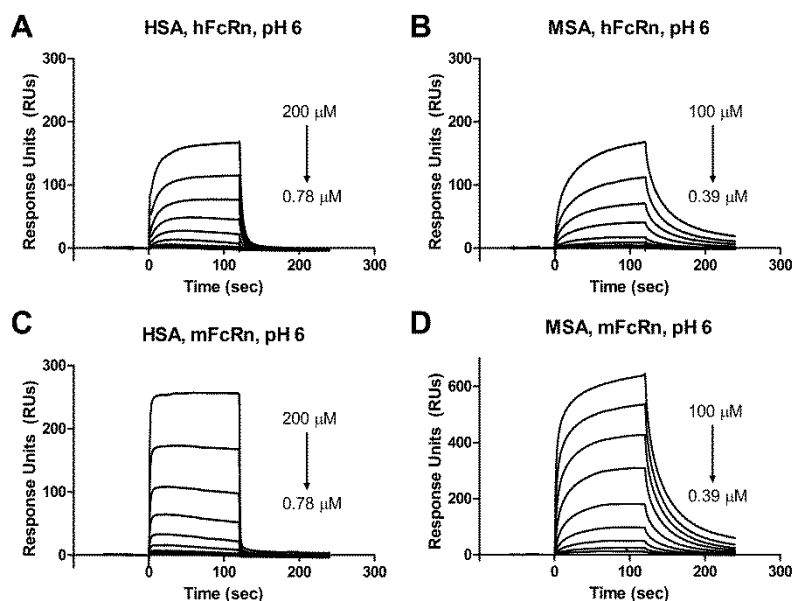


Figure 3.5 Surface plasmon resonance sensograms of mouse and human serum albumin binding to mouse and human FcRn at pH 6.

Serial dilutions of HSA (a,c) or MSA (b,d) were injected over immobilized human (a,b) and mouse FcRn (c,d) at pH 6. The resulting sensograms were fit to the 1:1 Langmuir model for derivation of binding kinetics and affinity summarized in Table 3.2.

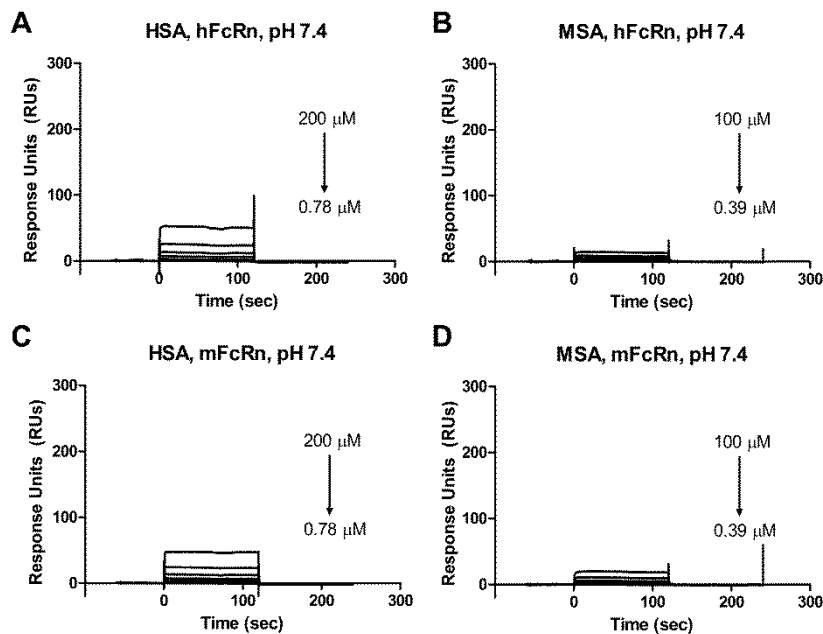


Figure 3.6 Surface plasmon resonance sensograms of mouse and human serum albumin binding to mouse and human FcRn at pH 7.4.

Serial dilutions of HSA (a,c) or MSA (b,d) were injected over immobilized human (a,b) and mouse FcRn (c,d) at pH 7.4. The resulting sensograms were not evaluated for kinetics or affinity derivation due to the low signal resulting from non-specific binding at high albumin concentrations.

3.3.4 Accumulation of FcRn ligands in MDCK hFcRn-EYFP/h β 2M cells by FACS

We quantitatively measured cellular accumulation of FcRn ligands in MDCK cells stably expressing hFcRn-EYFP/h β 2M by FACS. We used this cell model in chapter 2 to study human FcRn-mediated endocytosis, recycling, and transcytosis of mKate-cFcBP and hIgG1 *in vitro* and found that the concentration at which half-maximal uptake ($U_{1/2max}$) occurs for each protein correlated with our affinity measurements by SPR. Thus, this cell model provides an orthogonal method to quantify human FcRn binding and study FcRn-mediated trafficking. Human IgG1, rabIgG, and mKate-cFcBP exhibit dose- and pH-dependent accumulation in MDCK hFcRn-EYFP/h β 2M cells with a $U_{1/2max}$ at pH 6 of 2943 nM, 1488 nM, and 1269 nM, respectively, whereas accumulation of mIgG1 at pH 6 is negligible, in agreement with affinity measurements by SPR (Fig. 3.7a and Table 3.1).

HSA and MSA also exhibit dose- and pH-dependent accumulation in MDCK hFcRn-EYFP/h β 2m cells with a $U_{1/2max}$ at pH 6 of 17.9 μ M and 4.2 μ M, respectively (Fig. 3.7a). Although the $U_{1/2max}$ is significantly lower than the K_D measured by SPR (Table 3.2), the cross-species trends in human FcRn binding are consistent with the SPR results and the $U_{1/2max}$ values more closely match previously reported albumin-FcRn affinities¹⁵.

At pH 7.4, all ligands except mKate-cFcBP show negligible accumulation in MDCK hFcRn-EYFP/h β 2M cells in agreement with affinity measurements by SPR (Fig. 3.7b). Collectively, the data indicate that MSA has an \sim 4-fold higher affinity for human FcRn at pH 6 than HSA whereas hIgG1, rabIgG, and mKate-cFcBP have similar affinity for human FcRn at pH 6.

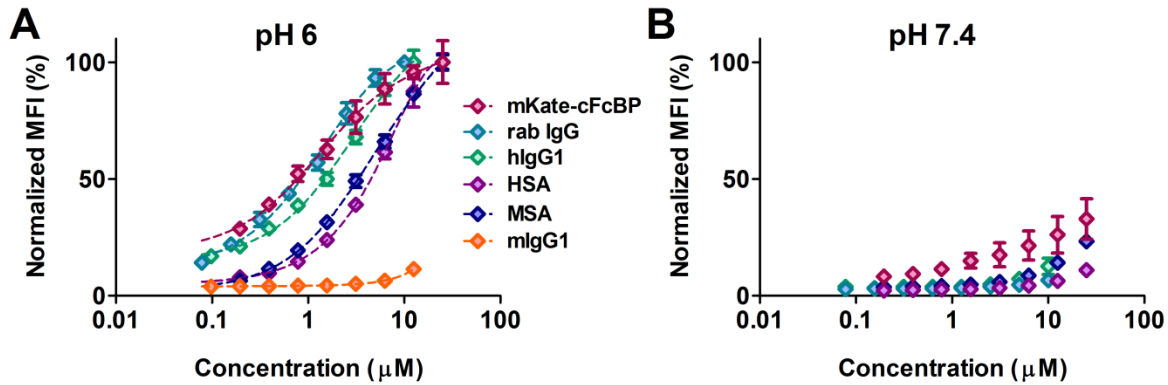


Figure 3.7 *In vitro* characterization of FcRn ligand accumulation in MDCK cells expressing hFcRn-EYFP/h β 2M by FACS.

Cellular accumulation of FcRn ligands at pH 6 (**a**) or pH 7.4 (**b**) in MDCK hFcRn-EYFP/h β 2m cells. Dashed lines represent data fit to a one-site total binding model in Prism and the concentrations at which half-maximal accumulation occurs ($U_{1/2,max}$) are summarized in Table 3.1 and 3.2. The mean fluorescent intensity, MFI, for each ligand was normalized internally to the maximum MFI observed for the same ligand except mIgG1 which was normalized to maximum MFI observed for hIgG1. The data shown in each panel are the mean (n=3) and error bars indicate s.d.

3.3.5 Plasma clearance of mouse and human IgG1 in mice

Collectively the FcRn-binding ligands evaluated *in vitro* are diverse in their species specificity, affinity, binding kinetics, valency, and pH-dependency enabling a comparison between various FcRn binding properties and plasma clearance *in vivo*. The promiscuity of mouse FcRn and selectivity of human FcRn enable the use of hIgG1 and mIgG1 as positive and negative controls, respectively, to verify the function human FcRn in the transgenic mouse models. We therefore first determined the plasma clearance of mouse and human IgG1 in wild type C57BL/6J mice [mFcRn^{+/+} hFcRn^{-/-}] and two homozygous human FcRn transgenic mouse models: Tg276 [mFcRn^{-/-} hFcRn (276) Tg/Tg] and Tg32 [mFcRn^{-/-} hFcRn (32) Tg/Tg]. Mice were dosed i.v. with 10 mg/kg labeled protein via the tail vein and decay of labeled protein in plasma was monitored by fluorometry.

Mouse IgG1 has a long terminal half-life ($t_{1/2}$) of ~ 13.9 days in wild type C57BL/6J mice but is rapidly cleared from Tg276 mice with a terminal $t_{1/2}$ of ~ 2.6 days, consistent with mIgG1 binding to mouse but not human FcRn (Fig. 3.8a and Table 3.3). Human IgG1 has a long terminal $t_{1/2}$ of 13.1 days, 10.0 days, and 7.1 days in C57BL/6J, Tg32, and Tg276 mice, respectively, consistent with the cross-species hIgG1 interaction with both mouse and human FcRn. The longer $t_{1/2}$ of hIgG1 in C57BL/6J compared to Tg276 and Tg32 mice agrees with the ~ 10 - 17 fold higher affinity for mouse FcRn compared to human FcRn at pH 6. Both human and mouse IgG1 have a similar $t_{1/2}$ in C57BL/6J mice ($t_{1/2} = 13.1$ days and $t_{1/2} = 13.9$ days) despite the ~ 4 - 9 fold higher affinity of the hIgG1-mFcRn compared to mIgG1-mFcRn interaction at pH 6, suggesting that alternative FcRn-dependent or independent factors contribute to the clearance of IgG in C57BL/6J mice.

Rabbit serum IgG also has a long terminal $t_{1/2}$ of ~ 10.8 days in Tg32 mice; however, the rabIgG levels in plasma were extremely variably at later time points suggesting the induction of anti-rabIgG antibodies leading to the accelerated clearance of rabIgG (Fig. 3.9). Therefore, we did not extend the analysis of rabIgG to wild type or Tg276 mice. Nonetheless, collectively the data clearly demonstrate the ability of mouse and human FcRn to extend the $t_{1/2}$ of IgG1 in wild type and human FcRn transgenic mice.

Table 3.3. Plasma half-life of hIgG1, mIgG1, HSA, and MSA in wild type and human FcRn transgenic mice.

Molecule	C57BL/6J		Tg276		Tg32	
	$t_{1/2, \alpha}$ (hrs)	$t_{1/2, \beta}$ (hrs)	$t_{1/2, \alpha}$ (hrs)	$t_{1/2, \beta}$ (hrs)	$t_{1/2, \alpha}$ (hrs)	$t_{1/2, \beta}$ (hrs)
hIgG1	2.6	313.8	4.1	169.8	2.4	239.8
mIgG1	2.5	332.8	4.2	63.2	n.d.	n.d.
HSA*	7.0	35.1	9.2	32.8	7.7	55.0
MSA*	5.7	48.5	4.3	42.3	5.3	68.6

(*) Data from alpha and beta phase % injected dose versus time were individually fit to a semilog line model, $Y = 10^{(k \cdot X + Y_0)}$, for derivation of $t_{1/2, \alpha}$ and $t_{1/2, \beta}$. n.d. = not determined.

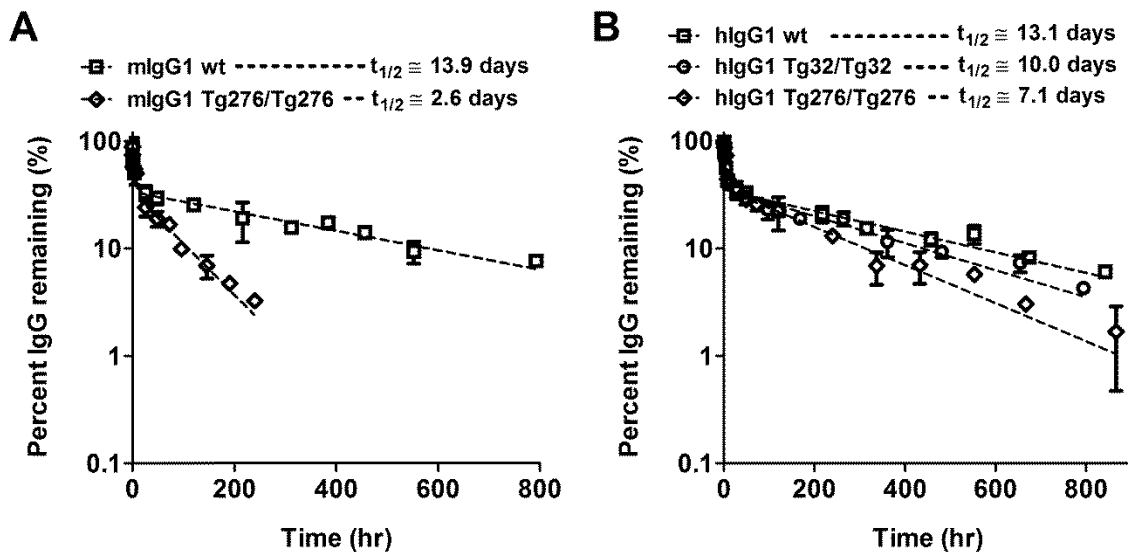


Figure 3.8 Plasma clearance of mouse and human IgG1 in wild type and human FcRn transgenic mice.

Labeled mouse IgG1 (a) or human IgG1 (b) were dosed i.v. at 10 mg/kg via the tail vein. Blood was collected at various time points into heparized tubes and the plasma clearance of labeled protein was determined via fluorometry. The % IgG remaining was calculated by normalizing the fluorescent emission at all time points to the maximum value observed in the first bleed 5 min after injection of each labeled protein. Dashed lines represent the data fit to a 2-compartment PK model in prism and the β -phase half-life shown in the figure was calculated as described in Section 3.2.8. The data shown in each panel are the mean (n=3 bleeds per time point) and error bars indicate s.d.

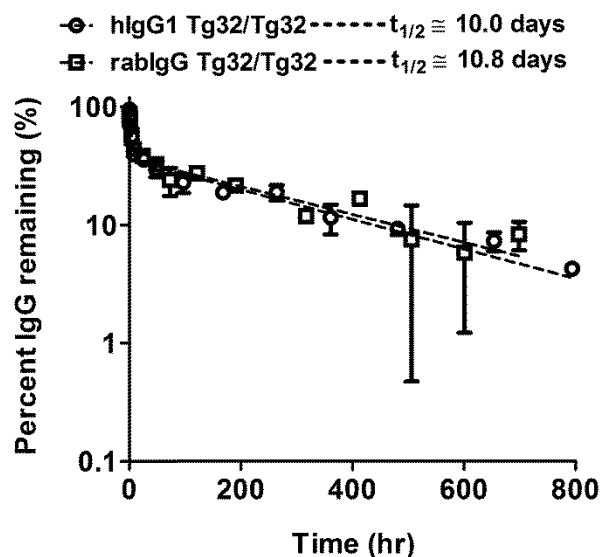


Figure 3.9 Plasma clearance of rabbit serum IgG and human IgG1 in Tg32 mice.

Labeled rabbit serum IgG or human IgG1 (reproduced from Fig. 3.8b) were dosed i.v. at 10 mg/kg via the tail vein. Blood was collected at various time points into heparinized tubes and the plasma clearance of labeled protein was determined via fluorometry. The % IgG remaining was calculated by normalizing the fluorescent emission at all time points to the maximum value observed in the first bleed 5 min after injection of each labeled protein. Dashed lines represent the data fit to a 2-compartment PK model in prism and the β -phase half-life shown in the figure was calculated as described in Section 3.2.8. The data shown in each panel are the mean (n=3 bleeds per time point) and error bars indicate s.d.

3.3.7 Plasma clearance of mouse and human serum albumin in mice

Although a number of studies highlight the utility of humanized FcRn transgenic mice to predict the pharmacokinetics of human IgG and Fc-containing proteins^{24,27,28,33-36}, to our knowledge there is only one recent report on the relationship between the HSA-hFcRn interaction *in vitro* and in human FcRn transgenic mice¹³. Therefore, we also evaluated the plasma clearance of human and mouse serum albumin in mice. Compared to IgG, MSA and HSA are rapidly eliminated from circulation (Fig. 3.10 and Table 3.3). The terminal t_{1/2} of HSA is 35 hrs, 33 hrs, and 55 hrs in C57BL/6J, Tg276 and Tg32 mice, respectively. The extended t_{1/2} of HSA in Tg32 versus C57BL/6J mice correlates with its higher affinity for human FcRn at pH 6; however, HSA t_{1/2} is similar in C57BL/6J and Tg276 mice (Fig. 3.10b) despite FcRn affinity

differences. The terminal $t_{1/2}$ of MSA is 49 hrs, 42 hrs, and 69 hrs in C57BL/6J, Tg276 and Tg32 mice, respectively, slightly longer than HSA in each respective strain and in agreement with affinity measurements by SPR. The $t_{1/2}$ of MSA is also similar in C57BL/6J and Tg276 mice despite differences in mouse and human FcRn affinity (Fig. 3.10a). Although there is no FcRn affinity to $t_{1/2}$ relationship between strains (e.g. C57BL/6J vs Tg276), the $t_{1/2}$ of MSA and HSA in the same strain correlates with FcRn affinity at pH 6. Collectively the data indicate a relationship between the albumin-FcRn interaction *in vitro* and plasma clearance *in vivo* supporting the role of FcRn in albumin clearance and the utility of humanized FcRn transgenic mice, especially the Tg32 strain, for the pharmacokinetic evaluation of human albumin-based therapeutics.

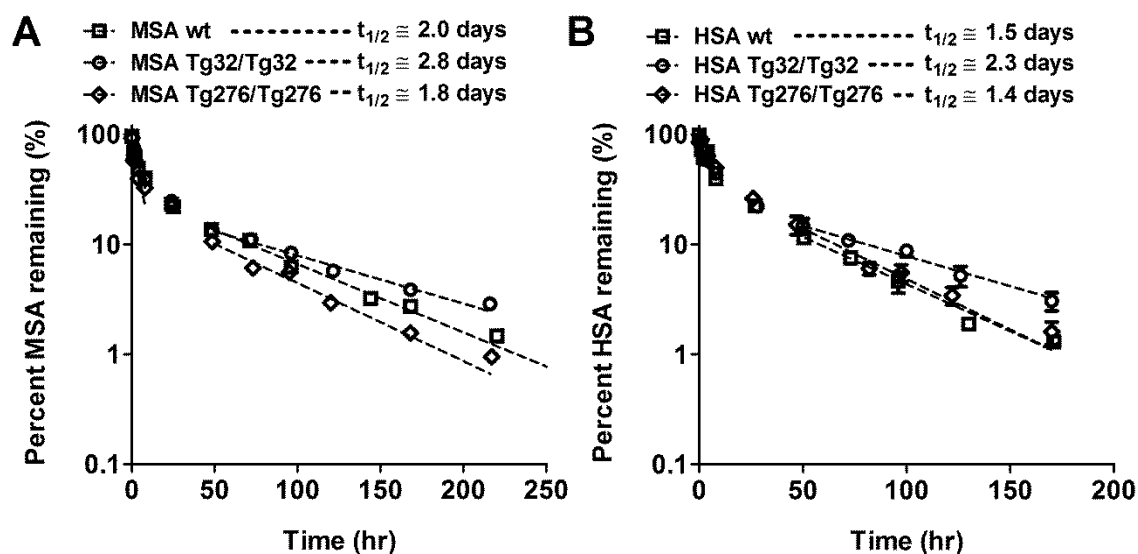


Figure 3.10 Plasma clearance of mouse and human serum albumin in wild type and human FcRn transgenic mice.

Labeled mouse serum albumin (a) or human serum albumin (b) were dosed i.v. at 10 mg/kg via the tail vein. Blood was collected at various time points into heparinized tubes and the plasma clearance of labeled protein was determined via fluorometry. The % albumin remaining was calculated by normalizing the fluorescent emission at all time points to the maximum value observed in the first bleed 5 min after injection of each labeled protein. Dashed lines represent the data fit to a semi-log line model in prism and the β -phase half-life shown in the figure was calculated as described in Section 3.2.8. The data shown in each panel are the mean (n=3 bleeds per time point) and error bars indicate s.d.

3.4 Conclusion

In this chapter, we characterized the two known endogenous FcRn ligands, IgG and albumin, from various species *in vitro* and demonstrate that cross-species FcRn binding influences their plasma clearance in wild type and human FcRn transgenic mice. IgG and albumin were used to validate the utility of human FcRn transgenic mice as an *in vivo* model to predict the behavior of alternative human FcRn-targeted “therapeutics.” IgG and albumin bind FcRn at distinct sites and with distinct biophysical and cross-species binding properties enabling a comparison between FcRn-affinity and plasma clearance. Both ligands can be purchased eliminating the need for laborious protein engineering efforts. In general we observed trends consistent with the literature that demonstrate the importance of FcRn in regulating the serum persistence of IgG and albumin, the utility of human FcRn transgenic mice for evaluating human IgG- and albumin-based molecules, and that cross-species IgG and albumin binding to FcRn *in vitro* correlates with plasma clearance *in vivo*. Thus, the results in this chapter confirm the functionality of human FcRn in transgenic mice and indicate that human FcRn transgenic mice should be useful to study the *in vivo* fate of FcBP fusion proteins.

The most convincing evidence of human FcRn function in Tg276 and Tg32 mice is the fact that mIgG1 is rapidly eliminated from circulation while hIgG1 has a long half-life. Mouse IgG1 does not bind human FcRn and as a consequence has a short half-life in Tg276 mice but circulates ~ 5-fold longer in wild type mice due to interaction with mouse FcRn, similar to that reported by Petkova et al.¹⁰. Human IgG1 on the other hand binds both mouse and human FcRn and as a result has extended circulation in all mouse strains. Interestingly, hIgG1 has an ~ 4-9-fold higher affinity than mIgG1 for mouse FcRn at pH 6 yet the half-life of both IgGs is similar in C57BL6/J mice. The increased affinity of the hIgG1-mFcRn interaction at pH 6 is also

accompanied by an increase in affinity at pH 7.4. Thus, the increased affinity at pH 6 may be offset by the increased affinity at pH 7.4 that could result in catabolism of hIgG1 that do not dissociate from FcRn during receptor turnover translating to faster plasma clearance³⁷. In agreement with these findings is the fact that antibodies engineered for high affinity binding to FcRn at both pH 6 and pH 7.4, or AbDegs³⁸, have faster clearance than wild type IgG³⁹. These data suggest there may be a fine balance between IgG affinity at pH 6 and pH 7.4 that must be considered when engineering the IgG-FcRn interaction to modulate serum persistence. However, we and others have not evaluated the half-life of hIgG1 variants with similar affinity at pH 6 but varying affinity at pH 7.4 and therefore cannot exclude the possibility that other FcRn-dependent or independent factors control IgG clearance *in vivo*.

As with any model caveats exist. First, because mouse IgG subclasses do not bind or bind weakly to human FcRn¹⁶, endogenous mouse serum IgG levels are low in human FcRn transgenic mice²⁷. In contrast, mouse serum albumin binds both mouse and human FcRn; therefore, serum albumin levels in human FcRn mice are normal or slightly elevated^{12,27}. Thus, the serum IgG and albumin composition in human FcRn mice does not replicate that of a wild type mouse or human. Pre-treatment of human FcRn transgenic mice with high dose IgG or albumin to “re-constitute” typical serum levels does not impact hIgG1 pharmacokinetics²⁷ suggesting that FcRn salvage of exogenous hIgG1 in these mice is not significantly altered by the lack or presence of endogenous IgG and/or albumin. The impact of serum components on human albumin clearance in human FcRn transgenic has not been determined. Improvements to the current transgenic models by humanizing both the IgG constant domain locus and the albumin locus could result in a more representative mouse model. Some of these improvements are currently in development at the Jackson Laboratory⁴⁰.

The function of the hybrid human-mouse FcRn/ β 2m receptor is another caveat. The Tg276 and Tg32 mice are wild type at the β 2m locus and thus express a hybrid human-mouse FcRn/ β 2m receptor at the protein level. β 2m is highly conserved between human and mouse with a 69% amino acid identity. β 2m residues involved in IgG binding or that form the interface of the FcRn- β 2m heterodimer are highly conserved between human and mouse (100% and 81%, respectively), suggesting that the human-mouse FcRn- β 2m hybrid receptor is likely to function. In fact, IgG has been shown to bind a soluble or cell-surface expressed hybrid human-mouse FcRn/ β 2m receptor *in vitro*^{10,15,41} and we and others show that the hybrid human-mouse FcRn/ β 2m receptor also appears to function *in vivo* to extend the half-life of human IgG and albumin, at least in Tg276 and Tg32 mice¹⁰. Furthermore, human IgG1 half-life in Tg32 mice and Tg32 mice intercrossed with human β 2M mice⁴² to generate a human-human FcRn/ β 2M mouse in a murine FcRn α -chain null background (Tg32/h β 2M) is similar suggesting that the addition of h β 2M does not impact IgG clearance²⁴. However, a major confounding factor in Tg32/h β 2M mice is the expression of endogenous mouse β 2m making it impossible to determine the relative contribution of the human-human or human-mouse FcRn/ β 2m receptor to IgG clearance. Further investigation of IgG in humanized FcRn and β 2M mice on a murine FcRn and β 2m null background is warranted. Nonetheless, the data indicate that the hybrid human-mouse FcRn/ β 2m receptor functions to regulate clearance *in vivo*, at least for IgG and albumin.

Alternative functions of hybrid FcRn- β 2m receptors such as surface stability, sub-cellular localization, cellular trafficking, etc., have not been evaluated. β 2m is also the light chain of MHC Class I molecules³. Hybrid mouse-human MHC Class I/ β 2m receptors have a profound effect on MHC Class I functions including peptide binding⁴³, co-receptor engagement⁴⁴, T-cell

activation⁴⁵, and NK cell recognition^{46,47}. Thus, it is plausible that certain yet unknown functions of hybrid FcRn/ β 2m receptors exist. Such investigations, although outside the scope of this dissertation, may identify novel β 2m regulated processes with importance to the selection of pre-clinical mouse models and the development of antibody and albumin-based therapeutics and engineering targets.

In summary, we have demonstrated in this chapter that human FcRn transgenic mice function to extend the plasma half-life of IgG and albumin. Therefore, these mouse models will be utilized to characterize FcBP fusion proteins *in vivo*.

3.5 References

1. Roopenian, D. C. & Akilesh, S. FcRn: the neonatal Fc receptor comes of age. *Nat Rev Immunol* **7**, 715–725 (2007).
2. Rath, T. *et al.* The immunologic functions of the neonatal Fc receptor for IgG. *J. Clin. Immunol.* **33 Suppl 1**, S9–17 (2013).
3. Wilson, I. A. & Bjorkman, P. J. Unusual MHC-like molecules: CD1, Fc receptor, the hemochromatosis gene product, and viral homologs. *Curr. Opin. Immunol.* **10**, 67–73 (1998).
4. Claypool, S. M., Dickinson, B. L., Yoshida, M., Lencer, W. I. & Blumberg, R. S. Functional reconstitution of human FcRn in Madin-Darby canine kidney cells requires co-expressed human beta 2-microglobulin. *J. Biol. Chem.* **277**, 28038–50 (2002).
5. Israel, E. J., Wilsker, D. F., Hayes, K. C., Schoenfeld, D. & Simister, N. E. Increased clearance of IgG in mice that lack beta 2-microglobulin: possible protective role of FcRn. *Immunology* **89**, 573–8 (1996).
6. Ghetie, V. *et al.* Abnormally short serum half-lives of IgG in beta 2-microglobulin-deficient mice. *Eur. J. Immunol.* **26**, 690–6 (1996).
7. Junghans, R. P. & Anderson, C. L. The protection receptor for IgG catabolism is the beta2-microglobulin-containing neonatal intestinal transport receptor. *Proc. Natl. Acad. Sci. U. S. A.* **93**, 5512–6 (1996).
8. Martin, W. L., West Jr., A. P., Gan, L. & Bjorkman, P. J. Crystal structure at 2.8 Å of an FcRn/heterodimeric Fc complex: mechanism of pH-dependent binding. *Mol Cell* **7**, 867–877 (2001).
9. Kim, J. K., Tsen, M. F., Ghetie, V. & Ward, E. S. Catabolism of the murine IgG1 molecule: evidence that both CH2-CH3 domain interfaces are required for persistence of IgG1 in the circulation of mice. *Scand. J. Immunol.* **40**, 457–65 (1994).
10. Petkova, S. B. *et al.* Enhanced half-life of genetically engineered human IgG1 antibodies in a humanized FcRn mouse model: potential application in humorally mediated autoimmune disease. *Int Immunol* **18**, 1759–1769 (2006).
11. Andersen, J. T. *et al.* Structure-based mutagenesis reveals the albumin-binding site of the neonatal Fc receptor. *Nat. Commun.* **3**, 610 (2012).
12. Chaudhury, C. *et al.* The major histocompatibility complex-related Fc receptor for IgG (FcRn) binds albumin and prolongs its lifespan. *J Exp Med* **197**, 315–322 (2003).

13. Schmidt, M. M. *et al.* Crystal Structure of an HSA/FcRn Complex Reveals Recycling by Competitive Mimicry of HSA Ligands at a pH-Dependent Hydrophobic Interface. *Structure* **21**, 1966–78 (2013).
14. Chaudhury, C., Brooks, C. L., Carter, D. C., Robinson, J. M. & Anderson, C. L. Albumin binding to FcRn: distinct from the FcRn-IgG interaction. *Biochemistry* **45**, 4983–90 (2006).
15. Andersen, J. T., Daba, M. B., Berntzen, G., Michaelsen, T. E. & Sandlie, I. Cross-species binding analyses of mouse and human neonatal Fc receptor show dramatic differences in immunoglobulin G and albumin binding. *J. Biol. Chem.* **285**, 4826–36 (2010).
16. Ober, R. J., Radu, C. G., Ghetie, V. & Ward, E. S. Differences in promiscuity for antibody-FcRn interactions across species: implications for therapeutic antibodies. *Int Immunol* **13**, 1551–1559 (2001).
17. Rath, T. *et al.* Fc-fusion proteins and FcRn: structural insights for longer-lasting and more effective therapeutics. *Crit. Rev. Biotechnol.* (2013). doi:10.3109/07388551.2013.834293
18. Sleep, D., Cameron, J. & Evans, L. R. Albumin as a versatile platform for drug half-life extension. *Biochim. Biophys. Acta* **1830**, 5526–34 (2013).
19. Ying, T., Chen, W., Gong, R., Feng, Y. & Dimitrov, D. S. Soluble Monomeric IgG1 Fc. *J. Biol. Chem.* **287**, 19399–408 (2012).
20. Mezo, A. R. *et al.* Reduction of IgG in nonhuman primates by a peptide antagonist of the neonatal Fc receptor FcRn. *Proc. Natl. Acad. Sci. U. S. A.* **105**, 2337–42 (2008).
21. Andersen, J. T. *et al.* Selection of Nanobodies that Target Human Neonatal Fc Receptor. *Sci. Rep.* **3**, (2013).
22. Wang, Z., Fraley, C. & Mezo, A. R. Discovery and structure-activity relationships of small molecules that block the human immunoglobulin G-human neonatal Fc receptor (hIgG-hFcRn) protein-protein interaction. *Bioorg. Med. Chem. Lett.* **23**, 1253–6 (2013).
23. Sockolosky, J. T., Tiffany, M. R. & Szoka, F. C. Engineering neonatal Fc receptor-mediated recycling and transcytosis in recombinant proteins by short terminal peptide extensions. *Proc. Natl. Acad. Sci. U. S. A.* **109**, 16095–16100 (2012).
24. Proetzl, G. & Roopenian, D. C. Humanized FcRn mouse models for evaluating pharmacokinetics of human IgG antibodies. *Methods* (2013).
25. Vaccaro, C., Zhou, J., Ober, R. J. & Ward, E. S. Engineering the Fc region of immunoglobulin G to modulate in vivo antibody levels. *Nat Biotechnol* **23**, 1283–1288 (2005).

26. Patel, D. a *et al.* Neonatal Fc receptor blockade by Fc engineering ameliorates arthritis in a murine model. *J. Immunol.* **187**, 1015–22 (2011).
27. Tam, S. H., McCarthy, S. G., Brosnan, K., Goldberg, K. M. & Scallon, B. J. Correlations between pharmacokinetics of IgG antibodies in primates vs. FcRn-transgenic mice reveal a rodent model with predictive capabilities. *MAbs* **5**, 397–405 (2013).
28. Zalevsky, J. *et al.* Enhanced antibody half-life improves in vivo activity. *Nat. Biotechnol.* **28**, 157–159 (2010).
29. Sockolosky, J. T. & Szoka, F. C. Periplasmic production via the pET expression system of soluble, bioactive human growth hormone. *Protein Expr. Purif.* **87**, 129–35 (2013).
30. Chaudhury, C., Brooks, C. L., Carter, D. C., Robinson, J. M. & Anderson, C. L. Albumin binding to FcRn: distinct from the FcRn-IgG interaction. *Biochemistry* **45**, 4983–90 (2006).
31. Andersen, J. T. *et al.* Single-chain Variable Fragment Albumin Fusions Bind the Neonatal Fc Receptor (FcRn) in a Species-dependent Manner: Implications for in vivo half-life evaluation of albumin fusion therapeutics. *J. Biol. Chem.* **288**, 24277–85 (2013).
32. West, A. P. & Bjorkman, P. J. Crystal Structure and Immunoglobulin G Binding Properties of the Human Major Histocompatibility Complex-Related Fc Receptor \dagger , \ddagger . *Biochemistry* **39**, 9698–9708 (2000).
33. Dall’Acqua, W. F., Kiener, P. a & Wu, H. Properties of human IgG1s engineered for enhanced binding to the neonatal Fc receptor (FcRn). *J. Biol. Chem.* **281**, 23514–24 (2006).
34. Roopenian, D. C., Christianson, G. J. & Sproule, T. J. Human FcRn transgenic mice for pharmacokinetic evaluation of therapeutic antibodies. *Methods Mol Biol* **602**, 93–104 (2010).
35. Christianson, G. J. *et al.* Monoclonal antibodies directed against human FcRn and their applications. *MAbs* **4**, 208–16 (2012).
36. Andersen, J. T. *et al.* Anti-carcinoembryonic antigen single-chain variable fragment antibody variants bind mouse and human neonatal Fc receptor with different affinities that reveal distinct cross-species differences in serum half-life. *J. Biol. Chem.* **287**, 22927–37 (2012).
37. Dall’Acqua, W. F. *et al.* Increasing the affinity of a human IgG1 for the neonatal Fc receptor: biological consequences. *J. Immunol.* **169**, 5171–80 (2002).

38. Vaccaro, C., Zhou, J., Ober, R. J. & Ward, E. S. Engineering the Fc region of immunoglobulin G to modulate in vivo antibody levels. *Nat. Biotechnol.* **23**, 1283–1288 (2005).
39. Vaccaro, C., Bawdon, R., Wanjie, S., Ober, R. J. & Ward, E. S. Divergent activities of an engineered antibody in murine and human systems have implications for therapeutic antibodies. *Proc. Natl. Acad. Sci.* **103**, 18709–18714 (2006).
40. Proetzel, G., Wiles, M. V & Roopenian, D. C. Genetically Engineered Humanized Mouse Models for Preclinical Antibody Studies. *BioDrugs* (2013). doi:10.1007/s40259-013-0071-0
41. Wang, W. *et al.* Monoclonal Antibodies with Identical Fc Sequences Can Bind to FcRn Differentially with Pharmacokinetic Consequences. *Drug Metab. Dispos.* **39**, 1469–77 (2011).
42. Krimpenfort, P. *et al.* Crosses of two independently derived transgenic mice demonstrate functional complementation of the genes encoding heavy (HLA-B27) and light (beta 2-microglobulin) chains of HLA class I antigens. *EMBO J.* **6**, 1673–6 (1987).
43. Pedersen, L. O. *et al.* The interaction of beta 2-microglobulin (beta 2m) with mouse class I major histocompatibility antigens and its ability to support peptide binding. A comparison of human and mouse beta 2m. *Eur. J. Immunol.* **25**, 1609–16 (1995).
44. Michaëlsson, J., Achour, A., Rölle, A. & Kärre, K. MHC class I recognition by NK receptors in the Ly49 family is strongly influenced by the beta 2-microglobulin subunit. *J. Immunol.* **166**, 7327–34 (2001).
45. Bjerager, L., Pedersen, L. O., Bregenholt, S., Nissen, M. H. & Claesson, M. H. MHC class I phenotype and function of human beta 2-microglobulin transgenic murine lymphocytes. *Scand. J. Immunol.* **44**, 615–22 (1996).
46. Mitsuki, M., Matsumoto, N. & Yamamoto, K. A species-specific determinant on beta2-microglobulin required for Ly49A recognition of its MHC class I ligand. *Int. Immunol.* **16**, 197–204 (2004).
47. Choi, T., Ferris, S. T., Matsumoto, N., Poursine-Laurent, J. & Yokoyama, W. M. Ly49-dependent NK cell licensing and effector inhibition involve the same interaction site on MHC ligands. *J. Immunol.* **186**, 3911–7 (2011).

Chapter 4: The *in vivo* fate of FcBP fusion proteins and liposomes in wild type and human FcRn transgenic mice

4.1 Introduction

The most common approaches to extend the half-life of low molecular weight proteins rely on increasing hydrodynamic diameter either by conjugation to large hydrophilic polymers, such as PEG¹, or by genetic fusion to long, flexible polypeptide extensions². Such strategies substantially increase molecular weight, which may alter tissue penetration and biological activity of the fusion protein. The neonatal Fc receptor (FcRn) has emerged as an exciting biological target to improve the pharmacokinetics and delivery of therapeutic agents and in particular protein-based drugs³. To date there are two clinically validated strategies that hijack FcRn to extend the half-life of protein drugs: Fc-⁴ or albumin-fusion⁵. Both strategies rely on the ability of FcRn to salvage IgG and albumin from intracellular catabolism and also on the substantial increase in molecular weight of the fusion protein due to the size of the Fc-domain and albumin (>50 kDa), which reduces renal clearance. Aside from Fc- and albumin-fusion, there are no alternative protein engineering strategies that hijack FcRn to improve the drug like properties of protein therapeutics.

Increasing protein half-life without increasing molecular weight is a challenge due to the rapid elimination of small proteins by the kidney. There are two examples of small peptide ligands that when genetically fused to proteins enable half-life extension *in vivo* either by engineering binding to serum albumin⁶ or to the surface of erythrocytes⁷. Both strategies target molecules that are present at high concentrations in the blood with relatively long serum half-lives. Upon injection, the peptide-protein fusions bind albumin or erythrocytes and are sequestered in the blood thereby restricting filtration through the glomerulus resulting in half-life

extension. A potential advantage of targeting FcRn over serum components is its ability to not only extend circulation but also enable non-invasive protein administration through a FcRn-dependent transcytosis process⁸. The latter is not possible when engineering albumin or erythrocyte binding.

Recently, Mezo and colleagues identified peptides from a phage library that bound human FcRn⁹. After extensive chemical modification^{10,11} a high affinity, pH-independent synthetic peptide inhibitor of the IgG-FcRn interaction was engineered as a candidate for the treatment of IgG-mediated autoimmune disease. The phage identified FcRn binding peptide (FcBP) however exhibits pH-dependent binding to FcRn through a series of ionic, hydrophobic, and hydrogen bond interactions, similar to the IgG-FcRn interaction^{12,13}. Therefore, we sought to re-mix the Mezo approach and hypothesized that the phage identified FcBP without further optimization would be an ideal ligand to engineer pH-dependent FcRn binding into proteins.

In Chapter 1 we demonstrated that genetic fusion of short, terminal FcBP extensions to proteins, termed FcBP fusion, mimics the IgG-FcRn interaction and enables FcRn-dependent recycling and transcytosis *in vitro* suggesting that FcBP fusion may be an attractive way to improve both protein half-life and delivery without substantially increasing molecular weight. In this chapter we determined the *in vivo* fate of FcBP fusion proteins in wild type and human FcRn transgenic mice with the intention of validating the FcBP fusion platform as a novel half-life extension and delivery strategy. To our surprise we found no correlation between the *in vitro* and *in vivo* properties of FcBP fusion proteins.

We investigated a number of potential factors that could explain the *in vivo* results such as: 1) the role of molecular weight and renal clearance, 2) peptide stability in blood, 3) serum competition for FcRn binding, 4) the function of the hybrid human-mouse FcRn/ β 2m receptor,

and 5) the role of valence using FcBP modified liposomes. Unfortunately, no single factor could explain the absence of a FcRn-dependent half-life improvement of either FcBP fusion proteins or liposomes *in vivo*. To account for this absence of protein half-life improvement, we speculate that alternative, unknown factor(s), in collaboration with FcRn, are important in regulating IgG homeostasis *in vivo* and are not mimicked by FcBP fusion.

4.2 Methods

4.2.1 Materials

Cholesterol, 1,2-dipalmitoyl-*sn*-glycero-3-phosphoethanolamine-N-(lissamine rhodamine B sulfonyl), (DPPE-Rho), 1,2-distearoyl-*sn*-glycero-3-phosphoethanolamine-N-[methoxy(polyethylene glycol)-2000] (PEG-DSPE), 1,2-distearoyl-*sn*-glycero-3-phosphoethanolamine-N-[maleimide(polyethylene glycol)-2000] (MAL-PEG-DSPE), and L- α -phosphatidylcholine, hydrogenated (Soy) (HSPC) were purchased from Avanti Polar Lipids (Alabaster, AL). α -[3-(3-Maleimido-1-oxopropyl)amino]propyl- ω -methoxy, polyoxyethylene, 40 kDa (mPEG-MAL-40) [Cat. ME-400MA, Lot M113102] was purchased from NOF America Corporation (White Plains, NY) and α -[3-(3-Maleimido-1-oxopropyl)amino]propyl- ω -methoxy, polyoxyethylene, 20 kDa (mPEG-MAL-20) [Cat. PJK-231, Lot ZQ46321] was purchased from Creative PEGWorks (Winston Salem, NC). Human IgG1 (Avastin®, bevacizumab) was obtained from the UCSF Medical Center and Mouse IgG1 (MOPC-21 isotype control) was obtained from the UCSF Monoclonal Antibody Core facility. Human serum albumin (A8763), N-acetyl-L-cysteine (NAC), Tris(2-carboxyethyl)phosphine hydrochloride (TCEP), dithiothreitol (DTT), iodoacetamide (IAM), ovalbumin, ampicillin, Terrific Broth (TB), heparin, and all buffer salts were purchased from Sigma-Aldrich (St. Louis, MO). AnaTag™ 5 – TAMRA protein labeling kit was purchased from AnaSpec (Fremont, CA). Succinimidyl-4-(*N*-maleimidomethyl)cyclohexane-1-carboxylate (SMCC) and 10 kDa MWCO SnakeSkin dialysis tubing were purchased from Thermo Scientific (Rockford, IL). Normal mouse serum (Cat. NC9256463) was purchased from Fisher Scientific (Waltham, MA). Human AB serum (Cat. 35-060-CI, Lot. 1L1900) was purchased from Mediatech, Inc. (Manassas, VA). Rabbit serum (Cat. 16120) was purchased from Gibco, Life Technologies (Grand Island, NY). Anti-rabbit goat pAB

IgG (HRP conjugated, Cat. ab6721, Lot 882103), rabbit mAb to beta 2 microglobulin (Cat. ab75853, Lot GR390-3), and rabbit mAb to human FcRn (Cat. ab139152) were purchased from Abcam (Cambridge, MA). Mouse monoclonal anti- β -Actin antibody (Cat. A5541, clone AC-15, Lot 061M4808) was purchased from Sigma (St. Louis, MO). Anti-mouse donkey IgG-HRP (Cat. 715-035-150, Lot 92320) was purchased from Jackson-ImmunoResearch (West Grove, PA). All restriction enzymes and buffers used for cloning were purchased from New England Biolabs (Beverly, MA) and all primers were purchased from IDT (San Diego, CA).

4.2.2 Cell Culture

MDCK wild type cells were cultured as described in Chapter 2, Section 2.2.2. MDCK hFcRn-EYFP/h β 2M cells were generated as previously described¹⁴ and maintained in MDCK wild type media supplemented with 0.3 mg/mL Hygromycin B and 0.4 mg/mL G418. Primary rabbit kidney cells (purchased from the UCSF cell culture facility) were maintained in DMEM high glucose (DME H-21) supplemented with 10% FBS. All cells were maintained in a humidified environment at 37 °C and 5% CO₂.

4.2.3 Mice

C57BL/6J, Tg276/Tg276, and Tg32/Tg32 mice were purchased from The Jackson Laboratory (Bar Harbor, ME), bred, and maintained as described in Chapter 3, Section 3.2.3.

We initially had difficulties breeding Tg276/Tg276 homozygous mice. Typical Tg276/Tg276 litters were small (~ 6 – 8 pups) and the number of mice that survived after weaning was even less (~ 4 – 6). We reasoned that the breeding phenotype was a result of the lack of mouse Fcgrt that could not be rescued by the human FCGRT transgene. Because we initially purchased only a single breeding pair of Tg276/Tg276 mice due to cost, to overcome the initial breeding bottleneck we generated heterozygous mice by crossing Tg276/Tg276 males to

C57BL/6J females. The resulting Tg276 heterozygous mice have one copy of mouse Fcgrt and human FCGRT. We also purchased a Tg32/Tg32 breeding pair after our initial Tg276/Tg276 breeding difficulties and generated Tg32 heterozygous mice as described for the Tg276 heterozygous strain. We utilized the heterozygous mice throughout our studies until we could generate a large enough colony of homozygous Tg276/Tg276 and Tg32/Tg32 mice. Interestingly, we did not have as many issues breeding Tg32/Tg32 mice although the litter sizes were typically small (~ 6 – 8 pups) when compared to the typical litter size for wild type C57BL/6J mice (~ 8 – 10 pups). Therefore, as the research progressed we switched our focus from Tg276 to the Tg32 strain and its derivatives as we had less breeding issues and the half-life of hIgG1 is slightly longer in this strain suggesting that any *in vivo* effect of FcBP modification would more likely be detected in Tg32/Tg32 versus Tg276/Tg276 mice.

To generate FcRn α -chain null mice (FcRn KO) we first crossed C57BL/6J females to Tg32 homozygous males to generate an intermediate mouse heterozygous for mouse Fcgrt and human FCGRT transgene [mFcRn^{-/+} hFcRn^{Tg32/+}], named mFcRn/Tg32. mFcRn/Tg32 siblings were intercrossed and pups null for both the mouse Fcgrt and human FCGRT transgene were selected for further breeding to establish a colony of FcRn KO mice for experiments. These mice are FcRn α -chain null but wild type at the mouse β 2m locus in a pure C57BL/6J background.

To generate human FCGRT and human β 2M transgenic mice we crossed male NOD.Cg-B2m^{tm1Unc} Tg(B2M)55Hpl/Dvs (hB2M; Jackson Laboratory stock number 003355) mice to female Tg32/Tg32 mice resulting in an intermediate mouse heterozygous for mouse Fcgrt, human FCGRT transgene, mouse β 2m, and human β 2M transgene, named Tg32/Tg55 [mFcRn^{-/+}; hFcRn^{Tg32/+}; m β 2m^{-/+}; h β 2M^{Tg55/+}]. We then intercrossed Tg32/Tg55 siblings to generate a

fully human FcGRT and β 2M transgenic mouse in a murine Fcgrt and β 2m null mixed background, named hFcRn^{Tg32/Tg32}/h β 2M^{Tg55/Tg55}. Mice of the correct genotype were used for further breeding to establish a colony of hFcRn^{Tg32/Tg32}/h β 2M^{Tg55/Tg55} for experiments. All mice genotypes were confirmed by qPCR analysis of genomic DNA isolated from tail biopsies. All genotyping was performed by TransnetYX, Inc. (Cordova, TN).

4.2.4 Mammalian expression vectors

Mammalian expression plasmids encoding hFcRn fused at its C-terminus to YFP and human β 2M are described in Chapter 2, Section 2.2.3 and reference¹⁴. The mammalian expression plasmid encoding mFcRn fused at its C-terminus to GFP¹⁵ was a kind gift of Dr. E. Sally Ward at the UT Southwestern Medical Center and the vector CP764 containing mouse β 2m cDNA was a kind gift of Dr. Lewis Lanier at the UCSF Helen Diller Family Comprehensive Cancer Center. The mouse β 2m expression plasmid was generated by PCR amplification of m β 2m cDNA from CP764 followed by restriction cloning into the 5' BamHI and 3' XhoI sites of the mammalian expression vector pcDNATM3.1/Hygro (+) (kindly provided by Dr. Kathy Giacomini, UCSF).

Cloning of rabbit FcRn and rabbit β 2m was performed by Dr. Vincent J Vinditto in the Szoka lab as a training exercise under the guidance of Jonathan Sockolosky. Rabbit mRNA was isolated from rabbit primary kidney cells using TRIzol® and converted to cDNA using the Superscript® III first-strand synthesis kit and oligo(dT) primers following the manufacturer's recommend protocol. The rabbit FcRn α -chain gene was PCR amplified from the rabbit cDNA library using primers designed based on the NCBI reference sequence: NM_001122937.1. The resulting PCR product was restriction cloned into the 5' EcoRI and 3' AgeI sites of the mammalian expression vector pEYFP-N1 (kindly provided by Dr. Alan Verkman, UCSF). The

rabbit β 2m light chain was PCR amplified from the rabbit cDNA library using primers designed based on the projected rabbit β 2m gene sequence on chromosome 17 of the rabbit (*Oryctolagus cuniculus*) genome. The resulting PCR product was restriction cloned into the 5' BamHI and 3' XhoI sites of the mammalian expression vector pcDNATM3.1/Hygro (+). All plasmids were confirmed by DNA sequencing. A complete list of primers used in this study is in Table 4.1.

4.2.5 *E. coli* expression vectors

The bacterial expression vectors for mKate and FcBP modified mKates were generated as described in Chapter 2, Section 2.2.5. The solvent exposed cysteine residues of mKate (Cys134 and Cys242) were mutated to Ser with mutagenic oligonucleotides using the QuikChange Lightning mutagenesis kit (Agilent Technologies; Santa Clara, CA) to yield the expression vector pETmKate Δ Cys. To create constructs for site-specific PEGylation of mKate and N-&-C-Term Linear FcBP mKate, a Ser128Cys substitution was generated by mutagenesis of pETmKate Δ Cys and pETmKNICl to yield pETmKate Δ CysPEG and pETmKNICIPEG. The resulting vectors encode mKate and N-&-C-Term Linear FcBP mKate with a single, solvent exposed Cys residue for site-specific conjugation to a maleimide containing PEG chain.

The gene encoding mKate modified at its C-terminus with an albumin binding polypeptide (ABP) sequence¹⁶ was constructed by PCR amplification of mKate from pETmKate Δ Cys with primers designed to insert DNA encoding a cyclic ABP sequence (Cyclic: QRLMEDICLPRWGCLWEDDF) separated from the C-terminus of mKate by a flexible linker (GGGGS). The resulting PCR product was purified and restriction cloned into the NdeI and BamHI restriction sites of the bacterial expression vector pET15b (Novagen; San Diego, CA) to yield the final expression vector pETmKateABP. All plasmids were confirmed by DNA sequencing. A complete list of primers used in this study is provided in the Table 4.1. Amino

acid sequences of proteins used in this study are provided in the Appendix A.

Table 4.1 Primers used in this study

Protein	Primer Pair	Restriction Site
Rabbit FcRn-YFP	F=5'-CTTCGAATTCCGGCCACGCAGCATGGGGC-3'	EcoRI
	R=5'-GCGACCGGTCCGGAGCCCCCTCCGCCGGAGCCCCCTCCGCCGGCAGTGGCCGGGAAGGCG-3'	AgeI
Rabbit B2m	F=5'-GCTCGGATCCACCATGTGCGCTCCGTCTTGG-3'	BamHI
	R=5'-CTAGACTCGAGTTAGTAATCTCGATCCCATTTC-3'	XhoI
Mouse B2m	F=5'-GCTCGGATCCACCATGGCTCGCTCGGTGACCCTGG-3'	BamHI
	R=5'-CTAGACTCGAGTCCACATGTCTCGATCCCAG-3'	XhoI
C-Term Cyclic ABP mKate	F=5'-CGGCAGCCATATGTCTGAACTGATCA-3'	NdeI
	R=5'-CAGCCGGATCCCCTAAAAGTCATCTTCCCACAGGCAGCCCCAACGAGGCAGGCAAATATCTTCCATAAGACGTGCGAGCCGCCGCCCTTTATGGCCCAGTTTAGAG-3'	BamHI
mKate C134S Mutagenesis	5'-CAGTCTGCAGGACGGTAGTCTGATCTATAACGT G-3'	---
mKate C242S Mutagenesis	5'-TGGCCGTCGCTCGTTATAGCGACCTGC-3'	---
mKate S128C Mutagenesis for PEGylation	5'-GGCGTAAACTTCCCCTGCAACGGTCCAGTGATGC-3'	---

4.2.6 Synthetic FcRn binding peptides

All synthetic peptides were synthesized and purified by CPC Scientific Inc. (Sunnyvale, CA) and supplied as a lyophilized powder. The synthetic FcBPs were designed to enable simple bioconjugate chemistries by installing a free N-terminal Cys residue followed by a short Gly₄Ser linker and the FcBP sequence. Two synthetic peptides were used in this chapter: 1) a linear FcBP [NH₂-CGGGGSQRFVTGHFGGLYPANG-NH₂] and 2) a cyclic FcBP [NH₂-CGGGGSQRF-cyclo-(-DTGHFGGLYP-Dap-)-NG-NH₂] constrained by a non-reducible lactam bridge between D and Dap (1,2-diaminopropionic acid) such that a free N-terminal Cys could be installed and the peptide could be purified without the risk of disulfide heterogeneity.

4.2.7 FcBP modified mKate protein expression and purification

Expression of mKate and all modified versions of mKate was carried out in BL21-Codon Plus (DE3)-RIPL *E. coli* cells harboring expression vectors described in Section 4.2.4 and in

Chapter 2, Section 2.2.5. Protein expression and purification was as described in Chapter 2, Section 2.2.6.

4.2.8 Affinity measurements by surface plasmon resonance

SPR measurements for N-&-C Term Cyclic FcBP mKate binding to human and mouse FcRn were obtained using a BIAcore T100 instrument as described in Chapter 3, Section 3.2.6

4.2.9 Size exclusion chromatography

Purification of proteins by size exclusion chromatography was as described in Chapter 3, Section 3.2.4.

4.2.10 FACS cellular accumulation, serum competition, ligand competition, and serum stability assays

Labeled protein or liposome accumulation in MDCK hFcRn-EYFP/h β ₂m cells was quantified as previously described¹⁴. Briefly, cells were washed twice in HBSS(+), pH 6 binding buffer [Hank's Balanced Salt Solution (HBSS), 1% ovalbumin, 50 mM MES, pH 6] and incubated with serial dilutions of proteins for 1 hr at 37 °C to permit cellular uptake. Cells were washed three times with cold binding buffer to remove unbound protein, trypsinized, and analyzed on a FACS Array cell sorter (BD Biosciences; San Jose, CA). Mean fluorescent intensities (MFI) for each test population were derived after gating for live and EYFP positive cells. Binding at pH 7.4 was as described above except all incubations and washes were done in HBSS(+), pH 7.4 [HBSS, 1% ovalbumin, 50 mM HEPES, pH 7.4]. Protein accumulation in wild type MDCK cells at pH 6 was as described above. All incubations were done in triplicate and data is represented as mean \pm SD.

Serum competition for accumulation of hIgG1, HSA, and FcBP modified mKates in MDCK hFcRn-EYFP/h β ₂m cells was evaluated by FACS. Cells were incubated with 1.5 μ M of hIgG1-TAMRA or FcBP modified mKates or 15 μ M HSA-TAMRA in serial dilutions of

purchased mouse or human serum, or freshly isolated C57BL/6J or Tg276/Tg276 plasma. Serum/plasma was first titrated to pH 6 by addition of 75 mM MES, pH 6 and passed through a 0.45 μ m clarifying filter. Serum containing labeled protein was serially diluted into HBSS, 50 mM MES, pH 6 also containing labeled protein both at the concentrations described above. Cells were washed twice with HBSS, pH 6 and incubated as described above prior to FACS analysis. All incubations were done in triplicate and data is represented as mean \pm SD.

Purified ligand (IgG and albumin) competition with mKate-cFcBP binding to MDCK hFcRn-EYFP/h β 2m cells was also evaluated by FACS. Unlabeled hIgG1 and HSA were first titrated to pH 6 by addition of 75 mM MES, pH 6 and passed through a 0.22 μ m sterilizing filter. HBSS, pH 6 containing 350 μ M unlabeled hIgG1 or 500 μ M unlabeled HSA and 1.5 μ M mKate-cFcBP was serially diluted into HBSS, pH 6 containing 1.5 μ M mKate-cFcBP. Cells were washed and incubated with protein solutions as described above prior to FACS analysis. All incubations were done in triplicate and data is represented as mean \pm SD.

4.2.11 Analysis of ligand binding to hybrid FcRn/ β 2m receptors in MDCK cells

The binding of IgGs, albumins, and N- & C-Term Cyclic FcBP mKate to FcRn/ β 2m receptor and receptor hybrids was evaluated by FACS after transient transfection of MDCK cells with the FcRn heavy chain and species-matched or mixed β 2m light chain. 175,000 MDCK cells per well were seeded in a 6-well plate and cultured overnight. MDCK cells were co-transfected with human, mouse, and rabbit FcRn-YFP/GFP expression plasmids in combination with human, mouse, and rabbit β 2m using Lipofectamine 2000 (Invitrogen) following the manufacturer's recommended 6-well plate protocol. A 1 μ g : 5 μ g ratio of FcRn-YFP/GFP to β 2m plasmid was used for all transient transfections as MDCK cells lacking over-expressed β 2m do not produce functional FcRn¹⁷. Cells were incubated with Lipofectamine / DNA complexes in OptiMEM

reduced serum media for 6 – 8 hrs, the media was exchanged with MDCK cell culture media, and cells were cultured overnight to allow for gene/protein expression. Transfected MDCK cells were washed twice with 1 mL HBSS(+), pH 6 binding buffer [Hank's Balanced Salt Solution (HBSS), 1% ovalbumin, 50 mM MES, pH 6] and incubated with 750 μ L of a 1 μ M solution of hIgG1-TAMRA, mIgG1-TAMRA, rabIgG-TAMRA or FcBP modified mKates, or 15 μ M HSA-TAMRA or MSA-TAMRA in binding buffer for 1 hr at 37 °C to permit cellular uptake. Cells were washed three times with 1 mL cold binding buffer to remove unbound protein, trypsinized, pelleted, re-suspended in 120 μ L binding buffer and analyzed on a FACS Array cell sorter. The mean fluorescent intensity corresponding to labeled-protein was derived by first gating for live cells based on the forward scatter (FSC) and side scatter (SSC), and then gating on the FcRn-positive cell population based on a YFP/GFP fluorescence greater than 1000 MFI. All FACS data were analyzed using FlowJo (Tree Star Inc.; Ashland, OR).

4.2.12 Western blot analysis of FcRn, β 2m, and β -actin

The relative expression of FcRn and β 2m after transient transfection of MDCK cells described in Section 4.2.11 was determined by western blot analysis of whole cell lysates. Transfected cells were washed twice in MDCK cell media to remove dead cells and lysed with 0.5 mL of 0.5 % CHAPS in D-PBS containing a Complete EDTA-free protease inhibitor tablet (Roche; Indianapolis, IN) for 1 hr at 4 °C with constant shaking. Cell debris was pelleted by centrifugation and the supernatant containing proteins of interest was isolated and stored at – 80 °C until use. An equal mass of total protein was loaded onto a 12% Tris-HCl SDS-PAGE gel under reducing conditions and separated at 180 V for 45 mins. The separated proteins were transferred to a PVDF membrane overnight at 4 °C under constant voltage (30 V). Blots were first blocked with blocking buffer [5% milk, 0.1% Tween 20 in D-PBS] then probed with either

anti-FcRn, anti- β 2m, or anti- β -actin primary antibody at a 1:200, 1:10000, and 1:5000 dilution, respectively, in blocking buffer. Blots were washed extensively with D-PBS and probed with an HRP conjugated secondary antibody at a 1:20000 dilution in blocking buffer. Blots were again washed extensively in D-PBS and developed with the SuperSignal West Pico Chemiluminescent Substrate kit following the manufactures recommended protocol (Thermo Scientific; Rockford, IL) and visualized using a Kodak Image Station (Kodak; Rochester, NY). All blocking, primary, and secondary antibody incubations were for 1 hr at room temperature.

4.2.13 PEGylation of N-&-C-Term Linear FcBP mKate (mKate-IFcBP)

mKate-IFcBP (15 mL at 1.8 mg/mL) was reduced overnight at room temperature with 10 mol excess DTT to mKate-IFcBP then dialyzed for 4 hrs against D-PBS using a 10 kDa MWCO membrane (Thermo) to remove excess reducing agent. Reduced mKate-IFcBP was split into 4 mL, 5 mL, and 5 mL aliquots and alkylated or PEGylated by addition of 2 mol excess IAM (0.5 M aqueous stock solution), mPEG-MAL-20 (~ 8.3 mg solid), or mPEG-MAL-40 (~ 21.6 mg solid), respectively, for 2.5 hrs at room temperature. Unreacted maleimide was quenched by addition of 1 mol NAC (0.25 M aqueous stock solution) to mol mPEG-MAL and incubated for 20 min at room temperature. PEGylated and alkylated mKate-IFcBPs were dialyzed overnight into D-PBS using a 10 kDa MWCO membrane to remove excess small molecule impurities. Alkylated and PEGylated proteins were analyzed by SDS-PAGE and size exclusion chromatography. Alkylated mKate-IFcBP was used as a negative control for *in vitro* and *in vivo* studies.

4.2.14 Preparation of synthetic FcBP modified liposomes

Fluorescently labeled unilamellar liposomes were prepared according to the method of Olson et al.¹⁸. HSPC, cholesterol, PEG-DSPE, MAL-PEG-DSPE, and DPPE-Rho in a

55:40:2.5:2.5:0.2 molar ratio (50 μ M total lipid) were dried under a rotary evaporator for ~ 2 hr and then overnight under high vacuum to form a thin lipid film. The synthetic cyclic FcBP (~ 6 mg) was hydrated in 5 mL of aqueous buffer containing 50 mM HEPES, 0.3 M Sucrose, pH 7 (buffer A) and reduced by addition of 2 mol excess TCEP (~ 1.7 mg) for 2 hr at room temperature. The reduced peptide solution was heated to 60 °C and dried lipids were re-hydrated in the peptide solution (2 mol excess peptide per mol MAL-PEG-DSPE) by vigorous vortexing followed by sonication for 10 minutes at 60 °C. A 2 mol excess of NAC per mol MAL-PEG-DSPE was added to inactivate all unreacted maleimide groups and incubated for 1 hr at room temperature. Liposomes were dialyzed overnight into buffer A using a 100 kDa MWCO membrane (Spectrum; New Brunswick, NJ) to remove excess FcBP and small molecule impurities. Immediately prior to use liposomes were diluted 1:1 in buffer A, heated to 60 °C, and subsequently extruded 5 times through a 100 nm polycarbonate filter and 10 times through a 80 nm polycarbonate filter. Liposome size was confirmed by dynamic light scattering using a Malvern Zetasizer NanoZS (Westborough, MA).

4.2.15 Preparation of mIgG1-SMCC-FcBP

Mouse IgG1 (5.2 mg/mL in D-PBS) was first labeled with 5-TAMRA as described in Chapter 3, Section 3.2.7 and desalted over a PD-10 column equilibrated in D-PBS to remove free dye. Labeled mIgG1 was then incubated with 8 mol SMCC (50 mM DMSO solution) per mol of mIgG1 for 1 hr at room temperature. The linear synthetic FcBP (~ 32 mg/mL DMSO solution) was added in excess at 2 mol FcBP per mol SMCC for 1 hr at room temperature. Free maleimides were quenched by addition of excess N-acetyl cysteine (NAC) at 2 mol NAC (250 mM aqueous solution) per mol SMCC for 1 hr at room temperature. mIgG1-SMCC-FcBP was dialyzed overnight into D-PBS using a 10 kDa MWCO membrane (Thermo Scientific; Rockford,

IL) to remove excess peptide, linker, and small molecule impurities and subsequently purified by size exclusion chromatography as described in Chapter 3, Section 3.2.5.

4.2.16 Plasma clearance in mice

Protein and liposome plasma clearance was evaluated in wild type C57BL/6J and human FcRn transgenic mice. Mice (n = 9 per group) received a 10 mg/kg intravenous (i.v.) tail vein injection of mKate or an equimolar 11.4 mg/kg i.v. injection of FcBP modified mKates in 200 μ L D-PBS. PEGylated FcBP modified mKates, mIgG1, and mIgG1-SMCC-FcBP were all dosed i.v. at 10 mg/kg. FcBP modified liposomes were dosed i.v. at 1 μ mol total lipid per mouse. Blood samples were collected into heparinized tubes through submandibular cheek pouch bleeds. Blood was centrifuged at 6,000 rpm for 6 min and the plasma was diluted 1:10 into D-PBS and assayed by fluorometry on a Spex Fluorolog fluorometer (Horiba Jobin Yvon; Edison, NJ) with 5 nm excitation and emission slits. mKate plasma clearance was assayed directly and label-free based on the intrinsic far-red fluorescent properties of mKate (Ex/Em: 588/620). mIgG1 and mIgG1-SMCC-FcBP were labeled with 5-carboxytetramethylrhodamine (5-TAMRA; Ex/Em: 547/574) using the AnaTagTM 5-TAMRA protein labeling kit at a ratio ~ 2 – 3 mol 5-TAMRA per mol protein to enable detection in mouse plasma via fluorescence. DPPE-Rho (Ex/Em: 560/583) was incorporated into FcBP modified liposome formulations to enable detection via fluorescence. All plasma samples were normalized to the maximum fluorescence observed in the first bleed 5 min after injection and plotted as % injected dose (%ID) versus time. The α - and β - phase half-life of mKate and FcBP modified mKates were calculated by fitting the plasma clearance curves (%ID vs. time) to a 1-compartment PK model, $Y = 10^{(k \cdot X + Y_0)}$, or 2-compartment PK model, $Y = C_0 e^{k_1 \cdot x} + C_1 e^{k_2 \cdot x}$, depending on the shape of the clearance curves using Prism 5 (GraphPad Software; La Jolla, CA).

4.3 Results

4.3.1 Binding kinetics between N-&-C-Term Cyclic FcBP mKate (mKate-cFcBP) and mouse and human FcRn

We first determined the binding kinetics of mKate-cFcBP to both human and mouse FcRn by surface plasmon resonance (SPR) to confirm the previously reported selectivity of the synthetic FcBP for human but not mouse FcRn⁹. As expected mKate-cFcBP binds human FcRn (Fig. 4.1a,b) with a K_D of ~ 1775 nM and ~ 34 μ M at pH 6 and pH 7.4, respectively, but lacks appreciable binding to mouse FcRn at concentrations up to 5 μ M (Fig. 4.1c,d). The lack of FcBP binding to mouse FcRn enables the use of wild type C57BL/6J mice as a negative control for all *in vivo* studies.

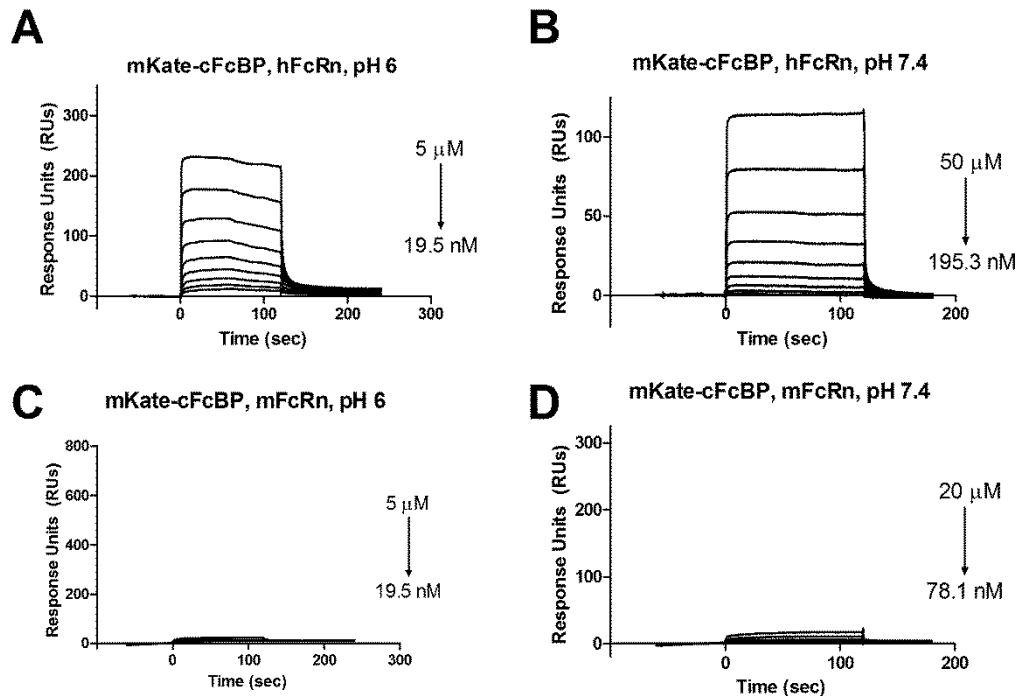


Figure 4.1. Surface plasmon resonance sensograms of mKate-cFcBP binding to mouse and human FcRn at pH 6 and pH 7.4

Serial dilutions of mKate-cFcBP were injected over immobilized human (a,b) and mouse FcRn (c,d) at pH 6 (a,c) or pH 7.4 (b,d). The resulting sensograms were fit to the bivalent analyte model for derivation of binding kinetics and affinity.

4.3.2 Plasma clearance of mKate and FcBP modified mKate

In chapter 3 we validated the utility of human FcRn transgenic mice to study the plasma clearance of the endogenous human FcRn ligands IgG and albumin. Therefore, we extended our analysis to determine if FcBP fusion results in a FcRn-dependent half-life extension in mice. Mice were dosed i.v. with 10 mg/kg mKate or equimolar 11.4 mg/kg FcBP modified mKate via the tail vein and decay of mKate in plasma was monitored by fluorometry. mKate is rapidly eliminated from circulation in C57BL/6J and Tg276/Tg276 mice with a terminal half-life of ~ 5 min (Fig. 4.2a and Table 4.2). The short half-life of mKate (~ 26 kDa) is likely the result of rapid elimination via the kidney as is the case for most plasma proteins with a molecular mass below ~ 50-60 kDa¹⁹ that readily pass through the fenestrated endothelium and podocyte slit diaphragm of the glomerulus²⁰. N-&-C-Term Linear FcBP mKate (mKate-lFcBP) is also rapidly eliminated from circulation in both Tg276/Tg276 and Tg32 mice with a $t_{1/2}$ of ~ 5 min (Fig. 4.3b) despite its pH-dependent interaction with human FcRn *in vitro*. N-&-C-Term Cyclic FcBP mKate (mKate-cFcBP) has an extended half-life compared to mKate or mKate-lFcBP with two distinct elimination phases: a rapid α -phase and a slightly extended β -phase (Fig 4.2c and Table 4.2). However, the α - and β -phase half-life of mKate-cFcBP are similar in wild type C57BL/6J, Tg276, Tg276/Tg276, and Tg32 mice indicating that the extended half-life of mKate-cFcBP compared to mKate and mKate-lFcBP is independent of interaction with human FcRn. mKate-cFcBP contains two Cys residues per peptide (4 total per mKate) that may contribute to the formation of disulfide aggregates during storage. Since mKate-cFcBP plasma clearance is not affected by the presence or zygosity of the human FcRn transgene in mice, it is likely that the half-life extension is an artifact due to the presence of low amounts of mKate related aggregates and not a result of human FcRn-mediated recycling.

As a comparison we determined the plasma half-life of mKate modified at its C-terminus with a serum albumin binding peptide (mKate-cABP) developed by Mark Dennis and colleagues at Genentech¹⁶. mKate-cABP has a half-life of ~ 8 hrs in Tg32 mice and likely in C57BL/6J mice; however, we did not calculate a half-life due to the lack of data points (Fig 4.2d). This represents an ~ 100-fold increase in half-life compared to unmodified mKate. Thus, targeting albumin, which is present at high concentrations in serum and immediately available for binding upon injection, is an attractive strategy to increase the plasma half-life of low molecular weight proteins without significantly altering hydrodynamic size.

In contrast, targeting FcRn with ligands that bind at acidic but not neutral pH requires endocytosis into FcRn-expressing cells prior to interaction with FcRn. The rate of protein endocytosis by parenchymal or hematopoietic cells that express FcRn^{21,22} may be much slower than the rate of renal filtration. Therefore, FcBP fusion may not be an attractive strategy to increase the half-life of low molecular weight proteins that are rapidly cleared from circulation via the kidney.

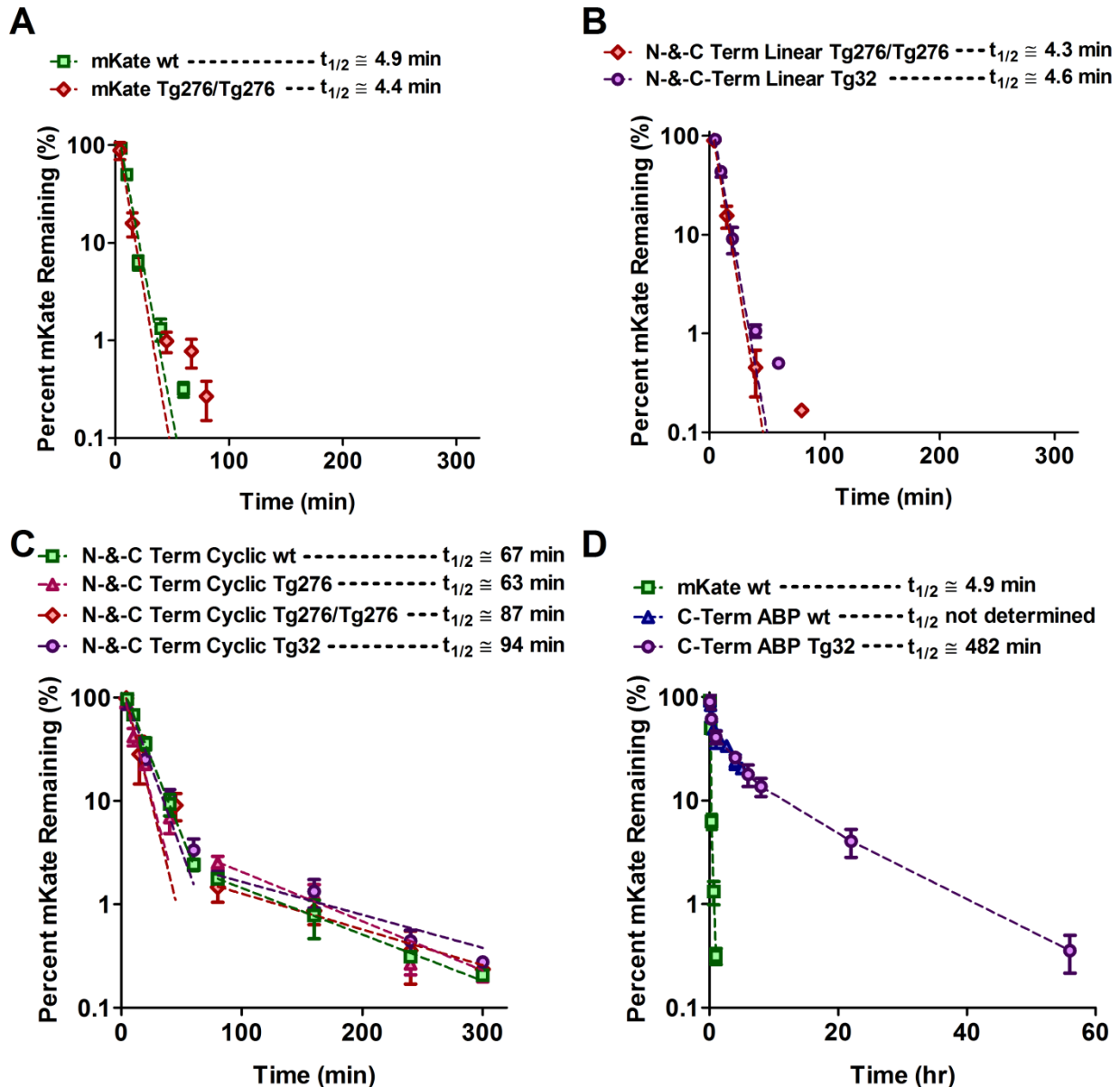


Figure 4.2. Plasma clearance of mKate and FcBP modified mKates in wild type and human FcRn transgenic mice

Equimolar i.v. dose of mKate (a), N-&-C-Term Linear FcBP mKate (b), N-&-C-Term Cyclic FcBP mKate (c), or C-Term Cyclic ABP mKate (d) at 10 mg/kg, 11.4 mg/kg, 11.4 mg/kg, and 11 mg/kg, respectively, via the tail vein. Blood was collected at various time points into heparized tubes and mKate plasma clearance was determined via fluorometry. The % mKate remaining was calculated by normalizing the fluorescent emission at all time points to the maximum value observed in the first bleed 5 min after injection of each labeled protein. Dashed lines represent the α - and β -phase data fit individually to a 1-compartment PK model in prism and the β -phase half-life shown in the figure was calculated as described in Section 4.2.16. The data shown in each panel are the mean (n=3 bleeds per time point) and error bars indicate s.d.

Table 4.2. Plasma half-life of mKate, FcBP modified mKates, ABP modified mKate in wild type, human FcRn transgenic, and human FcRn α -chain null (FcRn KO) mice.

Molecule	C57BL/6J		Tg276		Tg276/Tg276		Tg32		FcRn KO		Tg32/Tg55	
	$t_{1/2, \alpha}$ (min)	$t_{1/2, \beta}$ (min)	$t_{1/2, \alpha}$ (min)	$t_{1/2, \beta}$ (min)	$t_{1/2, \alpha}$ (min)	$t_{1/2, \beta}$ (min)	$t_{1/2, \alpha}$ (min)	$t_{1/2, \beta}$ (min)	$t_{1/2, \alpha}$ (min)	$t_{1/2, \beta}$ (min)	$t_{1/2, \alpha}$ (min)	$t_{1/2, \beta}$ (min)
mKate	4.9	---	4.0	---	4.4	---	n.d.	n.d.	n.d.	n.d.	n.d.	n.d.
mKate-cFcBP	10.3	67.1	6.9	63.2	6.3	87.0	9.4	94.3	8.8	56.1	5.8	54.0
mKate-lFcBP	n.d.	n.d.	n.d.	n.d.	4.3	---	4.6	---	n.d.	n.d.	n.d.	n.d.
mKate-cABP	NQ	NQ	n.d.	n.d.	n.d.	n.d.	11.5	482	n.d.	n.d.	n.d.	n.d.

Data from α - and β -phase % injected dose versus time were individually fit to a semilog line model, $Y = 10^{(k \cdot X + Y_0)}$, for derivation of $t_{1/2, \alpha}$ and $t_{1/2, \beta}$. NQ = not quantifiable due to lack of sufficient data points. n.d. = not determined.

4.3.3 Ligand binding to hybrid FcRn/ β 2m receptor *in vitro*.

Although mKate-cFcBP mimics the hIgG1 interaction with human FcRn *in vitro*, the half-life of FcBP fusion proteins in C57BL/6J and human FcRn transgenic mice is independent of FcRn binding whereas the half-life of IgG and albumin correlate with their species matched FcRn-binding affinity. These results prompted a cross-species evaluation of the FcRn heavy chain and β 2m light chain heterodimer interaction and ability to support ligand binding as the human FcRn transgenic mice express a hybrid human-mouse FcRn/ β 2m receptor. Although the hybrid human-mouse receptor has been shown to bind hIgG1 in cell-based²³ and SPR assays²⁴, in both cases the receptor is presented on the surface making it immediately available for ligand binding. Although useful to interrogate binding, these assays formats do not address potential differences in cellular trafficking, surface presentation, or stability of the hybrid FcRn/ β 2m receptors. To address this, we transiently transfected MDCK cells with full length mouse, rabbit, or human FcRn-YFP/GFP in combination with mouse, rabbit, or human β 2m and evaluated IgG, albumin, and mKate-cFcBP accumulation by FACS.

Accumulation of IgGs, albumins, and mKate-cFcBP in MDCK cells expressing the fully human or fully mouse FcRn/ β 2m receptor (Fig. 4.3a and Fig. 4.4a,b) correlate with affinity and

species specificity for FcRn determined by SPR in Chapter 3, Sections 3.3.2-3 and Chapter 4, Section 4.3.1. Negligible protein accumulation was observed in cells lacking exogenous β 2m consistent with the known dependence of FcRn function on β 2m expression in cells^{17,25,26}, mice²⁷⁻³⁰, and humans³¹. All ligands bind multiple combinations of human, rabbit, and mouse FcRn/ β 2m hybrid receptors (Fig. 4.3a and Fig. 4.4a,b) suggesting that the FcRn heavy chain is promiscuous in its partnership with β 2m and functional when expressed in MDCK cells. The reduced ligand accumulation in cells expressing human FcRn/ β 2m hybrid receptors is the result of reduced FcRn and β 2m protein levels determined by Western blot analysis of whole cell lysates (Fig. 4.3b). FcRn expression levels are also likely to explain the differences observed for mouse and rabbit FcRn ligand binding; however, the antibodies used did not cross react with mouse and rabbit FcRn or rabbit β 2m (Fig. 4.3b and Fig. 4.4c). Nonetheless, the data indicate that FcRn is promiscuous in its interaction with β 2m from various species and the hybrid receptors are functional in ligand binding *in vitro*. Therefore, the lack of correlation between half-life in mice and FcRn binding is not due to the lack of mKate-cFcBP binding to the hybrid human-mouse FcRn/ β 2m receptor, at least *in vitro*.

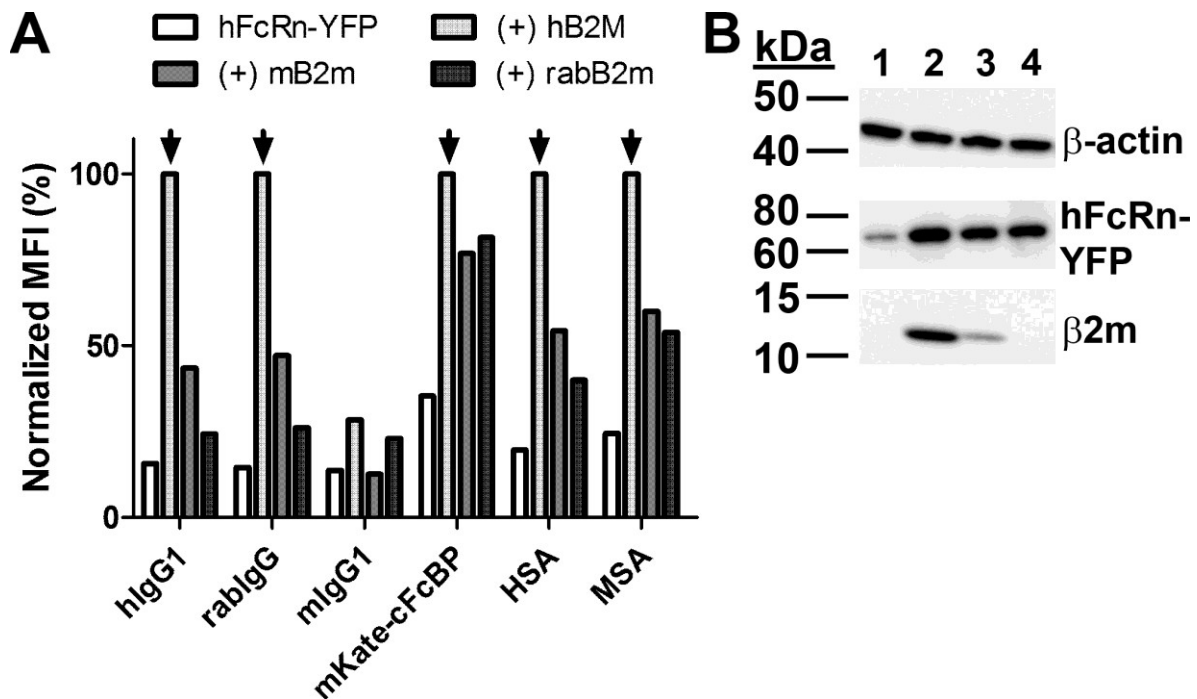


Figure 4.3. Ligand accumulation in MDCK cells expressing hybrid human FcRn / β 2m receptors

(a) MDCK cells transfected with human FcRn-YFP alone or in combination with either human, mouse, or rabbit β 2m were pulsed with 1 μ M hIgG1, mIgG1, rabIgG and mKate-cFcBP or 15 μ M HSA and MSA for 1 hr at pH 6, 37 $^{\circ}$ C and analyzed by FACS. The mean fluorescent intensity, MFI, for each ligand was normalized internally to the maximum MFI observed for the respective FcRn/ β 2m species combination indicated by the arrow. Note: mIgG1 was normalized to the maximum MFI observed for the mFcRn/h β 2M species combination indicated in Figure 4.X **(b)** Western blot analysis on whole cell lysates from MDCK cells transfected with hFcRn-YFP alone (lane 1) or in combination with either human (lane 2), mouse (lane 3), or rabbit β 2m (lane 4). Note: the anti- β 2m antibody used for western blot analysis does not cross react with rabbit β 2m.

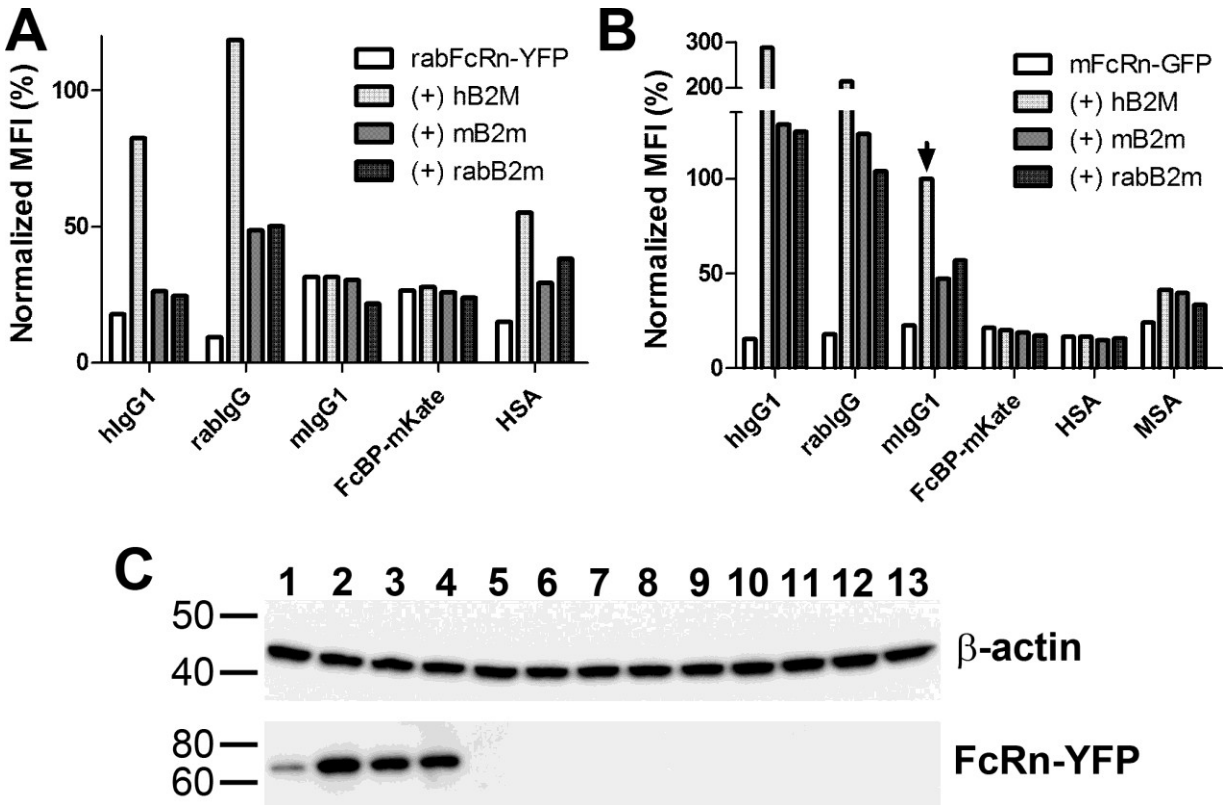


Figure 4.4. Ligand accumulation in MDCK cells expressing hybrid mouse or rabbit FcRn / β 2m receptors

MDCK cells transfected with rabbit FcRn-YFP (a) or mouse FcRn-GFP (b) alone or in combination with either human, mouse, or rabbit β 2m were pulsed with 1 μ M hlgG1, mlgG1, rablgG and mKate-cFcBP or 15 μ M HSA and MSA for 1 hr at pH 6, 37 $^{\circ}$ C and analyzed by FACS. The mean fluorescent intensity, MFI, for each ligand was normalized internally to the maximum MFI observed for the respective FcRn/ β 2m species combination indicated by the arrow. Note: Aside from mlgG1, ligands were normalized as indicated in Figure 4.X. (c) Western blot analysis on whole cell lysates from MDCK cells transfected with hFcRn-YFP (lanes 1-4), mFcRn-GFP (lanes 5-8), or rabFcRn-YFP (lanes 9-12) alone (lanes 1, 5, 9) or in combination with either human (lane 2, 6, 10), mouse (lane 3, 7, 11), or rabbit β 2m (lane 4, 8, 12). Lane 13 is the un-transfected MDCK cell negative control. Note: the anti-FcRn antibody used for western blot analysis does not cross react with mouse or rabbit FcRn.

4.3.4 mKate-cFcBP plasma clearance in FcRn knockout and Tg35/Tg55 heterozygous mice

To be certain that mouse FcRn present in wild type mice does not contribute to the plasma clearance of FcBP modified mKate *in vivo*, even though FcBP does not bind mouse FcRn *in vitro* (Fig 4.1 and reference⁹), we generated FcRn α -chain null mice that lack both the human and mouse FcRn (FcRn KO mice). The α - and β -phase half-life of mKate-cFcBP in FcRn KO

mice is ~ 9 min and ~ 56 min, respectively, similar to wild type and human FcRn transgenic mice (Fig. 4.5 and Table 4.2) confirming that C57BL/6J mice are a representative negative control. The β -phase half-life of mKate-cFcBP in FcRn KO mice is slightly shorter than in the other mouse strains. However, we believe this reflects the amount of aggregate in the protein preparation that varies with each expression and purification and not an FcRn-dependent effect as the α -phase half-life is very similar across strains (Table 4.2).

In addition, we evaluated the plasma clearance of mKate-cFcBP in Tg32/Tg55 mice that carry one copy each of hFcRn, mFcRn, h β 2M, and m β 2m. Therefore, if the hybrid human-mouse FcRn/ β 2m were non-functional in FcBP binding or trafficking *in vivo*, this heterozygous strain would presumably have some fraction of fully human-human FcRn/ β 2M receptor that could act to salvage FcBP modified mKates. The half-life of mKate-cFcBP is similar in Tg32/Tg55 and FcRn KO mice (Fig. 4.5) indicating that the human-human FcRn/ β 2M receptor does not act to extend the *in vivo* circulation time of mKate-cFcBP. The same protein preparation was used for PK studies in FcRn KO and Tg32/Tg55 mice further indicating that the small variations in the β -phase half-life across strains is an artifact of protein purity and not FcRn.

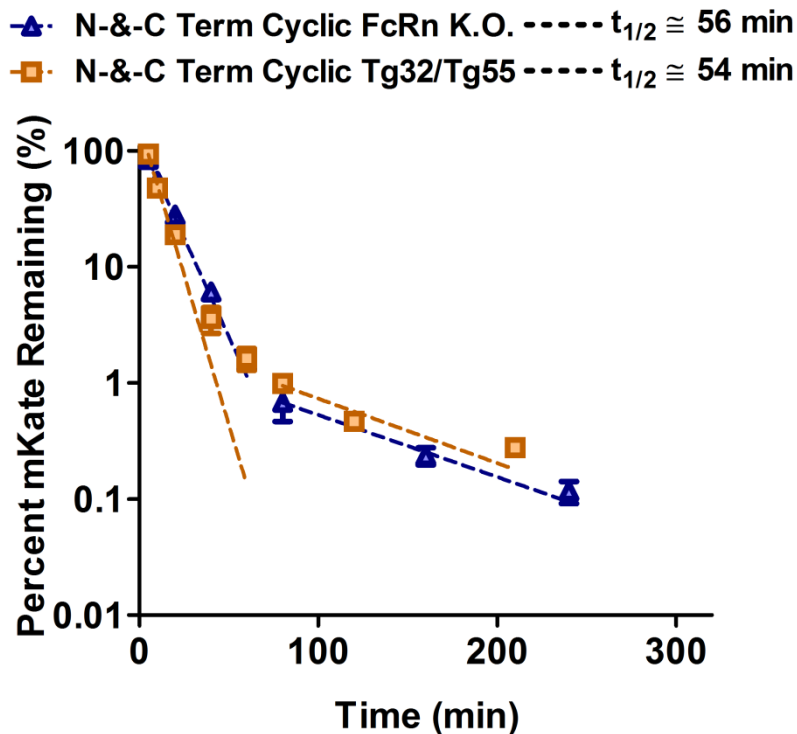


Figure 4.5. Plasma clearance of N-&-C-Term Cyclic FcBP mKate in FcRn knockout and Tg32/Tg55 transgenic mice

N-&-C-Term Cyclic FcBP mKate was dosed i.v. at 11.4 mg/kg via the tail vein. Blood was collected at various time points into heparinized tubes and plasma clearance was determined via fluorometry. The % mKate remaining (%ID) was calculated by normalizing the fluorescent emission at all time points to the maximum value observed in the first bleed 5 min after injection of each labeled protein. Dashed lines represent the α - and β -phase data fit individually to a 1-compartment PK model in prism and the β -phase half-life shown in the figure was calculated as described in Section 4.2.16. The data shown in each panel are the mean (n=3 bleeds per time point) and error bars indicate s.d.

4.3.5 PEGylation of mKate-IFcBP to reduce renal clearance

Although FcBP fusion did not extend the half-life of the low molecular weight protein mKate, FcBP fusion may be advantageous for proteins that are not rapidly eliminated by renal filtration. To test this we increased the hydrodynamic size of mKate-IFcBP by site-specific covalent conjugation to a 20 kDa or 40 kDa PEG chain. A single, solvent-exposed Cys residue was introduced into a flexible loop opposite the N-&-C-Term Linear FcBP mKate (mKate-IFcBP) termini to minimize the potential of disrupting binding to FcRn after PEGylation (Fig.

4.6a). mKate-IFcBP was subsequently alkylated or PEGylated by addition of thiol reactive IAM or MAL-PEG, respectively. Alkylated, 20 kDa, and 40 kDa PEGylated mKate-IFcBP migrate at ~ 25 kDa, ~ 60 kDa, and ~ 100 kDa by reducing SDS-PAGE (Fig. 4.6b) and with a predicted molecular weight of ~ 26 kDa, ~ 276 kDa, and ~ 550 kDa by size exclusion chromatography under non-denaturing conditions (Fig. 4.6c). Alkylated and 40 kDa PEGylated mKate-IFcBP bind human FcRn *in vitro* with a $U_{1/2, \max}$ of 2.4 μM and 4.3 μM , respectively, similar to hIgG1 (Fig. 4.6d). As expected, alkylated mKate-IFcBP is rapidly eliminated from circulation of Tg32 mice with a half-life of ~ 0.08 hrs (Fig 4.6e) due to its small size. PEGylation increases the half-life of mKate-IFcBP by ~ 175-fold to 14 hrs due to the substantial increase in molecular weight that reduces renal clearance; however, the half-life of 40 kDa PEG mKate-IFcBP is the same in both C57BL/6J and Tg32 mice (Fig. 4.6e). Thus, increasing the molecular weight of mKate-IFcBP by PEGylation does not result in a human FcRn-specific half-life *in vivo* despite the ability to bind human FcRn *in vitro*.

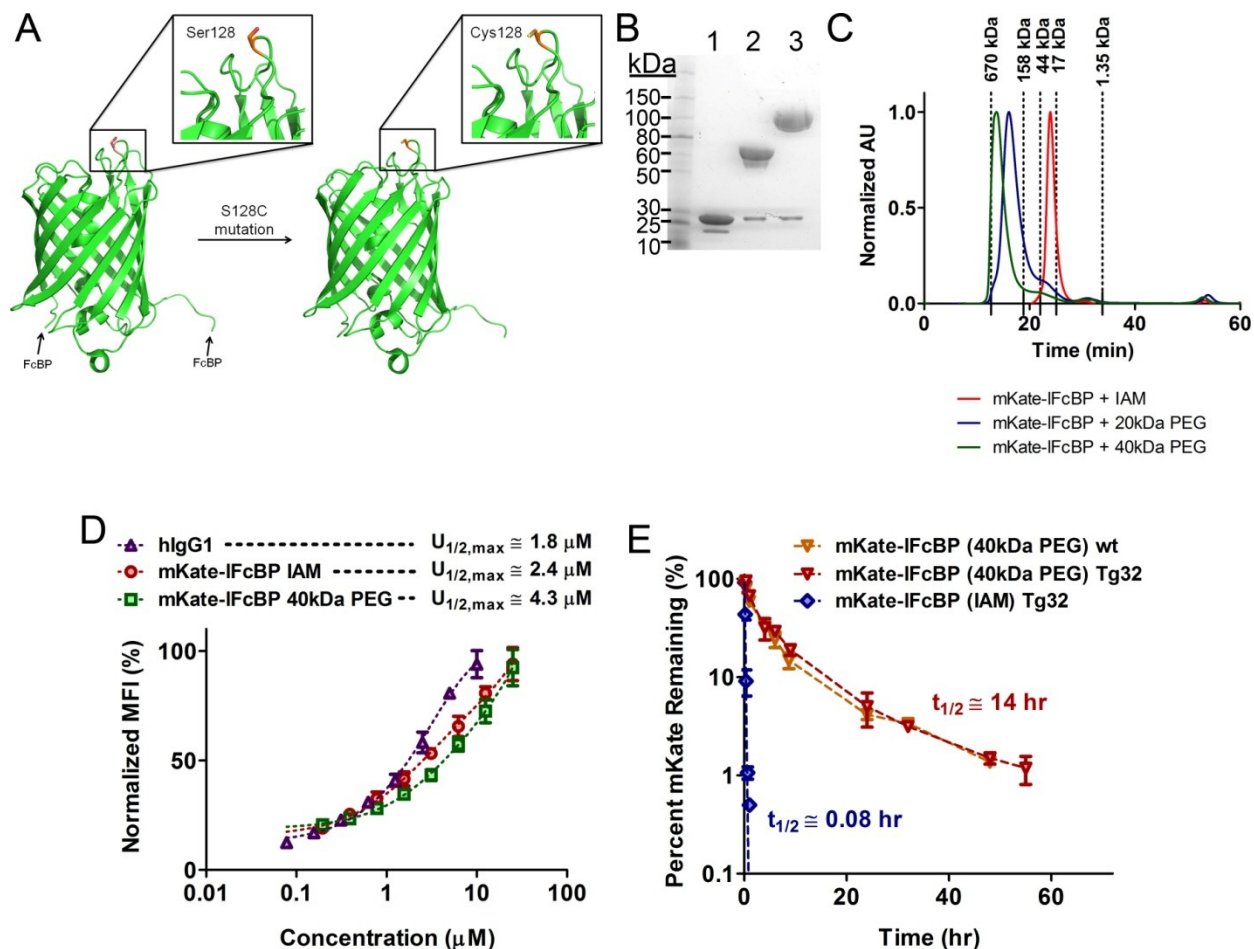


Figure 4.6. PEGylation does not impact FcRn-binding or result in human FcRn specific half-life extension in mice.

(a) A solvent exposed Cys residue was introduced into a flexible loop of mKate-IFcBP by mutagenesis of Ser128 for site specific PEGylation. (b) Reducing SDS-PAGE analysis of alkylated mKate-IFcBP (lane 1), 20 kDa PEGylated mKate-IFcBP (lane 2), and 40 kDa PEGylated mKate-IFcBP (lane 3). (c) Size exclusion chromatography analysis of alkylated mKate-IFcBP (red trace), 20 kDa PEGylated mKate-IFcBP (blue trace), and 40 kDa PEGylated mKate-IFcBP (green trace). Dashed lines indicate the retention time of the protein standards used to calibrate the size exclusion column and calculate an approximate molecular weight of the various mKate-IFcBP modified proteins. (d) Cellular accumulation of alkylated and PEGylated mKate-IFcBP in MDCK hFcRn-EYFP/hβ2M cells pulsed with increasing concentrations at pH 6. The dashed line represents data fit to a one-site total binding model in Prism. The data shown are the mean (n=3) and error bars indicate s.d. (e) Plasma clearance of alkylated and 40 kDa PEGylated mKate-IFcBP in wild type and Tg32 mice dosed i.v. with 10 mg/kg protein via the tail vein. The percent mKate remaining was calculated by normalizing the fluorescent emission at all time points to the maximum value observed in the first bleed 5 min after injection of each labeled protein. Dashed lines represent the α - and β -phase data fit individually to a 1-compartment PK model in prism and the α - and β -phase half-life shown in the figure was calculated as described in Section 4.2.16

4.3.6 Whole blood stability of FcBP modified mKates and hIgG1

The relatively flexible conformation of small polypeptides contributes to their enzymatic degradation in serum due to the presence of both membrane bound and soluble proteases³². Therefore, it is important to consider the serum stability of peptide-protein fusions as cleavage of peptide from the fusion protein, in this case mKate, could contribute to reduced activity *in vivo*. We evaluated the stability of FcBP modified mKates and hIgG1 in heparinized whole blood isolated from Tg276/Tg276 mice. FcBP modified mKates or hIgG1 were spiked into whole blood and incubated at 37 °C. At various time points plasma was isolated, diluted into HBSS(+), pH 6, and protein accumulation in MDCK hFcRn-EYFP/hβ2M cells was evaluated as a surrogate for blood stability. Human IgG1 is stable for up to 47 hrs in blood with little to no decline in accumulation in human FcRn-expressing MDCK cells (Fig. 4.7a). Both N-&-C-Term Cyclic and Linear FcBP mKate have a similar, gradual decline in accumulation over time with an ~ 40% reduction after 47 hrs (Fig. 4.7a). However, only a modest decline (~ 10% - 20%) in accumulation occurs over the relevant 0.5 to 5 hr time frame that FcBP modified mKates reside in serum *in vivo* (Fig. 4.7b). Collectively, the data indicate that FcBP modified mKates are relatively stable in blood and although there is a loss of activity after extended incubation, these data do not suggest that serum stability contributes significantly to the lack of FcBP fusion activity *in vivo*.

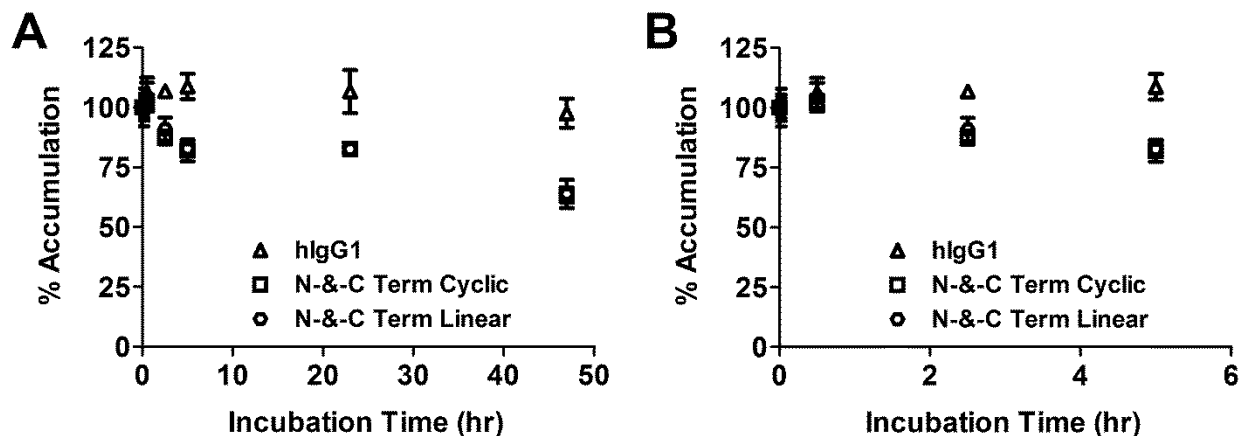


Figure 4.7. Whole blood stability of hIgG1, mKate-cFcBP, and mKate-IFcBP.

hIgG1, N-&-C-Term Cyclic FcBP mKate, or N-&-C-Term Linear FcBP mKate were spiked into heparinized blood isolated from Tg276/Tg276 mice to a final concentration of 5 μ M labeled protein and incubated at 37 $^{\circ}$ C. At the indicated times, blood was centrifuged and the plasma was diluted 1:5 into ice cold HBSS(+), pH 6. MDCK hFcRn-EYFP/h β 2M cells were pulsed for 1 hr at 37 $^{\circ}$ C with the diluted plasma samples and protein accumulation was analyzed by FACS. The % accumulation for each individual protein was calculated by normalizing the MFI for all time points to the maximum MFI observed at time zero. The data shown in each panel are the mean (n=3) and error bars indicate s.d. The data in panel (b) is the same as that in (a) but the scale on the x-axis was reduced to visualize changes in accumulation at early time points.

4.3.7 Serum competition for FcBP modified mKate and hIgG1 accumulation in MDCK hFcRn-EYFP/h β 2M cells

In addition to serum stability, the high concentrations of IgG and albumin in serum may compete with FcBP fusion proteins for salvage by FcRn *in vivo*. Therefore, we also determined the impact of plasma and serum on protein accumulation in MDCK hFcRn-EYFP/h β 2M cells. Human IgG1 and FcBP modified mKates were co-incubated with increasing concentrations of human or mouse plasma/serum titrated to pH 6 and the concentration at which half-maximal inhibition (IC₅₀) of ligand accumulation in MDCK hFcRn-EYFP/h β 2M cells occurs was determined by fitting the resulting data to a one site log IC₅₀ model in Prism.

Human serum potently inhibits the accumulation of hIgG1 in MDCK hFcRn-EYFP/h β ₂m cells with an IC₅₀ of ~15%, presumably due to the high levels of competing serum IgG (Figure 4.8b and Table 4.3). However, human serum only weakly inhibits N-&-C-Term Cyclic or Linear FcBP mKate (Fig. 4.8a and Table 4.3). The lack of potent competition may be due to subtle differences in binding kinetics, sterics, or binding mechanism that alter the rate of FcBP modified mKate binding and internalization by human FcRn compared to hIgG1. Tg276/Tg276 plasma has little to no effect on hIgG1 or FcBP modified mKate accumulation (Fig. 4.8b and Table 4.3) consistent with the low mouse serum IgG levels in Tg276/Tg276 mice³³ and the weak affinity of mouse serum IgG isotypes to human FcRn³⁴.

Surprisingly, C57BL/6J plasma inhibits hIgG1, N-&-C-Term Linear FcBP mKate, and N-&-C-Term Cyclic FcBP mKate accumulation (Fig. 4.8c and Table 4.3) with an IC₅₀ of ~ 12%, ~ 28%, and ~ 50%, respectively. However, mouse serum purchased from Fisher has little to no effect on hIgG1 and N-&-C-Term Cyclic FcBP mKate accumulation but potently inhibits human serum albumin accumulation, consistent with the cross-species binding of mouse serum albumin but not mouse serum IgG to human FcRn (Fig. 4.8d). These data suggest certain serum components may differ between C57BL/6J plasma and purchased mouse serum that result in differential and unexpected inhibition. Nonetheless, Tg276/Tg276 does not potently inhibit FcBP modified mKate accumulation in human FcRn expressing cells and does not explain the lack of FcBP function *in vivo*.

We also evaluated the ability of the purified endogenous FcRn ligands, IgG and albumin, to inhibit mKate-cFcBP accumulation in MDCK hFcRn-EYFP/h β ₂M cells. Human IgG1 inhibits mKate-cFcBP accumulation in human FcRn expressing cells with an IC₅₀ of ~ 300 μ M (Fig. 4.9) consistent with their overlapping binding sites on human FcRn¹². The weak inhibition

of mKate-cFcBP by purified hIgG1 explains lack of potent inhibition by human serum as the IgG concentration in human serum is less than $100 \mu\text{M}^{35}$. Human serum albumin does not compete with mKate-cFcBP accumulation (Fig. 4.9) consistent with their non-overlapping and non-competitive binding sites on human FcRn^{12,36}.

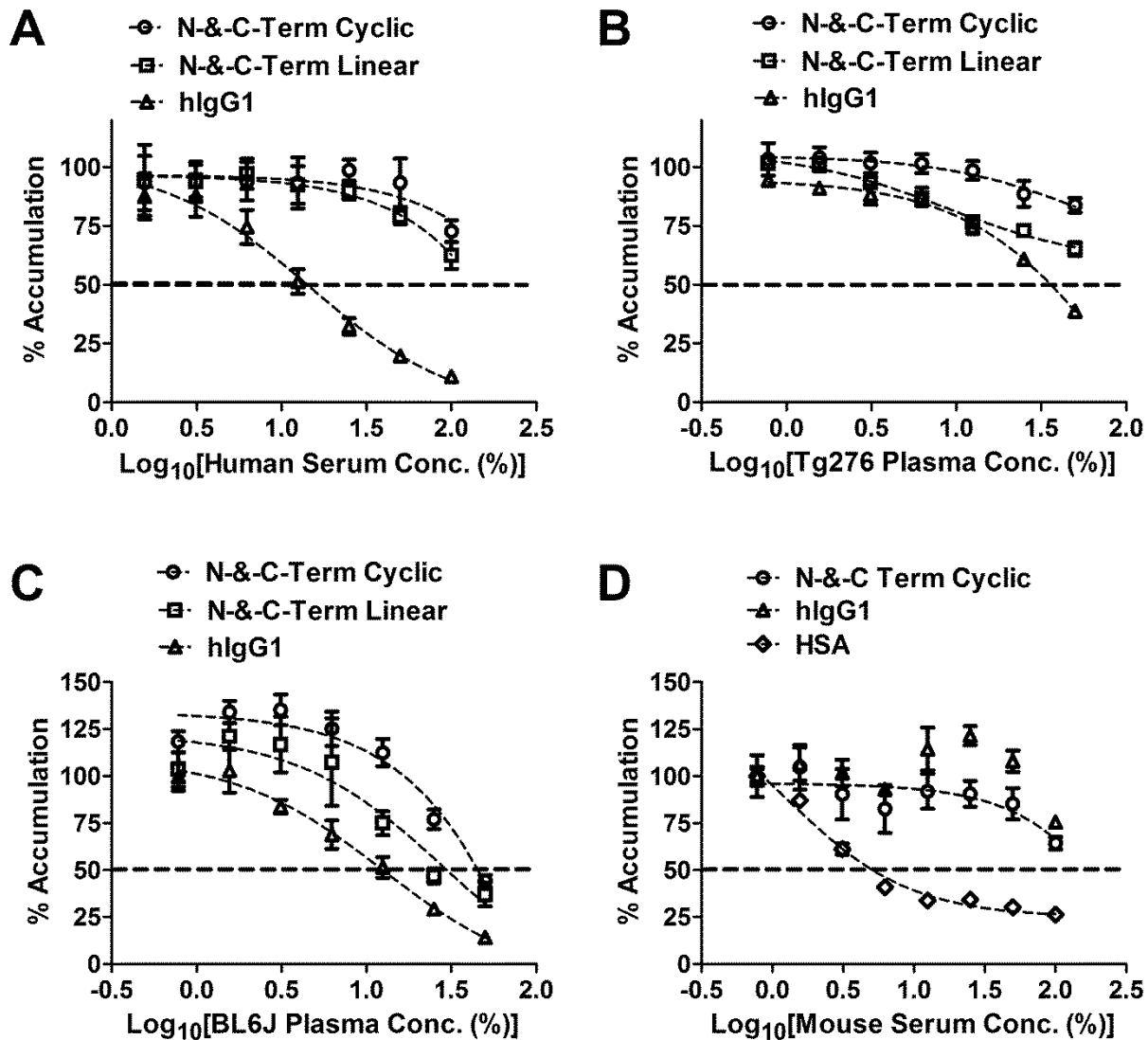


Figure 4.8. Serum competition of hIgG1, mKate-cFcBP, and mKate-IFcBP accumulation in MDCK hFcRn-EYFP/hβ2M cells by FACS.

Cellular accumulation of human FcRn ligands co-incubated with increasing concentrations of human serum (a), Tg276/Tg276 plasma (b), C57BL/6J plasma (c), or normal mouse serum (d) in MDCK hFcRn-EYFP/hβ2M at pH 6. Dashed lines represent data fit to a one-site log IC_{50} model in Prism. The % accumulation of each ligand was calculated by normalizing the MFI at each

serum/plasma concentration to the maximum observed MFI as the lowest plasma/serum concentration. The data shown in each panel are the mean (n=3) and error bars indicate s.d.

Table 4.3. Summary of IC₅₀ values derived from serum and plasma competition of IgG, albumin, and FcBP modified mKate accumulation in MDCK hFcRn-EYFP/hβ2M cells at pH 6 shown in Fig. 4.8.

Molecule	Human Serum IC ₅₀ (%)	Tg276 Plasma IC ₅₀ (%)	C57BL/6J Plasma IC ₅₀ (%)	Mouse Serum IC ₅₀ (%)
hIgG1	15	93	12	NQ
mKate-cFcBP	NQ	NQ	~ 50	NQ
mKate-lFcBP	NQ	NQ	28	n.d.
HSA	n.d.	n.d.	n.d.	1.3

(*) Data were fit to a one site LogIC50 model for derivation of IC₅₀. NQ, not quantifiable due to weak or no competition. n.d., not determined.

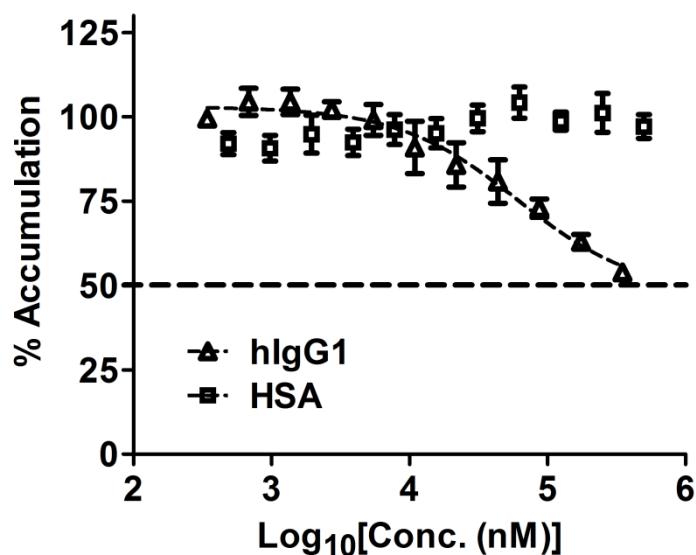


Figure 4.9. Purified hIgG1 and human serum albumin competition of mKate-cFcBP accumulation in MDCK hFcRn-EYFP/hβ2M cells by FACS.

Cellular accumulation of mKate-cFcBP co-incubated with increasing concentrations of human IgG1 or human serum albumin in MDCK hFcRn-EYFP/hβ2M at pH 6. Dashed lines represent data fit to a one-site log IC₅₀ model in Prism. The % accumulation of mKate-cFcBP was calculated by normalizing the MFI of each individual competitor concentration shown on the x-

axis to the maximum observed MFI at the lowest competitor concentration. The data shown in each panel are the mean (n=3) and error bars indicate s.d.

4.3.8 FcBP modified liposomes to probe the role of molecular weight and valency

Liposomes are predominantly cleared from circulation by cells of the mononuclear phagocyte system (MPS), primarily monocytes and macrophages, that reside in the lymph nodes, spleen, bone marrow, and liver^{37,38}. Hematopoietic cells derived from bone marrow progenitors are also major players in the FcRn-dependent catabolism of IgG²². Therefore, we reasoned that liposomes targeted to FcRn would provide the best opportunity to observe a FcRn-mediated *in vivo* effect. In addition, liposomes are large (~ 100 nm in diameter), have relatively long half-life in mice, and the valency of targeting ligand can be controlled by altering the amount of peptide displayed on the surface. We prepared PEGylated liposomes with varying amounts of FcBP displayed on the surface by conjugation to MAL-PEG-DSPE (Fig. 4.10a) and quantified dose-, pH-, and FcRn-dependent accumulation in MDCK hFcRn-EYFP/h β 2M cells *in vitro*. Liposomes containing 2.5 mol % or 5 mol % FcBP exhibit dose-dependent accumulation in MDCK hFcRn-EYFP/h β 2M cells at pH 6 whereas unmodified liposomes or liposomes containing 1 mol % FcBP are not endocytosed by human FcRn *in vitro* (Fig. 4.10b). At pH 7.4, accumulation of FcBP modified liposomes is dramatically reduced (Fig. 4.10c) confirming that FcBP modified liposomes retain pH-dependent binding to human FcRn. FcBP modified liposome accumulation in MDCK cells lacking human FcRn at pH 6 is negligible except at the highest concentration tested (250 μ M total lipid) presumably due to non-specific, ionic interactions between the protonated histidine residues within the FcBP and the negatively charged cell membrane (Fig 4.10d). Collectively, the data indicate that liposomes with at least

2.5 mol % FcBP interact specifically with human FcRn in MDCK cells in a pH-dependent manner.

We then determined the clearance of FcBP modified liposomes in wild type and Tg32/Tg32 transgenic mice. We chose to evaluate liposomes containing 2.5 mol % FcBP *in vivo* as this was the lowest concentration of FcBP that resulted in pH-dependent binding to human FcRn *in vitro* while minimizing the potential of non-specific binding (Fig. 4.10a,d). Mice were dosed i.v. with 1 μ mol total lipid via the tail vein and decay of FcBP modified liposomes in plasma was monitored by fluorometry. The half-life of FcBP modified liposomes is similar in both wild type C57BL/6J and Tg32/Tg32 mice (Fig. 4.11) indicating that liposome binding to human FcRn *in vitro* does not result in human FcRn-specific plasma clearance *in vivo*.

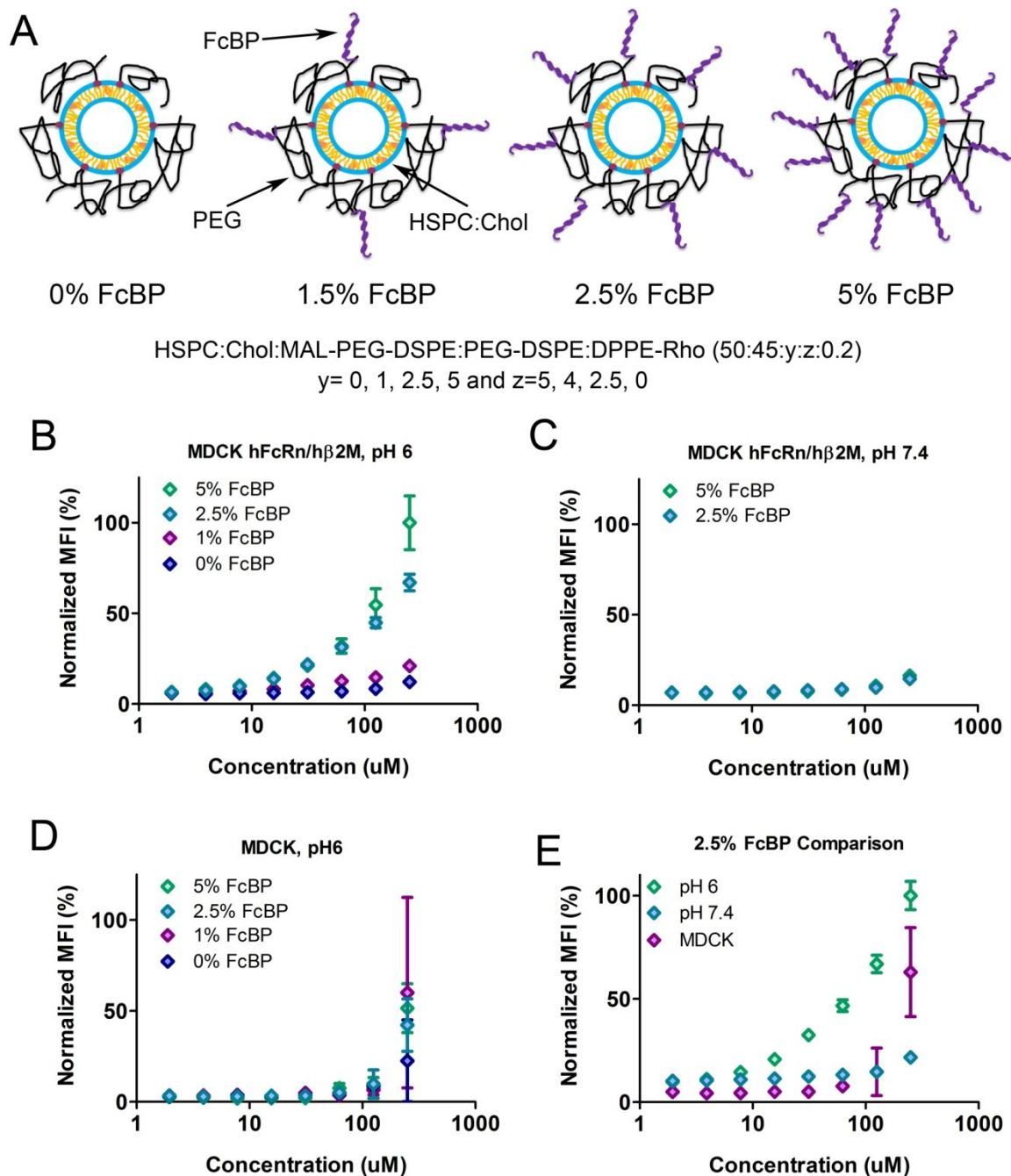


Figure 4.10. FcBP modified liposomes exhibit dose, pH, and FcRn dependent accumulation in MDCK hFcRn-EYFP/h β 2M cells

(a) Schematic depicting liposomes prepared from HSPC:Chol:PEG-DSPE containing increasing mol % of FcBP by increasing the mol % of MAL-PEG-DSPE. The final PEG-DSPE concentration was 5 mol % obtained by varying the respective concentration of PEG-DSPE and MAL-PEG-DSPE. Each formulation contains 0.2 mol % Rho-DSPE for to enable quantification of cellular accumulation by FACS. (b-e) Cellular accumulation of FcBP modified or control liposomes in MDCK hFcRn-EYFP/h β 2M cells (b, c) at pH 6 (b) or pH 7.4 (c) and in wild type MDCK cells at pH 6 (d). The MFI for FcBP modified or control liposomes was normalized to the maximum MFI for FcBP modified liposomes containing 5 mol % FcBP in panel b. (e)

Comparison of the cellular accumulation of FcBP modified liposomes containing 2.5 mol % FcBP, which was the selected formulation for *in vivo* studies, from panels b-d in MDCK hFcRn-EYFP/h β 2M cells at pH 6 (green diamonds) and pH 7.4 (blue diamonds) and in wild type MDCK cells at pH 6 (pink diamonds). The data shown in each panel are the mean (n=3) and error bars indicate s.d.

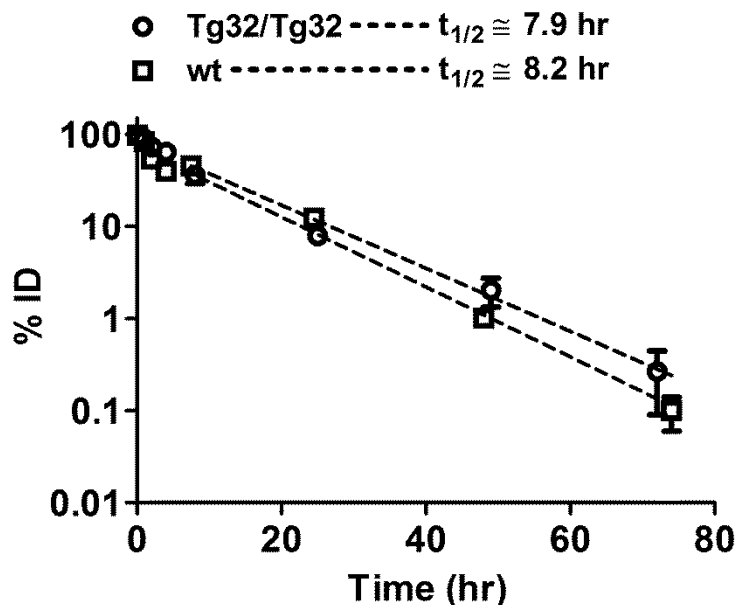


Figure 4.11. Plasma clearance of FcBP modified liposomes in wild type and human FcRn transgenic mice

Mice were dosed i.v. with 1 μ mol total lipid of liposomes containing 2.5 mol % cyclic FcBP via the tail vein. Blood was collected at various time points into heparinized tubes and FcBP modified liposome clearance was determined via fluorometry. The % FcBP modified liposomes remaining (%ID) was calculated by normalizing the fluorescent emission at all time points to the maximum value observed in the first bleed 5 min after injection of each labeled protein. Dashed lines represent the data fit to a 1-compartment PK model in prism and the β -phase half-life shown in the figure was calculated as described in Section 4.2.16. The data shown are the mean (n=3 bleeds per time point) and error bars indicate s.d.

4.3.9 mIgG1-SMCC-FcBP to probe alternative IgG regulatory mechanism

In this chapter we tested a number of variables that we hypothesized could contribute to the lack of FcBP function *in vivo* including: 1) the role of molecular weight and renal clearance, 2) peptide stability in blood, 3) serum competition for FcRn binding, 4) the function of the hybrid human-mouse FcRn/ β 2m receptor, and 5) the role of valence and alternative macromolecules. However, these variables do not adequately explain the lack of FcBP function *in vivo*. Either subtle differences in the FcBP-FcRn interaction do not enable FcRn-mediated recycling and transcytosis of FcBP fusion proteins *in vivo* or alternative unknown factors that contribute to the homeostasis of IgG are not replicated by the FcBP.

To probe the idea that an alternative factor contributes to the half-life of IgG *in vivo* we chemically coupled the FcBP to mouse IgG1 (Fig. 4.12a). If an additional IgG specific receptor is responsible for initiating or regulating FcRn function than engineering mIgG1 to bind human FcRn may result in the appropriate combination of unknown and FcRn receptor binding that translates to half-life extension, assuming mIgG1 interacts with the unknown factor in human FcRn transgenic mice. Also, if alternative physiochemical properties such as charge, hydrophobicity, size, etc. of a protein play a role in distribution and endocytosis into FcRn expressing cells, mIgG1 would be an ideal model protein as it is salvaged by mouse FcRn in wild type mice but not by human FcRn in human FcRn transgenic mice.

mIgG1-SMCC-FcBP potently accumulates in MDCK hFcRn-EYFP/h β 2M cells at pH 6 whereas unmodified mIgG1 has little to no detectable accumulation, indicating that conjugation of FcBP to mIgG1 confers binding to human FcRn *in vitro* (Fig. 4.12b). The mIgG1-SMCC-FcBP dose-response curve did not fit a one-site total binding model but was well described by a two-site binding model in Prism with a $U_{1/2, \max}$ of 31 nM and 915 nM for the high and low

affinity populations, respectively. This is likely the consequence of conjugation heterogeneity resulting in a distribution of mIgG1 with varying mol mIgG1 to mol peptide ratios and thus affinity to human FcRn. Regardless, the data indicate that mIgG1-SMCC-FcBP binds human FcRn at pH 6. Therefore, we evaluated the plasma clearance of mIgG1-SMCC-FcBP in human FcRn transgenic mice. mIgG1-SMCC-FcBP and mIgG1 have a similar, short half-life in Tg276/Tg276 mice of 2.4 days and 2.6 days (Fig. 4.12c), respectively, indicating that FcBP conjugation to mIgG1 does not alter plasma clearance. If our hypothesis were correct, we would expect a increase in the plasma half-life of FcBP modified mIgG1 unless by chance FcBP modification abrogates mIgG1 binding to the unknown factor or the unknown factor interacts directly with FcRn and not IgG.

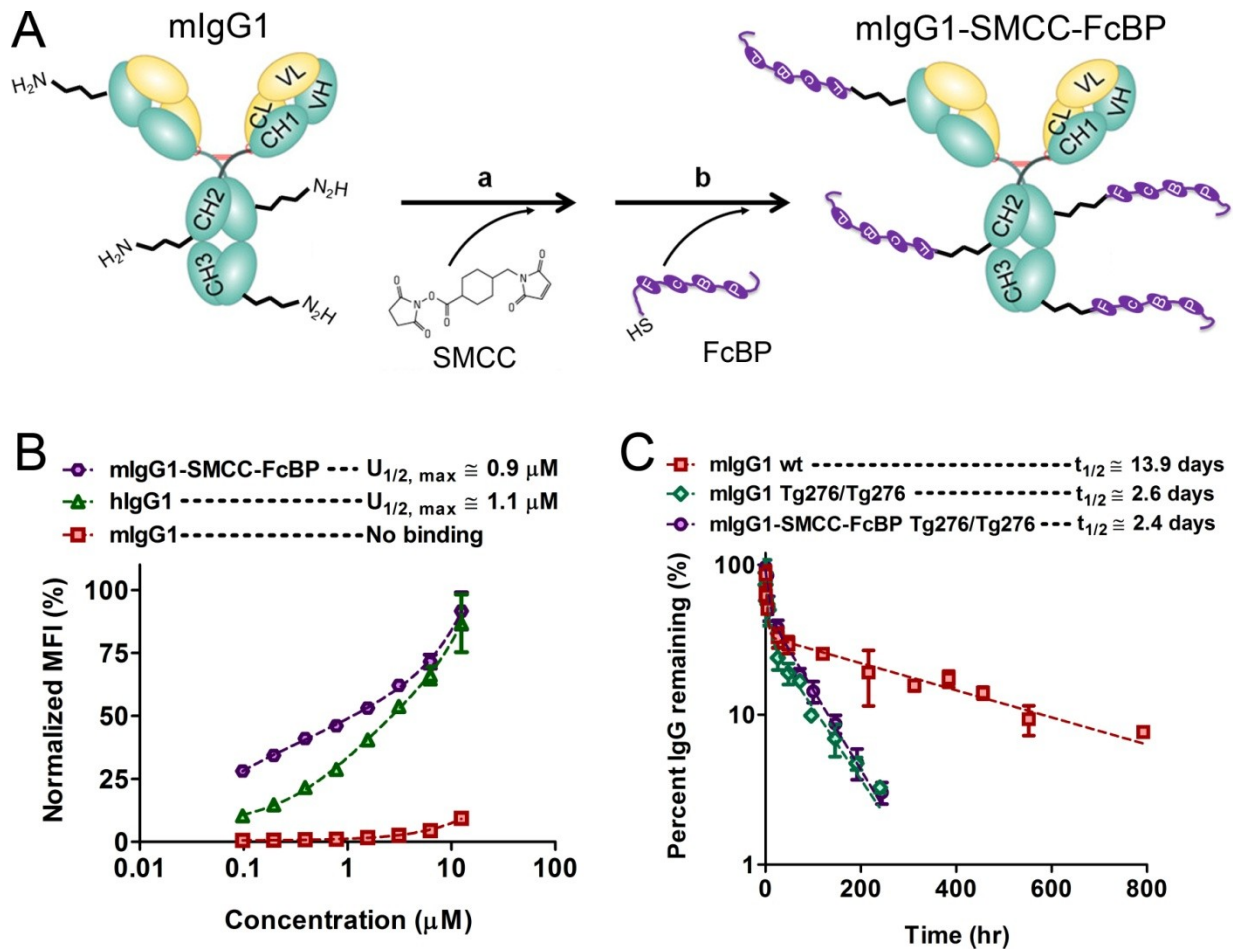


Figure 4.12. mIgG1-SMCC-FcBP fusion binds human FcRn but does not have an extended half-life in human FcRn transgenic mice

(a) Schematic depicting conjugation of FcBP to mIgG1. SMCC was first reacted with lysine residues on mIgG1 (a) leaving a reactive maleimide for conjugation to the N-terminal free thiol of the synthetic linear FcBP (b) to yield mIgG1-SMCC-FcBP. (b) Dose-dependent cellular accumulation of mIgG1, mIgG1-SMCC-FcBP, and hIgG1 in MDCK hFcRn-EYFP/h β 2M cells at pH 6. The dashed lines represents data fit to a one-site total binding model for hIgG1 and mIgG1 or a two-site binding model for mIgG1-SMCC-FcBP in Prism. The data shown are the mean ($n=3$) and error bars indicate s.d. (c) mIgG1 and mIgG1-SMCC-FcBP were dosed i.v. at 10 mg/kg via the tail vein. Blood was collected at various time points into heparinized tubes and plasma clearance was determined via fluorometry. The % mIgG1 remaining (%ID) was calculated by normalizing the fluorescent emission at all time points to the maximum value observed in the first bleed 5 min after injection of each labeled protein. Dashed lines represent the data fit to a 2-compartment PK model in prism and the β -phase half-life shown in the figure was calculated as described in Section 4.2.16. The data shown in each panel are the mean ($n=3$ bleeds per time point) and error bars indicate s.d.

4.4 Conclusion

Motivated by the promising *in vitro* results described in Chapter 2, we determined the *in vivo* fate of FcBP modified mKates in wild type and human FcRn transgenic mice to validate the FcBP fusion platform. We found that although FcBP modified mKates bind human FcRn with an affinity comparable to that of hIgG1, their half-life in mice is not influenced by the expression of human FcRn. Since mKate is rapidly eliminated from circulation ($t_{1/2} \cong 5$ min), we speculated that renal clearance was much faster than FcRn salvage. To overcome the rapid elimination we increased the molecular weight of FcBP modified cargo above the filtration threshold via two distinct mechanisms: 1) PEGylation of mKate-IgG and 2) coupling the FcBP to the surface of 100 nm liposomes. Both strategies result in macromolecules that are not readily filtered through the glomerulus. Regardless of the approach, FcBP fusion did not impact plasma clearance. We systematically tested a number of variables hypothesized to contribute to the lack of correlation between *in vitro* and *in vivo* results; however, no single factor explains why FcBP fusion does not affect the plasma clearance of various proteins and liposomes *in vivo*.

The findings described in this chapter raise a quandary regarding the mechanism(s) governing the half-life of IgG and FcBP fusion proteins. Why does IgG have a long, FcRn-dependent half-life *in vivo* but FcBP fusions do not, even though both IgG and FcBP have similar *in vitro* properties? We hypothesize that an alternative factor(s) acts in collaboration with FcRn to regulate IgG homeostasis that cannot be replicated by FcBP fusion proteins *in vivo* and the *in vitro* systems used to study the IgG and FcBP interaction with human FcRn are not representative of the *in vivo* biology.

It is widely believed that FcRn-dependent recycling initiates after non-specific, fluid-phase pinocytosis of IgG by parenchymal and hematopoietic cells. IgG then encounters FcRn in

acidified endosomes, a microenvironment conducive for an IgG-FcRn interaction, and is subsequently recycled or transcytosed. Pinocytosed serum proteins that do not bind a recycling receptor are destined for lysosomal degradation. It would be expected that exogenous serum proteins, such as FcBP fusions, are also pinocytosed by parenchymal or hematopoietic cells in circulation, although perhaps to varying degrees, enabling a chance encounter with endosomal FcRn resulting in salvage from intracellular catabolism and a FcRn-dependent half-life in mice. Our attempts to hijack FcRn-recycling with a synthetic FcBP have not translated to a FcRn-dependent increase in half-life of FcBP modified cargos *in vivo*. This observation forms the basis of our hypothesis that the IgG-FcRn recycling pathway involves an additional component(s) that acts in collaboration with FcRn to salvage IgG but not FcBP fusions from catabolism.

A number of observations in the literature also support the potential of an additional IgG salvage process. First, and most relevant, is the observation that $\beta 2m$ deficient mice catabolize IgG faster than FcRn α -chain deficient mice leading Kim, Anderson and coworkers to suggest an alternative $\beta 2m$ -associated IgG salvage mechanism³⁹. Unfortunately, $\beta 2m$ is required for FcRn function^{17,27} making it impossible with current mouse models to decouple the relative contribution of FcRn or an alternative $\beta 2m$ -dependent process that regulates IgG half-life. Also of relevance is the observation that the varying plasma clearance of IgG subclasses (1, 2, 3, and 4) and isotypes (λ or κ) cannot be explained by a simple FcRn-IgG affinity relationship⁴⁰⁻⁴², suggesting alternative factors contribute to IgG serum persistence.

We speculate that such a mechanism may involve a yet unknown receptor or known receptor with unknown/additional function, termed “Factor X.” In this conclusion, we outline three alternative IgG salvage mechanisms based on data in this dissertation and examples in the

literature (Fig. 4.13). In the first hypothesized mechanism, IgG binds Factor X at the cell surface. Factor X then shuttles IgG from the blood to FcRn-containing endosomes in a “bait and switch” type endocytosis and recycling mechanism (Fig. 4.13a). This contrasts with the widely accepted mechanism of non-specific, fluid-phase uptake to deliver serum IgG to intracellular FcRn. FcBP fusion proteins would not be internalized if FcBP does not bind Factor X at the cell surface and therefore cannot access intracellular FcRn. In the “bait and switch” mechanism only serum proteins that bind both Factor X and FcRn complete the intracellular FcRn-mediated recycling process.

Interestingly, placental alkaline phosphatase (AP) can bind IgG at the cell surface but alone is not sufficient for IgG transcytosis across MDCK cells⁴³. In contrast, IgG is transported across trophoblast-derived BeWo cells that express both AP and FcRn^{43,44}, as well as other IgG receptors (IgRs)⁴⁵. Specific binding of hIgG to placental membranes occurs at both pH 6 and pH 7.4⁴⁶, suggesting the involvement of additional receptors since IgG does not bind FcRn at pH 7.4. The exact mechanism of maternofetal IgG transfer has not been elucidated; however, FcRn is required but alone is not sufficient for IgG transfer.

A similar two-component “bait-n-switch” could also regulate IgG salvage in parenchymal and hematopoietic cells as these cells both express known (or possibly unknown) IgRs⁴⁷ and are the major cell types involved in regulating IgG serum persistence in mice^{21,22}. Even a low affinity interaction between IgG and an IgR could result in receptor-mediated endocytosis given the high concentration of IgG in serum while dissociation of IgG during endosomal transit, either due to weak or pH-dependent affinity, would enable capture by FcRn.

Alternative to the “bait and switch,” an additional membrane component may interact directly with the FcRn α -chain and/or β 2m light-chain and influence the IgG-FcRn interaction

resulting in a cooperative (**P**artner **I**nitiated) or competitive (**P**artner **I**nhibited) **R**ecycling process, or “**PAI**Red.” The human hemochromatosis protein (HFE) acts as a “**P**artner **I**nhibited” regulator of iron absorption by competing with transferrin-bound iron (Tf-Fe) for transferrin receptor binding⁴⁸. HFE function, like FcRn, is dependent on association with β 2m⁴⁹. In a similar fashion, Factor X may compete with IgG for binding to FcRn providing an additional regulatory component to control IgG homeostasis (Fig. 4.13b). IgG may be an effective competitor of the Factor X-FcRn interaction resulting in salvage by FcRn whereas FcBP modified cargo may be a poor competitor. The fact that a pH-dependent FcBP does not alter the plasma clearance of FcBP modified cargo but a high affinity, pH-independent FcBP can compete with IgG binding to FcRn *in vitro* and increase the catabolism of IgG *in vivo* suggests that a competition based regulatory factor may be a likely mechanism.

Alternatively, an additional membrane component may induce affinity between IgG and FcRn at physiological pH, resulting in FcRn-mediated endocytosis of the ternary Factor X-FcRn-IgG complex (Fig. 4.13c). Again, even weak affinity at pH 7.4 would be sufficient to capture serum IgG. At some point along the recycling pathway Factor X may dissociate from FcRn while IgG stays bound to FcRn due to its high affinity at low pH. The binary FcRn-IgG complex may be trafficked back to the plasma membrane resulting in release of IgG from FcRn due to the elevated pH and absence of Factor X. FcBP fusion proteins on the other hand may be unable to bind the Factor X-FcRn binary complex at the cell surface and are not specifically salvaged by FcRn.

A major question that remains is why FcBP fusion proteins are recycled and transcytosed by human FcRn *in vitro*, if in fact an alternative regulatory process exists? We postulate that there may be cross-species differences in the Factor X interaction with FcRn, β 2m, and/or IgG in

our *in vitro* MDCK cell model. The MDCK cell systems used to study the IgG and FcBP interaction with human FcRn has caveats. First, to detect both IgG and FcBP accumulation in MDCK cells FcRn must be over-expressed such that a high fraction of the receptor is present on the cell surface. In this model we may be relying on FcRn-dependent endocytosis to quantify cellular accumulation of IgG and FcBP fusion proteins not fluid-phase pinocytosis or alternative receptor mediated endocytosis processes. Second, MDCK cells may not express Factor X or may express a species of Factor X that does not interact with human FcRn/ β 2m or human IgG.

If Factor X acts in a “bait and switch” or “partner initiated” type process then its absence from our MDCK cell model would go unnoticed as cell-surface FcRn alone is sufficient to initiate endocytosis. If Factor X acts in a “partner inhibited” type process and is absent or non-functional in MDCK cells then there would be no competition for human FcRn binding between Factor X and FcBP resulting in efficient recycling and transcytosis of FcBP fusion proteins. Thus, if Factor X exists our *in vitro* model may not reflect the *in vivo* biology. We are in the process of evaluating the uptake and recycling mechanisms of IgG and FcBP fusions in immortalized and primary human microvascular endothelial cells as this cell type is thought to be a major contributor to FcRn function *in vivo*²¹ and possibly a more representative cell model.

A species specific interaction between Factor X and FcRn/ β 2m may also explain why the synthetic FcBP can accelerate the clearance of hIgG in fully human FcRn/ β 2m transgenic mice⁹. If mouse Factor X interacts with mouse but not human β 2m, the FcBP may function in fully human transgenic mice as there would be no competition between Factor X and FcBP for binding FcRn; however, mouse Factor X may interact with the human-mouse FcRn/ β 2m in Tg32 or Tg276 mice and contribute to the lack of FcBP function *in vivo*. We are in the process of generating a fully human FcRn/ β 2M mouse to address this question.

The suggestions in this conclusion are highly speculative; however, we would not be surprised that an additional regulatory component influences IgG homeostasis in combination or collaboration with FcRn, as has been suggested for the maternofetal transfer of IgG⁵⁰. Our hypotheses are built upon published data and our observation that a synthetic peptide specific for human FcRn does not enable half-life extension of its fused cargos *in vivo* even though it mimics the IgG-FcRn interaction in single component model systems *in vitro*. These data suggest an alternative IgG-salvage component that cannot be mimicked by the FcBP. However, we cannot rule out that subtle, unidentified differences in FcBP-FcRn binding kinetics, affinity, site, or mechanism contribute to its lack of function *in vivo*. We are developing methods to test these hypotheses, since the identification of an IgG or FcRn regulatory component may have a significant impact on FcRn biology and provide new opportunities to engineer IgG, albumin, or alternative FcRn-targeted molecules for enhanced serum persistence.

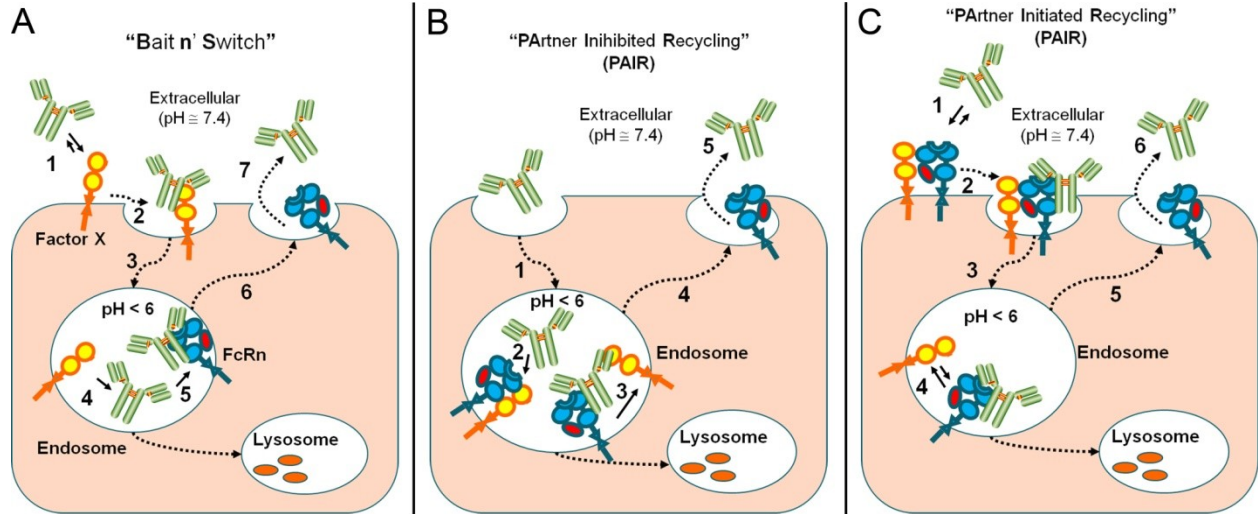


Figure 4.13. Alternative IgG salvage theories that act in combination with FcRn.

(a) In this “bait n’ switch” type mechanism an unknown cell-membrane anchored receptor, Factor X, binds IgG in serum (1) triggering receptor-mediated endocytosis (2). As IgG is trafficked along the endosomal pathway (3) the pH decreases to 6 resulting in dissociation of IgG from Factor X (4) and subsequent transfer to FcRn (5). FcRn then recycles IgG back to the plasma membrane (6) where IgG is released into blood due to its weak affinity for FcRn at blood pH (7). FcBP fusion proteins would not be readily endocytosed because they cannot bind Factor X (b) In the PARTner Inhibited Recycling mechanism IgG is endocytosed into FcRn expressing cells by non-specific pinocytosis (1) and is trafficked to the endosome. The IgG binding site on FcRn is blocked by Factor X at steady state; however, IgG can effectively compete with the Factor X (2) resulting in dissociation of Factor X from FcRn and the formation of the FcRn-IgG complex (3). FcRn then recycles IgG back to the plasma membrane (4) where IgG is released into blood due to its weak affinity for FcRn at blood pH (5). FcBP fusion proteins cannot compete with the Factor X-FcRn interaction and are not salvaged by FcRn (c) Alternatively, in a PARTner Initiated Recycling process an additional, unknown cell-membrane anchored FcRn binding partner increases the affinity of FcRn for IgG at physiological pH (1) resulting in FcRn-mediated endocytosis of IgG (2). As the complex is trafficked along the endosomal pathway (3) the pH decreases to 6 resulting in dissociation of Factor X from the FcRn-IgG complex (4). IgG stays bound to FcRn due to its high affinity at pH 6 and is trafficked back to the plasma membrane (5) where IgG is released into blood due to its weak affinity for FcRn at blood pH in the absence of Factor X (6). In all cases, IgG, FcBP fusion proteins, or additional serum components that do not bind FcRn or cannot compete with Factor X for binding FcRn are trafficked to the lysosome and degraded.

4.5 References

1. Alconcel, S. N. S., Baas, A. S. & Maynard, H. D. FDA-approved poly(ethylene glycol)–protein conjugate drugs. *Polym. Chem.* **2**, 1442 (2011).
2. Schellenberger, V. *et al.* A recombinant polypeptide extends the in vivo half-life of peptides and proteins in a tunable manner. *Nat. Biotechnol.* **27**, 1186–90 (2009).
3. Roopenian, D. C. & Akilesh, S. FcRn: the neonatal Fc receptor comes of age. *Nat. Rev. Immunol.* **7**, 715–725 (2007).
4. Rath, T. *et al.* Fc-fusion proteins and FcRn: structural insights for longer-lasting and more effective therapeutics. *Crit. Rev. Biotechnol.* (2013). doi:10.3109/07388551.2013.834293
5. Sleep, D., Cameron, J. & Evans, L. R. Albumin as a versatile platform for drug half-life extension. *Biochim. Biophys. Acta* **1830**, 5526–34 (2013).
6. Dennis, M. S. *et al.* Albumin binding as a general strategy for improving the pharmacokinetics of proteins. *J Biol Chem* **277**, 35035–35043 (2002).
7. Kontos, S. & Hubbell, J. A. Improving protein pharmacokinetics by engineering erythrocyte affinity. *Mol. Pharm.* **7**, 2141–7 (2010).
8. Bitonti, A. J. & Dumont, J. A. Pulmonary administration of therapeutic proteins using an immunoglobulin transport pathway. *Adv Drug Deliv Rev* **58**, 1106–1118 (2006).
9. Mezo, A. R. *et al.* Reduction of IgG in nonhuman primates by a peptide antagonist of the neonatal Fc receptor FcRn. *Proc. Natl. Acad. Sci. U. S. A.* **105**, 2337–42 (2008).
10. Mezo, A. R., McDonnell, K. A., Castro, A. & Fraley, C. Structure-activity relationships of a peptide inhibitor of the human FcRn:human IgG interaction. *Bioorg. Med. Chem.* **16**, 6394–405 (2008).
11. McDonnell, K. A. *et al.* Synthesis and Structure–Activity Relationships of Dimeric Peptide Antagonists of the Human Immunoglobulin G–Human Neonatal Fc Receptor (IgG–FcRn) Interaction. *J. Med. Chem.* **53**, 1587–1596 (2010).
12. Mezo, A. R., Sridhar, V., Badger, J., Sakorafas, P. & Nienaber, V. X-ray Crystal Structures of Monomeric and Dimeric Peptide Inhibitors in Complex with the Human Neonatal Fc Receptor, FcRn. *J. Biol. Chem.* **285**, 27694–27701 (2010).
13. West, A. P. & Bjorkman, P. J. Crystal Structure and Immunoglobulin G Binding Properties of the Human Major Histocompatibility Complex-Related Fc Receptor † , ‡. *Biochemistry* **39**, 9698–9708 (2000).

14. Sockolosky, J. T., Tiffany, M. R. & Szoka, F. C. Engineering neonatal Fc receptor-mediated recycling and transcytosis in recombinant proteins by short terminal peptide extensions. *Proc. Natl. Acad. Sci. U. S. A.* **109**, 16095–16100 (2012).
15. Vaccaro, C., Zhou, J., Ober, R. J. & Ward, E. S. Engineering the Fc region of immunoglobulin G to modulate in vivo antibody levels. *Nat Biotechnol* **23**, 1283–1288 (2005).
16. Dennis, M. S. Albumin Binding as a General Strategy for Improving the Pharmacokinetics of Proteins. *J. Biol. Chem.* **277**, 35035–35043 (2002).
17. Claypool, S. M., Dickinson, B. L., Yoshida, M., Lencer, W. I. & Blumberg, R. S. Functional reconstitution of human FcRn in Madin-Darby canine kidney cells requires co-expressed human beta 2-microglobulin. *J. Biol. Chem.* **277**, 28038–50 (2002).
18. Olson, F., Hunt, C. A., Szoka, F. C., Vail, W. J. & Papahadjopoulos, D. Preparation of liposomes of defined size distribution by extrusion through polycarbonate membranes. *Biochim. Biophys. Acta - Biomembr.* **557**, 9–23 (1979).
19. Kontermann, R. E. Strategies to extend plasma half-lives of recombinant antibodies. *BioDrugs* **23**, 93–109 (2009).
20. Deen, W. M., Lazzara, M. J. & Myers, B. D. Structural determinants of glomerular permeability. *Am J Physiol Ren. Physiol* **281**, F579–596 (2001).
21. Montoyo, H. P. *et al.* Conditional deletion of the MHC class I-related receptor FcRn reveals the sites of IgG homeostasis in mice. *Proc. Natl. Acad. Sci.* **106**, 2788–2793 (2009).
22. Akilesh, S., Christianson, G. J., Roopenian, D. C. & Shaw, A. S. Neonatal FcR Expression in Bone Marrow-Derived Cells Functions to Protect Serum IgG from Catabolism. *J. Immunol.* **179**, 4580–4588 (2007).
23. Petkova, S. B. *et al.* Enhanced half-life of genetically engineered human IgG1 antibodies in a humanized FcRn mouse model: potential application in humorally mediated autoimmune disease. *Int Immunol* **18**, 1759–1769 (2006).
24. Wang, W. *et al.* Monoclonal Antibodies with Identical Fc Sequences Can Bind to FcRn Differentially with Pharmacokinetic Consequences. *Drug Metab. Dispos.* **39**, 1469–77 (2011).
25. X, Z. *et al.* The heavy chain of neonatal Fc receptor for IgG is sequestered in endoplasmic reticulum by forming oligomers in the absence of β 2-microglobulin association. **367**, 703–14 (2002).

26. Praetor, A. & Hunziker, W. β 2-microglobulin is important for cell surface expression and pH-dependent IgG binding of human FcRn. *J. Cell Sci.* **115**, 2389–97 (2002).
27. Israel, E. J., Wilsker, D. F., Hayes, K. C., Schoenfeld, D. & Simister, N. E. Increased clearance of IgG in mice that lack beta 2-microglobulin: possible protective role of FcRn. *Immunology* **89**, 573–8 (1996).
28. Israel, E. J., Patel, V. K., Taylor, S. F., Marshak-Rothstein, A. & Simister, N. E. Requirement for a beta 2-microglobulin-associated Fc receptor for acquisition of maternal IgG by fetal and neonatal mice. *J. Immunol.* **154**, 6246–51 (1995).
29. Ghetie, V. *et al.* Abnormally short serum half-lives of IgG in beta 2-microglobulin-deficient mice. *Eur. J. Immunol.* **26**, 690–6 (1996).
30. Junghans, R. P. & Anderson, C. L. The protection receptor for IgG catabolism is the beta2-microglobulin-containing neonatal intestinal transport receptor. *Proc. Natl. Acad. Sci. U. S. A.* **93**, 5512–6 (1996).
31. Wani, M. A. *et al.* Familial hypercatabolic hypoproteinemia caused by deficiency of the neonatal Fc receptor, FcRn, due to a mutant beta2-microglobulin gene. *Proc Natl Acad Sci U S A* **103**, 5084–5089 (2006).
32. Walsh, J. S. D. and A. F. / E. by G. W. and F. S., Sato, A. K., Viswanathan, M., Kent, R. B. & Wood, C. R. Therapeutic peptides: technological advances driving peptides into development. *Curr. Opin. Biotechnol.* **17**, 638–642 (2006).
33. Tam, S. H., McCarthy, S. G., Brosnan, K., Goldberg, K. M. & Scallon, B. J. Correlations between pharmacokinetics of IgG antibodies in primates vs. FcRn-transgenic mice reveal a rodent model with predictive capabilities. *MAbs* **5**, 397–405 (2013).
34. Ober, R. J., Radu, C. G., Ghetie, V. & Ward, E. S. Differences in promiscuity for antibody-FcRn interactions across species: implications for therapeutic antibodies. *Int Immunol* **13**, 1551–1559 (2001).
35. Stoop, J. W., Zegers, B. J., Sander, P. C. & Ballieux, R. E. Serum immunoglobulin levels in healthy children and adults. *Clin. Exp. Immunol.* **4**, 101–12 (1969).
36. Schmidt, M. M. *et al.* Crystal Structure of an HSA/FcRn Complex Reveals Recycling by Competitive Mimicry of HSA Ligands at a pH-Dependent Hydrophobic Interface. *Structure* **21**, 1966–78 (2013).
37. Hämmerling, D. H. and P. H. / S. P. and G. & Hume, D. A. The mononuclear phagocyte system. *Curr. Opin. Immunol.* **18**, 49–53 (2006).
38. Allen, T. M. & Hansen, C. Pharmacokinetics of stealth versus conventional liposomes: effect of dose. *Biochim. Biophys. Acta - Biomembr.* **1068**, 133–141 (1991).

39. Kim, J. *et al.* Beta 2-microglobulin deficient mice catabolize IgG more rapidly than FcRn-alpha-chain deficient mice. *Exp. Biol. Med. (Maywood)*. **233**, 603–9 (2008).
40. Zuckier, L. S., Chang, C. J., Scharff, M. D. & Morrison, S. L. Chimeric human-mouse IgG antibodies with shuffled constant region exons demonstrate that multiple domains contribute to in vivo half-life. *Cancer Res.* **58**, 3905–8 (1998).
41. Montaña, R. F. & Morrison, S. L. Influence of the isotype of the light chain on the properties of IgG. *J. Immunol.* **168**, 224–31 (2002).
42. Gurbaxani, B., Dela Cruz, L. L., Chintalacheruvu, K. & Morrison, S. L. Analysis of a family of antibodies with different half-lives in mice fails to find a correlation between affinity for FcRn and serum half-life. *Mol Immunol* **43**, 1462–1473 (2006).
43. Stefaner, I., Stefanescu, A., Hunziker, W. & Fuchs, R. Expression of placental alkaline phosphatase does not correlate with IgG binding, internalization and transcytosis. *Biochem. J.* **327**, 585–92 (1997).
44. Ellinger, I., Schwab, M., Stefanescu, A., Hunziker, W. & Fuchs, R. IgG transport across trophoblast-derived BeWo cells: a model system to study IgG transport in the placenta. *Eur. J. Immunol.* **29**, 733–44 (1999).
45. Simister, N. E. & Story, C. M. Human placental Fc receptors and the transmission of antibodies from mother to fetus. *J. Reprod. Immunol.* **37**, 1–23 (1997).
46. Simister, N. E., Story, C. M., Chen, H. L. & Hunt, J. S. An IgG-transporting Fc receptor expressed in the syncytiotrophoblast of human placenta. *Eur. J. Immunol.* **26**, 1527–31 (1996).
47. Ravetch, J. V & Kinet, J. P. Fc receptors. *Annu. Rev. Immunol.* **9**, 457–92 (1991).
48. Salter-Cid, L. *et al.* Transferrin receptor is negatively modulated by the hemochromatosis protein HFE: Implications for cellular iron homeostasis. *Proc. Natl. Acad. Sci.* **96**, 5434–5439 (1999).
49. Santos, M. Defective iron homeostasis in beta 2-microglobulin knockout mice recapitulates hereditary hemochromatosis in man. *J. Exp. Med.* **184**, 1975–1985 (1996).
50. Gafencu, A., Heltianu, C., Burlacu, A., Hunziker, W. & Simionescu, M. Investigation of IgG Receptors Expressed on the Surface of Human Placental Endothelial Cells. *Placenta* **24**, 664–676 (2003).

Chapter 5: Conclusions

5.1 Overview

Genetic engineering has enabled the production of numerous recombinant proteins in large quantities in effect transforming the biotechnology industry by enabling the cost effective manufacture of human proteins¹⁻³. Protein-based therapeutic sales in the biotech sector continue to grow reaching ~ \$54 billion in 2011⁴. Arguably monoclonal antibodies (mAbs) are the most successful class of protein drugs due to their remarkable pharmacokinetics, mediated by FcRn, safety, and target specificity. Monoclonal antibody sales account for ~ 40% of all biologic sales in 2011; however, not far behind are the growing classes of hormones, cytokines, growth factors, enzymes, and blood factors. Unlike mAbs, these classes of human proteins are rapidly eliminated from circulation which necessitates frequent injection or continuous infusion to maintain therapeutic concentrations in the blood. To overcome these limitations a number of half-life extension strategies have been devised⁵. Fusion of therapeutic proteins to the Fc-domain of IgG or to albumin is a clinically validated strategy to improve both protein half-life and delivery.

In this dissertation we investigated a novel genetic fusion approach with the goal of improving both protein half-life and delivery by hijacking FcRn-mediated recycling and transcytosis. We developed a strategy, termed FcBP fusion, to target proteins to FcRn by genetic fusion of short FcRn binding peptides to the termini of proteins. We hypothesized that proteins modified with FcBPs would have an increased circulating lifetime due to FcRn-dependent recycling and would be delivered across FcRn expressing epithelial cells, such as in the lung, due to FcRn-mediated transcytosis enabling non-invasive protein administration. In this chapter, I will briefly discuss the findings presented in this dissertation and make the argument that a

deeper understanding of FcRn biology is necessary in order to develop alternative protein engineering approaches with the goal of improving protein half-life and delivery or developing therapeutic strategies dependent on the biological functions of FcRn.

5.2 Summary of findings

In chapter 2, we describe a strategy to engineer protein mimetics of the IgG-FcRn interaction by installing short FcRn binding peptides to the termini of the model fluorescent protein mKate. We first demonstrated that FcBP modified mKates can be easily produced in *E. coli* unlike Fc- or albumin-fusion proteins that necessitate mammalian expression systems due to their complex structure and glycosylation pattern. We then characterized the interaction between a family of FcBP modified mKates and human FcRn through a series of molecular and cell-based assays. We found that the affinity and kinetics of the FcBP modified mKate and hIgG1 interaction with FcRn were almost identical at pH 6 with the only difference being the weak affinity of the FcBP-FcRn interaction at pH 7.4 whereas hIgG1 does not bind human FcRn at pH 7.4. Guided by the crystal structure⁶ we designed a mutant (Y286H) with negligible affinity at pH 7.4 and used the wild type and Y286H mutant to demonstrate that affinity at pH 7.4 is advantageous for initiating endocytosis and subsequent transcytosis across FcRn expressing MDCK cell monolayers. We also studied the intracellular fate of FcBP fusion proteins in MDCK hFcRn-EYFP/h β 2M cells and identified a number of FcRn-mediated trafficking events that are consistent with the FcRn processing of IgG. Finally we demonstrated that FcBP modified mKates are recycled and transcytosed across FcRn expressing cell monolayers. Collectively, the results in Chapter 2 suggest that FcBP fusion may be a viable strategy to improve protein half-life and delivery.

The promising proof-of-concept results described in Chapter 2 provided the rationale for *in*

in vivo studies. The FcBP used is specific for human FcRn with little to no binding to mouse FcRn. Therefore, wild type mice are not a suitable *in vivo* model to study FcBP fusion proteins. Derry Roopinean and colleagues at the Jackson Laboratory developed human FcRn transgenic mice that are null for the mouse FcRn heavy chain and express human FcRn⁷. IgG and albumin have distinct cross-species binding properties to FcRn that we took advantage of to validate the human FcRn transgenic mouse model. We demonstrated in Chapter 3 that the half-life of both mouse and human IgG and albumin in wild type and human FcRn transgenic mice correlate with their species matched affinity for FcRn. The results provide strong evidence that human FcRn transgenic mice are a predictive *in vivo* model to evaluate the pharmacokinetics of human FcRn specific ligands, at least IgG and albumin.

Building upon the *in vitro* and *in vivo* characterization of FcBP modified mKates and human FcRn transgenic mice in Chapters 2 and 3, respectively, we determined the *in vivo* fate of FcBP modified mKates, liposomes, and mouse IgG1 in Chapter 4. To our surprise we were unable to demonstrate that FcBP fusion alters the plasma clearance of macromolecule cargos. We evaluated a number of variables that we hypothesized might contribute to the lack of function *in vivo* such as peptide stability in blood, serum competition for binding FcRn, the function of the hybrid human-mouse FcRn/ β 2m receptor, the role of renal clearance by increasing the hydrodynamic size of FcBP modified cargos, and the potential for an alternative IgG specific salvage pathway. However, no single variable adequately explained the lack of FcBP function *in vivo*.

We are left with two potential explanations. First, it is possible that subtle differences in FcBP binding to FcRn that we have not detected in our *in vitro* assays do not enable salvage by FcRn *in vivo*. The *in vitro* assays used to characterize the FcBP-FcRn interaction are performed

under equilibrium conditions using single-component molecular and cell-based assays that rely on surface presentation of FcRn to detect binding and initiate endocytosis. However, *in vivo* it is unlikely that the FcBP-FcRn interaction is at equilibrium. Thus, the affinity or kinetics of the FcBP-FcRn interaction at pH 6 and/or pH 7.4 under non-equilibrium conditions may not be adequate to hijack FcRn-mediated recycling and transcytosis *in vivo* when compared to IgG.

Second, we speculate that an additional, unknown factor in collaboration with FcRn is responsible for controlling the serum persistence of IgG and thus cannot be replicated by FcBP fusion. We are currently developing methods to address both hypotheses in an effort to make new discoveries regarding the biology of FcRn and understand the factors important to the design of exogenous FcRn targeting ligands.

In the field of drug delivery, a deep understanding of underlying biological mechanisms that contribute to human physiology and disease is a prerequisite to the development of effective drug carriers. FcRn is a prime example of how basic biology and incremental discoveries can be translated into therapeutics and will be highlighted in the next section to conclude this dissertation and provide a perspective on the future of FcRn as a therapeutic target for drug delivery.

5.3 Historical and future perspectives: the not so well characterized neonatal Fc receptor?

The discovery of FcRn as the receptor responsible for the transfer of maternal IgG from mother to fetus⁸ in the late 80s and long serum persistence of IgG in the 90s resulted in an explosion in the field of FcRn biology⁹⁻¹¹. The crystal structure of the rat FcRn-rat Fc complex solved by Pamela Bjorkman and colleagues¹² and the identification of Fc-domain amino acid residues that influence the plasma clearance of mouse IgG1¹³ guided engineering efforts that resulted in the first engineered Fc-domain with enhanced serum persistence as a result of

increased affinity for FcRn at pH 6¹⁴. These seminal discoveries paved the way for the now vast number of reports on approaches to alter the serum persistence of therapeutic human antibodies, modulate the endogenous IgG-FcRn interaction, and hijack FcRn to enable non-invasive protein administration, reviewed in¹⁵⁻¹⁷.

The discovery that FcRn also salvages albumin from degradation by Clark Anderson and colleagues¹⁸ came almost a decade after discovery of the IgG-FcRn interaction; however, the impact was similar and triggered a number of albumin-based drug delivery approaches guided by the basic understanding of the endogenous albumin-FcRn interaction¹⁹.

The next notable discovery in FcRn biology was its expression in immune cells such as monocytes, macrophages and dendritic cells suggesting FcRn may contribute in some manner to immune regulation and antigen presentation²⁰. Sure enough FcRn has a profound effect on both innate and adaptive immunity by shuttling IgG-antigen complexes across mucosal barriers enabling phagocytosis by antigen presenting cells²¹ and diverting immune complexes to the lysosome for degradation and presentation of foreign antigens to T-cells^{22,23}. Yet another combination of basic biological discoveries that triggered novel drug delivery approaches that hijack FcRn to improve the immunogenicity of protein antigens²⁴ and protein-subunit mucosal vaccination²⁵. So what is next for FcRn?

Aside from the hypothesis regarding alternative mechanisms that act in collaboration with FcRn to regulate IgG homeostasis *in vivo*, a number of unexplored drug delivery strategies may be useful when considering the known biology of FcRn. For instance, FcRn expressed in the lung and intestinal epithelia provides a route for the transport of Fc-fusion proteins across the epithelium and into the blood stream, enabling non-invasive protein administration via FcRn-mediated transcytosis^{26,27}. However, FcRn also recycles its ligands and may act to increase lung

retention of pulmonary administered therapeutics, which is hampered by rapid mucociliary and alveolar macrophage clearance²⁸. It is unknown whether FcRn can increase the residence time of therapeutics delivered to the lung or what role alveolar macrophages play in the disposition of FcRn-targeted therapeutics. An investigation into these processes may identify useful FcRn-dependent strategies to improve the efficacy of pulmonary therapeutics.

Interestingly, intense expression of FcRn in human small intestine crypt cells was recently reported²⁹. The cells also stained positive for chromogranin A, Glucagon-Like Peptide (GLP)-1, GLP-2 by immunohistochemistry suggesting their identity as enteroendocrine cells. Although the biology of FcRn in this specific cell type is unknown, the crosstalk between endocrine and immune cells in the gut³⁰ suggests FcRn may play a specialized role in maintaining mucosal immunity in this cell type. Endocrine cells in the gut also play an important role in nutrient absorption and metabolism³¹. Thus, targeting therapeutics to FcRn expressing endocrine cells may be a strategy for the treatment of metabolic disease and gastrointestinal disorders but requires a significant amount of further investigation. In general, organ specific functions of FcRn have not been thoroughly investigated.

There may also still be unexplored antibody engineering strategies that alter the biodistribution or pharmacokinetics of mAbs mediated by FcRn. Increasing the affinity the IgG-FcRn interaction at pH 6 can extend IgG half-life; however, there appears to be a direct correlation between affinity gains at pH 6 and pH 7.4³² that place a ceiling on increasing the affinity of the IgG-FcRn interaction at pH 6 as subsequent affinity gains at pH 7.4 can decrease IgG serum persistence³³. IgG can simultaneously bind two FcRn molecules due to the homodimeric nature of the Fc-domain³⁴. Therefore, an interesting idea may be to engineer a heterodimeric Fc with each subunit having a differential affinity for FcRn at either pH 6 or pH

7.4. Such engineered heterodimeric Fc molecules may alter the pH 6 to pH 7.4 affinity correlations, could be useful to study the role of FcRn affinity and dimerization on recycling, transcytosis, and half-life, and may result in IgGs with unusual *in vivo* properties.

The role of FcRn in the protection and transport of albumin has lagged IgG. The recent crystal structure of an engineered human serum albumin variant in complex with human FcRn³⁵ will certainly provide new insights into the albumin-FcRn interaction that should guide albumin engineering approaches. Compared to IgG, there is little knowledge of the FcRn-mediated recycling and transcytosis and intracellular fate of albumin. Albumin is a carrier of numerous endogenous compounds and exogenous drugs, thus engineering inhibitors of the albumin-FcRn interaction may be a viable strategy to enhance the clearance of albumin-bound molecules. Interestingly, albumin is not actively transported across the placental barrier even though IgG transport from mother to fetus is dependent on FcRn³⁶. This suggests that the maternofetal transfer of IgG requires an additional FcRn-independent mechanism that is not replicated by albumin. Perhaps a similar step also regulates IgG circulation in blood?

With continual discovery of the vast biological functions of FcRn, the development of new tools to study FcRn *in vitro* and *in vivo*, and clever engineering approaches and creative minds, I anticipate research in the field to have a profound impact on the development of novel therapeutic strategies to treat human disease.

5.4 References

1. Itakura, K. *et al.* Expression in *Escherichia coli* of a chemically synthesized gene for the hormone somatostatin. *Science* **198**, 1056–63 (1977).
2. Morrow, J. F. *et al.* Replication and transcription of eukaryotic DNA in *Escherichia coli*. *Proc. Natl. Acad. Sci. U. S. A.* **71**, 1743–7 (1974).
3. Cohen, S. N., Chang, A. C., Boyer, H. W. & Helling, R. B. Construction of biologically functional bacterial plasmids in vitro. *Proc. Natl. Acad. Sci. U. S. A.* **70**, 3240–4 (1973).
4. Aggarwal, S. R. What's fueling the biotech engine-2011 to 2012. *Nat. Biotechnol.* **30**, 1191–7 (2012).
5. Kontermann, R. *Therapeutic Proteins: Strategies to Modulate Their Plasma Half-Lives*. (Wiley-VCH Verlag GmbH & Co. KGaA, 2012).
6. Mezo, A. R., Sridhar, V., Badger, J., Sakorafas, P. & Nienaber, V. X-ray Crystal Structures of Monomeric and Dimeric Peptide Inhibitors in Complex with the Human Neonatal Fc Receptor, FcRn. *J. Biol. Chem.* **285**, 27694–27701 (2010).
7. Petkova, S. B. *et al.* Enhanced half-life of genetically engineered human IgG1 antibodies in a humanized FcRn mouse model: potential application in humorally mediated autoimmune disease. *Int Immunol* **18**, 1759–1769 (2006).
8. Simister, N. E. & Mostov, K. E. An Fc receptor structurally related to MHC class I antigens. *Nature* **337**, 184–7 (1989).
9. Ghetie, V. *et al.* Abnormally short serum half-lives of IgG in beta 2-microglobulin-deficient mice. *Eur. J. Immunol.* **26**, 690–6 (1996).
10. Junghans, R. P. & Anderson, C. L. The protection receptor for IgG catabolism is the beta2-microglobulin-containing neonatal intestinal transport receptor. *Proc. Natl. Acad. Sci. U. S. A.* **93**, 5512–6 (1996).
11. Israel, E. J., Wilsker, D. F., Hayes, K. C., Schoenfeld, D. & Simister, N. E. Increased clearance of IgG in mice that lack beta 2-microglobulin: possible protective role of FcRn. *Immunology* **89**, 573–8 (1996).
12. Burmeister, W. P., Gastinel, L. N., Simister, N. E., Blum, M. L. & Bjorkman, P. J. Crystal structure at 2.2 Å resolution of the MHC-related neonatal Fc receptor. *Nature* **372**, 336–43 (1994).
13. Kim, J. K., Tsen, M. F., Ghetie, V. & Ward, E. S. Identifying amino acid residues that influence plasma clearance of murine IgG1 fragments by site-directed mutagenesis. *Eur. J. Immunol.* **24**, 542–8 (1994).

14. Ghetie, V. *et al.* Increasing the serum persistence of an IgG fragment by random mutagenesis. *Nat. Biotechnol.* **15**, 637–40 (1997).
15. Roopenian, D. C. & Akilesh, S. FcRn: the neonatal Fc receptor comes of age. *Nat. Rev. Immunol.* **7**, 715–725 (2007).
16. Rath, T. *et al.* Fc-fusion proteins and FcRn: structural insights for longer-lasting and more effective therapeutics. *Crit. Rev. Biotechnol.* (2013). doi:10.3109/07388551.2013.834293
17. Low, S. C. & Mezo, A. R. Inhibitors of the FcRn:IgG protein-protein interaction. *AAPS J.* **11**, 432–4 (2009).
18. Chaudhury, C. *et al.* The Major Histocompatibility Complex-related Fc Receptor for IgG (FcRn) Binds Albumin and Prolongs Its Lifespan. *J. Exp. Med.* **197**, 315–322 (2003).
19. Sleep, D., Cameron, J. & Evans, L. R. Albumin as a versatile platform for drug half-life extension. *Biochim. Biophys. Acta* **1830**, 5526–34 (2013).
20. Zhu, X. *et al.* MHC class I-related neonatal Fc receptor for IgG is functionally expressed in monocytes, intestinal macrophages, and dendritic cells. *J Immunol* **166**, 3266–3276 (2001).
21. Yoshida, M. *et al.* Human neonatal Fc receptor mediates transport of IgG into luminal secretions for delivery of antigens to mucosal dendritic cells. *Immunity* **20**, 769–783 (2004).
22. Qiao, S.-W. *et al.* Dependence of antibody-mediated presentation of antigen on FcRn. *Proc. Natl. Acad. Sci. U. S. A.* **105**, 9337–42 (2008).
23. Rath, T. *et al.* The immunologic functions of the neonatal Fc receptor for IgG. *J. Clin. Immunol.* **33 Suppl 1**, S9–17 (2013).
24. Mi, W. *et al.* Targeting the neonatal fc receptor for antigen delivery using engineered fc fragments. *J. Immunol.* **181**, 7550–61 (2008).
25. Ye, L., Zeng, R., Bai, Y., Roopenian, D. C. & Zhu, X. Efficient mucosal vaccination mediated by the neonatal Fc receptor. *Nat. Biotechnol.* **29**, 158–63 (2011).
26. Low, S. C., Nunes, S. L., Bitonti, A. J. & Dumont, J. A. Oral and pulmonary delivery of FSH-Fc fusion proteins via neonatal Fc receptor-mediated transcytosis. *Hum Reprod* **20**, 1805–1813 (2005).
27. Dumont, J. A. *et al.* Delivery of an erythropoietin-Fc fusion protein by inhalation in humans through an immunoglobulin transport pathway. *J Aerosol Med* **18**, 294–303 (2005).

28. Patton, J. S. & Byron, P. R. Inhaling medicines: delivering drugs to the body through the lungs. *Nat Rev Drug Discov* **6**, 67–74 (2007).
29. Hornby, P. J. *et al.* Human and Non-Human Primate Intestinal FcRn Expression and Immunoglobulin G Transcytosis. *Pharm. Res.* (2013). doi:10.1007/s11095-013-1212-3
30. Moran, G. W., Leslie, F. C., Levison, S. E., Worthington, J. & McLaughlin, J. T. Enteroendocrine cells: neglected players in gastrointestinal disorders? *Therap. Adv. Gastroenterol.* **1**, 51–60 (2008).
31. Janssen, S. & Depoortere, I. Nutrient sensing in the gut: new roads to therapeutics? *Trends Endocrinol. Metab.* **24**, 92–100 (2013).
32. Yeung, Y. A. *et al.* Engineering human IgG1 affinity to human neonatal Fc receptor: impact of affinity improvement on pharmacokinetics in primates. *J Immunol* **182**, 7663–7671 (2009).
33. Acqua, W. F. D. *et al.* Increasing the Affinity of a Human IgG1 for the Neonatal Fc Receptor: Biological Consequences. *J. Immunol.* **169**, 5171–5180 (2002).
34. West, A. P. & Bjorkman, P. J. Crystal structure and immunoglobulin G binding properties of the human major histocompatibility complex-related Fc receptor. *Biochemistry* **39**, 9698–708 (2000).
35. Schmidt, M. M. *et al.* Crystal Structure of an HSA/FcRn Complex Reveals Recycling by Competitive Mimicry of HSA Ligands at a pH-Dependent Hydrophobic Interface. *Structure* **21**, 1966–78 (2013).
36. Gitlin, D. & Koch, C. On the mechanisms of maternofetal transfer of human albumin and gamma-G globulin in the mouse. *J. Clin. Invest.* **47**, 1204–9 (1968).

Appendix A: Periplasmic production via the pET expression system of soluble, bioactive human growth hormone

A.1 Introduction

The pET expression system pioneered by Studier and Moffat¹ and commercialized by Novagen is one of the most widely used systems for recombinant protein production in *E. coli*. The multitude of commercially available vectors, *E. coli* strains, and related products enables expression and purification of a wide variety of foreign proteins. Of particular interest for the expression of disulfide bonded proteins is a family of pET vectors containing the N-terminal pelB secretion signal, which directs synthesized polypeptides to the *E. coli* periplasm². Disulfide oxidoreductases and isomerases located in the *E. coli* periplasm catalyze the formation of disulfide bonds enabling the accumulation of properly folded, soluble protein making the periplasm an ideal compartment for expression of certain therapeutic proteins³.

Human growth hormone (hGH) is a 191 amino acid, disulfide-linked, pituitary-derived protein that regulates a number of metabolic processes involved in growth and development⁴. *E. coli* derived recombinant hGH is approved for the treatment of multiple human diseases and new indications, treatment modalities, and novel delivery systems represent an active area of research in growth hormone based therapy⁵⁻¹². The lack of glycosylation makes *E. coli* an ideal host for hGH production, which can be achieved in the cytoplasm¹³⁻¹⁶ or periplasm¹⁷⁻²³. Over-expression of hGH in the cytoplasm results in the formation of insoluble aggregates, or inclusion bodies. The isolation of hGH from inclusion bodies requires a re-folding step to obtain soluble protein that adds process complexity and contributes to reduced yields. Recombinant hGH directed to the periplasm can be easily isolated in its native state by selective disruption of the *E. coli* outer membrane resulting in a reduction in processing steps, complexity, and time.

There are a number of reports on the periplasmic expression of recombinant human growth hormone¹⁷⁻²³; however, each uses custom prepared vectors, a range of *E. coli* strains, expression conditions, and purification schemes making replication difficult for the academic laboratory. We describe simple methods for the expression, purification, and characterization of recombinant hGH produced at the shake flask level using the pET expression system. All components necessary for cloning, expression, and purification are commercially available. This process results in an average yield of 1.4 mg/L culture of purified protein from ~ 10 – 15 g wet cells. The recombinant hGH isolated using this system is soluble, monomeric, binds the hGH receptor with high affinity, and potently stimulates cell growth comparable to pharmaceutical grade hGH. Thus, the pET expression system provides a rapid and economical method for production of recombinant human growth hormone in *E. coli*.

A.2 Methods

A.2.1 Materials

Ampicillin, Terrific Broth (TB), 3,3',5,5'-tetramethylbenzidine (TMB), and all buffer salts were purchased from Sigma-Aldrich (St. Louis, MO). Nickel Sepharose high performance resin prepacked in 5 mL HiTrap columns (HisTrap FF), PD-10 desalting columns, and Superdex 75 size exclusion chromatography (SEC) column were purchased from GE Healthcare (Piscataway, NJ). Complete EDTA-free protease inhibitor cocktail tablets and isopropyl β -D-1-thiogalactopyranoside (IPTG) were purchased from Roche Diagnostics (Indianapolis, IN). Stericup 0.45 μ m vacuum filters and Amicon 10 kDa MWCO spin filters were from Millipore (Billerica, MA). TEV-TROPIN (Teva Pharmaceuticals; North Wales, PA) was obtained from the UCSF pharmacy. Anti-human growth hormone antibodies and human growth hormone receptor Fc fusion (hGHR-Fc) were purchased from R&D systems (Minneapolis, MN). The bacterial expression vector pET22b was purchased from Novagen (San Diego, CA). All restriction enzymes and buffers used for cloning were purchased from New England Biolabs (Beverly, MA) and all primers were purchased from IDT (San Diego, CA).

A.2.2 *E. coli* expression vectors.

Human growth hormone cDNA was purchased from OpenBiosystems (Huntsville, AL) and maintained in the vector pCR4-TOPO. The gene encoding hGH was PCR amplified from pCR4-TOPO with primers designed to incorporate 5' NcoI and 3' XhoI restriction sites. All PCR reactions were performed with Phusion DNA polymerase (New England BioLabs) as follows: 98 °C 1 min; 98 °C 15 sec, 69 °C 30 sec, 72 °C 15 sec, repeat for 35 cycles; 72 °C 10 min, 4 °C hold. The resulting PCR product was purified and restriction cloned into the NcoI and XhoI sites of the bacterial expression vector pET22b (Novagen; San Diego, CA). The

resulting vector, pET22b_pelB_hGH, encodes hGH containing a N-terminal pelB leader sequence to enable periplasmic secretion via the Sec translocation machinery and a C-terminal poly-histidine tag for purification by immobilized metal affinity chromatography (IMAC). The corresponding vector, pET22b_ompA_hGH was generated by PCR amplification of the gene encoding hGH from pCR4-TOPO with primers designed to incorporate a 5' NdeI site followed by the ompA signal sequence and a 3' XhoI site. The resulting PCR product was restriction cloned into the NdeI and XhoI sites of pET22b. The resulting vector encodes hGH containing a N-terminal ompA leader sequence to enable periplasmic secretion and a C-terminal poly-histidine tag for purification. All plasmids were confirmed by DNA sequencing. A complete list of primers used in this study is provided in Table A.1.

A.2.3 Protein expression and purification.

Expression of hGH was carried out in BL21-Codon Plus (λ DE3)-RIPL *E. coli* cells (Stratagene; La Jolla, CA) harboring the pET22b-hGH vectors described above. A single colony was selected and cultured overnight at 37 °C in 10 mL of terrific broth (TB) containing 100 μ g/mL ampicillin. The 10 mL overnight *E. coli* culture was used to inoculate a 1L culture of TB containing 100 μ g/mL ampicillin. Cells were cultured at 37 °C until $OD_{600} = 0.7 - 0.9$. Protein expression was induced by addition of 0.1 mM IPTG and cultured for an additional 16 – 18 hrs at 25 °C. Cells were harvested by centrifugation (7650 g for 30 min) and the periplasmic *E. coli* fraction was extracted via osmotic shock as previously described^{24,25}. Briefly, harvested cells were suspended in a hypertonic solution of 30 mM Tris, 20% w/v sucrose, 1 mM EDTA, pH 8 (25 mL) and incubated for 30 min at 4 °C. Cells were centrifuged and the supernatant collected. Cells were re-suspended in a hypotonic solution of 5 mM MgSO₄ (25mL) and incubated for 30 min at 4 °C followed by an additional centrifugation. The supernatant from the hypotonic

solution was combined with the supernatant from the hypertonic solution, centrifuged to remove debris, and dialyzed against D-PBS overnight at 4 °C.

The periplasmic solution containing soluble hGH was clarified over a 0.45 µm filter and purified by Ni²⁺ affinity chromatography as follows. A 5mL HisTrap FF column charged with Ni²⁺ was equilibrated with 20 mM Tris, 300 mM NaCl, 40 mM imidazole, pH 8. The clarified osmotic shock fluid was loaded onto the HisTrap FF column and washed with equilibration buffer for 8 column volumes (CV). Bound protein was eluted with 3 CVs of 20 mM Tris, 300 mM NaCl, 500 mM imidazole, pH 8. Fractions with an absorbance at 280 nm greater than 0.05 were pooled, concentrated and buffer exchanged into D-PBS, and subject to analysis by reducing and non-reducing SDS-PAGE. Protein concentrations were measured based on absorbance at 280 nm assuming an extinction coefficient of 17670 M⁻¹ m⁻¹ predicted based on the mature hGH amino acid sequence using ExPASy ProtParam tool (www.expasy.org). The hGHs characterized in this study contain a carboxy terminal poly-histidine tag with the exception of TEV-TROPIN. The amino acid sequence of the tag appended to the carboxy-terminus of hGH is LVPRGSLEHHHHHH.

A.2.4 Matrix-assisted laser desorption and ionization (MALDI)-time of flight (TOF) mass spectrometry.

The intact mass of purified hGH was determined by MALDI-TOF mass spectrometry. Purified hGHs and TEV-TROPIN were desalted using C₄ ZipTips (Millipore; Billerica, MA) per the manufactures recommended protocol and eluted with 4 µL of 75% acetonitrile, 0.1% TFA in water. Desalted proteins (1 µL) were mixed with 1 µL of a saturated solution of sinapinic acid (SA) and spotted on top of a pre-formed layer of SA matrix. Mass spectra were obtained on a Microflex LT mass spectrometer (Bruker Daltonics; Billerica, MA) operated in linear, positive mode at a laser frequency of 60 Hz (100 shots total). The spectra were calibrated using the

protein Standard II from Bruker-Daltonics. Mass spectra were analyzed with the FLEX Analysis software (Bruker Daltonics).

A.2.5 Size exclusion chromatography.

The size and composition of purified hGH was analyzed by size exclusion chromatography on a Dionex FPLC equipped with a Superdex 75 column (GE Healthcare). The column was operated at a flow rate of 0.5 mL/min in D-PBS and the eluate was monitored at 280 nm. Column calibration was performed using gel filtration standards (Bio-Rad; Hercules, CA) containing bovine thyroglobulin (670 kDa), bovine γ -globulin (158 kDa), chicken ovalbumin (44 kDa), horse myoglobin (17 kDa), and vitamin B₁₂ (1.35 kDa) and plotted as Log₁₀ molecular weight, in kilo-daltons, versus retention time. The standard curve was used to estimate the molecular weight of purified hGH.

A.2.6 In vitro receptor binding assay.

An enzyme-linked immunosorption assay (ELISA) was used to evaluate binding of hGH to its receptor^{5,26} with minor modifications. The wells of a Costar 3690 plate were coated with 25 ng of recombinant human growth hormone receptor Fc fusion (hGHR-Fc; R&D Systems, Minneapolis, MN) from a 0.63 μ g/mL solution in D-PBS overnight at 4 °C. Wells were washed 3 times with 150 μ L of PBS-T (PBS, 0.05% Tween-20) and blocked with 200 μ L of a 2% BSA solution in PBS-T. Serial dilutions of purified hGH in blocking buffer were incubated with hGHR-Fc coated wells, washed 3 times with PBS-T and probed with a 1:500 dilution of biotinylated anti-hGH antibody (R&D Systems). After 3 washes with PBS-T, wells were incubated with a 1:2000 dilution of streptavidin-horseradish peroxidase (HRP), washed 6 times with PBS-T, and bound hGH was detected by addition of the HRP substrate TMB. Color was developed for 5 minutes, quenched with a 1M sulfuric acid solution and absorbance was

measured at 450 nm with blank subtraction at 550 nm. All incubations were for 1 hr at room temperature in a 40 μ L volume unless otherwise noted. Antibody and streptavidin-HRP dilutions were prepared in 1/5 strength blocking buffer.

A.2.7 Nb2 cell proliferation assay.

Nb2 cells were obtained from the UCSF cell culture facility and cultured in suspension in Fischer's medium containing L-glutamine supplemented with 10% horse serum, 10% FBS, 0.055 mM 2-mercaptoethanol, 0.075% sodium bicarbonate, and 1% penicillin/streptomycin. Cells were collected by centrifugation, re-suspended in medium lacking FBS (assay medium), seeded at a density of 4000 cells per well (in 100 μ L) in a 96-well tissue culture plate, and serum starved for 24 hrs. Nb2 cell growth was stimulated by addition of hGH diluted in assay medium (100 μ L) to a final concentration between 0.1 pM and 500 pM in a final volume of 200 μ L. Cells were cultured for an additional 3 days at 37 °C in a CO₂ controlled and humidified incubator then counted on a FACS Array cell sorter (BD Biosciences; San Jose, CA). Cell counts for each test population were derived after gating for live cells based on the forward scatter (FSC) and side scatter (SSC). Data were analyzed using FlowJo (Tree Star Inc.; Ashland, OR) and all incubations were done in triplicate with data represented as mean \pm SD.

A.2.8 Affinity measurements by surface plasmon resonance.

SPR measurements were obtained using a BIAcore T100 instrument (BIAcore Inc.; Piscataway, NJ). The hGHR-Fc fusion protein (R&D Systems) was captured on a CM5 sensor chip by amine coupling at pH 4.5 to a final immobilization density of \sim 680 resonance units (RU). Un-reacted sites were blocked with 1M ethanolamine. A control flow cell without immobilized hGHR-Fc was prepared for reference subtraction. Dilutions of hGH in running buffer [10 mM HEPES, 150 mM NaCl, 0.005% Tween 20, pH 7.4 (HBS-T) or 50 mM phosphate,

100 mM NaCl, 0.01% Tween 20, pH 6] were injected over the chip for 90 sec followed by a 200 sec dissociation in running buffer. The chip was regenerated with a 30 sec injection of 10 mM glycine, pH 2.5 and two 45 sec injections of HBS-T. The flow rate used for all methods was 30 μ L/min. Binding affinities were derived by analysis of the generated sensograms using the Biacore T100 evaluation software. The equilibrium RU observed for each injection was plotted against protein concentration and fit to a steady-state affinity model included in the evaluation software for determination of the equilibrium binding affinity (K_D).

A.3 Results

A.3.1 Construction of pET22b hGH expression vectors.

The plasmid pET22b (Novagen) was used as a template to construct vectors that target hGH to the *E. coli* periplasm. The plasmid contains a T7 promoter, lacI gene, N-terminal pelB signal sequence for periplasmic localization, multiple cloning sites, and an optional C-terminal poly-histidine tag. The pET22b-pelB hGH secretion vector was created by PCR amplification of the gene encoding hGH with primers (Table A.1) that add a 5' NcoI and 3' XhoI restriction site and restriction cloned into the NcoI and XhoI sites of pET22b (Fig. A.1). The resulting pET22b-pelB hGH vector encodes a N-terminal pelB sequence in frame with the hGH sequence followed by a poly-histidine tag. The pET22b-ompA hGH secretion vector was created by PCR amplification of the gene encoding hGH with primers that add a 5' NdeI site followed by the ompA signal sequence and a 3' XhoI site. The ompA-hGH PCR product was subsequently restriction cloned into the NdeI and XhoI sites of pET22b resulting in replacement of the pelB sequence with ompA. The resulting pET22b-ompA hGH vector encodes a N-terminal ompA sequence in frame with hGH followed by a poly-histidine tag.

Table A.1 Primers used in this study.

Vector	Primer Pair	Restriction Site
pET22b-pelB	F = 5'-GATGGCCATGGGCTTCCCAACCATTCCCTTATC-3'	NcoI
hGH	R = 5'-GGTGCTCGAGGCTGCCGCGCGGCACCAGGAAGCCACAGCTGCCCTC-3'	XhoI
pET22b-ompA	F = 5'-CATACATATGAAAAAACC GCGATTGCGATTGCGGTGGCGTTAGCGGGCT TTGCGACCGTGGCGCAGGCGTTCCCAACCATTCCCTTATC-3'	NdeI
hGH	R = 5'-GGTGCTCGAGGCTGCCGCGCGGCACCAGGAAGCCACAGCTGCCCTC-3'	XhoI

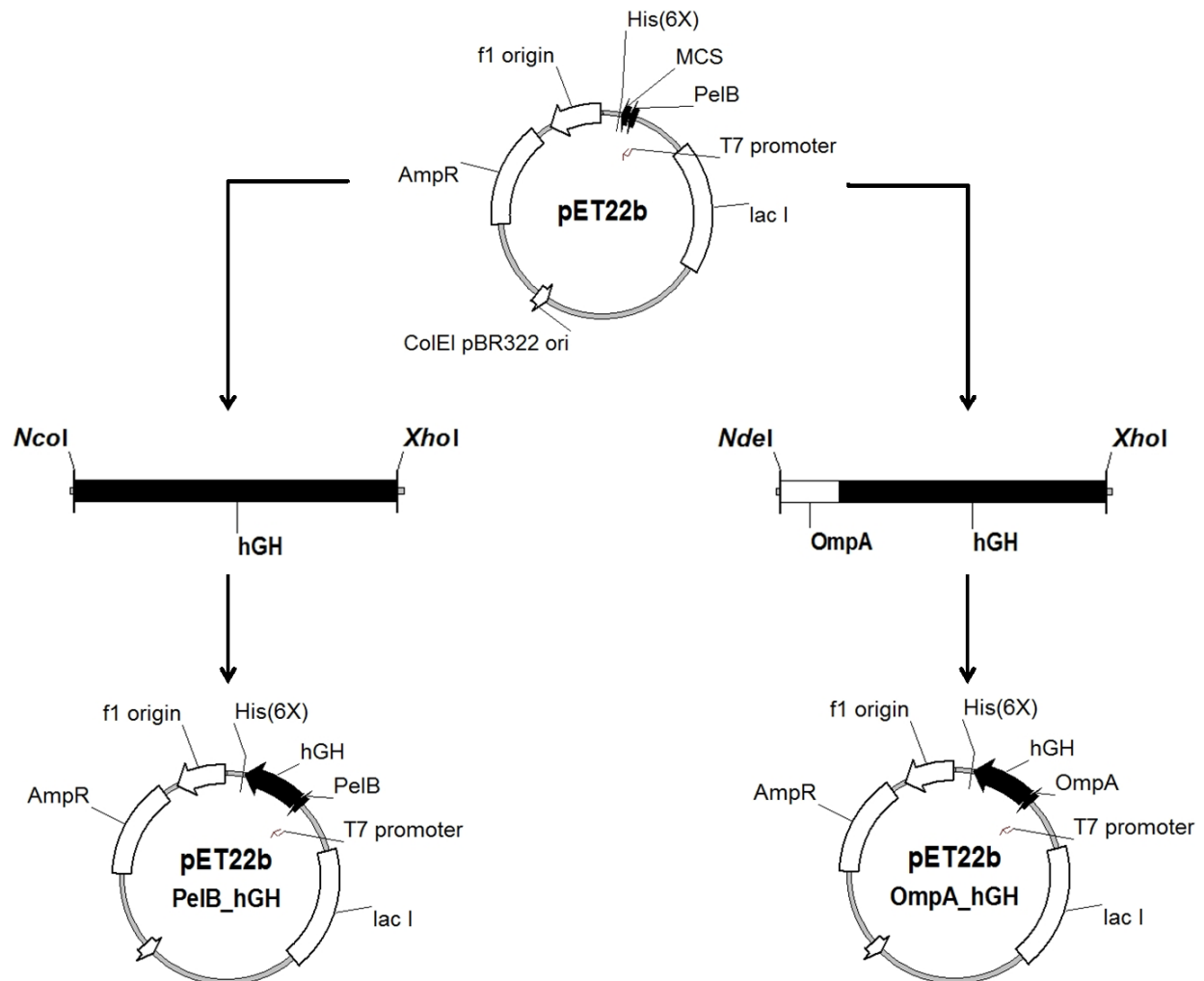


Figure A.1 Schematic depicting the construction of pET22b-pelB hGH (left) and pET22b-ompA hGH (right) expression vectors.

The gene encoding hGH was PCR amplified as described in Section A.2.2 and restriction cloned into the pET22b *E. coli* expression vector.

A.3.2 Protein expression, purification, and characterization.

Vectors encoding hGH with either the pelB or ompA secretion signal were transformed into BL21-Codon Plus (DE3)-RIPL *E. coli* cells for recombinant protein production. This *E. coli* strain carries a chromosomal copy of the T7 RNA polymerase gene under control of the *lacUV5* promoter. IPTG addition induces expression of T7 RNA polymerase resulting in transcription of the hGH gene under control of the T7 promoter in cells harboring the pET22b-hGH vectors. The N-terminal pelB and ompA secretion signals target the translated polypeptide in its unfolded state to the *E. coli* periplasm via the Sec-dependent transport pathway². The signal peptide is cleaved and the protein folds in the periplasm with the help of chaperones and disulfide bond isomerases. Although the pelB and ompA leader sequences are removed upon secretion to the periplasm, the terms pelB-hGH and ompA-hGH are used throughout to indicate the hGH described was produced from either pET22b_pelB_hGH or pET22b_ompA_hGH vectors, respectively. It is expected that an amino-terminal methionine or phenylalanine is generated upon cleavage of the pelB or ompA secretion signals, respectively, resulting in the mature hGH sequences. Both pelB- and ompA-hGH were purified from osmotic shock fluid containing *E. coli* periplasmic proteins. Purification was facilitated by the C-terminal poly-histidine tag which enabled separation of soluble, periplasmic hGH from contaminating *E. coli* cell proteins by Ni²⁺ affinity chromatography. No distinct over-expression of hGH was observed in the lysate or periplasmic fraction by SDS-PAGE; therefore, we report yields as the amount of hGH recovered after the Ni²⁺ affinity chromatography step. Yields after purification ranged from 0.64 to 2.57 mg/L culture (0.39 – 1.13 mg/L/OD₆₀₀) for pelB-hGH and 0.32 to 2.29 mg/L culture (0.24 – 1.37 mg/L/OD₆₀₀) for ompA-hGH from ~ 10 – 15 grams of wet cells. The variability in yield from batch to batch is likely due to colony selection as each round of expression and purification

started with a colony selected from freshly transformed *E. coli*. It is therefore important to screen for high-expressing colonies to maximize yield of hGH using the pET expression system. It is difficult to compare yields to previous reports given the variation in expression systems, scale, and analytical methods; however, based on yields summarized by Soares et al.¹⁷ the pET system is within the reported range, although notably lower than yields from industrial expression systems^{18,19}, as expected.

Purified pelB- and ompA-hGH migrate at approximately ~ 24 kDa under reducing and ~ 19 kDa under non-reducing SDS-PAGE (Fig. A.2). The observed shift in electrophoretic mobility is consistent with that of pharmaceutical grade recombinant hGH (TEV-TROPIN) and indicates the formation of native disulfide bonds resulting in a more compact tertiary structure and faster migration under non-reducing conditions. There are no detectable high molecular weight aggregates by SDS-PAGE; however, a low proportion of an ~ 25 kDa band is present in both the pelB- and ompA-hGH preparations under non-reducing conditions. Upon reduction the 25 kDa species migrates as two low molecular weight fragments suggesting that the 25 kDa species is the result of a previously characterized endoproteolytic cleavage between Thr-142 and Tyr-143 of hGH during culture²². This “two chain” hGH is commonly observed in periplasmic preparations and has equivalent biological activity as non-cleaved hGH in both the hypophysectomized rat weight-gain and Nb2 cell growth assay^{18,22,27}. Further optimization of culture conditions such as pH, temperature, cation concentration, etc. may reduce proteolytic cleavage and improve product quality.

Affinity purified hGHs were analyzed by size exclusion chromatography under non-denaturing conditions (Fig. A.3a-c). All proteins migrate as monomers with a predicted molecular weight of ~ 23 kDa, ~ 22 kDa, and ~ 25 kDa for TEV-TROPIN, pelB-hGH, and

ompA-hGH, respectively. Intact mass was further confirmed by MALDI-TOF MS (Fig. A.3d-f). The observed molecular weights are in agreement with the expected molecular weights of mature hGH indicating proper cleavage of the pelB and ompA signal peptides upon secretion into the *E. coli* periplasm. A peak corresponding to the mass of hGH dimer is present by MALDI-TOF MS analysis in all hGH samples, including TEV-TROPIN, that is not detectable by SDS-PAGE or size exclusion chromatography. This likely represents a very small fraction of the total protein that is detectable due to the sensitivity of MALDI-TOF MS and may be exaggerated due to ionization differences between monomer and dimer.

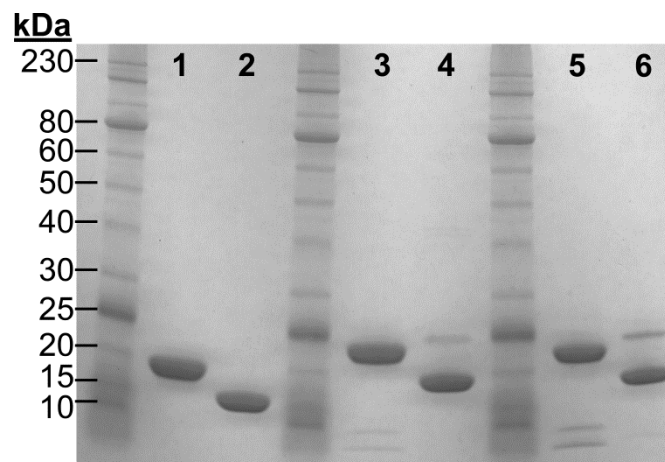


Figure A.2 Reducing and non-reducing SDS-PAGE analysis of recombinant hGH. Reduced TEV-TROPIN (lane 1), non-reduced TEV-TROPIN (lane 2), reduced pelB-hGH (lane 3), non-reduced pelB-hGH (lane 4), reduced ompA-hGH (lane 5), non-reduced ompA-hGH (lane 6). 7.5 μ g of protein were loaded in each lane.

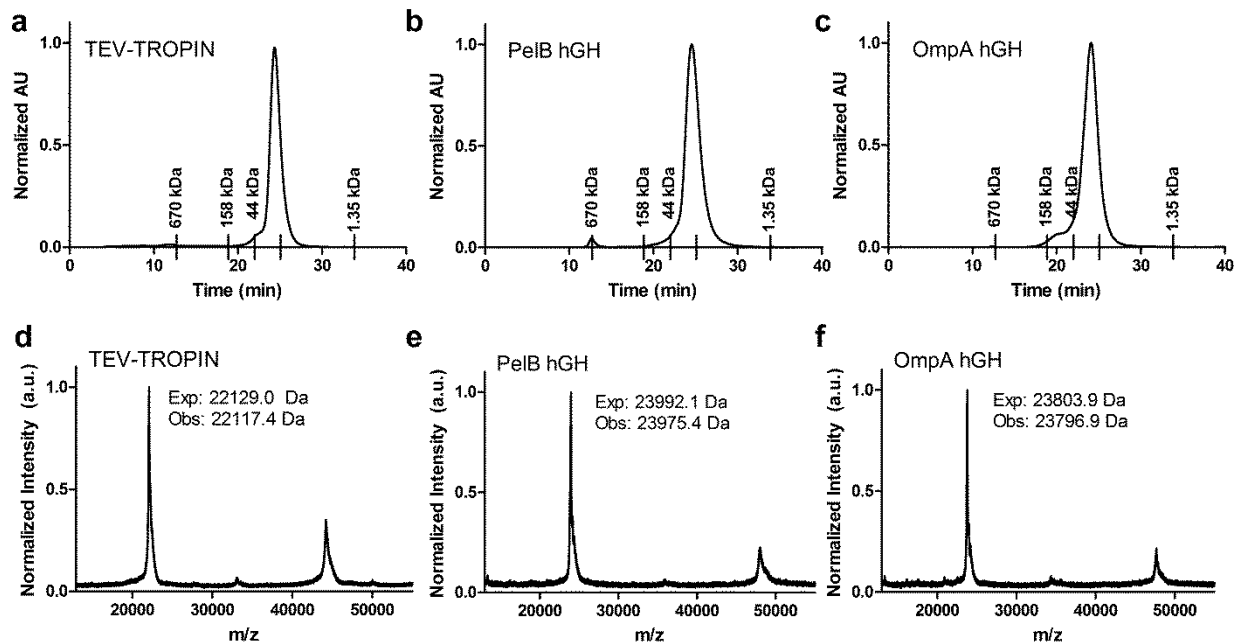


Figure A.3 Size exclusion chromatography (a-c) and MALF-TOF (d-f) analysis of TEV-TROPIN (a,d), pelB-hGH (b,e), and ompA-hGH (c,f).

The retention time of the SEC calibration standards are indicated by tick marks on the x-axis. The standards include thyroglobulin 670 kDa, gamma-globulin 158 kDa, ovalbumin 44kDa, myoglobin 17 kDa, and vitamin B12 1.35 kDa. The unlabeled tick under the hGH peak in each panel corresponds to the retention time of the 17 kDa myoglobin standard. Obs: = Observed, Exp: = Expected.

A.3.3 Affinity measurement by surface plasmon resonance and ELISA.

We characterized binding between purified hGHs and the hGH receptor (hGH-R) by surface plasmon resonance and ELISA. One hGH molecule contains two hGH-R binding sites allowing the formation of a 2:1 complex between hGH-R and hGH^{28,29}. Both pelB- and ompA-hGH bind the hGH-R with similar affinity (Fig. A.4a and Table A.2) indicating the choice of secretion sequence for periplasmic targeting does not influence receptor binding. The affinity of pelB- and ompA-hGH by SPR and ELISA is slightly lower than that of TEV-TROPIN likely due to the C-terminal poly-histidine tag given alternative peptide fusions to the carboxy-terminus of hGH also have reduced potency³⁰. Analysis of the SPR sensograms indicates the slight reduction in affinity at pH 7.4 is mainly attributed to a reduction in the rate of association (Fig A.5). We also evaluated whether binding of hGH to the hGH-R is affected by pH. A slight increase in affinity is observed at pH 6 compared to pH 7.4 for pelB- and ompA-hGH, whereas the affinity of TEV-TROPIN does not change with pH (Fig. A.5 and Table A.2). Again, this slight increase in affinity at pH 6 may be attributed to the protonated histidine residues in the poly-histidine tag given there is no difference in affinity as a function of pH for TEV-TROPIN. Therefore, for certain applications it may be necessary to remove the poly-histidine tag prior to evaluation.

Table A.2 Binding affinity to hGH receptor measured by SPR and ELISA and *in vitro* hGH potency in Nb2 cell growth bioassay.

(*) Data were fit to a steady state affinity model for derivation of apparent K_D .

Molecule	K_D (SPR) [*] pH 7.4, (nM)	K_D (SPR) [*] pH 6, (nM)	K_D (ELISA) pH 7.4, (nM)	EC_{50} (pM)
TEV-TROPIN	14.8	11.6	0.52 ± 0.05	10.2 ± 4.8
PelB hGH	32.9	12.8	0.81 ± 0.28	23.7 ± 9.9
OmpA hGH	35.3	13.1	1.17 ± 0.38	21.6 ± 12.7

(*) Data were fit to a steady state affinity model for derivation of apparent K_D .

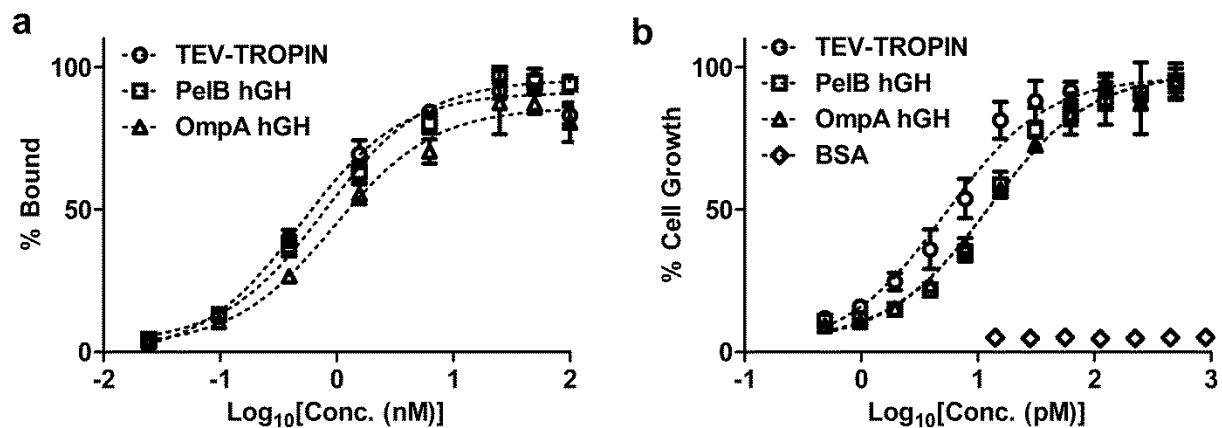


Figure A.4 *In vitro* hGH receptor binding ELISA (a) and Nb2 cell potency bioassay (b). Each data point represent the mean (n=3) and error bars indicate standard deviation (s.d.). The dashed line indicates data fit to a log(agonist) vs. response model using Prism for derivation of K_D and EC_{50} . Data points were normalized to the maximum observed hGH receptor binding (a) or Nb2 cell count (b) and plotted as percentage of maximum binding or growth. The data shown in (a) and (b) are representative of at least 3 independent protein preparations.

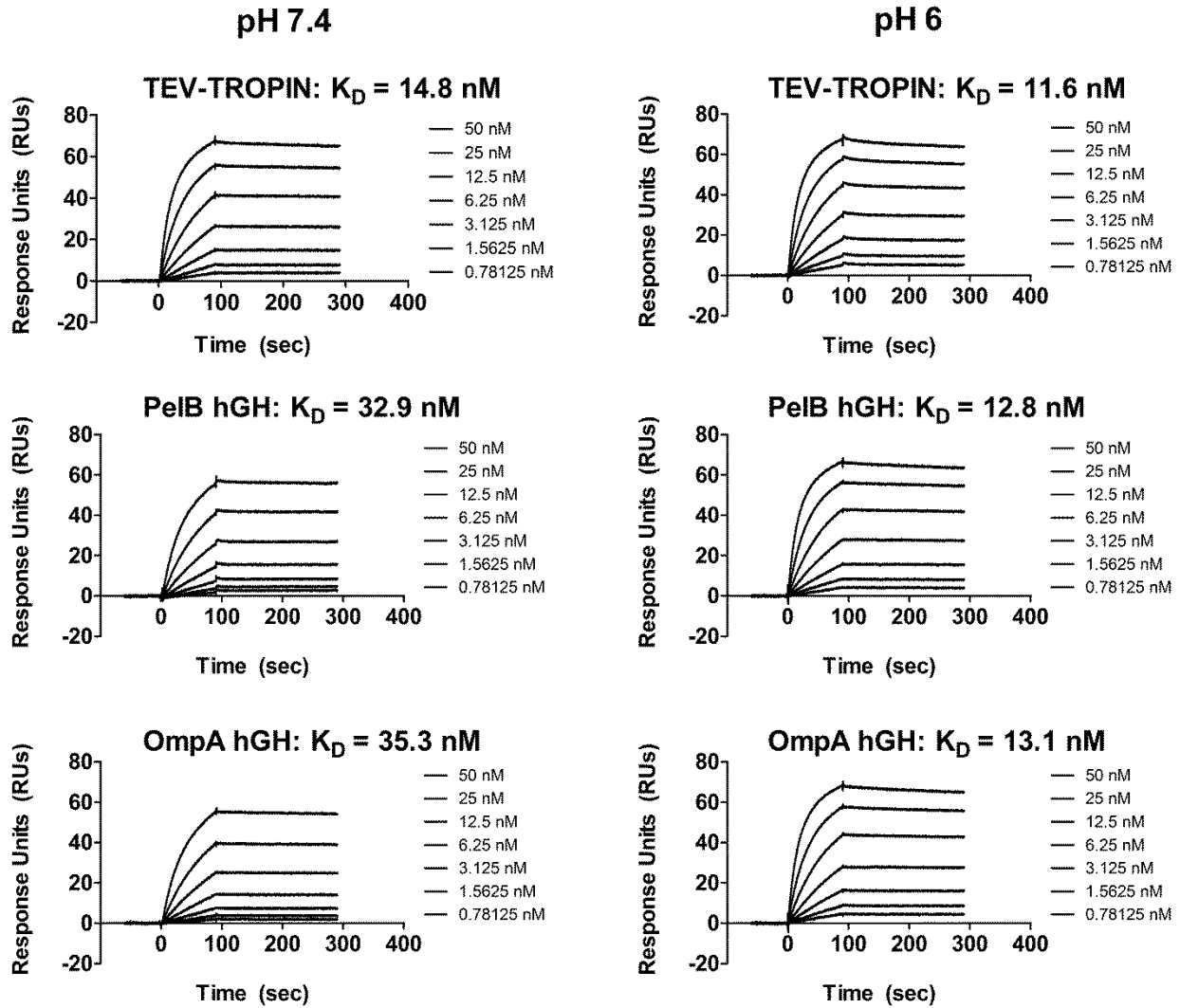


Figure A.5 Surface plasmon resonance sensograms of hGH binding to immobilized hGH-R. Increasing concentrations of TEV-TROPIN, pelB-hGH, or ompA-hGH (0.78 nM to 50 nM) were injected over immobilized hGHR-Fc at pH 7.4 (left) or pH 6 (right) as described in Section A.2.8. The resulting sensograms were fit to a steady state affinity model for derivation of K_D . All data were baseline-adjusted and reference cell-subtracted.

A.3.4 Nb2 cell bioassay for growth hormone activity.

The Nb2 rat node lymphoma cell line was used to quantify the *in vitro* bioactivity of purified hGH³¹. Nb2 cell growth is dependent on mammalian lactogens, such as prolactin and hGH, and is a useful tool for quantifying the potency of recombinant hGH³². Nb2 cells starved of FBS undergo cell cycle arrest which can be rescued by addition of exogenous hGH. The ability of hGH to elicit a biological response (e.g. cell growth) is dependent on hGH induced receptor dimerization. Each hGH contains two separate hGH-R binding sites. hGH first binds the hGH-R using site 1 with subsequent binding to a second hGH-R using site 2²⁸. Sequential binding and receptor dimerization make hGH a potent agonist whereas dimerization blockade through site 2 mutagenesis or high hGH concentrations that saturate hGH receptors with site 1 binders act as antagonists³³. TEV-TROPIN, pelB-, and ompA-hGH stimulate Nb2 cell growth in a dose-dependent manner with an EC₅₀ of 10.2 pM, 23.7 pM, and 21.6 pM, respectively, whereas BSA has no effect on cell growth at concentrations up to 14 nM (Fig. A.4b and Table A.2). The data indicate that pelB- and ompA-hGH contain 2 functional hGH-R binding sites and form the appropriate receptor-hormone complex necessary for potent growth stimulation.

A.4 Conclusion

In summary, we report a simple system for production of recombinant human growth hormone directed to the *E. coli* periplasm via the pET based expression platform to yield soluble, properly folded hGH containing a C-terminal poly-histidine tag. The hGH isolated by a single affinity chromatography step is monomeric, binds the hGH receptor with high affinity, and potently stimulates cell growth with only a slight reduction in potency compared to pharmaceutical grade recombinant hGH. The amount of hGH recovered per batch is suitable for *in vitro* and *in vivo* studies. This system will be useful for the average research laboratory wishing to produce material to study hGH biology or design novel hGH variants and delivery systems.

A.5 References

1. Studier, F. W. & Moffatt, B. A. Use of bacteriophage T7 RNA polymerase to direct selective high-level expression of cloned genes. *J. Mol. Biol.* **189**, 113–30 (1986).
2. Yoon, S. H., Kim, S. K. & Kim, J. F. Secretory production of recombinant proteins in *Escherichia coli*. *Recent Pat. Biotechnol.* **4**, 23–9 (2010).
3. Berkmen, M. Production of disulfide-bonded proteins in *Escherichia coli*. *Protein Expr. Purif.* **82**, 240–51 (2012).
4. CORPAS, E., HARMAN, S. M. & BLACKMAN, M. R. Human Growth Hormone and Human Aging. *Endocr. Rev.* **14**, 20–39 (1993).
5. Cleland, J. L. *et al.* A novel long-acting human growth hormone fusion protein (VRS-317): enhanced in vivo potency and half-life. *J. Pharm. Sci.* **101**, 2744–54 (2012).
6. Illum, L., Jordan, F. & Lewis, A. L. CriticalSorbTM: A novel efficient nasal delivery system for human growth hormone based on Solutol HS15. *J. Control. Release* **162**, 194–200 (2012).
7. De Schepper, J., Rasmussen, M. H., Gucev, Z., Eliakim, A. & Battelino, T. Long-acting pegylated human GH in children with GH deficiency: a single-dose, dose-escalation trial investigating safety, tolerability, pharmacokinetics and pharmacodynamics. *Eur. J. Endocrinol.* **165**, 401–9 (2011).
8. Péter, F., Bidlingmaier, M., Savoy, C., Ji, H.-J. & Saenger, P. H. Three-year efficacy and safety of LB03002, a once-weekly sustained-release growth hormone (GH) preparation, in prepubertal children with GH deficiency (GHD). *J. Clin. Endocrinol. Metab.* **97**, 400–7 (2012).
9. Amet, N., Wang, W. & Shen, W.-C. Human growth hormone-transferrin fusion protein for oral delivery in hypophysectomized rats. *J. Control. Release* **141**, 177–82 (2010).
10. Kirk, J. Indications for growth hormone therapy in children. *Arch. Dis. Child.* **97**, 63–8 (2012).
11. Cuatrecasas, G. *et al.* Growth hormone treatment for sustained pain reduction and improvement in quality of life in severe fibromyalgia. *Pain* **153**, 1382–9 (2012).
12. Sockolosky, J. T., Tiffany, M. R. & Szoka, F. C. Engineering neonatal Fc receptor-mediated recycling and transcytosis in recombinant proteins by short terminal peptide extensions. *Proc. Natl. Acad. Sci. U. S. A.* **109**, 16095–16100 (2012).

13. Patra, A. K. *et al.* Optimization of inclusion body solubilization and renaturation of recombinant human growth hormone from *Escherichia coli*. *Protein Expr. Purif.* **18**, 182–92 (2000).
14. Peterson, F. C., Anderson, P. J., Berliner, L. J. & Brooks, C. L. Expression, folding, and characterization of small proteins with increasing disulfide complexity by a pT7-7-derived phagemid. *Protein Expr. Purif.* **15**, 16–23 (1999).
15. Singh, S. M., Sharma, A. & Panda, A. K. High throughput purification of recombinant human growth hormone using radial flow chromatography. *Protein Expr. Purif.* **68**, 54–9 (2009).
16. Mukhija, R., Rupa, P., Pillai, D. & Garg, L. C. High-level production and one-step purification of biologically active human growth hormone in *Escherichia coli*. *Gene* **165**, 303–6 (1995).
17. Soares, C. R. J., Gomide, F. I. C., Ueda, E. K. M. & Bartolini, P. Periplasmic expression of human growth hormone via plasmid vectors containing the lambdaPL promoter: use of HPLC for product quantification. *Protein Eng.* **16**, 1131–8 (2003).
18. Hsiung, H. M., Mayne, N. G. & Becker, G. W. High-Level Expression, Efficient Secretion and Folding of Human Growth Hormone in *Escherichia coli*. *Bio/Technology* **4**, 991–995 (1986).
19. Chang, C. N., Rey, M., Bochner, B., Heyneker, H. & Gray, G. High-level secretion of human growth hormone by *Escherichia coli*. *Gene* **55**, 189–96 (1987).
20. Gray, G. L., Baldridge, J. S., McKeown, K. S., Heyneker, H. L. & Chang, C. N. Periplasmic production of correctly processed human growth hormone in *Escherichia coli*: natural and bacterial signal sequences are interchangeable. *Gene* **39**, 247–54 (1985).
21. Ghorpade, A. & Garg, L. C. Efficient processing and export of human growth hormone by heat labile enterotoxin chain B signal sequence. *FEBS Lett.* **330**, 61–65 (1993).
22. Chang, J. Y., Pai, R. C., Bennett, W. F. & Bochner, B. R. Periplasmic secretion of human growth hormone by *Escherichia coli*. *Biochem. Soc. Trans.* **17**, 335–7 (1989).
23. Teresa, M., Ribela, C. P., Camargo, I. M., Oliveira, J. E. & Bartolini, P. Single-step purification of recombinant human growth hormone (hGH) directly from bacterial osmotic shock fluids, for the purpose of (125)I-hGH preparation. *Protein Expr. Purif.* **18**, 115–20 (2000).
24. Zhou, Y. & Marks, J. D. Antibody Engineering. *Antib. Eng.* **1**, 183–195 (2010).
25. Koshland, D. & Botstein, D. Secretion of beta-lactamase requires the carboxy end of the protein. *Cell* **20**, 749–60 (1980).

26. Schellenberger, V. *et al.* A recombinant polypeptide extends the in vivo half-life of peptides and proteins in a tunable manner. *Nat. Biotechnol.* **27**, 1186–1190 (2009).
27. CANOVA-DAVIS, E. *et al.* Properties of a cleaved two-chain form of recombinant human growth hormone. *Int. J. Pept. Protein Res.* **35**, 17–24 (2009).
28. Cunningham, B. *et al.* Dimerization of the extracellular domain of the human growth hormone receptor by a single hormone molecule. *Science* **254**, 821–825 (1991).
29. De Vos, A., Ultsch, M. & Kossiakoff, A. Human growth hormone and extracellular domain of its receptor: crystal structure of the complex. *Science* **255**, 306–312 (1992).
30. Langenheim, J. F. & Chen, W. Y. Improving the pharmacokinetics/pharmacodynamics of prolactin, GH, and their antagonists by fusion to a synthetic albumin-binding peptide. *J. Endocrinol.* **203**, 375–87 (2009).
31. Gout, P. W., Beer, C. T. & Noble, R. L. Prolactin-stimulated growth of cell cultures established from malignant Nb rat lymphomas. *Cancer Res.* **40**, 2433–6 (1980).
32. Tanaka, T. *et al.* A new sensitive and specific bioassay for lactogenic hormones: measurement of prolactin and growth hormone in human serum. *J. Clin. Endocrinol. Metab.* **51**, 1058–63 (1980).
33. Fuh, G. *et al.* Rational design of potent antagonists to the human growth hormone receptor. *Science* **256**, 1677–80 (1992).

Appendix B

B.1 Amino acid sequences of proteins studied in this dissertation

The FcBP sequence in each protein is in **bold** letters. Mutants of the FcBP sequence or protein sequence are shown in ***bold italic*** letters. The thrombin cleavage site is *underlined in italic*. Signal peptide sequences for periplasmic secretion in *E. coli* or endogenous mammalian signal peptide sequences are in *italic*.

mKate

MGSSHHHHHHSSGL***LVPRG***SHMSELIKENMHMKLYMEGTVNNHHFKCTSEGEGKPYEGTQTMRI
KVVEGGPLPFAFDILATSFMYGSKTFINHTQGIPDFFKQSFPEGFTWERVTTYEDGGVLTATQDTS
LQDGCLIYNVKIRGVNFPSNGPVMQKKT LGWEASTEMLYPADGGLEGRSDMALKLVGGGHLIC
NLKTTYRSKKPAK***NLKMPGVYYVDRRLERIKEADKETYVEQHEVAVARYCDLPSKLGHK***

mKate S128C mutant for PEGylation

MGSSHHHHHHSSGL***LVPRG***SHMSELIKENMHMKLYMEGTVNNHHFKCTSEGEGKPYEGTQTMRI
KVVEGGPLPFAFDILATSFMYGSKTFINHTQGIPDFFKQSFPEGFTWERVTTYEDGGVLTATQDTS
LQDGSLIYNVKIRGVNFP***CNG***PVMQKKT LGWEASTEMLYPADGGLEGRSDMALKLVGGGHLIC
NLKTTYRSKKPAK***NLKMPGVYYVDRRLERIKEADKETYVEQHEVAVARYSDLPSKLGHK***

C-Terminal Linear FcBP mKate

MGSSHHHHHHSSGL***LVPRG***SHMSELIKENMHMKLYMEGTVNNHHFKCTSEGEGKPYEGTQTMRI
KVVEGGPLPFAFDILATSFMYGSKTFINHTQGIPDFFKQSFPEGFTWERVTTYEDGGVLTATQDTS
LQDGCLIYNVKIRGVNFPSNGPVMQKKT LGWEASTEMLYPADGGLEGRSDMALKLVGGGHLIC
NLKTTYRSKKPAK***NLKMPGVYYVDRRLERIKEADKETYVEQHEVAVARYCDLPSKLGHKGGG***
GSQRFTGHFGGLYPANG

C-Terminal Cyclic FcBP mKate

MGSSHHHHHHSSGL***LVPRG***SHMSELIKENMHMKLYMEGTVNNHHFKCTSEGEGKPYEGTQTMRI
KVVEGGPLPFAFDILATSFMYGSKTFINHTQGIPDFFKQSFPEGFTWERVTTYEDGGVLTATQDTS
LQDGSLIYNVKIRGVNFPSNGPVMQKKT LGWEASTEMLYPADGGLEGRSDMALKLVGGGHLIC
NLKTTYRSKKPAK***NLKMPGVYYVDRRLERIKEADKETYVEQHEVAVARYSDLPSKLGHKGGG***
GSQRFACTGHFGGLYPCNG

N-Terminal Cyclic FcBP mKate

MGSSHHHHHHSSGL***LVPRG******QRFCTGHFGGLYPCNGGGGG***SSELIKENMHMKLYMEGTVNNHH
FKCTSEGEGKPYEGTQTMRIKVVEGGPLPFAFDILATSFMYGSKTFINHTQGIPDFFKQSFPEGFT
WERVTTYEDGGVLTATQDTS***LQDGSLIYNVKIRGVNFPSNGPVMQKKT LGWEASTEMLYPADG***
GLEGRSDMALKLVGGGHLICNLKTTYRSKKPAKNLKMPGVYYVDRRLERIKEADKETYVEQHE
VAVARYSDLPSKLGHK

N-&-C-Terminal Cyclic FcBP mKate

MGSSHHHHHHSSGL***LVPRG******QRFCTGHFGGLYPCNGGGGG***SSELIKENMHMKLYMEGTVNNHH
FKCTSEGEGKPYEGTQTMRIKVVEGGPLPFAFDILATSFMYGSKTFINHTQGIPDFFKQSFPEGFT
WERVTTYEDGGVLTATQDTS***LQDGSLIYNVKIRGVNFPSNGPVMQKKT LGWEASTEMLYPADG***
GLEGRSDMALKLVGGGHLICNLKTTYRSKKPAKNLKMPGVYYVDRRLERIKEADKETYVEQHE
VAVARYSDLPSKLGHKGGGG***QRFCTGHFGGLYPCNG***

N-&-C-Terminal Cyclic FcBP mKate Y286H

MGSSHHHHHHSSGLVPRGQRFCTGHFGGLYPCNGGGGGSSSELIKENMHMKLYMEGTVNNHH
FKCTSEGEGKPYEGTQTMRIKVVVEGGPLPFAFDILATSFMYGSKTFINHTQGIPDFFKQSFPEGFT
WERVTTYEDGGVLTATQDTSLQDGS LIY NVKIRGVNFPSNGPVMQKKT LGWEASTEMLYPADG
GLEGRSDMALKLVGGGH LICNLKTTYRSKKPAKNLKM PGVYYVDRRLRIKEADKETYVEQHE
VAVARYSDLPSKLGHKGGGGSQRFCTGHFGGLHPCNG

N-Linear & C-Cyclic FcBP mKate

MGSSHHHHHHSSGLVPRGQRFVTGHFGGLYPANGGGGGSSSELIKENMHMKLYMEGTVNNHHF
KCTSEGEGKPYEGTQTMRIKVVVEGGPLPFAFDILATSFMYGSKTFINHTQGIPDFFKQSFPEGFTW
ERVTTYEDGGVLTATQDTSLQDGS LIY NVKIRGVNFPSNGPVMQKKT LGWEASTEMLYPADGG
LEGRSDMALKLVGGGH LICNLKTTYRSKKPAKNLKM PGVYYVDRRLRIKEADKETYVEQHEV
AVARYSDLPSKLGHKGGGGSQRFCTGHFGGLYPCNG

N-&-C-Terminal Linear FcBP mKate

MGSSHHHHHHSSGLVPRGQRFVTGHFGGLYPANGGGGGSSSELIKENMHMKLYMEGTVNNHH
FKCTSEGEGKPYEGTQTMRIKVVVEGGPLPFAFDILATSFMYGSKTFINHTQGIPDFFKQSFPEGFT
WERVTTYEDGGVLTATQDTSLQDGS LIY NVKIRGVNFPSNGPVMQKKT LGWEASTEMLYPADG
GLEGRSDMALKLVGGGH LICNLKTTYRSKKPAKNLKM PGVYYVDRRLXRIKEADKETYVEQHE
VAVARYSDLPSKLGHKGGGGSQRFVTGHFGGLYPANG

N-&-C-Terminal Linear FcBP mKate S128C for PEGylation

MGSSHHHHHHSSGLVPRGQRFVTGHFGGLYPANGGGGGSSSELIKENMHMKLYMEGTVNNHH
FKCTSEGEGKPYEGTQTMRIKVVVEGGPLPFAFDILATSFMYGSKTFINHTQGIPDFFKQSFPEGFT
WERVTTYEDGGVLTATQDTSLQDGS LIY NVKIRGVNFPCNGPVMQKKT LGWEASTEMLYPADG
GLEGRSDMALKLVGGGH LICNLKTTYRSKKPAKNLKM PGVYYVDRRLRIKEADKETYVEQHE
VAVARYSDLPSKLGHKGGGGSQRFVTGHFGGLYPANG

hGH (OmpA Leader)

MKKTAAIAVALAGFATVAQAFPTIPLSRLFDNAMLR AHR LHQLAFD TYQEFEEAYIPKEQKYSFLQ
NPQTSLCFSESIPTSPNREETQQKSNLELLRISLLLIQSWLEPVQFLRSVFANSLVYGASDSNVYDL
LKDLEEGIQTLMGRLEDGSPRTGQIFKQTYSKFDTNSHNDDALLKNYGLLYCFRKDMDKVETFL
RIVQCRSVEGSCGFLVPRGSLEHHHHHH

hGH (PelB Leader)

MKYLLPTAAAGLLLLAAQPAMAMGFPTIPLSRLFDNAMLR AHR LHQLAFD TYQEFEEAYIPKEQKY
SFLQNPQTSLCFSESIPTSPNREETQQKSNLELLRISLLLIQSWLEPVQFLRSVFANSLVYGASDSNV
YDLLKDLEEGIQTLMGRLEDGSPRTGQIFKQTYSKFDTNSHNDDALLKNYGLLYCFRKDMDKVE
TFLRIVQCRSVEGSCGFLVPRGSLEHHHHHH

C-Terminal Cyclic ABP mKate

MGSSHHHHHHSSGLVPRGSHMSELIKENMHMKLYMEGTVNNHHFKCTSEGEGKPYEGTQTMRI
KVVVEGGPLPFAFDILATSFMYGSKTFINHTQGIPDFFKQSFPEGFTWERVTTYEDGGVLTATQDTS
LQDGS LIY NVKIRGVNFPSNGPVMQKKT LGWEASTEMLYPADGGLEGRSDMALKLVGGGH LIC
NLKTTYRSKKPAKNLKM PGVYYVDRRLRIKEADKETYVEQHEVAVARYSDLPSKLGHKGGG
GSQRLMEDICLPRWGCLWEDDF

hFcRn-YFP

MGVPRPQPWALGLLLFLLPGLGAESHLSLLYHLTA VSSPAPGTPAFWVSGWLGPQQYLSYNSLR

GEAEPGAWWENQVSWYWEKETDRLRIKEKLFLEAFKALGGKGPYTLQGLLGCELGPDNTSV
PTAKFALNGEEFMNFDLKQGTWGGDWPEALAISQRWQQDKAANKELTFLLFSCPHRLREHLE
RGRGNLEWKEPPSMRLKARPSSPGFSVLTCSAFSFYPPQLRFLRNGLAAGTGQGDFGPNSDGS
FHASSLTVKSGDEHHYCCIVQHAGLAQPLRVELESPAKSSVLVVGIVIGVLLLAAA VGGALLW
RRMRGLPAPWISLRGDDTGVLPTPGEAQDADLKDVNVIPATAGGGGSGGGGSGPVATMVSK
GEELFTGVVPILVELDGDVNGHKFSVSGEGEGDATYGKLTCLKFICTTGKLPVPWPTLVTTFGYGL
QCFARYPDHMKQHDFFKSAMPEGYVQERTIFFKDDGNYKTRAEVKFEGDTLVNRIELKGIDFKE
DGNILGHKLEYNYNSHNVYIMADKQKNGIKVNFKIRHNIEDGSVQLADHYQQNTPIGDGPVLLP
DNHYLSYQSALS KDPNEKRDMVLEFVTAAGITLGMDELYK

hβ2M

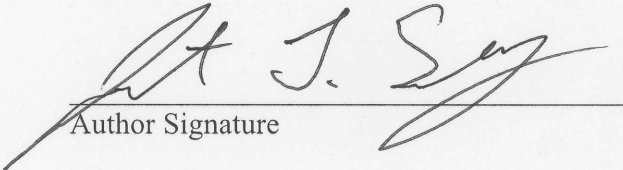
*MSRSVALAVLALLSLSGLEAIQRTPKIQVYSRHPAENGKSNFLNCYVSGFHPSDIEVDLLKNGERIEK
VEHSDLSFSKDWSFYLLYYTEFTPTEKDEYACRVNHVTL SQPKIVKWDRDM*

Publishing Agreement

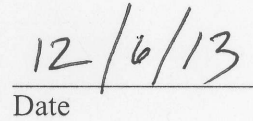
It is the policy of the University to encourage the distribution of all theses, dissertations, and manuscripts. Copies of all UCSF theses, dissertations, and manuscripts will be routed to the library via the Graduate Division. The library will make all theses, dissertations, and manuscripts accessible to the public and will preserve these to the best of their abilities, in perpetuity.

Please sign the following statement:

I hereby grant permission to the Graduate Division of the University of California, San Francisco to release copies of my thesis, dissertation, or manuscript to the Campus Library to provide access and preservation, in whole or in part, in perpetuity.



Author Signature



Date